JANUARY-MARCH 2018 VOL. 10 № 1 (36)

ISSN 2075-8251

ActaNaturae

"Social Life" of Senescent Cells: What Is SASP and Why Study It?

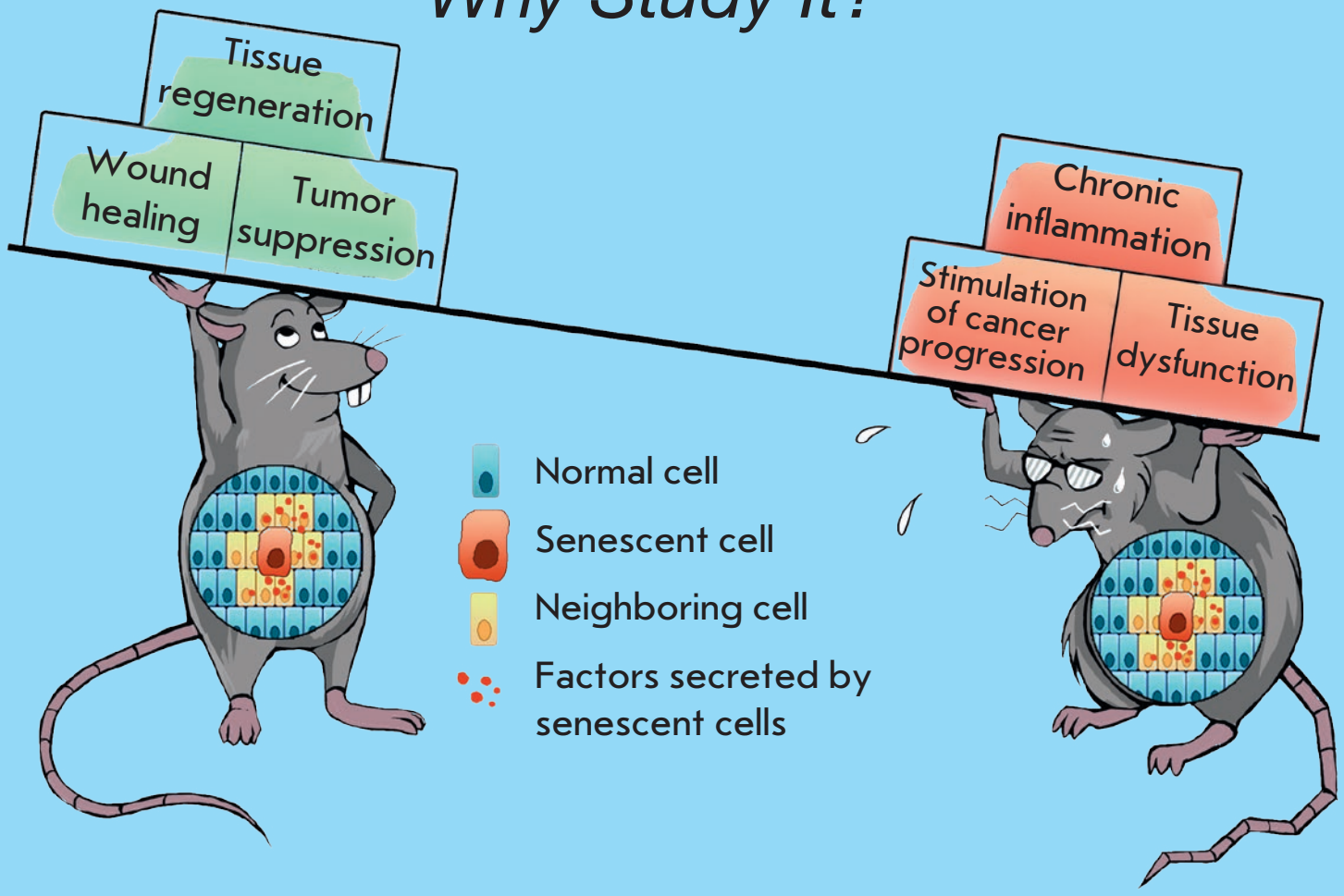

Organismal aging

MERCK

Comprehensive solutions for cell analysis

- Cell lines and primary cells
- Traditional and specialized culture media
- Sterilizing filtration
- Biochemical reagents
- Water purification systems
- Cell counting and analysis
- Cryopreservation

An extensive range and top quality of cell lines from our partner, the European Collection of Authenticated Cell Cultures (ECACC):

- 4000 animal and human cell lines;
- Cells of 45 animal species and 50 tissue types;
- 370 B-lymphoblastoid cell lines for which human leukocyte antigen (HLA) typing data are available;
- 480 hybridoma cell lines secreting monoclonal antibodies;
- DNA, RNA, and cDNA extracted from the cell lines from our collection;

SIGMAaldrich.com/ECACC

LLC Merck
Valovaya Str., 35, Moscow, 115054, Russia;
Tel. +7 (495) 937-33-04
E-mail: mm.russia@merckgroup.com, ruorder@sial.com

SIGMAaldrich.com/cellculture
MERCKmillipore.com/cellculture

SIGMA-ALDRICH® is now MERCK

A Highly Productive CHO Cell Line Secreting Human Blood Clotting Factor IX

S. V. Kovnir, N. A. Orlova, M. I. Shakhparonov, K. G. Skryabin, A. G. Gabibov, I. I. Vorobiev

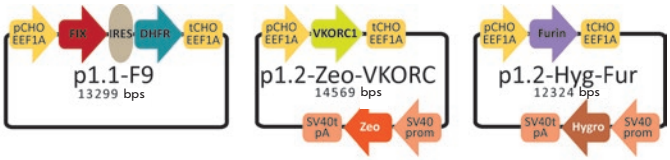

Maps of the expression plasmids p1.1-F9, p1.2-Zeo-VKORC, and p1.2-Hyg-Fur

Recombinant human blood clotting factor IX is produced in the cultured CHO cells; the productivity of the known cell lines is relatively low. The titer of active factor IX upon cultivation can be significantly increased by overexpression of the endogenous enzyme, vitamin K oxidoreductase, from Chinese hamster. The 3B12-86 cell line with the final titer of the product of 6 IU/ml was obtained using p1.1 plasmid vectors. The secreted factor IX was purified using three chromatography rounds to specific activity of 230 IU/mg, with the overall yield > 30%.

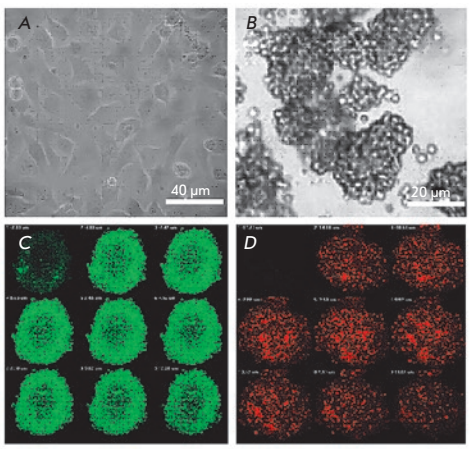

Morphology of Ea.hy926 cells under 2D and 3D cultivation conditions

The Effect of TNF and VEGF on the Properties of Ea.hy926 Endothelial Cells in a Model of Multi-Cellular Spheroids

S. Sh. Gapizov, L. E. Petrovskaya, L. N. Shingarova, E. V. Svirschevskaya, D. A. Dolgikh and M. P. Kirpichnikov

The study demonstrates for the first time that cultivation of Ea.hy926 cells on an anti-adhesive substrate under static conditions leads to the formation of spheroids (3D cultures). Expression of ICAM-1 and VEGFR-2 and production of cytokines by Ea.hy926 cells cultured under 2D and 3D conditions in the presence of TNF and VEGF are studied by flow cytometry, confocal microscopy, and qPCR.

The *PTENP1* Pseudogene, Unlike the *PTEN* Gene, Is Methylated in Normal Endometrium as well as in Endometrial Hyperplasias and Carcinomas in Middle-Aged and Elderly Females

T. F. Kovalenko, K. V. Morozova, L. A. Ozolinya, I. A. Lapina, L. I. Patrushev

Methylation of the *PTEN* gene and its pseudogene *PTENP1* in tumor cells, endometrial hyperplasia, and normal endometrial tissues is studied by methylation-sensitive PCR. None of the analyzed tissue samples carried the methylated *PTEN* gene. However, the *PTENP1* pseudogene was methylated in all the analyzed tissues except for peripheral blood. Significant differences in *PTENP1* methylation rates in normal endometrium were revealed between young (4%) and middle-aged or elderly (58%) females.

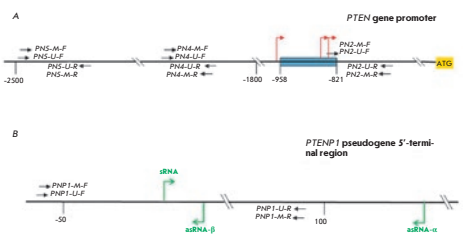

The studied regions of the *PTEN* gene (A) and *PTENP1* pseudogene (B)

ActaNaturae
JANUARY-MARCH 2018 VOL. 10 № 1 (36)

Founders
Ministry of Education and
Science of the Russian Federation,
Lomonosov Moscow State University,
Park Media Ltd

Phone/Fax: +7 (495) 727 38 60
E-mail: vera.knorre@gmail.com, actanaturae@gmail.com

Номер подписан в печать 27 марта 2018 г.
Тираж 200 экз. Цена свободная.
Отпечатано в типографии «МИГ ПРИНТ»

Indexed in Pubmed, Web of Science, Scopus, and RISC

CONTENTS

REVIEWS

RESEARCH ARTICLES

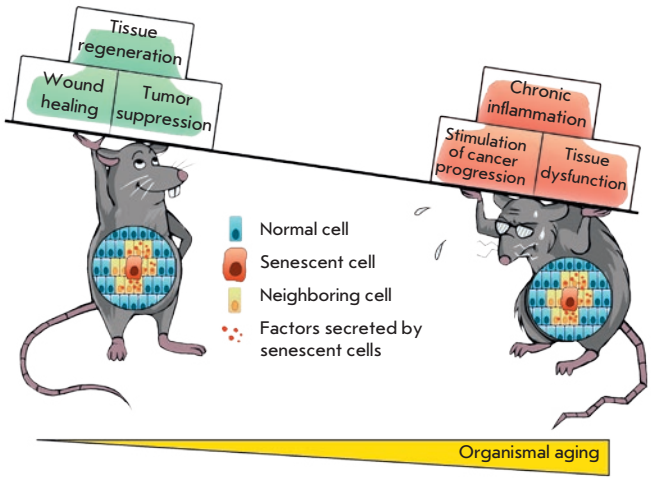

IMAGE ON THE COVER PAGE
(see the article by Borodkina *et al.*)

"Social Life" of Senescent Cells: What Is SASP and Why Study It?

A. V. Borodkina*, P. I. Deryabin, A. A. Giukova, N. N. Nikolsky
Institute of Cytology, Russian Academy of Sciences, Tikhoretsky Ave. 4, St. Petersburg, 194064, Russia
Received May 16, 2017; in final form February 12, 2018
*E-mail: borodkina618@gmail.com

ABSTRACT **Cellular senescence was first described as a failure of normal human cells to divide indefinitely in culture. Until recently, the emphasis in the study of cell senescence has been focused on the accompanying intracellular processes. The focus of the attention has been on the irreversible growth arrest and two important physiological functions that rely on it: suppression of carcinogenesis due to the proliferation loss of damaged cells, and the acceleration of organism aging due to the deterioration of the tissue repair mechanism with age. However, the advances of the past years have revealed that senescent cells can impact the surrounding tissue microenvironment, and, thus, that the main consequences of senescence are not solely mediated by intracellular alterations. Recent studies have provided evidence that a pool of molecules secreted by senescent cells, including cytokines, chemokines, proteases and growth factors, termed the senescence-associated secretory phenotype (SASP), via autocrine/paracrine pathways can affect neighboring cells. Today it is clear that SASP functionally links cell senescence to various biological processes, such as tissue regeneration and remodeling, embryonic development, inflammation, and tumorigenesis. The present article aims to describe the "social" life of senescent cells: basically, SASP constitution, molecular mechanisms of its regulation, and its functional role.**
KEYWORDS **antagonistic pleiotropy, cellular senescence, immune clearance, senescence-associated secretory phenotype, stem cells, tumor suppression, tumorigenesis.**

INTRODUCTION

The history of cellular senescence (CS) studies can be viewed within the framework of the well-known dialectic law of "negation of the negation," which represents a process of development as a spiral (*Fig. 1*). The first turn of this imaginary spiral dates back to more than 100 years ago and reflects a view that had remained the prevailing one in science for a long time: aging is a phenomenon unique to organisms and can be avoided in cell culture. The basic proof of this hypothesis was gathered and published in the work of Nobel Laureate A. Carrel [1]. In his experiments, Carrel demonstrated the feasibility of endless proliferation of cells in culture, given adequate conditions, sufficient quantities of nutrients and, as he himself put it, "due diligence." The paradigm shift and the transition to a new turn in the spiral occurred almost 50 years later, thanks to the work of L. Hayflick, who established the existence of a limit in the division of normal human fibroblasts *in vitro* [2]. Later, this limit was named the Hayflick limit, and the author himself interpreted his findings as a manifestation of human aging at the cellular level [3]. The next important stage in the study of cellular senescence dates back to the early 1970s, when independently of each other A. Olovnikov and D. Watson described the issue of terminal DNA underreplication [4, 5]. According to this hypothesis, the 5'-terminal daughter DNA chain is shortened with each cell division, which ultimately leads to the Hayflick limit. This discovery led to the elucidation of the telomere theory, according to which telomere shortening is what mediates replicative senescence [4]. Shortly afterwards, the structure of telomeres was elucidated and their properties were investigated [6]. Approximately at the same time, other authors began publishing papers which indicated that there is another type of CS that is independent of telomere length [7, 8]. This type of senescence was called 'premature senescence,' since its signs manifested themselves in cells during early passages, long before the onset of replicative senescence. Various stress factors and overexpression of oncogenes are considered to be the main inducers of premature senescence [7–10].

Despite the progress achieved in the study of the mechanisms of CS, for a long time the relationship between cellular and organismal aging remained hypothetical. The experimental evidence for the existence of senescent cells in human tissue samples was obtained

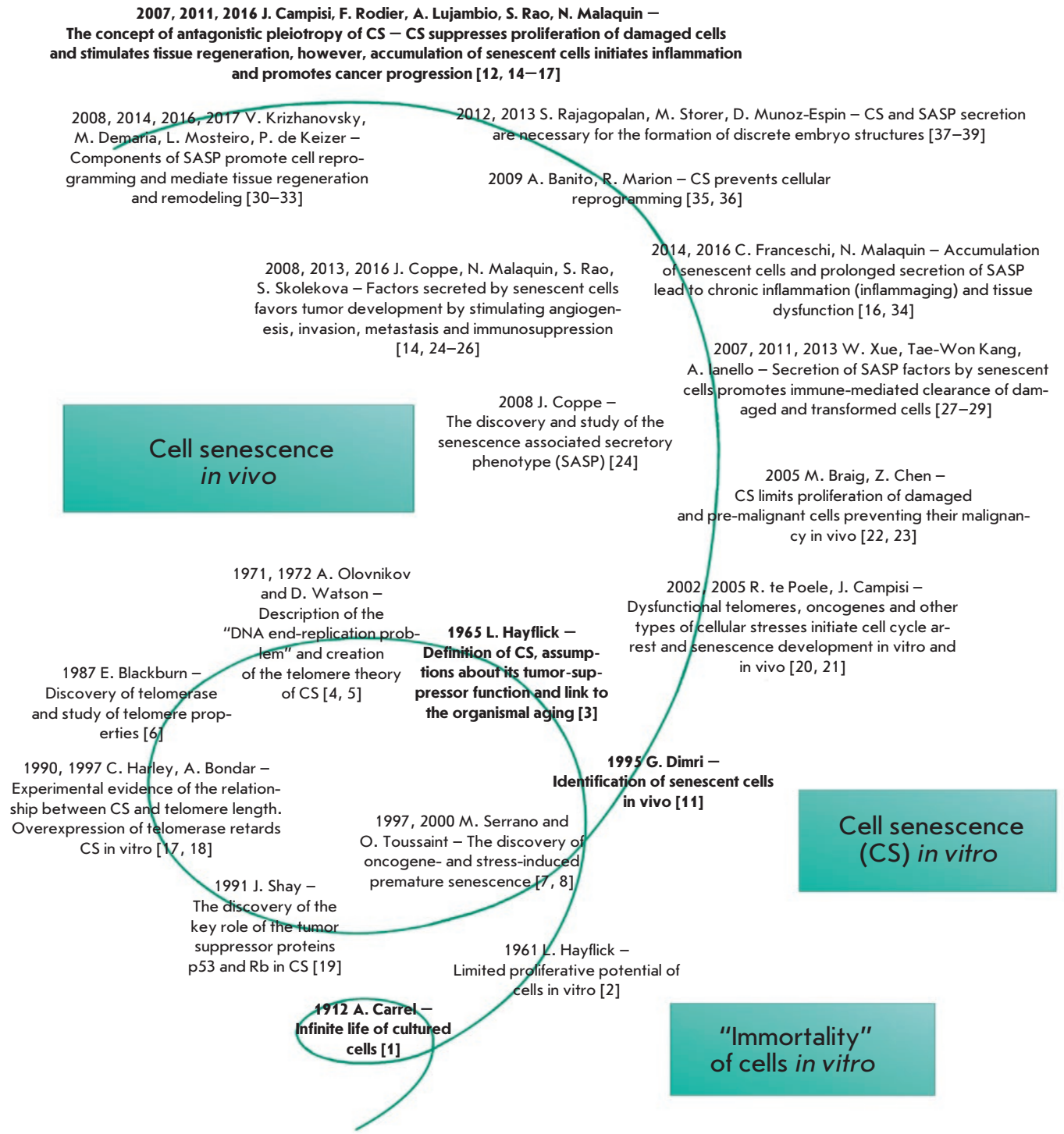

Fig. 1. The timeline of cellular senescence research

only in 1995 [11]. By linking the processes taking place *in vivo* and *in vitro*, these observations drew a line under the previous turns of the spiral and serve as the point of origin for the next phase, which continues up to this day. Previously, manifestations of CS at the organismal level had been considered as something unidirectional, associated exclusively with age and age-related diseases. Today, the effects of CS are described

using the concept of antagonistic pleiotropy, implying a role in the most diverse and sometimes opposite processes, such as repair, regeneration, tissue remodeling, embryogenesis, inflammation, tumor suppression and tumorigenesis [12–16].

PHENOMENOLOGY OF CELLULAR SENESCENCE

Before delving into the heart of this review, which is devoted to the changes that accompany CS and its role in various biological processes, one needs first to understand the essence of this phenomenon. From a mechanistic point of view, the term CS implies an irreversible loss of the proliferative potential of metabolically active cells, which is caused by irreparable DNA damage [40]. If CS is considered at the organismal level, it becomes obvious that preventing the proliferation of cells that are damaged due to their senescence upholds tissue homeostasis. The generally accepted view of the moment that logically follows from the statements above is that senescence is exclusively characteristic of proliferating cells.

During ontogenesis, cell proliferation begins from the moment of the first fragmentation of the zygote. The blastomeres formed as a result of mitotic divisions and subsequent embryonic stem cells (ESCs) are known to possess an unlimited replicative potential. At the molecular level, ESCs lack of replicative senescence is mediated by telomerase activity, which compensates for the shortening of telomeres in each cell division [41, 42]. It is important that these cells also do not exhibit premature senescence: in case of irreparable damage, ESCs are eliminated from the population by apoptosis, which is necessary to preserve the stability of the genome [43]. Due to unrestricted proliferation and their ability to differentiate, ESCs give rise to all types of cells in an adult organism.

In an adult organism, most cells are differentiated and are in a quiescent state [44]. It is worth emphasizing that this state is characterized by a prolonged arrest of proliferation, but it is fundamentally different from CS [45]. First of all, the arrest of growth in this case is not a consequence of DNA damage. Secondly, this arrest can be reversed: with certain stimuli, differentiated cells in the G0 phase of the cell cycle can re-enter the cycle and start proliferating. One such stimuli is the disruption of the functioning of tissues or organs caused by damage. In this case, quiescent cells, such as skin fibroblasts, smooth muscle cells, endothelial cells, the epithelial cells of many internal organs, including the pancreas, liver, kidneys, lungs, prostate and mammary glands, may begin to proliferate to replace cells in damaged areas [44]. Most of these types of cells are susceptible to both replicative and premature senescence [40, 46–48]. It is interesting, however, that damage does not induce CS equally in all types of cells [49]. For example, the epithelium is a very dynamic tissue, characterized by a high rate of renewal. In this tissue homeostasis is supported mainly through the death of damaged and the proliferation of normal cells, and, therefore, epithelial cells are more prone to apoptosis than they are to triggering CS [50]. The opposite is typical for the stromal cells that form the framework of all internal organs. These cells are resistant to apoptosis and are more likely to enter the state of senescence [49].

Despite the examples of recovery of proliferation by certain types of epithelial and stromal cells described above, *in vivo* most of the cells that perform specialized functions are in the terminal differentiated state and, with rare exceptions, are incapable of proliferating even in the case of severe damage [44]. In this case, regeneration is carried out by the division and differentiation of adult stem cells (SCs). Pools of resident stem cells have been found in virtually every tissue [51]. However, it turns out that adult SCs are also susceptible to senescence. First of all, these cells have no active telomerase, and, therefore, SCs, just like all other proliferating cells, experience replicative senescence [52, 53]. Secondly, recently it has been demonstrated that various stress factors can induce premature senescence of SCs [54–56]. Taking into account the unique role of SCs in tissue regeneration in an adult organism, one has to emphasize the negative consequences of the aging of these cells. The senescent SCs lose their ability to proliferate, and their migration activity and differentiation potential decrease [57]. Thus, CS leads to a gradual depletion of the pool of functional SCs: on the one hand, their number decreases, and on the other, they cease to respond properly to external stimuli [58]. There is a view today that holds that SCs senescence is related to organismal aging, and the amount of data describing the contribution of senescent SCs to the development of various age-related diseases is increasing [58, 59].

While speaking about CS, one also has to mention a very special case: the senescence of transformed cells. Given that cancer cells possess unlimited proliferative potential, this, of course, is not about replicative, but about premature, senescence. In normal proliferating cells, premature CS is a physiological response to stress. However, in transformed cells, it can be induced only under specific circumstances, such as treatment with chemotherapeutic agents, irradiation, and overexpression of growth inhibitory genes [60]. Therefore, the induction of CS in transformed cells can be considered as one of the ways available to arrest tumor growth [60].

"SOCIAL LIFE" OF SENESCENT CELLS

It is well known that the main features of CS are similar across its different forms and different types of proliferating cells [40]. *Figure 2* shows the most important

"individual" intracellular changes that accompany CS, which are subdivided into events occurring in the nucleus and in the cytoplasm. The change in the secretory profile occupies a special place among the modifications accompanying CS. It is generally accepted that the senescence-associated secretory phenotype (SASP) defines the engagement of senescent cells in a wide range of processes, such as reparation, propagation of senescence, immune clearance, embryogenesis, and tumorigenesis [29, 31, 38 , 79, 80].

Classification of SASP factors

The term SASP was first used in 2008 to refer to the factors secreted by senescent cells [24]. The following classification of SASP components has been adopted: soluble signaling factors, proteases, insoluble extracellular matrix proteins, and non-protein components [78]. SASP factors can be divided into the following groups based on molecular mechanisms [81]:

1) Factors binding to a receptor. This group includes soluble signaling molecules, such as cytokines, chemokines, and growth factors. These factors can influence cells of the microenvironment by interacting with the corresponding surface receptors on their membranes and, thus, triggering various intracellular signaling cascades [82, 83]. The most well known representatives of this group are interleukins IL-6, IL-8, IL-1a, chemokines GROα, GROβ, CCL-2, CCL-5, CCL-16, CCL-26, CCL-20, and the growth factors HGF, FGF, TGFβ, and GM-CSF.

2) Factors acting directly. This group includes matrix metalloproteases MMP-1, MMP-10, MMP-3 and serine proteases: the tissue plasminogen activator (tPA) and urokinase plasminogen activator (uPA). These factors are capable of cleaving membrane-bound proteins, destroying signaling molecules and remodeling the extracellular matrix, to enable senescent cells to modify their microenvironment [84]. Small non-protein components, such as reactive oxygen (ROS) and nitrogen species that damage neighboring cells, can also be included in this group [78, 85].

3) Regulatory factors. This group includes tissue inhibitors of metalloproteases (TIMP), the plasminogen activator inhibitor (PAI), and insulin-like growth factor binding proteins (IGFBP). These factors do not have their own enzymatic activity. However, when they bind to factors from the first and second groups, they regulate their functioning. For example, TIMP inhibits the activity of most MMPs [86], PAI-1 functions primarily as an inhibitor of tPA and uPA [87], and IGFBP function as IGF transport proteins [88].

In addition to all the factors mentioned above, which are secreted by senescent cells, another component has recently begun to be viewed as part of SASP: extracellular vesicles, in particular vesicles associated with microRNAs [89]. It turns out that such vesicles can affect neighboring cells and cells located at a considerable distance, both by initiating and suppressing CS, depending on the composition of microRNAs.

It should be emphasized that the specific qualitative and quantitative composition of the secreted factors largely depends on the type of cells and the inducer of senescence, which makes it very difficult to study this CS feature. Several approaches to the study of SASP and elucidation of the functions of its individual components have been described to date. The main approaches are presented at *Fig. 3*.

Mechanisms of SASP regulation

It is well known that cellular senescence is not a one-time phenomenon, but one that develops over time [99]. Remarkably, SASP has also recently begun to be viewed as a dynamic process which can be subdivided into several phases [16]. It is believed that the first phase of secretion begins immediately after DNA damage and lasts for the first 36 hours. It should be noted that the onset of this phase is not sufficient evidence in favor of initiation of senescence, since it does not preclude complete repair or apoptosis [99]. The next phase is the "early" SASP phase, which continues for several days after the initiation of CS. It is during this period that the most important SASP factors, for example IL-1α, start to appear. During the next 4–10 days, the secretion of most factors intensifies due to the autocrine effect of SASP, which ultimately leads to the formation of "mature" SASP [16]. Such a wave-like secretion of factors during the development of CS is largely attributed to positive feedback loops and complex regulatory mechanisms. The most common mechanisms for SASP regulation are presented below.

It should be noted that SASP is regulated both at the transcriptional and post-transcriptional levels. The key role in the regulation of SASP components expression, including IL-6, IL-8, CXCL1, and CXCR2, belongs to the nuclear factor kappa-light-chain-enhancer of activated B cells, NF-kB [100–102]. For most of these factors, control over transcription is achieved through positive feedback loops. A vivid example of such "self-amplifying" loops is the regulation of IL-1α secretion [15, 103]. It has been reported that another transcription factor, C/EBPβ, is also involved: by binding directly to the promoter of the *IL-6* gene, where it initiates its expression [82, 104].

At the post-transcriptional level of SASP regulation, it is customary to identify DDR (DNA Damage

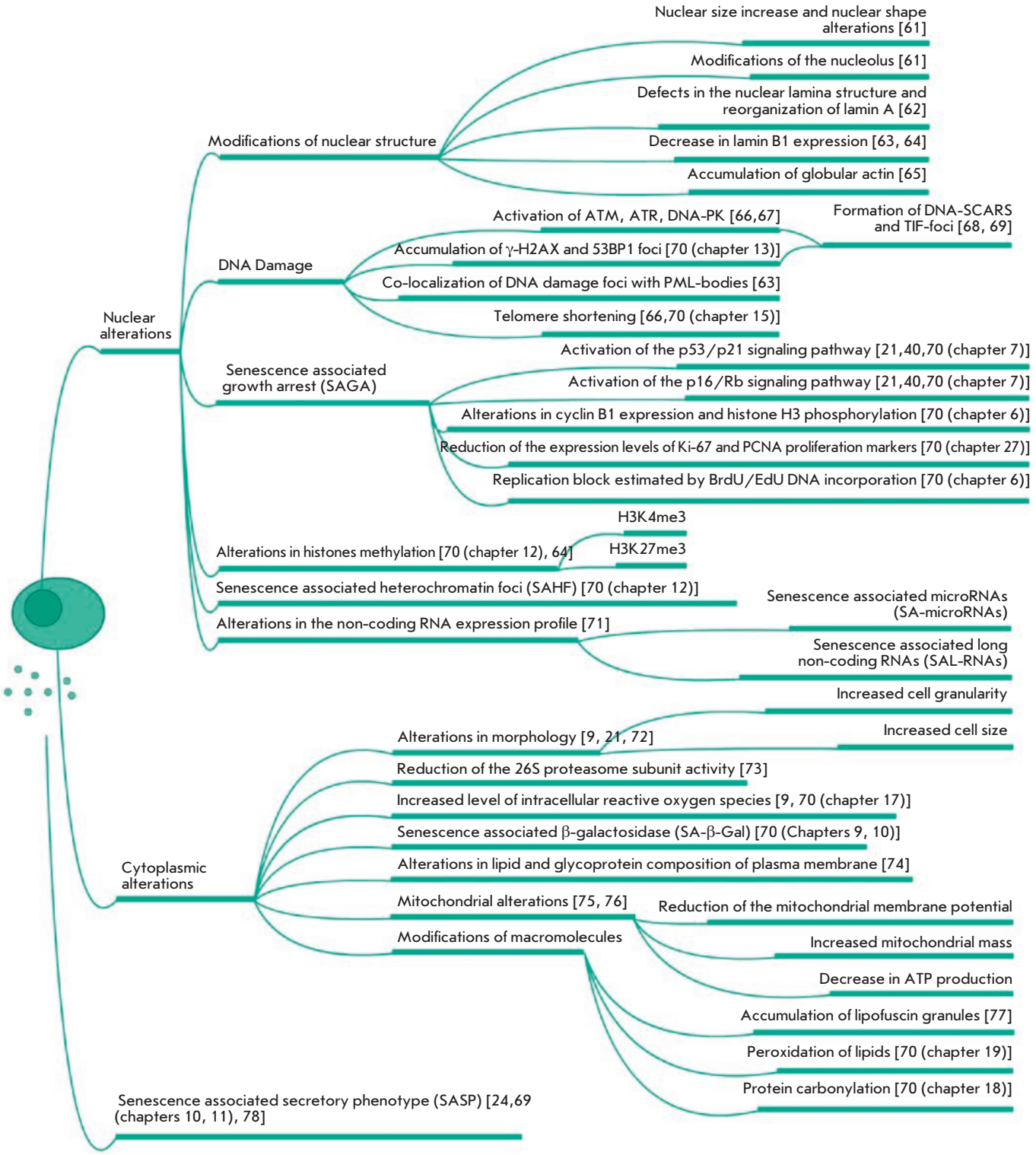

Fig. 2. Biomarkers of senescent cells. The main features of senescent cells and references describing experimental approaches for their estimation are provided

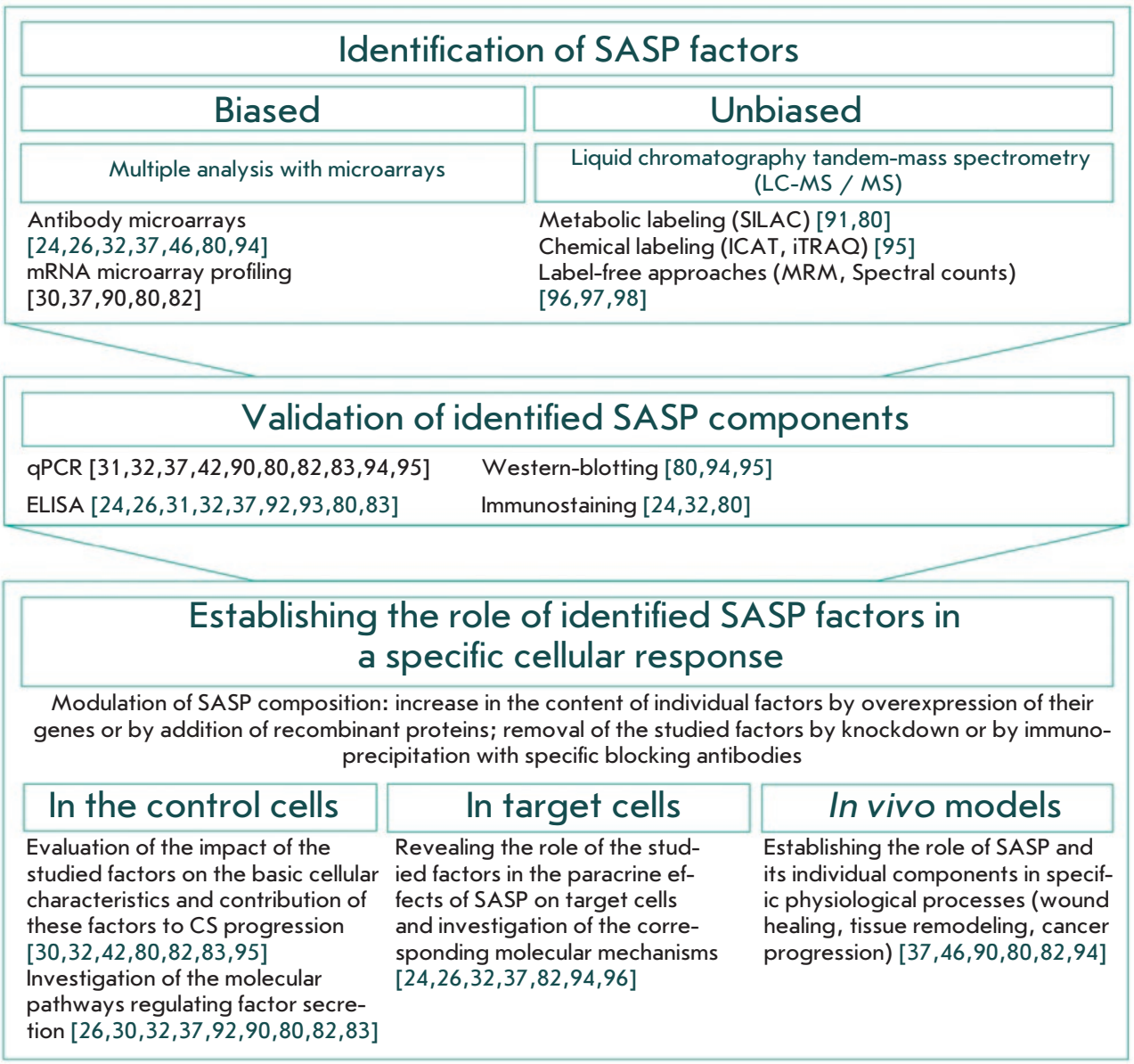

Fig. 3. Experimental approaches to study SASP and to identify the functional role of its individual components

Response)-dependent and independent mechanisms [15]. As mentioned above, one of the most important features of CS is the DNA damage response. It has been shown that knockdowns of such DDR components as ATM, Chk2, NBS1, and H2AX reduce the expression and, accordingly, the secretion of a number of SASP factors, including IL-6 and IL-8 [104–106]. Despite evidence that DDR is involved in SASP regulation, the detailed mechanisms for their relationships are not fully understood. The signaling pathways known today are associated with the ability of DDR components, in particular ATM kinase, to somehow regulate NF-kB activity. For example, ATM can form complexes with the NEMO protein, which, due to the initiation of DDR, are exported from the nucleus to the cytoplasm, where NEMO binds to and activates IKK kinase. IKK promotes the dissociation of the inhibitory IkB protein from its complex with NF-kB and activation of the latter [107]. More recently, the involvement of the transcription factor GATA4 in the DDR-dependent mechanism of SASP regulation has been demonstrated [108]. Normally, GATA4 is degraded by p62-mediated au-

tophagy. However, autophagy is suppressed in most senescent cells, and, therefore, GATA4 stabilizes, and this process is ATM-dependent. The accumulation of GATA4 in senescent cells facilitates the initiation and maintenance of NF-kB activity.

In the DDR-independent mechanism of SASP regulation, the key role is played by the stress-kinase p38, which is involved in the activation of the $p16^{Ink4a}$/Rb signaling pathway that mediates the arrest of the cell cycle in senescent cells [109]. A number of studies have demonstrated that suppression of p38 expression prevents the secretion of most of the cytokines, chemokines and growth factors that make up SASP [110, 111]. In addition, maintaining p38 in the active state for a long time can initiate SASP in the absence of any other stimuli that cause senescence [110]. The following chain of signaling events was proposed for the mechanism of p38 involvement in SASP regulation: p38 activates its underlying targets – MSK1 and MSK2 kinases – which then phosphorylate p65, the transactivation subunit of NF-kB, thereby initiating the expression of many SASP factors [16, 112 , 113].

Recently, the role of the mTOR protein in the regulation of SASP was identified [114, 115]. On the one hand, it has been shown that mTOR can control the translation of IL-1α and thus regulate SASP [115]. On the other hand, mTOR controls the translation of MK-2 kinase, which phosphorylates the specific RNA-binding protein ZFP36L1, preventing the degradation of the transcripts of a large number of SASP factors [114]. Another possible option for mTOR involvement in the regulation of SASP is associated with the presence on the trans side of the Golgi apparatus of a special compartment (TOR-autophagy spatial coupling compartment, TASCC) in which autolysosomes and mTOR are accumulated during senescence [116]. It is assumed that the accumulation of mTOR in this compartment helps accelerate the synthesis of SASP factors.

The regulatory mechanisms described above are the most well studied to date. However, the huge diversity of the proteins included in SASP, as well as the fact that the composition of the secreted factors depends on the cellular context and the type of senescence, leads to an increase in the number of studies focused on detailing the molecular mechanisms of SASP regulation. In most publications, the emphasis is on the relationship between regulatory mechanisms and the functional role of SASP in specific biological processes, which will be discussed in the next chapter. It should be noted that most of the research is performed on cancer cells or on fibroblasts. Paradoxically, despite the obvious biological significance of stem cell senescence, the molecular mechanisms of SASP regulation in these cells are relatively poorly studied.

Functional role of SASP

To understand the mechanisms that mediate the involvement of SASP in a variety of biological processes, one first needs to answer a fundamental question: why do senescent cells secrete so many specific factors? Based on composition, it is logical to assume that *in vivo* SASP can serve as a signal that indicates the appearance of senescent cells in the body. Schematically, this process can be described as follows: the secreted proinflammatory cytokines and chemokines form the focus of the inflammation and attract cells of the immune system to the areas of senescent cells localization for their elimination; the proteins that remodel the extracellular matrix facilitate the entry of immune system cells to these areas; and the secreted growth factors stimulate the proliferation of neighboring cells for subsequent replacement of the removed cells. In a young healthy organism, this mechanism is well regulated. However, with age or in case of lesions, its effectiveness can be significantly impaired, leading to the accumulation of senescent cells in the population and, consequently, to prolonged secretion of SASP factors. Therefore, the outcome of the influence of SASP components on the microenvironment is defined by the balance between how long the senescent cells remain in the population and their rate of elimination by the cells of the immune system [12, 14–16]. Thus, the effects of SASP that are positive for the organism are due to the temporary presence of senescent cells, whereas its negative effects are associated with the accumulation of senescent cells and the emergence of a focus of chronic inflammation.

The opposite consequences of the phenomenon of "auto/paracrine senescence" can be cited as an example of such time dependence of the SASP effects. It is established that once the molecules secreted by the senescent cells get into the extracellular space, they are able to act on adjacent normal cells through the auto/paracrine pathway and initiate the arrest of the cell cycle, stop proliferation, greatly accelerating the development of CS in the population [80, 83, 117]. For example, a conditioned medium derived from replicatively, oncogen or etoposide-aged fibroblasts containing high levels of IL-1, IL-6, and TGFβ contributes to an increase in the level of ROS, damage to DNA and, accordingly, the onset of senescence in normal cells [117]. The role of such SASP factors as activin A, GDF15, VEGF, CCL2, and CCL20 chemokines in the regulation of senescence has also been established [80]. It has been shown that compounds inhibiting the activity or the binding receptors of these factors prevent the development of senescence in a population of fibroblasts. According to our preliminary results, the cultivation of endometrial stem cells in a conditioned medium obtained from

senescent cells also initiates premature senescence in young cells, with the PAI-1 protein playing an important role in this process. Returning to the duality of the cummulative effects of SASP, it should be noted that autocrine senescence plays a positive role in the case of temporary presence of senescent cells: first of all, it prevents the proliferation of the damaged cells, and secondly, it activates the immune response that leads to their removal [28–31, 118].

However, the accumulation of senescent cells and the prolonged secretion of SASP, which promotes the spread of premature senescence to neighboring cells, can lead to disruption in the functioning of tissues, accelerate the development of aging, and various age-associated diseases [33, 119]. For example, the increased secretion of matrix metalloproteases by senescent cells plays an important role in the progression of such pathologies as ischemic heart disease, osteoporosis, and osteoarthritis [120, 121]. Senescent smooth muscle cells secreting large amounts of pro-inflammatory cytokines are involved in the development of atherosclerosis [122]. The increased secretion of TNFα by senescent T cells is involved in the mechanism of bone loss [123]. It is also known that overexpression of IL-6 can lead to hyperinsulinemia, liver inflammation and pulmonary hypertension [124, 125]. In addition, the term 'inflammaging' has been introduced comparatively recently to describe the non-infectious chronic systemic inflammation that accompanies aging, and SASP factors secreted by old cells play a crucial role in its progression [34].

Another manifestation of the duality of the functional effects of SASP is its tumor-suppressing and tumor-promoting activities [2, 14, 28, 78]. A number of works that highlight the tumorigenic role of SASP have demonstrated that factors secreted by senescent fibroblasts stimulate the proliferation of various precancerous and transformed cell lines [24, 25, 126, 127]. Later, it was established that SASP induces an epithelial-mesenchymal transition and enhances the invasion of cells in the culture of precancerous epithelial cells, in particular through an increased content IL-6 and IL-8 [24]. It has been established that SASP factors secreted by senescent stem cells also contribute to the progression of cancer, accelerating the proliferation and migration of transformed cells [57]. For example, SASP factors secreted by SCs stimulate the division and migration of breast cancer cells both *in vitro* and in a mouse model [57]. In addition, it was established that senescent SCs secreting large amounts of IL-6 and IL-8 increase the resistance of breast cancer cells to cisplatin [26]. Based on the data available to date, it is most likely that SASP components induce proliferation, survival, and metastasis in already committed precancerous cells [14].

The tumor suppressing function is based on the ability of SASP factors to attract cells of the immune system to eliminate damaged senescent cells. Thus, a mouse model shows that Ras overexpression results in oncogen-induced hepatocyte senescence, which is accompanied by activation of SASP, stimulation of the $CD4^+$-mediated immune response and, as a consequence, in the removal of these cells [28]. Another piece of evidence of the tumor-suppressing role of SASP was also obtained in a mouse model of hepatocarcinoma: however, in this case CS was induced by overexpression of p53 [29]. The secretion of various chemokines by senescent cancer cells led to the recruitment of natural killers (natural killers, NK) for their clearance. Remarkably, the removal of CCL2 chemokine by antibodies prevents the recruitment of NK cells and reduces the elimination of senescent cells.

The involvement of SASP in the regeneration of tissues deserves special attention. It is known that SASP factors can influence the signaling and differentiation of stem cells [33, 128, 129]. For example one of the key components of SASP, IL-6, promotes the induction and maintenance of pluripotency, in particular by regulating the expression of Nanog [130, 131]. Moreover, *in vivo* experiments have shown that secretion of SASP promotes the reprogramming of microenvironment cells [32]. This SASP-mediated tissue regeneration is another example of the time dependence of the cummulative effects of SASP. In a young organism, short-term action of SASP promotes tissue regeneration through temporary reprogramming and subsequent proliferation and differentiation of neighboring cells, whereas in an elderly organism ineffective elimination of senescent cells and prolonged secretion of SASP can lead to a prolongation of the dedifferentiated state of neighboring cells, and, accordingly, to the inhibition of regeneration [33].

Interesting results concerning the role of SASP in tissue regeneration and remodeling were obtained by studying the molecular mechanisms of wound healing. It has been established that senescent fibroblasts and endothelial cells can be detected at wound sites for several days, which promote wound healing through secretion of PDGF-A, the SASP factor responsible for the differentiation of myofibroblasts [31]. In addition, the role of SASP in tissue remodeling during embryonic development has been established [31, 37–39]. It has been shown that SASP-mediated remodeling occurs both from the maternal body and from the embryo. For example, SASP was implicated in the remodeling of the maternal vasculature in early pregnancy [131]. Senescent cells appear in the process of embryonic development and use SASP to act as a primary signal that triggers macrophage-mediated cell removal, which is

necessary for the proper development of individual embryonic structures [31, 38, 39].

CONCLUSION

Summing up all the above, let's revisit the last turn of the spiral, which corresponds to the current stage in the history of cellular senescence studies, and once again emphasize the pleiotropy of CS effects. It is obvious that the experimental approaches that involve the elimination of senescent cells from the body and considered as "anti-aging" therapy can have a number of concomitant, undesirable consequences. Therefore, the most promising approach seems to be the development of strategies aimed at modulating the composition of the factors secreted by old cells, in order to enhance the positive and minimize the potential negative effects of SASP. Modulation of the SASP factors of senescent SC acquires particular importance in this context. Taking into account that at present the most probable mechanism of SC influence on tissue repair is their paracrine activity, the issue of changes in the secretory profile of SC as a result of their aging becomes very urgent and requires additional studies. ●

This work was supported by the Russian Science Foundation (Project No. 14-50-00068).

REFERENCES

1. Carrel A. // J. Exp. Med. 1912. V. 15. № 5. P. 516–528.
2. Hayflick L., Moorhead P.S. // Exp. Cell Res. 1961. V. 25. P. 585–621.
3. Hayflick L. // Exp. Cell Res. 1965. V. 37. P. 614–636.
4. Olovnikov A.M. // Dokl. Akad. Nauk SSSR. 1971. V. 201. P. 1496–1499.
5. Watson J.D. // Nat. New Biol. 1972. V. 239. P. 197–201.
6. Greider C.W., Blackburn E.H. // Cell. 1987. V. 51. № 6. P. 887–898.
7. Serrano M., Lin A.W., McCurrach M.E., Beach D., Lowe S.W. // Cell. 1997. V. 88. № 5. P. 593–602.
8. Toussaint O., Medrano E.E., von Zglinicki T. // Exp. Gerontol. 2000. V. 35. № 8. P. 927–945.
9. Kuilman T., Michaloglou C., Mooi W.J., Peeper D.S. // Genes Dev. 2010. V. 24. № 22. P. 2463–2479.
10. Fridlyanskaya I.I., Alekseenko L.L., Nikolsky N.N. // Exp. Gerontol. 2015. V. 72. P. 124–128.
11. Dimri G.P., Lee X., Basile G., Acosta M., Scott G., Roskelley C., Medrano E.E., Linskens M., Rubelj I., Pereira-Smith O., et al. // Proc. Natl. Acad. Sci. USA. 1995. V. 92. № 20. P. 9363–9367.
12. Rodier F., Campisi J. // J. Cell Biol. 2011. V. 192. № 4. P. 547–556.
13. Childs B.G., Durik M., Baker D.J., van Deursen J.M. // Nat. Med. 2015. V. 21. № 12. P. 1424–1435.
14. Rao S.G., Jakson J.G. // Trends Cancer. 2016. V. 2. № 11. P. 676–687.
15. Lujambio A. // Bioessays. 2016. V. 38. № 1. P. 56–64.
16. Malaquin N., Martinez A., Rodier F. // Exp. Gerontol. 2016. V. 82. P. 39–49.
17. Harley C.B., Futcher A.B., Greider C.W. // Nature. 1990. V. 345. № 6274. P. 458–460.
18. Bodnar A.G., Ouellette M., Frolkis M., Holt S.E., Chiu C.P., Morin G.B., Harley C.B., Shay J.W., Lichtsteiner S., Wright W.E. // Science. 1998. V. 279. № 5349. P. 349–352.
19. Shay J.W., Pereira-Smith O.M., Wright W.E. // Exp. Cell. Res. 1991. V. 196. № 1. P. 33–39.
20. te Poele R.H., Okorokov A.L., Jardine L., Cummings J., Joel S.P. // Cancer Res. 2002. V. 62. № 6. P. 1876–1883.
21. Campisi J. // Cell. 2005. V. 120. № 4. P. 513–522.
22. Braig M., Lee S., Loddenkemper C., Rudolph C., Peters A.H., Schlegelberger B., Stein H., Dörken B., Jenuwein T., Schmitt C.A. // Nature. 2005. V. 436. № 7051. P. 660–665.
23. Chen Z., Trotman L.C., Shaffer D., Lin H.K., Dotan Z.A., Niki M., Koutcher J.A., Scher H.I., Ludwig T., Gerald W., et al. // Nature. 2005. V. 436. № 7051. P. 725–730.
24. Coppe J.P., Patil C.K., Rodier F., Sun Y., Munoz D.P., Goldstein J., Nelson P.S., Desprez P.Y., Campisi J. // PLoS Biol. 2008. V. 6. P. 2853–2868.
25. Malaquin N., Vercamer C., Bouali F., Martien S., Deruy E., Wernert N., Chwastyniak M., Pinet F., Abbadie C., Pourtier A. // PLoS One. 2013. V. 8. № e63607.
26. Skolekova S., Matuskova M., Bohac M., Toro L., Demkova L., Gursky J., Kucerova L. // Cell Commun. Signal. 2016. V. 14. № 4. P. 1–13.
27. Xue W., Zender L., Miething C., Dickins R.A., Hernando E., Krizhanovsky V., Cordon-Cardo C., Lowe S.W. // Nature. 2007. V. 445. № 7128. P. 656–660.
28. Kang T.W., Yevsa T., Woller N., Hoenicke L., Wuestefeld T., Dauch D., Hohmeyer A., Gereke M., Rudalska R., Potapova A., et al. // Nature. 2011. V. 479. P. 547–551.
29. Iannello A., Thompson T.W., Ardolino M., Lowe S.W., Raulet D.H. // J. Exp. Med. 2013. V. 210. P. 2057–2069.
30. Krizhanovsky V., Yon M., Dickins R.A., Hearn S., Simon J., Miething C., Yee H., Zender L., Lowe S.W. // Cell. 2008. V. 134. P. 657–667.
31. Demaria M., Ohtani N., Youssef S.A., Rodier F., Toussaint W., Mitchell J.R., Laberge R.M., Vijg J., van Steeg H., Dolle M.E., et al. // Dev. Cell. 2014. V. 31. P. 722–733.
32. Mosteiro L., Pantoja C., Alcazar N., Marión R.M., Chondronasiou D., Rovira M., Fernandez-Marcos P.J., Muñoz-Martin M., Blanco-Aparicio C., Pastor J., et al. // Science. 2016. V. 25. № 354. P. af4445.
33. de Keizer P.L. // Trends Mol. Med. 2017. V. 23. № 1. P. 6–17.
34. Franceschi C., Campisi J. // J. Gerontol. A Biol. Sci. Med. Sci. 2014. V. 69. P. S4–S9.
35. Banito A., Rashid S.T., Acosta J.C., Li S., Pereira C.F., Geti I., Pinho S., Silva J.C., Azuara V., Walsh M., et al. // Genes Dev. 2009. V. 23. № 18. P. 2134–2139.
36. Marión R.M., Strati K., Li H., Murga M., Blanco R., Ortega S., Fernandez-Capetillo O., Serrano M., Blasco M.A. // Nature. 2009. V. 460. № 7259. P. 1149–1153.
37. Rajagopalan S., Long E.O. // Proc. Natl. Acad. Sci. USA. 2012. V. 109. № 50. P. 20596–20601.
38. Munoz-Espin D., Canamero M., Maraver A., Gomez-Lopez G., Contreras J., Murillo-Cuesta S., Rodriguez-Baeza A., Varela-Nieto I., Ruberte J., Collado M., et al. // Cell. 2013. V. 155. P. 1104–1118.
39. Storer M., Mas A., Robert-Moreno A., Pecoraro M., Ortells M.C., Di Giacomo V., Yosef R., Pilpel N., Krizhanovsky V., Sharpe J., Keyes W.M. // Cell. 2013. V. 155. № 5. P. 1119–1130.
40. Campisi J., d'Adda di Fagagna F. // Nat. Rev. Mol. Cell.

Biol. 2007. V. 8. P. 729–740.
41. Rosler E.S., Fisk G.J., Ares X., Irving J., Miura T., Rao M.S., Carpenter M.K. // Dev. Dyn. 2004. V. 229. P. 259–274.
42. Miura T., Mattson M.P., Rao M.S. // Aging Cell. 2004. V. 3. P. 333–343.
43. Dumitru R., Gama V., Fagan B.M., Bower J.J., Swahari V., Pevny L.H., Deshmukh M. // Mol. Cell. 2012. V. 46. P. 573–583.
44. Cooper G.M. The Cell: A Molecular Approach. 2nd ed. Washington, D.C.: ASM Press, 2000. 689 p.
45. Buttitta L.A., Edgar B.A. // Curr. Opin. Cell Biol. 2007. V. 19. № 6. P. 697–704.
46. Jeyapalan J.C., Ferreira M., Sedivy J.M., Herbig U. // Mech. Ageing Dev. 2007. V. 128. P. 36–44.
47. Bertram C., Hass R. // Mech. Ageing Dev. 2009. V. 130. № 10. P. 657–669.
48. Papadopoulou A., Kletsas D. // Int. J. Oncol. 2011. V. 39. № 4. P. 989–999.
49. Georgakopoulou E., Evangelou K., Havaki S., Townsend P., Kanavaros P., Gorgoulis V.G. // Mech. Ageing Dev. 2016. V. 156. P. 17–24.
50. Guillot C., Lecuit T. // Science. 2013. V. 340. P. 1185–1189.
51. da Silva Meirelles L., Chagastelles P.C., Nardi N.B. // J. Cell Sci. 2006. V. 119. № 11. P. 2204–2213.
52. Zimmermann S., Voss M., Kaiser S., Kapp U., Waller C.F., Martens U.M. // Leukemia. 2003. V. 17. P. 1146–1149.
53. Banfi A., Bianchi G., Notaro R., Luzzatto L., Cancedda R., Quarto R. // Tissue Eng. 2002. V. 8. P. 901–910.
54. Cmielova J., Havelek R., Soukup T., Jiroutova A., Visek B., Suchanek J., Vavrova J., Mokry J., Muthna D., Bruckova L., et al. // Int. J. Radiat. Biol. 2012. V. 88. P. 393–404.
55. Larsen S.A., Kassem M., Rattan S.I. // Chem. Cent. J. 2012. V. 6. P. 18.
56. Burova E.B., Borodkina A.V., Shatrova A.N., Nikolsky N.N. // Oxid. Med. Cell Longev. 2013. V. 2013. № 474931.
57. Turinetto V., Vitale E., Giachino C. // Int. J. Mol. Sci. 2016. V. 17. № 7. P. E1164.
58. Wehrwein P. // Nature. 2012. V. 492. P. 12–13.
59. Bell D.R., van Zant G. // Oncogene. 2004. V. 23. № 43. P. 7290–7296.
60. Roninson I.B. // Cancer Res. 2003. V. 63. № 11. P. 2705–2715.
61. Mehta I.S., Figgitt M., Clements C.S., Kill I.R., Bridger J.M. // Ann. N.Y. Acad. Sci. 2007. V. 1100. P. 250–263.
62. Righolt C.H., van't Hoff M.L., Vermolen B.J., Young I.T., Raz V. // Aging (Albany NY). 2011. V. 3. № 12. P. 1192–1201.
63. Freund A., Laberge R.M., Demaria M., Campisi J. // Mol. Biol. Cell. 2012. V. 23. № 11. P. 2066–2075.
64. Shah P.P., Donahue G., Otte G.L., Capell B.C., Nelson D.M., Cao K., Aggarwala V., Cruickshanks H.A, Rai T.S., McBryan T., et al. // Genes Dev. 2013. V. 27. № 16. P. 1787–1799.
65. Kwak I.H., Kim H.S., Choi O.R., Ryu M.S., Lim I.K. // Cancer Res. 2004. V. 64. № 2. P. 572–580.
66. d'Adda di Fagagna F. // Nat. Rev. Cancer. 2008. V. 8. № 7. P. 512–522.
67. Borodkina A.V., Shatrova A.N., Abushik P.A., Nikolsky N.N., Burova E.B. // Aging (Albany NY). 2014. V. 6. № 6. P. 481–495.
68. Rodier F., Muñoz D.P., Teachenor R., Chu V., Le O., Bhaumik D., Coppé J.P., Campeau E., Beauséjour C.M., Kim S.H., et al. // J. Cell Sci. 2011. V. 124. P. 68–81.
69. Herbig U., Ferreira M., Condel L., Carey D., Sedivy J.M. // Science. 2006. V. 311. № 5765. P. 1257.
70. Galluzzi L., Vitale I., Kepp O., Kroemer G. Cell senescence. Methods and protocols. N.Y.: Springer Science+Businces Media, LLC, 2013. 538 p.
71. Abdelmohsen K., Gorospe M. // Wiley Interdiscip. Rev. RNA. 2015. V. 6. № 6. P. 615–629.
72. Yang J., Dungrawala H., Hua H., Manukyan A., Abraham L., Lane W., Mead H., Wright J., Schneider B.L. // Cell Cycle. 2011. V. 10. № 1. P. 144–155.
73. Chondrogianni N., Stratford F.L., Trougakos I.P., Friguet B., Rivett A.J., Gonos E.S. // J. Biol. Chem. 2003. V. 278. № 30. P. 28026–28037.
74. Matjusaitis M., Chin G., Sarnoski E.A., Stolzing A. // Ageing Res. Rev. 2016. V. 29. P. 1–12.
75. Correia-Melo C., Passos J.F. // Biochim. Biophys. Acta. 2015. V. 1847. № 11. P. 1373–1379.
76. Passos J.F., Nelson G., Wang C., Richter T., Simillion C., Proctor C.J., Miwa S., Olijslagers S., Hallinan J., Wipat A., et al. // Mol. Syst. Biol. 2010. V. 6. № 347. P. 1–14..
77. Georgakopoulou E.A., Tsimaratou K., Evangelou K., Fernandez Marcos P.J., Zoumpourlis V., Trougakos I.P., Kletsas D., Bartek J., Serrano M., Gorgoulis V.G. // Aging (Albany NY). 2013. V. 5. № 1. P. 37–50.
78. Coppe J.P., Desprez P.Y., Krtolica A. Campisi J. // Annu. Rev. Pathol. 2010. V. 5. P. 99–118.
79. Parrinello S., Coppe J.P., Krtolica A., Campisi J. // J. Cell Sci. 2005. V. 118. P. 485–496.
80. Acosta J.C., Banito A., Wuestefeld T., Georgilis A., Janich P., Morton J.P., Athineos D., Kang T.W., Lasitschka F., Andrulis M., et al. // Nat. Cell Biol. 2013. V. 15. № 8. P. 978–990.
81. Byun H.O., Lee Y.K., Kim J.M., Yoon G. // BMB Rep. 2015. V. 48. № 10. P. 549–558.
82. Kuilman T., Michaloglou C., Vredeveld L.C., Douma S., van Doorn R., Desmet C.J., Aarden L.A., Mooi W.J., Peeper D.S. // Cell. 2008. V. 133. № 6. P. 1019–1031.
83. Acosta J.C., O'Loghlen A., Banito A., Guijarro M.V., Augert A., Raguz S., Fumagalli M., Da Costa M., Brown C., Popov N., et al. // Cell. 2008. V. 133. P. 1006–1018.
84. Hornebeck W., Maquart F.X. // Biomed. Pharmacother. 2003. V. 57. P. 223–230.
85. Finkel T., Serrano M., Blasco M.A. // Nature. 2007. V. 448. № 7155. P. 767–774.
86. Brew K., Dinakarpandian D., Nagase H. // Biochim. Biophys. Acta. 2000. V. 1477. P. 267–283.
87. Parfyonova Y.V., Plekhanova O.S., Tkachuk V.A. // Biochemistry (Mosc.). 2002. V. 67. № 1. P. 119–134.
88. Hwa V., Oh Y., Rosenfeld R.G. // Endocr. Rev. 1999. V. 20. № 6. P. 761–787.
89. Urbanelli L., Buratta S., Sagini K., Tancini B., Emiliani C. // Int. J. Mol. Sci. 2016. V. 17. № 9. P. E1408.
90. Pearson M., Carbone R., Sebastiani C., Cioce M., Fagioli M., Saito S., Higashimoto Y., Appella E., Minucci S., Pandolfi P.P., et al. // Nature. 2000. V. 406. № 6792. P. 207–210.
91. Acosta J.C., Snijders A.P., Gil J. // Methods Mol. Biol. 2013. V. 965. P. 175–184.
92. Rodier F., Muñoz D.P., Teachenor R., Chu V., Le O., Bhaumik D., Coppé J.P., Campeau E., Beauséjour C.M., Kim S.H., et al. // J. Cell Sci. 2011. V. 124. P. 68–81.
93. Freund A., Laberge R.M., Demaria M., Campisi J. // Mol. Biol. Cell. 2012. V. 23. № 11. P. 2066–2075.
94. Coppé J.P., Patil C.K., Rodier F., Krtolica A., Beauséjour C.M., Parrinello S., Hodgson J.G., Chin K., Desprez P.Y., Campisi J. // PLoS One. 2010. V. 5. № 2. P. e9188.
95. Elzi D.J., Song M., Hakala K., Weintraub S.T., Shiio Y. // Mol. Cell Biol. 2012. V. 32. № 21. P. 4388–4399.
96. Severino V., Alessio N., Farina A., Sandomenico A., Cipollaro M., Peluso G., Galderisi U., Chambery A. // Cell Death

Dis. 2013. V. 4. P. e911.
97. Pasillas M.P., Shields S., Reilly R., Strnadel J., Behl C., Park R., Yates J.R., Klemke R., Gonias S.L., Coppinger J.A. // Mol. Cell Proteomics. 2015. V. 14. № 1. P. 1–14.
98. Özcan S., Alessio N., Acar M.B., Mert E., Omerli F., Peluso G., Galderisi U. // Aging (Albany NY). 2016. V. 8. № 7. P. 1316–1329.
99. Baker D.J., Sedivy J.M. // J. Cell Biol. 2013. V. 202. P. 11–13.
100. Chien Y., Scuoppo C., Wang X., Fang X., Balgley B., Bolden J.E., Premsrirut P., Luo W., Chicas A., Lee C.S., et al. // Genes Dev. 2011. V. 25. P. 2125–2136.
101. Ohanna M., Giuliano S., Bonet C., Imbert V., Hofman V., Zangari J., Bille K., Robert C., Bressac-de Paillerets B., Hofman P., et al. // Genes Dev. 2011. V. 25. P. 1245–1261.
102. Rovillain E., Mansfield L., Caetano C., Alvarez-Fernandez M., Caballero O.L., Medema R.H., Hummerich H., Jat P.S. // Oncogene. 2011. V. 30. P. 2356–2366.
103. Orjalo A.V., Bhaumik D., Gengler B.K., Scott G.K., Campisi J. // Proc. Natl. Acad. Sci. USA. 2009. V. 106. № 4. P. 17031–17036.
104. Rodier F., Coppe J.P., Patil C.K., Hoeijmakers W.A., Munoz D.P., Raza S.R., Freund A., Campeau E., Davalos A.R., Campisi J. // Nat. Cell Biol. 2009. V. 11. P. 973–979.
105. Rodier F., Munoz D.P., Teachenor R., Chu V., Le O., Bhaumik D., Coppe J.P., Campeau E., Beausejour C.M., Kim S.H., et al. // J. Cell Sci. 2011. V. 124. P. 68–81.
106. Pazolli E., Alspach E., Milczarek A., Prior J., Piwnica-Worms D., Stewart S.A. // Cancer Res. 2012. V. 72. P. 2251–2261.
107. Miyamoto S. // Cell Res. 2011. V. 21. P. 116–130.
108. Kang C., Xu Q., Martin T.D., Li M.Z., Demaria M., Aron L., Lu T., Yankner B.A., Campisi J., Elledge S.J. // Science. 2015. V. 349. № 6255. P. aaa5612.
109. Bulavin D.V., Phillips C., Nannenga B., Timofeev O., Donehower L.A., Anderson C.W., Appella E., Fornace A.J. Jr. // Nat. Genet. 2004. V. 36. P. 343–350.
110. Freund A., Patil C.K., Campisi J. // EMBO J. 2011. V. 30. P. 1536–1548.
111. Alspach E., Flanagan K.C., Luo X., Ruhland M.K., Huang H., Pazolli E., Donlin M.J., Marsh T., Piwnica-Worms D., Monahan J., et al. // Cancer Discov. 2014. V. 4. P. 716–729.
112. Vermeulen L., De Wilde G., van Damme, P., Vanden Berghe W., Haegeman G. // EMBO J. 2003. V. 22. P. 1313–1324.
113. Kefaloyianni E., Gaitanaki C., Beis I. // Cell. Signal. 2006. V. 18. P. 2238–2251.
114. Herranz N., Gallage S., Mellone M., Wuestefeld T., Klotz S., Hanley C.J., Raguz S., Acosta J.C., Innes A.J., Banito A., et al. // Nat. Cell Biol. 2015. V. 17. P. 1205–1217.
115. Laberge R.M., Sun Y., Orjalo A.V., Patil C.K., Freund A., Zhou L., Curran S.C., Davalos A.R., Wilson-Edell K.A., Liu S., et al. // Nat. Cell Biol. 2015. V. 17. P. 1049–1061.
116. Narita M., Young A.R., Arakawa S., Samarajiwa S.A., Nakashima T., Yoshida S., Hong S., Berry L.S., Reichelt S., Ferreira M., et al. // Science. 2011. V. 332. № 6032. P. 966–970.
117. Hubackova S., Krejcikova K., Bartek J., Hodny Z. // Aging (Albany NY). 2012. V. 4. P. 932–951.
118. Munoz-Espin D., Serrano M. // Nat. Rev. Mol. Cell. Biol. 2014. V. 15. P. 482–496.
119. Baker D.J., Wijshake T., Tchkonia T., LeBrasseur N.K., Childs B.G., van de Sluis B., Kirkland J.L., van Deursen J.M. // Nature. 2011. V. 479. P. 232–236.
120. Nanni S., Melandri G., Hanemaaijer R., Cervi V., Tomasi L., Altimari A., van Lent N., Tricoci P., Bacchi L., Branzi A. // Transl. Res. 2007. V. 149. P. 137–144.
121. Price J.S., Waters J.G., Darrah C., Pennington C., Edwards D.R., Donell S.T., Clark I.M. // Aging Cell. 2002. V. 1. P. 57–65.
122. Minamino T., Yoshida T., Tateno K., Miyauchi H., Zou Y., Toko H., Komuro I. // Circulation. 2003. V. 108. P. 2264–2269.
123. Effros R.B. // Exp. Gerontol. 2004. V. 39. P. 517–524.
124. Franckhauser S., Elias I., Rotter Sopasakis V., Ferré T., Nagaev I., Andersson C.X., Agudo J., Ruberte J., Bosch F., Smith U. // Diabetologia. 2008. V. 51. № 7. P. 1306–1316
125. Steiner M.K., Syrkina O.L., Kolliputi N., Mark E.J., Hales C.A., Waxman A.B. // Circ. Res. 2009. V. 104. № 2. P. 236–244.
126. Krtolica A., Parrinello S., Lockett S., Desprez P.Y., Campisi J. // Proc. Natl. Acad. Sci. USA. 2001. V. 98. P. 12072–12077.
127. Sun Y., Nelson P.S. // Clin. Cancer Res. 2012. V. 18. P. 4019–4025.
128. Pietras E.M., Mirantes-Barbeito C., Fong S., Loeffler D., Kovtonyuk L.V., Zhang S., Lakshminarasimhan R., Chin C.P., Techner J.M., Will B., et al. // Nat. Cell Biol. 2016. V. 18. P. 607–618.
129. Brady J.J., Li M., Suthram S., Jiang H., Wong W.H., Blau H.M., et al. // Nat. Cell Biol. 2013. V. 15. P. 1244–1252.
130. Cahu J., Bustany S., Sola B. // Cell Death Dis. 2012. V. 3. P. e446.
131. Chang T.S., Wu Y.C., Chi C.C., Su W.C., Chang P.J., Lee K.F., Tung T.H., Wang J., Liu J.J., Tung S.Y., et al. // Clin. Cancer Res. 2015. V. 21. P. 201–210.

The Role of TAL1 in Hematopoiesis and Leukemogenesis

E. R. Vagapova*, P. V. Spirin, T. D. Lebedev, V. S. Prassolov
The Engelhardt Institute of Molecular Biology, Russian Academy of Sciences, Vavilova Str. 32, Moscow, 119991, Russia
*E-mail: elmira-mi@mail.ru
Received: September 22, 2017; in final form January 29, 2018

ABSTRACT **TAL1 (SCL/TAL1, T-cell acute leukemia protein 1) is a transcription factor that is involved in the process of hematopoiesis and leukemogenesis. It participates in blood cell formation, forms mesoderm in early embryogenesis, and regulates hematopoiesis in adult organisms. TAL1 is essential in maintaining the multipotency of hematopoietic stem cells (HSC) and keeping them in quiescence (stage G0). TAL1 forms complexes with various transcription factors, regulating hematopoiesis (E2A/HEB, GATA1–3, LMO1–2, Ldb1, ETO2, RUNX1, ERG, FLI1). In these complexes, TAL1 regulates normal myeloid differentiation, controls the proliferation of erythroid progenitors, and determines the choice of the direction of HSC differentiation. The transcription factors TAL1, E2A, GATA1 (or GATA2), LMO2, and Ldb1 are the major components of the SCL complex. In addition to normal hematopoiesis, this complex may also be involved in the process of blood cell malignant transformation. Upregulation of *C-KIT* expression is one of the main roles played by the SCL complex. Today, TAL1 and its partners are considered promising therapeutic targets in the treatment of T-cell acute lymphoblastic leukemia.**
KEWORDS **hematopoiesis, acute myeloid leukemia, receptor tyrosine kinase C-KIT, T-cell acute lymphoblastic leukemia.**
ABBREVIATIONS **HSC — hematopoietic stem cell, ESC — embryonic stem cell, CMP — common myeloid progenitor, CLP — common lymphoid progenitor, T-ALL — T-cell acute lymphoblastic leukemia, DMSO — dimethyl sulfoxide.**

INTRODUCTION

Hematopoiesis comprises a series of steps, including the formation of early hematopoietic progenitor cells from mesoderm, the formation of hematopoietic stem cells (HSC), and their further differentiation into mature blood cells. Dysregulation of these processes in hematopoietic precursor cells often leads to their abnormal differentiation and proliferation and, as a result, malignant transformation. The transcription factor TAL1 is one of the main regulators of hematopoiesis. It comprises a helix-loop-helix domain which binds to DNA through its regulatory regions, interacting with the E-box sequence (CANNTG, where N is any nucleotide), and GATA, Ets, and Runx factor binding sites [1]. It has been shown that inhibition of *TAL1* gene expression leads to a complete absence of hematopoiesis in the yolk sac [2]. In an adult organism, a mximum level of *TAL1* expression is characteristic of pluripotent HSCs, multipotent myeloid and lymphoid progenitors, as well as erythroid and megakaryocytic cells [3]. TAL1 participates in the formation of complexes with various transcription factors (E47/E2A, LMO2, GATA1–3, Ldb1/2, Ldb1, ETO2, Runx1, ERG, FLI1) [4, 5]. The composition of the complex may vary. The composition of the complex determines the intracellular targets it interacts with, activating or inhibiting the expression of the factors associated with differentiation of myeloid and lymphoid cells [6–8]. An abnormal expression level or mutations in genes whose translation products comprise the SCL complex can lead to malignant transformation of blood cells. Approximately 60% of cases of T-cell acute lymphoblastic leukemia (T-ALL) are characterized by an abnormally high level of *TAL1* expression [9]. Mutant forms of TAL1 in lymphoid and myeloid leukemia cells are diagnosed in 20% of patients [10]. The promoter portion of the *C-KIT* gene encoding the receptor tyrosine kinase is considered as one of the main TAL1 targets in malignant blood cells. In some cases, it has been shown that progression of malignant hematological diseases (including acute myeloid leukemia) is accompanied by an abnormally high expression of C-KIT [11, 12].

TAL1: GENE STRUCTURE, KNOWN ISOFORMS OF THE PROTEIN AND THEIR FUNCTION IN HEMATOPOIESIS

The *TAL1* gene locus is located on human chromosome 1. TAL1 belongs to the family of transcription factors that possess a helix-loop-helix (bHLH) motif.

The *TAL1* gene contains six exons, including the coding exons 4–6. According to the PubMed database as of 2017, six different transcripts of the *TAL1* gene have been described (*Fig. 1*). There are two isoforms to the TAL1 protein: a long (TAL1-l) one, with a molecular weight of 34.3 kDa and composed of 331 amino acid residues, and a short (TAL1-s) one, consisting of 156 amino acid residues. The TAL1-l to TAL1-s ratio differs in megacaryocyte-erythroid cells [13]. *TAL1* pre-mRNA is alternatively spliced, producing mRNA without the exons 1–4. The ETO2-binding domain and phosphorylation sites are absent in the TAL1-s protein translation product of this mRNA, while DNA-binding domains and the helix-loop-helix domain are maintained. Furthermore, the third exon of the *TAL1* comprises a highly conserved uORF sequence, an upstream open reading frame which acts as a *cis*-regulatory element in the formation of TAL1 isoforms. The presence of uORF enables the initiation of translation, involving the eIF2 and eIF4E factors from the alternative sites located in exons 4–5 [14], producing a truncated form of the TAL1 protein.

The truncated form TAL1-s is required for erythroid progenitors differentiation, while the full-length protein TAL1-l is required for megakaryocytic differentiation of progenitor cells. It has been shown that treatment of the human erythroid leukemia cell lines TF1 and HEL with erythroid differentiation inducers (DMSO and erythropoietin) produces not only the primary (full-length) form of the TAL1-l protein, but also a truncated TAL1-s form [15]. It has been established that some anticancer agents acting on the components of the signaling pathways involved in the regulation of translation initiation may affect the TAL1-l to TAL1-s ratio. In particular, rapamycin (Rap,mTOR inhibitor) blocks the formation of truncated forms, while 2-Aminopurine (2AP, eIF2α-kinase inhibitor) blocks the formation of full-length forms [14].

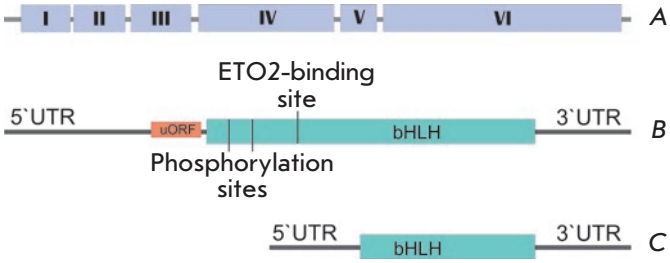

Fig. 1. a. The structure of TAL1 gene – I–VI exons b. Long TAL1 transcript variant. Long isoform TAL1-L and short isoform TAL1-S are translated from this mRNA. UTR – untranslated mRNA region. uORF – upstream open reading frame. bHLH – mRNA region encoding the helix-loop-helix domain. c. Short TAL1 transcript variant from which only the TAL1-S isoform is translated

TAL1 FUNCTIONS IN EMBRYOGENESIS

The TAL1 transcription factor is essential for normal embryogenesis. Its expression starts on the 7th day after fertilization, a day before the beginning of the development of circulatory system components. *TAL1* expression has been found in the blood islet cells of the yolk sac, endothelial cells, and angioblasts, and then in the liver and spleen of a fetus, the major hematopoietic organs in embryogenesis. It has been shown that the cells involved in the formation of skeletal and nervous tissues also express *TAL1* [16]. In the yolk sac and fetal liver, the *Runx1* gene promoter and *Runx3* gene enhancer are the major targets of TAL1 [17]. Ets, GATA, and the Runx factor binding sites, as well as a E-box sequence, have been found in the regulatory regions of these genes. TAL1 and its partners GATA1, GATA2, E47, Ldb1, and LMO2 may form complexes at these DNA sites [18]. Hematopoietic progenitor cells can also be derived from hemogenic endothelial cells, a process that involves the Runx1 transcription factor. TAL1 is required in order to produce hemogenic endothelial cells from mesoderm [19]. At later stages of embryonic development, TAL1 regulates the differentiation of hematopoietic progenitors into red blood cells, megakaryocytes, and platelets [20]. During embryogenesis, the cells that form blood vessels also express *TAL1* [16]. A lack of *TAL1* expression not only results in impaired hematopoiesis, but also in early embryonic death [2, 21]. It has been demonstrated in a murine model that embryonic stem cells (ESCs) not expressing *TAL1* are not differentiated into hematopoietic cells under the action of hematopoietic differentiation factors [21]. Ectopic expression of *TAL1* in ESCs induces the formation of hematopoietic cells. *In vitro* experiments have demonstrated that ESCs without *TAL1* expression are characterized by a low effectiveness of differentiation into erythroid progenitor cells and cannot form colonies of lymphoid and myeloid progenitor cells [22].

Thus, TAL1 directs the differentiation of hematopoietic progenitors at all three stages of hematopoiesis during embryonic development. TAL1 acts on blood progenitor cells in the yolk sac (the first stage of hematopoiesis), determines the development and differentiation of hemangioblasts from their aggregation in the primary strip until their migration into the hematopoietic islets of the yolk sac (the second stage of hematopoiesis). At the beginning of the third stage of hematopoiesis, TAL1 is required for hemangioblast differentiation in HSCs. It activates the expression of genes important for the maturation of erythroid, meg-

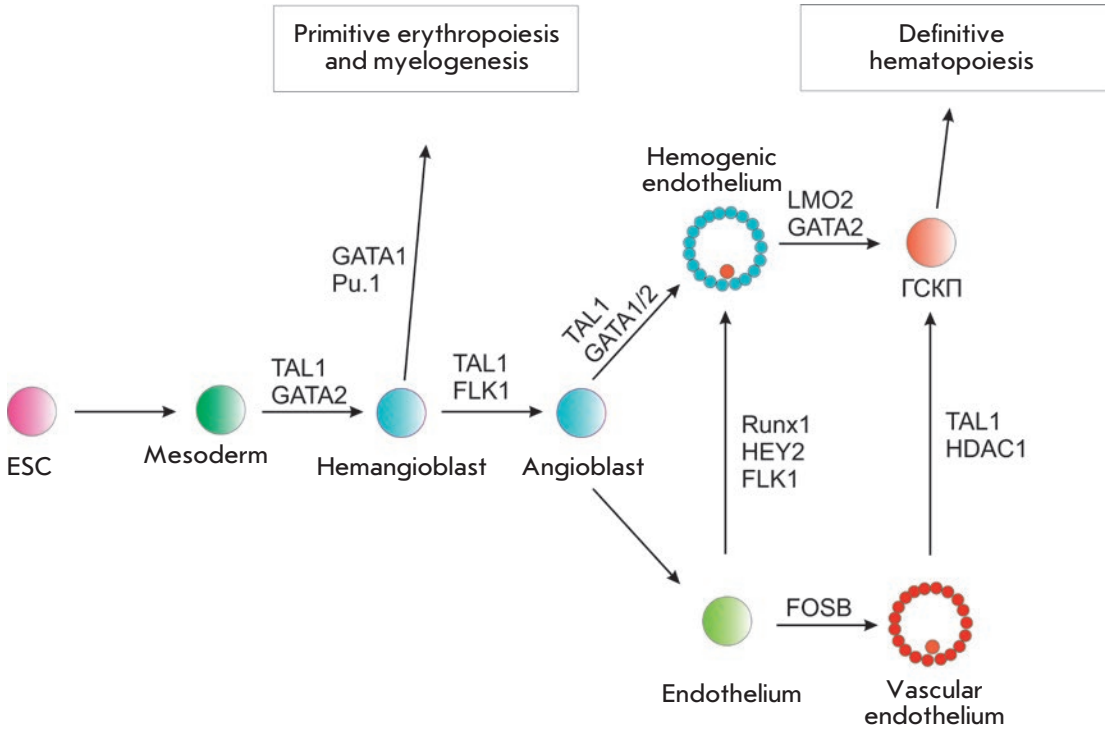

Fig. 2. The process of hematopoietic cell development during embryogenesis. Some transcription factors defining the differentiation direction are shown above the arrows. ESC – embryonic stem cell, HSCP – hematopoietic stem cell progenitor

acaryotic, and mast cells, and it is likewise involved in vascular system remodeling *(Fig. 2)* [23].

THE ROLE OF TAL1 IN THE REGULATION OF HEMATOPOIESIS

In adults, mature blood cells are derived from pluripotent HSCs. HSCs are retained in the bone marrow during replication quiescence stage G0, due to the interaction between their superficial cellular receptor protein (C-KIT, MPL, CXCR4) and the ligands on stromal cell surfaces [24, 25]. The pluripotent HSCs respond to hematopoietic stress by terminating the quiescent phase and initiating active proliferation, receiving signals for further differentiation, and leading to the appearance of myeloid and lymphoid progenitor cells. Some transcription factors essential to the hematopoiesis process are also the key factors in maintaining HSCs in the quiescent stage. These include the TAL1, E47, GATA2, and Ldb1, LMO2 components of the SCL complex [26]. Transformation of $KLS^+/CD150^+/CD48^+$ HSCs from the quiescent phase G0 to stage G1 is assisted by the cyclin-dependent kinase P21/CDKN1A. TAL1 blocks this transition, increasing the expression of the P21/CDKN1A inhibitor [27]. Simultaneously, TAL1 enhances the expression of the transcription factor ID1. Importantly, TAL1 does not belong to the proteins essential for the survival and self-renewal of HSCs [3]. Its related protein LYL1 supports HSC survival in the case of *TAL1* knockout [28]. Interestingly, TAL1 plays the opposite role in cord blood HSCs, where it, contrarily, activates G0–G1 transition, which is regulated using the mTOR signaling pathway [29]. However, TAL1 and LYL1 are not interchangeable in differentiation processes and both proteins are required for normal erythropoiesis and the formation of B-cells, respectively [30]. Unlike HSCs, TAL1 functions as a cell cycle activator in myeloid and lymphoid progenitors, inhibiting the expression of the cyclin-dependent kinase inhibitors p21 and p16/Ink4a [31, 32]. The hematopoietic transcription factors TAL1, GATA2, and LMO2, whose expression level differs in each cell type, regulate the process of blood cell differentiation and maturation *(Fig. 3)* [33]. The expression of *TAL1* is not identical in all hematopoietic cells. High expression levels of this gene have been detected in HSCs, in myeloid progenitors, and in some mature myeloid cells (megakaryocytes, erythrocytes, mast cells, and basophils). Low levels of TAL1 are characteristic of lymphoid progenitors, eosinophils, macrophages, and neutrophils [34–36]. Mature T- and B-cells do not express *TAL1* [37]. Certain genes specific to erythroid cells are activated by a complex formed by GATA1 and TAL1 [38].

An analysis of the ChIP-seq has shown that TAL1 controls both the processes common to all cells (cell cycle regulation, proliferation, apoptosis) and those specific only to erythroid cells (redox processes, heme

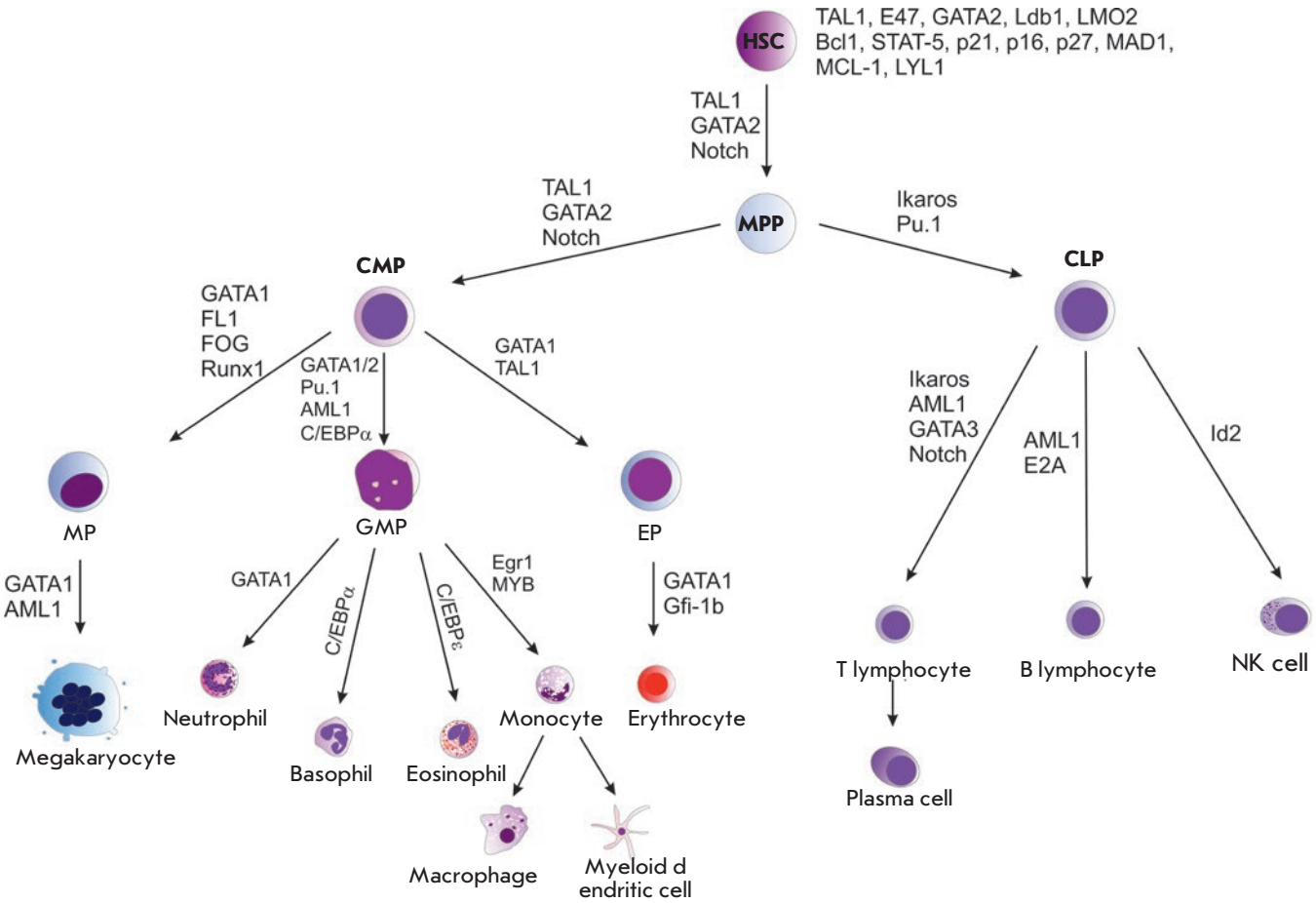

Fig. 3. Adult hematopoiesis scheme with some key transcriptional factors. HSC – hematopoietic stem cell, MPP – multipotential progenitor, CMP – common myeloid progenitor, CLP – common lymphoid progenitor, MP – megakaryocyte progenitor, EP – erythropoietin progenitor, EBP – eosinophil–basophil progenitor

biosynthesis, organization of the cytoskeleton), which is indirectly indicative of its multifunctionality [39]. In myeloid and lymphoid progenitor cells, the genes that control proliferation and apoptosis play the role of TAL1 targets. Additionally, the pattern of TAL1 binding to target genes widely varies with cell maturation. The dynamic changes in *TAL1* expression suggest that the TAL1 factor demonstrates differing activity in cells during the initial choice of differentiation direction and formation of mature blood cells, while its multifunctionality is directly related to its ability to form multicomponent complexes in the regulatory regions of target genes [8]. There is evidence that the role of TAL1 in the differentiation of erythroid cells is effected, among others, using caspase-3, inducing cleavage of this protein. It has been shown that its activity eventually leads to a decrease in the expression of *GATA1* and *BCL-XL*, thereby inducing apoptosis in these cells [40]. Some amino acid residues of TAL1 may undergo phosphorylation. For example, in erythrocytes, Akt kinase phosphorylates Thr 90 in TAL1. This modification reduces the ability of TAL1 to repress the *EPB42* gene promoter, whose product, the 4.2 protein, is required to build the erythrocyte cytoskeleton [41]. The Ser172 residue may also be phosphorylated by the cAMP-dependent protein kinase (PKA), which affects TAL1 binding to the E-box in the regulatory sites of various genes [42].

SCL-COMPLEX: ITS COMPONENTS AND TARGETS IN NORMAL HEMOPOIESIS

The proteins involved in normal hematopoiesis (LMO2, Ldb1–2, Gata1–3, Lyl–1, E2A/HEB, Runx1, ETO2, ERG, FL1) are the main partners of TAL1 in hematopoietic cells (*Fig. 4*). TAL1 directly binds to the LIM-domain of the LMO2 protein, which, in turn, interacts with Ldb1. LMO2 has no DNA-binding domain and acts as a bridge factor, which complexes TAL1 with oth-

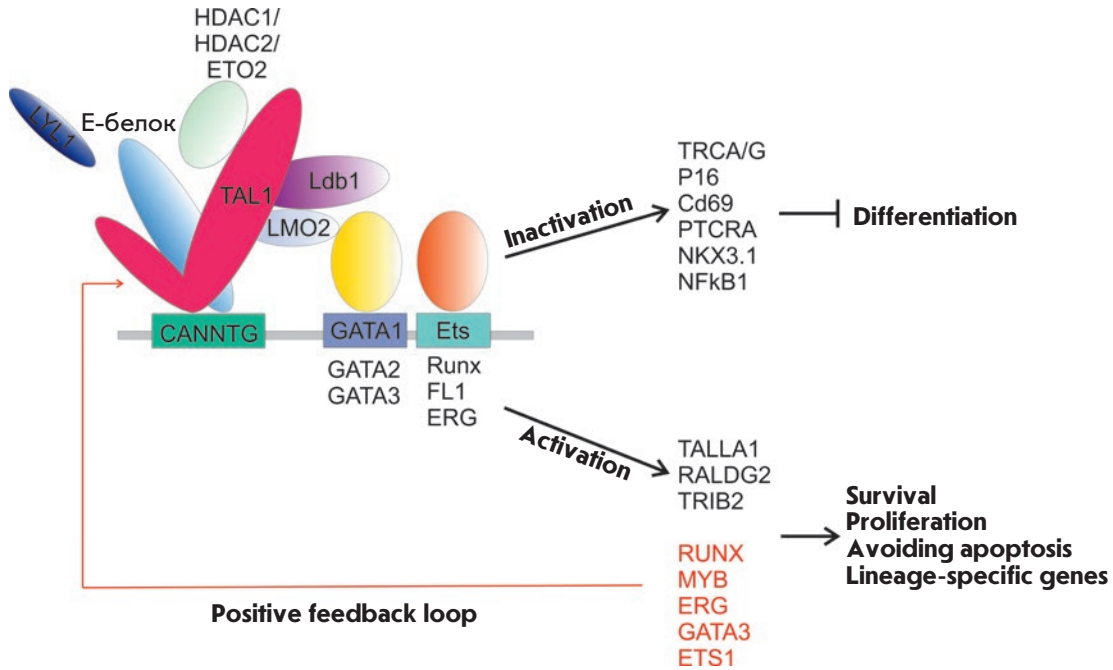

Fig. 4. TAL1 and its partners involved in the differentiation, proliferation, and survival of hematopoietic cells

er transcription factors in hematopoietic cells [43, 44]. It may also form an extended complex, binding ETO2, RUNX1, ERG, or FLI1 [45]. E-proteins (E12, E47), containing helix-loop-helix domains, are required for TAL1 binding to the E-box sequences (CANNTG) in the regulatory regions of genomic DNA. In the complex, TAL1 regulates the activity of certain signaling pathways during the differentiation of hematopoietic cells. For example, TAL1 is essential for the survival of hematopoietic precursors cultured in the presence of SCF, a ligand of the receptor tyrosine kinase C-KIT, which plays an important role in hematopoiesis [46]. The main role of the SCL complex in C-KIT regulation is associated with its ability to bind the promoter of this gene. It has also been established thatcomponents of the SCL complex may bind to various components of the C-KIT signaling pathway and change its activity [46–51].

Furthermore, there is a direct correlation between the level of *TAL1* expression and phosphorylated forms of MEK and ERK1/2 kinases, the components of the MEK/ERK signaling pathway [40]. In hematopoietic cells, the activity of MEK and ERK1/2 kinases is associated with the differentiation of myeloid, erythroid, and megakaryocytic hematopoietic cells [52]. TAL1 probably participates in the differentiation of $CD34^+$ hematopoietic cells through the MEK/ERK signals [52, 53].

THE FUNCTIONS OF THE SCL COMPLEX AND ITS INDIVIDUAL COMPONENTS IN CARCINOGENESIS

As noted above, the normal level of *TAL1* expression in lymphoid cells is much lower than that in myeloid ones [37]. Enhanced expression of *TAL1* in T-cells often leads to their malignant transformation. Abnormally high expression of *TAL1* can result from chromosomal rearrangements, deletions, and mutations affecting the gene [54]. The chromosomal translocation t (1; 14) (p32; q11) was found in 3% of cases of T-cell leukemia. The chromosomal translocation t (1; 14) (p32; q11), leading to the formation of the TRA/TAL1 fusion gene, was detected in 3% of cases of T-cell leukemia. Deletion of 90 bps between the 5`-noncoding region of the *TAL1* gene and *SIL* gene results in the formation of a *SIL-TAL1* fusion gene controlled by the *SIL* gene promoter [54]. The expression level of *SIL* in T-cells is normally very high, and, therefore, this translocation results in a high expression of the *SIL-TAL1* fusion gene [55]. This deletion has been detected in 20–25% of patients with T-ALL [54, 56, 57]. However, in most TAL1-positive cases of T-cell leukemia, an abnormally high expression of *TAL1* is effected without the participation of chromosomal rearrangements. Along with a high expression of *TAL1*, significant expression levels of *TLX1* and *LMO2* were detected in most primary T-ALL samples [58]. Increased activity of *TAL1* in T-cells results in an increased lifetime for lymphoid cells in the form of immature thymocytes. It is assumed that this can be considered as an event initiating the development of T-cell leukemia [59].

In T-ALL cells, TAL1 preferably binds to CAGGTG E-box sequences. Although GATA1–3 factors often serve as intermediaries in TAL1 binding to the regulatory sites of DNA in T-cell leukemia cells, there are alternative binding sites, in particular Runx and Ets [59].

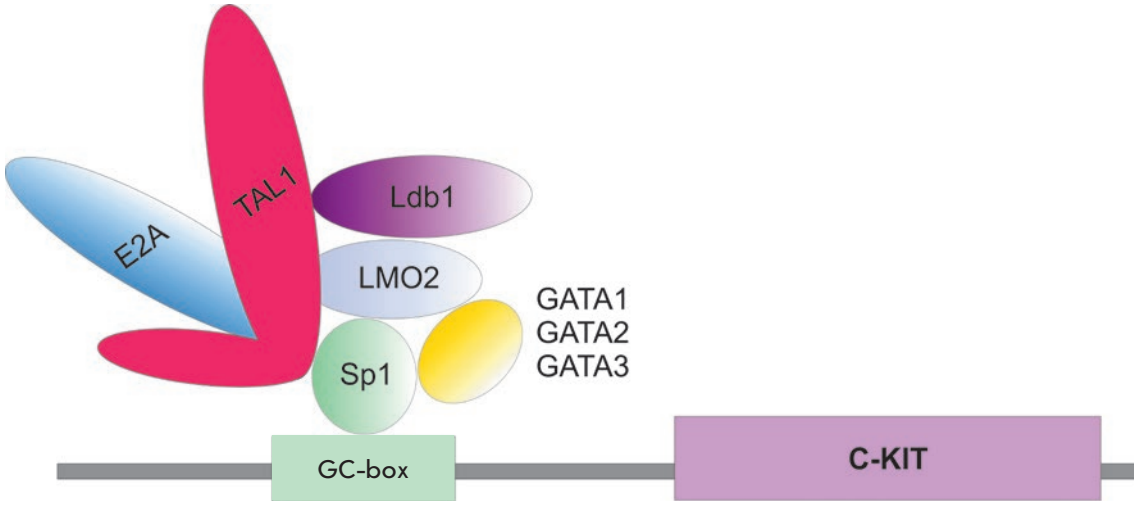

Fig. 5. The structure of the SCL complex in the promoter region of the receptor tyrosine kinase *C-KIT* gene

It has been shown that the TAL1 transcription factor directly activates the expression of *Runx1*, *Ets1,* and *GATA3* in the blast cells of patients with T-ALL [60]. Furthermore, the GATA3 and Runx1 factors enhance the expression of the *TAL1* gene, which may indicate the need for a positive feedback loop for the abnormal expression of the factors involved in blood cell malignant transformation. In 45% of cases of TAL1-positive leukemia, LMO1 and LMO2 mutant proteins formed due to chromosomal rearrangements of their encoding genes were detected [61]. Expression of all these factors leads to the fact that double negative (CD4-CD8-) preleukemic thymocytes become capable of division. Additionally, the Notch signaling pathway, whose components are involved in the accumulation of mutations and impairment of differentiation processes, is often activated in these cells. This leads to initiation and progression of T-cell leukemia [62]. In the case of malignant transformation , TAL1 is often involved in the abnormal transcription of various genes. In this case, as in normal hematopoiesis, it forms complexes with the hematopoietic factors LMO2, Ldb1, and E12/E47 [46,47]. It has been established that overexpression of TAL1 and LMO2 is often observed in T-ALL cells. Normally, LMO2 and TAL1 independently regulate the transcription of their own target genes, but they cooperatively disrupt the functioning of the E2A factor in T-ALL cells, which contributes to the development of leukemia [63, 64]. It has been shown that the transcription factor FOXP3 can act as a tumor suppressor in T-cell leukemia. It binds to LMO2 and reduces the likelihood of it interacting with TAL1, resulting in reduced transcriptional activity of the TAL1/LMO2 complex [65].

C-KIT receptor tyrosine kinase is one of the main targets of TAL1 [48, 66]. Hematopoietic progenitor cells are characterized by a high expression level of *TAL1* and *C-KIT*. It has been shown that ectopic expression of *TAL1* results in the induction of *C-KIT* expression in B-lymphocytes, which normally do not express these genes [66]. Some hematological malignancies, including acute myeloid leukemia and chronic myeloid leukemia, are associated with an abnormally high expression of *C-KIT*. The SCL complex acts as a specific activator receptor tyrosine kinase *C-KIT* gene promoter *(Fig.*5). All the components of the complex (TAL1, LMO2, Ldb1, GATA2, E47) are required for it to function at its maximum. Studies in a murine embryonic fibroblast model have shown that the transcription factors E47 and GATA, taken alone, do not affect the activity of the *C-KIT* gene promoter despite the fact that they activate the transcription of many genes in human hematopoietic cells [66]. The same murine system was used to show that the promoter is only activated in the case of formation of a multicomponent complex whose main component is TAL1. GATA1 and GATA2 are interchangeable: however, the complex comprising GATA1 possess a lower transcriptional activity. The Sp1 protein, comprising zinc fingers and binding GC-rich sequences, is also required to form the active SCL-protein complex. It has been shown that removal of E-box and GATA from the promoter region of *C-KIT* does not reduce the activating activity of the SCL complex. Probably, Sp1 is also involved in attracting complex components to certain target genes.

CLINICAL SIGNIFICANCE OF TAL1

The extensive body of evidence of TAL1 participation in the development of T-cell leukemia suggests that inhibitors of this protein, as well as inhibitors of the associated signaling cascades, can be used as promising therapeutic agents to treat leukemia characterized by an abnormal activity of TAL1. At the moment, novel

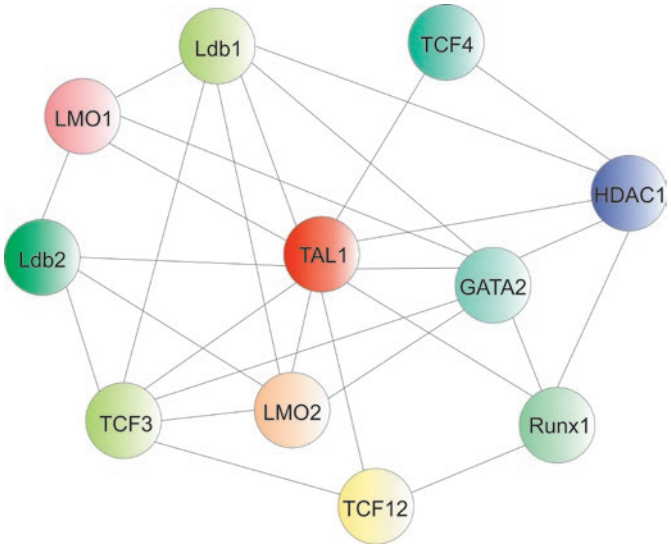

Fic. 6. Possible partners of TAL1 and their interactions in normal and malignant hematopoietic cells

low-molecular-weight inhibitors of TAL1 are being developed and synthesized in many laboratories. However, sufficiently strong and specific inhibitors of this protein have not been achieved so far. Phosphorylation of TAL1 with MEK/ERK kinases is required to effect its transcriptional activity. The prospects of using the inhibitors of MAPK/MEK/ERK signaling pathway components as potential therapeutic targets are being discussed [67]. At the same time, there is evidence that treatment of a mesenchymal stromal cell culture (stromal components of the bone marrow) with MEK inhibitors results in the secretion of proinflammatory cytokine interleukin-18 by these cells [68]. This improves the survival chances of T-ALL blast cells. The potential TAL1 protein targets associated with the implementation of its transcriptional activity are considered as promising targets for the therapy of TAL1-associated T-cell leukemia *(Fig. 6)*. These proteins include UTX demethylase (also known as KDM6A). It has been shown that treatment of TAL1-positive blast cells with the T-ALL UTX inhibitor reduces the rate of their proliferation and stimulates apoptosis [69]. It has been determined that the use of HDAC histone deacetylase inhibitors leads to a decrease in *TAL1* expression and induces the apoptosis of blast cells of T-cell leukemia [70]. At the moment, the stoichiometry of the SCL complex is being actively explored. The results of such studies are expected to open up new possibilities for the development of highly effective therapeutic agents targeting TAL1-positive leukemia, which could act by interfering with the protein-protein interactions between the components of the SCL complex but not affect the viability of normal hematopoietic cells [41]. ●

This study was carried out as a part of the Program for Basic Research of the State Academies of Sciences in 2013–2020 (topic No 01201363823) and supported by the Russian Science Foundation (Project No 14-50-00060).

REFERENCES

1. Hoang T., Lambert J.A., Martin R. // Curr. Top. Dev. Biol. 2016. V. 118. P. 163–204.
2. Robb L., Lyons I., Li R., Hartley L., Kontgen F., Harvey R.P., Metcalf D., Begley C.G. // Proc. Natl. Acad. Sci. USA. 1995. V. 92. № 15. P. 7075–7079.
3. Mikkola H.K., Klintman J., Yang H., Hock H., Schlaeger T.M., Fujiwara Y., Orkin S.H. // Nature. 2003. V. 421. № 6922. P. 547–551.
4. Lécuyer E., Hoang T. // Exp. Hematol. 2004. V. 32. № 1. P. 11–24.
5. Goardon N., Lambert J.A., Rodriguez P., Nissaire P., Herblot S., Thibault P., Dumenil D., Strouboulis J., Romeo P.H., Hoang T. // EMBO J. 2006. V. 25. № 2. P. 357–366.
6. Anderson K.P., Crable S.C., Lingrel J.B. // J. Biol. Chem. 1998. V. 273. № 23. P. 14347–14354.
7. Org T., Duan D., Ferrari R., Montel-Hagen A., van Handel B., Kerenyi M.A., Sasidharan R., Rubbi L., Fujiwara Y., Pellegrini M., et al. // EMBO J. 2015. V. 34. № 6. P. 759–777.
8. Wu W., Morrissey C.S., Keller C.A., Mishra T., Pimkin M., Blobel G.A., Weiss M.J., Hardison R.C. // Genome Res. 2014. V. 24. № 12. P. 1945–1962.
9. Ferrando A.A., Neuberg D.S., Staunton J., Loh M.L., Huard C., Raimondi S.C., Behm F.G., Pui C.H., Downing J.R., Gilliland D.G., et al. // Cancer Cell. 2002. V. 1. № 1. P. 75–87.
10. Begley C.G., Aplan P.D., Davey M.P., Nakahara K., Tchorz K., Kurtzberg J., Hershfield M.S., Haynes B.F., Cohen D.I., Waldmann T.A., et al. // Proc. Natl. Acad. Sci. USA. 1989. V. 86. № 6. P. 2031–2035.
11. Spirin P.V., Lebedev T.D., Orlova N.N., Gornostaeva A.S., Prokofjeva M.M., Nikitenko N.A., Dmitriev S.E., Buzdin A.A., Borisov N.M., Aliper A.M., et al. // Leukemia. 2014. V. 28. № 11. P. 2222–2228.
12. Orlova N.N., Lebedev T.D., Spirin P.V., Prassolov V.S. // Molec. Biol. 2016. V. 50. № 3. P. 344–352.
13. Jin S., Su H., Tran N.T., Song J., Lu S.S., Li Y., Huang S., Abdel-Wahab O., Liu Y., Zhao X. // PLoS One. 2017. V. 12. № 5. P. e0175523.
14. Calkhoven C.F., Muller C., Martin R., Krosl G., Pietsch H., Hoang T., Leutz A. // Genes Dev. 2003. V. 17. № 8. P. 959–964.
15. Zhen F., Lan Y., Yan B., Zhang W., Wen Z. // Development. 2013. V. 140. № 19. P. 3977–3985.
16. Kallianpur A.R., Jordan J.E., Brandt S.J. // Blood. 1994. V. 83. № 5. P. 1200–1208.

17. Landry J.R., Kinston S., Knezevic K., de Bruijn M.F., Wilson N., Nottingham W.T., Peitz M., Edenhofer F., Pimanda J.E., Ottersbach K., et al. // Blood. 2008. V. 111. № 6. P. 3005–3014.
18. Real P.J., Ligero G., Ayllon V., Ramos-Mejia V., Bueno C., Gutierrez-Aranda I., Navarro-Montero O., Lako M., Menendez P. // Mol. Ther. 2012. V. 20. № 7. P. 1443–1453.
19. Lancrin C., Sroczynska P., Stephenson C., Allen T., Kouskoff V., Lacaud G. // Nature. 2009. V. 457. № 7231. P. 892–895.
20. Toscano M.G., Navarro-Montero O., Ayllon V., Ramos-Mejia V., Guerrero-Carreno X., Bueno C., Romero T., Lamolda M., Cobo M., Martin F., et al. // Mol. Ther. 2015. V. 23. № 1. P. 158–170.
21. Shivdasani R.A., Mayer E.L., Orkin S.H. // Nature. 1995. V. 373. № 6513. P. 432–434.
22. Robertson S.M., Kennedy M., Shannon J.M., Keller G. // Development. 2000. V. 127. № 11. P. 2447–2459.
23. Porcher C., Chagraoui H., Kristiansen M.S. // Blood. 2017. V. 129. № 15. P. 2051–2060.
24. Curtis D.J., Hall M.A., van Stekelenburg L.J., Robb L., Jane S.M., Begley C.G. // Blood. 2004. V. 103. № 9. P. 3342–3348.
25. Gottgens B., Nastos A., Kinston S., Piltz S., Delabesse E.C., Stanley M., Sanchez M.J., Ciau-Uitz A., Patient R., Green A.R. // EMBO J. 2002. V. 21. № 12. P. 3039–3050.
26. Zhang Y., Payne K.J., Zhu Y., Price M.A., Parrish Y.K., Zielinska E., Barsky L.W., Crooks G.M. // Stem Cells. 2005. V. 23. № 6. P. 852–860.
27. Lacombe J., Herblot S., Rojas-Sutterlin S., Haman A., Barakat S., Iscove N.N., Sauvageau G., Hoang T. // Blood. 2010. V. 115. № 4. P. 792–803.
28. Capron C., Lecluse Y., Kaushik A.L., Foudi A., Lacout C., Sekkai D., Godin I., Albagli O., Poullion I., Svinartchouk F., et al. // Blood. 2006. V. 107. № 12. P. 4678–4686.
29. Benyoucef A., Calvo J., Renou L., Arcangeli M.L., van den Heuvel A., Amsellem S., Mehrpour M., Larghero J., Soler E., Naguibneva I., et al. // Stem Cells. 2015. V. 33. № 7. P. 2268–2279.
30. Souroullas G.P., Salmon J.M., Sablitzky F., Curtis D.J., Goodell M.A. // Cell Stem Cell. 2009. V. 4. № 2. P. 180–186.
31. Chagraoui H., Kassouf M., Banerjee S., Goardon N., Clark K., Atzberger A., Pearce A.C., Skoda R.C., Ferguson D.J., Watson S.P., et al. // Blood. 2011. V. 118. № 3. P. 723–735
32. Dey S., Curtis D.J., Jane S.M., Brandt S.J. // Mol. Cell. Biol. 2010. V. 30. № 9. P. 2181–2192.
33. Zhu J., Emerson S.G. // Oncogene. 2002. V. 21. № 21. P. 3295–3313.
34. Akashi K., Traver D., Miyamoto T., Weissman I.L. // Nature. 2000. V. 404. P. 193–197.
35. Green A.R., Salvaris E., Begley C.G. // Oncogene. 1991. V. 6. № 3. P. 475–459.
36. Hall M.A., Curtis D.J., Metcalf D., Elefanty A.G., Sourris K., Robb L., Gothert J.R., Jane S.M., Begley C.G. // Proc. Natl. Acad. Sci. USA. 2003. V. 100. № 3. P. 992–997.
37. Mouthon M.A., Bernard O., Mitjavila M.T., Romeo P.H., Vainchenker W., Mathieu-Mahul D. // Blood. 1993. V. 81. № 3. P. 647–655.
38. Moignard V., Macaulay I.C., Swiers G., Buettner F., Schutte J., Calero-Nieto F.J., Kinston S., Joshi A., Hannah R., Theis F.J., et al. // Nat. Cell Biol. 2013. V. 15. № 4. P. 363–372.
39. Kassouf M.T., Hughes J.R., Taylor S., McGowan S.J., Soneji S., Green A.L., Vyas P., Porcher C. // Genome Res. 2010. V. 20. № 8. P. 1064–1083.
40. Zhou R.Q., Wu J.H., Gong Y.P., Guo Y., Xing H.Y. // Blood Cells Mol. Dis. 2014. V. 53. P. 39–46.
41. Palamarchuk A., Efanov A., Maximov V., Aqeilan R.I., Croce C.M., Pekarsky Y. // Cancer Res. 2005. V. 65. № 11. P. 4515–4519.
42. Prasad K.S., Brandt S.J. // J. Biol. Chem. 1997. V. 272. № 17. P. 11457–11462.
43. Wadman I.A., Osada H., Grutz G.G., Agulnick A.D., Westphal H., Forster A., Rabbitts T.H. // EMBO J. 1997. V. 16. № 11. P. 3145–3157.
44. Osada H., Grutz G.G., Axelson H., Forster A., Rabbitts T.H. // Leukemia. 1997. V. 11. P. 307–312.
45. Schuh A.H., Tipping A.J., Clark A.J., Hamlett I., Guyot B., Iborra F.J., Rodriguez P., Strouboulis J., Enver T., Vyas P., et al. // Mol. Cell. Biol. 2005. V. 25. № 23. P. 10235–10250.
46. Krosl G., He G., Lefrancois M., Charron F., Romeo P.H., Jolicoeur P., Kirsch I.R., Nemer M., Hoang T. // J. Exp. Med. 1998. V. 188. № 3. P. 439–450.
47. Rojas-Sutterlin S., Lecuyer E., Hoang T. // Curr. Opin. Hematol. 2014. V. 21. № 4. P. 256–264.
48. Lacombe J., Krosl G., Tremblay M., Gerby B., Martin R., Aplan P.D., Lemieux S., Hoang T. // Blood. 2013. V. 122. № 7. P. 1150–1161.
49. Cheng J.T., Cobb M.H., Baer R. // Mol. Cell. Biol. 1993. V. 13. № 2. P. 801–808.
50. Tang T., Prasad K.S., Koury M.J., Brandt S.J. // Biochem. J. 1999. V. 343. P. 615–620.
51. Tang T., Arbiser J.L., Brandt S.J. // J. Biol. Chem. 2002. V. 277. № 21. P. 18365–18372.
52. Bugarski D., Krstic A., Mojsilovic S., Vlaski M., Petakov M., Jovcic G., Stojanovic N., Milenkovic P. // Exp. Biol. Med. (Maywood). 2007. V. 232. № 1. P. 156–163.
53. Zeuner A., Eramo A., Testa U., Felli N., Pelosi E., Mariani G., Srinivasula S.M., Alnemri E.S., Condorelli G., Peschle C., et al. // Cell Death Differ. 2003. V. 10. № 8. P. 905–913.
54. Liu Y., Easton J., Shao Y., Maciaszek J., Wang Z., Wilkinson M.R., McCastlain K., Edmonson M., Pounds S.B., Shi L., et al. // Nat. Genet. 2017. V. 49. № 8. P. 1211–1218.
55. Chen Q., Cheng J.T., Tasi L.H., Schneider N., Buchanan G., Carroll A., Crist W., Ozanne B., Siciliano M.J., Baer R. // EMBO J. 1990. V. 9. № 2. P. 415–424.
56. Correia N.C., Arcangeli M.L., Pflumio F., Barata J.T. // Leukemia. 2016. V. 30. № 10. P. 1968–1978.
57. Begley C.G., Green A.R. // Blood. 1999. V. 93. № 9. P. 2760–2770.
58. Sayitoglu M., Erbilgin Y., Hatirnaz Ng O., Yildiz I., Celkan T., Anak S., Devecioglu O., Aydogan G., Karaman S., Sarper N., et al. // Turk. J. Haematol. 2012. V. 29. № 4. P. 325–333.
59. Zhou Y., Kurukuti S., Saffrey P., Vukovic M., Michie A.M., Strogantsev R., West A.G., Vetrie D. // Blood. 2013. V. 122. № 26. P. 4199–4209.
60. Liau W.S., Ngoc P.C., Sanda T. // Adv. Exp. Med. Biol. 2017. V. 962. P. 139–147.
61. Palii C.G., Perez-Iratxeta C., Yao Z., Cao Y., Dai F., Davison J., Atkins H., Allan D., Dilworth F.J., Gentleman R., et al. // EMBO J. 2011. V. 30. № 3. P. 494–509.
62. Aplan P.D., Jones C.A., Chervinsky D.S., Zhao X., Ellsworth M., Wu C., McGuire E.A., Gross K.W. // EMBO J. 1997. V. 16. № 9. P. 2408–2419.
63. Ryan D.P., Duncan J.L., Lee C., Kuchel P.W., Matthews J.M. // Proteins. 2008. V. 70. № 4. P. 1461–1474.
64. Patterson L.J., Gering M., Eckfeldt C.E., Green A.R., Verfaillie C.M., Ekker S.C., Patient R. // Blood. 2007. V. 109. № 6. P. 2389–2398.
65. Fleskens V., Mokry M., van der Leun A.M., Huppel-

schoten S., Pals C.E., Peeters J., Coenen S., Cardoso B.A., Barata J.T., van Loosdregt J., et al. // Oncogene. 2016. V. 35. № 31. P. 4141–4148.
66. Lecuyer E., Herblot S., Saint-Denis M., Martin R., Begley C.G., Porcher C., Orkin S.H., Hoang T. // Blood. 2002. V. 100. № 7. P. 2430–2440.
67. Spirin P., Lebedev T., Orlova N., Morozov A., Poymenova N., Dmitriev S.E., Buzdin A., Stocking C., Kovalchuk O., Prassolov V. // Oncotarget. 2017. V. 8. № 34. P. 56991–57002.
68. Uzan B., Poglio S., Gerby B., Wu C.L., Gross J., Armstrong F., Calvo J., Cahu X., Deswarte C., Dumont F., et al. // EMBO Mol. Med. 2014. V. 6. № 6. P. 821–834.
69. Benyoucef A., Palii C.G., Wang C., Porter C.J., Chu A., Dai F., Tremblay V., Rakopoulos P., Singh K., Huang S., et al. // Genes Devel. 2016. V. 30. № 5. P. 508–521.
70. Cardoso B.A., de Almeida S.F., Laranjeira A.B., Carmo-Fonseca M., Yunes J.A., Coffer P.J., Barata J.T. // Leukemia. 2011. V. 25. № 10. P. 1578–1586.

Pathogenesis of Type 1 Diabetes Mellitus and Rodent Experimental Models

I. G. Gvazava[1,2*], O. S. Rogovaya[1,2], M. A. Borisov[1,2], E. A. Vorotelyak[1,2,3], A. V. Vasiliev[1,3]
[1]Koltsov Institute of Developmental Biology, Russian Academy of Sciences, Vavilova Str. 26, Moscow, 119334, Russia
[2]Pirogov Russian National Research Medical University, Ministry of Health of the Russian Federation, Ostrovitianov Str. 1–9, Moscow, 117997, Russia
[3]Lomonosov Moscow State University, Faculty of Biology, Leninskiye Gory 1–12, Moscow, 119234, Russia
*E-mail: gvazava.inessa@yandex.ru
Received May 25, 2017; in final form October 26, 2017

ABSTRACT **The global prevalence of diabetes mellitus and its severe complications is on the rise. The study of the pathogenesis of the onset and the progression of complications related to the disease, as well as the search for new therapeutic agents and methods of treatment, remains relevant. Experimental models are extremely important in the study of diabetes. This survey contains a synthesis of the most commonly used experimental animal models described in scientific literature. The mechanisms of the streptozotocin model are also analyzed and discussed, as it is considered as the most adequate and easily reproducible diabetes model. A review of the significant advantages and disadvantages of the described models has also been conducted.**
KEYWORDS **beta-cells, diabetes, experimental laboratory animals, hyperglycemia, Langerhans islets, pathogenesis, streptozotocin.**
ABBREVIATIONS **T1DM – type 1 diabetes mellitus; STZ – streptozotocin; β-cells – beta-cells.**

INTRODUCTION

Diabetes mellitus (DM) is currently one of the leading pathologies among the so-called diseases of civilization in terms of its high rates of incidence, disability, and mortality. According to the most recent data, there were 382 million people suffering from diabetes in the world in 2013, and the number of such patients is estimated to reach 592 million by 2035; i.e. an increase of 55% [1]. DM is a chronic condition characterized by a relative or absolute lack of insulin, which leads to hyperglycemia. Chronic hyperglycemia promotes the development of various complications, such as neuropathy, nephropathy, and retinopathy, and it also increases the risk of cardiovascular diseases. According to current classification, there are two main types of DM with numerous clinical, immunological, and genetic differences. Predisposition to DM is related to several groups of genes. It should be noted that the disease's development is associated with certain alleles of the genes of the major histocompatibility complex (MHC) class II system. Aside from genetic factors, the genesis of diabetes mellitus involves environmental factors; thus the reference to this pathology as a multifactorial disease [2].

T1DM is an autoimmune disease associated with the destruction of the insulin-producing β-cells of the pancreas. T1DM is most often diagnosed amongst children and young people, and the production of endogenous insulin in patients is significantly down by the time of the diagnosis; therefore, regular insulin injections and continuous monitoring of blood glucose are necessary to reduce the risk of hyperglycemia. The most popular theory of T1DM pathogenesis was proposed by G.S. Eisenbarth [3]. According to this theory, T1DM develops in genetically predisposed individuals. Autoimmune processes in T1DM are triggered by environmental factors. The initial stage of T1DM – death of islet cells – is asymptomatic but can be detected by autoantibody tests. The clinical signs appear only at the latest stages, when most β-cells are dead, and absolute insulin deficiency develops [3, 4]. Initially, the genetics of T1DM were considered to be relatively simple. The presence of certain alleles of the HLA system genes was believed to lead to an almost complete dominance of the disease [5].

To date, there are more than 20 loci and 100 candidate genes that affect, to varying degrees, the development of T1DM [6]. However, the wide prevalence of

this disease and the absence of significant correlations with genetic abnormalities suggest that people genetically not predisposed to the disease can also develop T1DM. For example, 85–90% of T1DM cases have been shown to occur in families without a primary history of T1DM in first-line relatives. V. Hyttinen and co-authors believe that the genetic predisposition amounts to about 30% [7].

The modern theory of T1DM pathogenesis proposed by M.A. Atkinson and G.S. Eisenbarth suggests that the disease's development is facilitated or impeded by interactions among genes, rather than by a genetic predisposition [8]. In addition, these genes are believed to affect susceptibility and resistance to T1DM not only in the period preceding the induction of an autoimmune reaction, but also during the entire period preceding the disease.

T1DM symptoms are believed to manifest themselves usually when 90–95% of β-cells die [4]. However, there are many variations in this regard. In addition, the phenomenon of β-cell loss is not yet completely understood. The severity of this phenomenon is supposed to vary significantly depending on the type of insulitis, extent of β-cell death, and the β-cell ability to regenerate [9].

At present, there is no clear understanding of the mechanism of the autoimmune reaction that precedes the destruction of β-cells, in particular β-cell response to autoimmune antibodies.

According to modern concepts of T1DM pathogenesis, β-cells can die as a result of various pathological processes. One of these is the destruction or necrosis of β-cells, and another is apoptosis or genetically programmed cell death [10]. β-Cells undergo necrosis in the presence of an excessive amount of free radicals (oxygen radicals or nitric oxide) or under the action of pro-inflammatory cytokines [3, 11].

In recent years, the processes of necrosis and apoptosis have been demonstrated not to antagonize each other. Cytokines play an important role in the cell death process. Cytokines, such as IFN and IL-2, are considered triggers of insulitis, which are capable of activating a mechanism of signaling leading to the death of pancreatic β-cells [11].

Like all endocrine disorders, DM is a rather complex disease that involves various body systems. Despite the tremendous progress achieved in molecular genetics research, the issues of prevention and pathogenetic treatment of diabetes are yet to be developed to an adequate level. The main tool used in pathophysiology today is research conducted on experimental models; in this case, the choice of a model and its etiological and pathogenetic conformity to a human disease underlies not only the success of any theoretical study, but also the development of prevention and treatment modalities. Experimental models of DM provide valuable information for understanding the mechanism that underlies the antidiabetic action of various agents, which is necessary for their targeted use. To date, a variety of experimental DM models have been developed [12–16]. Objective assessment of the advantages and disadvantages of each model, in accordance with the target goal, is important to avoid erroneous results.

For more than 50 years, the only model of experimental diabetes mellitus has been diabetes induced by removal of the pancreas. The quantity of preserved pancreatic tissue is of paramount importance for the development of diabetic impairments in the postoperative period. Depending on this factor, diabetes can develop between a period of several hours (complete removal) and 9 months (removal of 80% of the organ). Subtotal pancreatectomy is often used to model chronic diabetes with a prolonged high blood glucose level. The main cause behind diabetes in this case is insulin deficiency: i.e., absolute insulin insufficiency. The use of this model at the first stage of experimental diabetology development enabled researchers to understand many aspects of the mechanisms of insulin action, the metabolic changes related to insulin deficiency, and the pathogenesis of diabetes-associated disorders. However, a number of the causes that complicate the use of operative removal of the pancreas have stimulated a search for new models. The emergence of non-operative models of DM sharply reduced the use of the previous method. In recent years, that method has been used in some cases to study the mechanism of action of natural compounds on insulin resistance and insulin secretion in various animals: rats, guinea pigs, and dogs. The effects of glucose uptake in various tissues upon removal of 90% of the pancreas and the significant hypoinsulinemia associated with subtotal resection of the organ, followed by additional resection, were studied [17, 18].

This review analyzes existing experimental models in an effort to identify the most adequate and widely used animal model of T1DM.

The main feature of type 1 diabetes mellitus is the autoimmune destruction of pancreatic β-cells, which leads to insufficient insulin production. Insufficient insulin production in animal models is caused by the action of many different mechanisms, ranging from chemical ablation of β-cells to the spontaneous development of autoimmune diabetes.

Genetic and non-genetic experimental models are used depending on the task at hand. Over recent years, the progress achieved in genetic engineering has resulted in the generation of many animals with genetically determined development of diabetes mellitus.

SPONTANEOUS AUTOIMMUNE MODELS OF TYPE 1 DIABETES MELLITUS

In 1974, the so-called Non-Obese Diabetic (*NOD*) mouse strain was generated in Japan. These mice, along with other rodents such as *AKITA* mice, biobreeding (*BB*) rats, *LEW.1AR1* rats, etc., are characterized by the ability to spontaneously develop autoimmune diabetes [16, 19, 20]. The spontaneous development of diabetes is likely associated with a genetic mutation affecting the selection of T-lymphocytes and leading to the impairment of the mechanisms of autotolerance control. *NOD* mice whose immunological characteristics are similar to those of insulin-dependent T1DM in humans have been routinely used as models of spontaneous autoimmune type 1 diabetes mellitus for the last 25 years [21–26]. These mice develop insulitis 3–4 weeks after birth. At this pre-diabetic stage, pancreatic islets are primarily infiltrated with CD4+ and CD8+ lymphocytes [27]. Insulitis causes the destruction of β-cells, but the pancreas of these animals produces up to 90% of its insulin until week 10–14, and the animals can develop diabetes up to the age of 30 weeks. In *NOD* mice, diabetes is more common among females (60–90%), while 10–30% of males develop the disease in most colonies [28]. *NOD* mice are characterized by the typical clinical symptoms of diabetes (hyperglycemia, glycosuria, polydipsia, and polyuria), but they do not develop ketoacidosis. If not treated with endogenous insulin, the animals die due to dehydration, not ketoacidosis, 2–4 weeks after the disease's onset [23, 29]. In *NOD* mice, many genes are associated with a predisposition to T1DM and MHC alleles play an important role, as in humans, in this process. However, MHC class II alleles providing resistance or susceptibility to the disease in *NOD* mice have a structure that is different from that of human MHC class II alleles [27, 30, 31].

NOD mice are useful models in studying the genetics and mechanism of T1DM. These mice are potentially suitable for testing drugs that modulate the autoimmune response [23]. The advantages of *NOD* mice include the possibility of blocking cytokines by specific antisera and studying changes in the development and course of the disease [11, 32, 33]. It is this method that has been used to collect substantial data on the role of individual cytokines (interleukins, tumor necrosis factor, interferon γ) in the pathogenesis of autoimmune insulitis in diabetes [34]. However, it should be noted that, despite the high sensitivity of *NOD* mice to streptozotocin (STZ), β-cell death in them occurs in the absence of poly(ADP-ribose) polymerase (PARP) activation [35]. This fact can significantly affect the integrity of studies of β-cell sensitivity to diabetogenic factors in these animals [25, 26].

The initial optimism that accompanied the identification of a method for preventing T1DM by using animal models led to both discoveries and disappointments in the use of similar methods in humans. More than 192 methods that can be used to prevent T1DM in *NOD* mice have been reported [36–38]. Prevention of diabetes is relatively simple in mice, but it is extremely complicated in humans [5]. One of the causes may be that greater importance is attached to the similarity of T1DM in *NOD* mice and humans than to the differences [39]. In fact, diabetes in both mice and humans has a polygenic etiology characterized by impaired regulation of the immune response and the ability for remission after bone marrow transplantation. Differences in the action of maternal autoantibodies in mice and humans were revealed. In addition, there are differences in the incidence rate and gender. In *NOD* mice, the insulitis course is mild and benign [19]. Finally, there are significant differences in the functioning of immune systems in mice and humans [40].

Another commonly used model of autoimmune diabetes is *BB* rats generated from a colony of outbred Wistar rats in Canada (BioBreeding Laboratories) in the 1970s. Usually, after puberty, 90% of *BB* rats (males and females aged 8–16 weeks) develop spontaneous diabetes with a rather severe phenotype and the need for insulin therapy [41]. The animals have insulitis with the presence of T cells, B cells, macrophages, and NK cells, but with a sharply decreased number of CD4+ T cells and almost complete absence of CD8+ T cells. T cell lymphopenia characteristic of these animals is not typical of T1DM in humans and *NOD* mice and is considered as the model's drawback. It should be noted that insulitis in *BB* rats is not preceded by peri-insulitis [42]. However, *BB* rats are used as a small animal model for the induction of tolerance after islet transplantation [41], as well as for the investigation of diabetic neuropathy.

GENETICALLY INDUCED INSULIN-DEPENDENT DIABETES

AKITA mice were generated in Japan from C57BL/6NSIc mice with a spontaneous mutation in the *ins 2* gene, which prevents correct pro-insulin processing and leads to endoplasmic reticulum stress (ER stress). Starting at the age of 3–4 weeks, mice with this mutation develop insulin-dependent diabetes that is characterized by hyperglycemia, hypoinsulinemia, polyuria, and polydipsia. The absence of β-cell mass in this model makes it an alternative to the STZ-induced model used in transplantation studies [22]. *AKITA* mice are also used as a model of T1DM in studies of macrovascular diseases [43] and neuropathies [44]. This model has been widely used to investigate potential ER-stress suppressors in pancreatic islet cells: therefore, *AKITA*

mice can be used to study certain pathologies associated with T2DM [45].

However, the results obtained in rodents cannot be used in clinical medicine because there are both specific differences in the immune system of rodents and humans and the species-specific features of pancreatic Langerhans islets. Human and mouse islets that are intended for use as targets for autoimmune attack differ in many aspects, including the architecture and composition of the cells, proliferative activity, susceptibility to injuries, and ability to form islet amyloid, as well as in the expression of heat shock proteins, islet transcription factors, antioxidant enzymes, and the main glucose transporter (GLUT-1 or GLUT-2). For example, the inner β-cell mass in rodents is surrounded not by β-endocrine cells, whereas endocrine islet cells in humans are more mixed. In addition, unlike rodent β-cells capable of restoring or regenerating in response to some stimuli (insulin resistance, β-cell ablation, and partial pancreatectomy), the proliferative potential of human β-cells is either very small or absent [46].

The differences in the immune system of rodents and humans are primarily associated with the major histocompatibility complex (MHC). Transplantation of human immune cells and tissues onto immunodeficient mice produces the promising mouse models used to study natural human immune responses. There have been attempts to improve experimental models of diabetes mellitus by using humanized transgenic mice expressing human MHC class II molecules that predispose to diabetes. There have been new strains of immunodeficient mice suitable for the survival of grafted human functional tissues, including hematopoietic stem cells, mature lymphocytes, and pancreatic islets. For example, *NOD-SCID* mice were used to develop unique strains of *NSG* mice with a targeted mutation of the $IL2ry^{null}$ receptor common γ chain. *NSG* mice are considered perfect for studying the functions of the human immune system *in vivo* and determining the action mechanisms of drugs in T1DM [47–50].

Models based on immunodeficient mice have a number of disadvantages. First, they have natural killer (NK) cells, and human pancreatic islets are very sensitive to NK cells. Second, they do not enable engraftment of the functional human immune system [37, 39]. Deficiency of the $IL2ry^{null}$ receptor common γ chain completely blocks NK cells, causing additional defects of innate immunity. *NSG* mice are completely devoid of NK cells. *NSG* mice are a convenient model for studying the functions of transplanted islets of the human pancreas in the absence of the potential toxic effects of glucose, despite the fact that the euglycemia (120–160 mg/dL) in these animals is characterized by a higher blood glucose level in contrast to that in humans (80–100 mg/dL). Normoglycemic *NSG* mice are available in an unlimited amount; cells transplanted to them are not exposed to high glucose levels; fewer cells are required for an analysis of the function than for the regulation of hyperglycemia in recipients with diabetes [47–50]. Therefore, *NSG* mice have been shown to be readily available; they enable optional induction of hyperglycemia and restoration of normoglycemia by grafting Langerhans islets and suspensions of human and mouse pancreas cells; most important, these mice can be grafted with a functioning human immune system. However, when these mice are exposed to STZ, they, despite a number of the described advantages, also exhibit disadvantages: unstable induction of hyperglycemia, possibility of using endogenous mouse islets to restore normoglycemia, and STZ toxicity.

Genetic models of hyperglycemia were developed to induce hyperglycemia without the use of toxic compounds [47, 48]. These include the mouse models $NOD\text{-}Rag1^{null}\ Prf1^{null}\ Ins2^{Akita}$, $NOD\text{-}Rag1^{null}\ IL\text{-}2ry^{null}\ Ins2^{Akita}$, etc. The advantages of these models include: 1) spontaneous development of hyperglycemia without the use of toxic agents; 2) persistent and severe hyperglycemia; 3) no return to normoglycemia, due to endogenous mouse islets; 4) no need for exogenous insulin to prevent the development of metabolic decompensation and death. These models are able to support engraftment of the functional human immune system; therefore, they may be used to study alloimmunity and autoimmunity.

Despite the significant contribution of research on genetically modified animals to our understanding of the mechanism of diabetes pathogenesis, their role should not be overestimated. When using these models, acquired predisposition issues that play an important role in the development of type 1 diabetes mellitus may remain out of sight. T1DM is known to be strictly genetically determined in only 6–7% of cases, while in other cases the disease develops without significant hereditary predisposition [51]. The disease was found to develop not in all carriers of diabetes-associated alleles [52]. Therefore, experimental studies of the action mechanisms of unfavorable environmental factors seem promising. In this case, β-cell death mechanisms are largely versatile and independent of the acting factor, which enables an extrapolation of the results obtained in experimental models to humans [52].

CHEMICALLY INDUCED TYPE 1 DIABETES MELLITUS

Chemically induced T1DM is associated with the destruction of a large number of endogenous β-cells, which leads to a reduced production of endogenous insulin, followed by the development of hyperglycemia and weight loss. Chemically induced diabetes in

rodents and higher animals is a simple and relatively cheap model of this disease [53].

T1DM induced by chemical substances (STZ, alloxan, dithizone) is appropriate for an evaluation of drugs or therapeutic approaches that decrease the blood glucose level independently of β-cells; for example, for testing new insulin forms [54, 55]. This model is also appropriate for assessing the effectiveness of transplantation therapy that also reduces the blood glucose level [56, 57]. It is considered necessary to exclude spontaneous regeneration of β-cells in transplantation [58, 59] and also to perform a histological study of the endogenous pancreas for identifying insulin-positive cells and measuring the insulin level [59]. However, in the case of a chemically induced model of T1DM, the presence of β-cells has been shown not to necessarily correlate with their function [60].

One of the drawbacks of chemically induced diabetes is the potential toxicity of chemicals to other organs. It should be noted that administration of STZ and alloxan has been associated with changes in the expression level of P450 isoenzymes in the liver, kidneys, lungs, intestines, testes, and brain. This fact should be considered when testing drugs in animal models [61].

The STZ-induced model of T1DM is the most widely used at this moment. It has replaced the alloxan model [36, 40], the essential drawbacks of which are associated with the neurotoxicity and nephrotoxicity of alloxan and the lack of a clear dose-response relationship.

The natural antibiotic STZ is produced by *Streptomyces achromogenes* actinomycetes; this is N-acetylglucosamine (2-deoxy-2-(3-methyl-3-nitrosourea)-1-D-glucopyranose) that contains a nitrosourea moiety in lieu of acetate [36, 37]. STZ exhibits antibacterial and antitumor activities and is used in antitumor therapy. However, STZ has been found to cause the development of hypoglycemic conditions. STZ has been shown to be capable of inducing specific necrosis of β-cells in laboratory animals. The observed insulinemic syndrome has been called streptozotocin-induced diabetis, and STZ has been used to induce experimental T1DM. Let us consider this model in more detail.

STREPTOZOTOCIN-INDUCED DIABETES MELLITUS

Currently, streptozotocin diabetes is induced in most laboratory animals: rats, mice, guinea pigs, rabbits, dogs, and monkeys. However, different animal species, even within the same family, often differ significantly in sensitivity to STZ. Investigation of interspecies and intergroup differences in resistance to STZ is one of the important tasks of experimental diabetology. It is believed that rodents, especially rats, are most sensitive to STZ, while humans and fish are maximally resistant to it [62]; in this case, human β-cells are much more resistant to STZ than the β-cells of other anthropoid primates [62]. This phenomenon is genetically determined and is associated with the expression of different types of glucose transporters on the cell membrane, the features of enzymatic glucose oxidation systems in mitochondria, and differences in the DNA repair system [63].

INTRASPECIES DIFFERENCES

There are significant intergroup differences in the resistance to STZ within the same species. Inbred strains of rats and mice differ widely in their sensitivity to STZ [64, 65]. The diabetogenic action of STZ is enhanced by androgens and inhibited by estrogens, which leads to significant differences in the sensitivity to STZ in males and females [66]. An important role in sensitivity to diabetogenic factors is played not only by gender-related differences, but also by certain individual characteristics. For example, Wistar rats may be allocated into three groups of animals with differing resistance to diabetogenic factors, which manifests itself in the number of β-cells that die when exposed to STZ. This heterogeneity is related not to the breadth of the reaction norm but to the existence of isolated groups of animals with differing resistance. Animals of the first group are characterized by rapid development of hyperglycemia and significant destruction of pancreatic islets already at the initial stages of diabetes. The second group is characterized by a prolonged latent course of the pathological process when fasting euglycemia is associated with impaired glucose tolerance. The third group that is characterized by periodically occurring hyperglycemia falls in between the first two groups [63].

STZ DOSES AND ADMINISTRATION PROCEDURES

Single administration of a high STZ dose leads to the development of hyperglycemia, and experimental models of laboratory rodents generated in this way may be useful in grafting and testing insulins. Multiple administrations of low STZ doses are also used to model T1DM. However, T1DM models based on the development of autoimmune insulitis have been developed only in a few strains of mice with a genetic predisposition [62, 67]. This method is not appropriate for the generation of an adequate model of human T1DM in other animal species [62]. In these cases, a single injection of a diabetogenic dose of STZ (which depends on the animal species) is desirable to use for the induction of a self-progressive pathological process with an autoimmune component [62].

Diabetogenic doses of STZ, like procedures of their administration, are different for different animal species. The sub-diabetogenic dose of STZ for rats is

25 mg/kg, with the optimal diabetogenic dose being about 50–75 mg/kg [62, 68, 69]. In most animals, this dose leads to diabetes manifestation with hyperglycemia, hypoinsulinemia, dyslipidemia, and significant destruction of pancreatic islets, in combination with their lymphoid infiltration. For other rodent species, diabetogenic doses are significantly higher and range from 100 to 200 mg/kg [62, 70]. Fish β-cells show high resistance to STZ that, even at high doses (350 mg/kg), causes only short-term impairment of insulin synthesis and secretion, without destruction of pancreatic islets. This phenomenon is associated not with accelerated degradation of STZ in the liver or kidneys, but with the peculiarities of β-cell metabolism in these animals. Because of the instability and short half-life of STZ, its intravenous administration is considered to be the most reliable. However, there are also other ways of administering the drug to induce experimental diabetes: the intraperitoneal method and direct infusion into the pancreatic vessels. STZ is stable only at low temperatures in an acidic medium, while under neutral and alkaline conditions, it rapidly (within a few minutes) degrades to inactive metabolites lacking diabetogenic effect [71]. For this reason, STZ, dissolved *ex tempore*, should be administered in citrate buffer at acidic pHs ~ 4.5 [66].

PATTERNS OF EXPERIMENTAL T1DM DEVELOPMENT

The blood glucose concentration changes in response to a change in the plasma insulin concentration after STZ administration [72]. These changes occur in three phases. Unlike alloxan, STZ does not inhibit glucokinase. One hour after administration, the first hyperglycemic phase starts; it reaches a maximum after 2 h and lasts up to 4 h. The development of early hyperglycemia is believed to be caused by the suppression of insulin secretion due to the toxic effect of STZ on pancreatic β-cells [73]. Some authors associate it with an increased rate of hepatic glycogenolysis or consider it as secondary to the elevation in the free fatty acid content [13, 74]. Ultrastructural changes in the synthesis and energy apparatus of β-cells, which are accompanied by disruptions in the biosynthesis of proinsulin and insulin, were observed in the hyperglycemic phase [75]. After 4–8 h, the next hypoglycemic phase occurs, which lasts for several hours (up to a day) and is considered to be caused by the release of insulin from damaged β-cells. Loss of secretory granules develops in association with irreversible changes in subcellular organelles and nuclei. The final phase of the glycemic curve is characterized by persistent hyperglycemia and the development of permanent diabetes 24 h after STZ administration. Morphological and ultrastructural analyses indicate complete degranulation and disintegration of β-cells. Secondary hyperglycemia is considered as the result of absolute insulin deficiency.

According to other authors, hyperglycemia in experimental STZ-induced diabetes also develops in several consecutive stages but they are more prolonged: for example, the primary hyperglycemic reaction for 1–4 days; a period of euglycemia in the setting of impaired glucose tolerance (5–9th day); and a period of stable hyperglycemia, hyperphagia, and polyuria (10 days and more) [66]. Twelve hours after STZ administration, a primary hyperglycemic response develops; it is caused by the death of a significant portion of β-cells in pancreatic islets. The peak of hyperglycemia occurs on day 2 or 3, followed by a short period of euglycemia. This is associated with the potential ability of β-cells to enter mitosis under the influence of a high glucose concentration [5]. Activation of β-cell proliferation is believed to occur on the 3rd day of diabetes [63]. An increase in the β-cell mass further leads to a rapid decrease in glycemia to physiological values (before the end of day 9) and corresponds to incomplete compensation of the pancreatic insulin apparatus function. Inadequacy of the compensatory response is manifested as impaired glucose tolerance. By the 10–14th day, animals experience a repeated increase in the glycemia level [63]. Probably, an expanded autoimmune response to the neoantigens of pancreatic islets develops during this period, which leads to the death of most β-cells, fibrosis and sclerosis of the islets, and proliferation of alpha-cells. In preserved β-cells, glucose-induced insulin secretion is largely impaired. This is associated with several causes: a nonspecific response of β-cells to any damaging factors (including STZ) and the specific action of IL-1B and NO on glucose metabolism in mitochondria, which disrupts normal activation of β-cells [75, 76]. In addition, activated islet macrophages and T lymphocytes produce the neuropeptide γ (NPY) that inhibits insulin secretion [76].

FACTORS UNDERLYING DIFFERENCES IN RESISTANCE TO STZ

The differences in sensitivity to STZ are largely caused by intracellular events occurring after the transfer of STZ through the cell membrane to the cytosol and before depletion of NAD+ stores [63]. According to published data, resistance to STZ is controlled by a number of factors.

1. Sensitivity to diabetogenic action depends primarily on the physiological properties of β-cells. This underlies the differences in the rate of inactivation and excretion of STZ [62, 71].

2. A different degree of expression of type 2 glucose transporters (GLUT-2) that are specific STZ carriers into the cytoplasm of β-cells. High resistance of human

β-cells to STZ is caused by preferential expression of GLUT-1, not GLUT-2, on the β-cell surface [62].

3. Differences in the activity of oxidation systems; for example, a lower activity of glycolysis enzymes causes greater susceptibility to and toxicity of STZ in voles than in mice.

4. Intracellular accumulation of various STZ metabolites, some of which promote, like STZ, the generation of free radical products and mutations [77, 78].

5. Differing sensitivity of inbred mouse strains to STZ is caused by a difference in the activity of poly(ADP-ribose) polymerase (PARP) [77].

6. Expression of heat shock proteins that are potent factors of pancreatic β-cell resistance to the toxic effect of STZ. The level of their expression in both nonspecific (effect of STZ) inflammation and autoimmune inflammation is considered as one of the most important parameters controlling the viability of β-cells in insulitis [79, 80].

7. Differences in the activity of antioxidant systems, in particular the higher activity of glutathione peroxidase in mice, are one of the factors underlying the high resistance of mice to STZ [63].

8. Transgenic mouse strains expressing interferon γ in β-cells are significantly more resistant to the induction of diabetes than the initial strain [81]. This example demonstrates the role of intra-islet paracrine factors [81]. However, the molecular mechanisms of this phenomenon remain as yet not fully understood.

9. The cumulative effect of damaging factors is also considered as a cause of the differences in resistance to STZ. Adverse environmental factors (especially those acting during early ontogeny) that cause a stress response through a high level of glucocorticoids and changes in the neuroendocrine regulation of the pancreatic islet function can lead to endocrine imprinting associated with significant rearrangement of the intracellular systems of β-cell function regulation [63]. In adult animals that have undergone stress in the prenatal period, glucose-stimulated insulin secretion and glucose tolerance are impaired and the sensitivity of β-cells to the toxic effect of STZ is significantly increased [5].

The tropicity of STZ to β-cells is controlled by a glucose residue in the STZ molecule [82], which enables its selective binding to the GLUT-2 glucose transporter and transport to the cytoplasm [83]. Therefore, cell sensitivity to STZ depends on the expression of the GLUT-2 carriers that are expressed exclusively by pancreatic islet β-cells in most animals. This is also confirmed by the following observations: insulin-producing cells not expressing the glucose transporter are resistant to STZ; they become sensitive to the toxic effect of the drug only after the expression of GLUT-2 in the cell membrane [84]. In addition, other cells expressing this transporter, such as hepatocytes and epithelial cells of the renal tubules, are also exposed to the toxic action of STZ. Therefore, administration of STZ to animals leads to the development of not only diabetes, but also damage to the liver and kidneys [63].

TOXIC EFFECT

STZ is capable of non-enzymatic release of free NO associated with the toxic effect of STZ [39, 85]. In this case, islet β-cells accumulate a large amount of STZ, which results in a high concentration of NO that, being in a liquid medium, rapidly transforms into peroxynitrate, which leads to the activation of free radical oxidation processes [39]. This leads to disruption of the cell membrane integrity, reduced efficiency of oxidative phosphorylation in mitochondria [37, 67], and point mutations in DNA, such as covalent modification of purine bases and the emergence of N-7-methylguanine, O-6-methylguanine, and 3-methyladenine. STZ and its metabolites are alkylating agents that methylate guanine and, to a lesser extent, adenine residues in DNA [86]. DNA damage leads to the activation of repair systems. The key enzyme involved in the repair of point mutations is PARP that replaces a defective base with a poly-ADP-ribose tail [59, 77]. The repair process requires NAD, which, given the huge number of NO- and STZ-induced mutations, leads to depletion of the cell NAD pool and cell death [71, 87, 88]. In this case, transgenic mice with PARP deficiency are resistant to diabetogenic factors. Recent studies have shown that, although STZ also methylates proteins, it is DNA methylation that is responsible for the death of β-cells [73]. The ability of STZ to cause energy deficiency in cells was shown to play the decisive role in its toxic effect towards β-cells [71, 87, 88].

PARP is the key factor involved in the death of β-cells [37, 62]. PARP is activated regardless of whether DNA damage is caused by chemical factors (STZ, alloxan), inflammatory factors (NO, cytokines, reactive oxygen species), or β-cytotropic viruses [62, 89].

On the other hand, the specific effect of NO on β-cells also includes activation of guanylate cyclase, an increase in the cGMP level, and inhibition of mitochondrial aconitase, which leads to impairment of aerobic glucose oxidation and, as a consequence, suppression of glucose-stimulated insulin secretion and synthesis [67, 90, 91]. In this case, inhibition of aconitase (that participates in the Krebs cycle) in the setting of PARP hyperactivation leads to complete depletion of intracellular NAD and ATP stores, which is the direct cause of β-cell necrosis. In the case of STZ-induced β-cell death, apoptosis processes are also blocked due to complete depletion of intracellular ATP and NAD stores [92, 93].

NO generation is responsible for both the initiation and development of diabetes caused both by viruses [89] and toxic substances [94] and by an autoimmune response. The alkylating agent methyl methanesulfonate, being the most toxic compound, is not a donor of NO; thereby proving that NO is unnecessary to the toxic effect of alkylating agents, including diabetogenic streptozotocin. NO and free nitroxide radicals can enhance STZ toxicity, but NO is certainly not a decisive factor of toxicity to β-cells [51]. However, the ability of STZ to cause ATP pool depletion and, therefore, energy deficit is important to the toxic effect on β-cells. The biological effects of STZ on the homeostasis of glucose and insulin are a result of damage to β-cells. On the one hand, glucose homeostasis disturbance (oxygen consumption and glucose oxidation) and inhibition of insulin biosynthesis and secretion are obvious. On the other hand, STZ has been found not to immediately and directly affect the transport of glucose or its phosphorylation by glucokinase [33, 95]. Inhibition of insulin biosynthesis and secretion is supposed to be initially caused by STZ-induced depletion of NAD+ [96].

Cytokines, such as IL-1, in the immunocompetent and endocrine cells of pancreatic islets have been shown to trigger the expression of the inducible nitric oxide synthase (iNOS) [85, 97] that produces significant amounts of the major biological mediator and, thus, causes β-cell death [39, 98].

Therefore, STZ activates the same pathogenetic mechanisms (suppression of glucose oxidation, DNA mutations, NAD depletion) as those activated by other poisons and viruses toxic to β-cells, and the key agents implementing these processes, regardless of the damaging factor, are NO and PARP. Thus, it should be concluded that the streptozotocin model of diabetes is etiologically and pathogenetically very close to human T1DM.

Despite the variety of experimental DM models reported to date, STZ-induced diabetes is the preferable one. The advantages of this model include relatively simple reproducibility, a highly selective effect, and induction of diabetes of varying severity and duration, which enables the modeling of both progressively developing β-cell dysfunction and impaired glucose tolerance with associated disorders. A number of the disadvantages of nongenetic STZ-induced diabetes models (scattering of glycemia level data, spontaneous normalization of insulin secretion function) can be eliminated by a judicious choice of the diabetogenic dose of the drug and adequate planning of the experiment.

Experimental DM models in laboratory rodents are undoubtedly a very useful tool for studying the pathophysiology and clinical aspects of the disease and are used as the first step in the investigation of new promising therapies. However, animal models, in general, and rodent T1DM models, in particular, are imperfect and exhibit certain drawbacks when their results are extrapolated to humans. Furthermore, the results obtained in rodents may sometimes prove misleading when studying the prevention of T1DM [64, 99]. To avoid compromised results, a degree of caution is necessary when choosing the model and drug dose for the induction of experimental diabetes. It is necessary to standardize the models and experiments specifically for studies of DM prevention, clearly interpret reliable results, and create a database after multiple iterations of the experiments.

The question of to which extent the results obtained in models may be extrapolated to humans is both the most important and most difficult one when laboratory animals are used [100, 101]. However, the question of how relevant a particular model is to the processes occurring in the human body remains open. Evaluation of the adequacy of experimental models includes a body of evidence that demonstrate that the results obtained in animals may be, to a certain degree, extrapolated to humans.

The data presented here do not reflect the entire spectrum of the T1DM models developed to date. The number of models is constantly growing, but they have not been sufficiently explored. In this case, it should be remembered that each experimental model simulates only certain aspects of the T1DM pathogenesis and does not completely match the development and course of the disease in humans. Therefore, there is ongoing research on the modification of existing models and development of new, more advanced models that most adequately reflect the changes typical of T1DM in humans.

It should be emphasized that adequate modeling of T1DM is a necessary basis for the preclinical testing of antidiabetic agents, and the use of various models enables to substantiate the extrapolation of experimental results to T1DM patients. ●

The research was carried out within the state assignment of Koltsov Institute of Developmental Biolog ("Mechanisms of cell differentiation in morphogenesis and restoration processes" No. 0108-2018-0004).

REFERENCES

1. WHO Bulletin No. 312, April 2016
2. Balabolkin M.I., Dedov I.I. // Diabetes mellitus. 2000. № 3. P. 2–10.
3. Eisenbarth G.S. // N. Engl. J. Med. 1986. № 314. P. 1360–1368.
4. Daaboul J., Schtz D. // Rev. Endocr. Metab. Disord. 2003. № 4. P. 317–323.
5. Nikonova T.V. // Diabetes mellitus. 2006. № 3. P. 59–64.
6. Ide A., Eisenbarth G.S. // Rev. Endocr. Metab. Disord . 2003. № 4. P. 243–253.
7. Hyttinen V., Kaprio J., Kinnunen L., Koskenvuo M., Tuomilehto J. // Diabetes. 2003. № 52. P. 1052–1055.
8. Atkinson M.A. // Diabetes. 2005. V. 54. № 5. P. 1253–1263.
9. Homo-Delarche F., Drexhage H.A. // Trends Immunol. 2004. № 25. P. 222–229.
10. Mokhort T.V., Melnov S.V., Goranov V.A. // Problems of Endocrinology. 2000. V. 46. № 2. P. 8–13.
11. Kawasaki E., Abiru N., Eguchi K. // Diabetes Res. Clin. Practice. 2004. № 66. P. 27–32.
12. Rees D.A., Alcolado J.C. // Diabetic Medicine. 2005. № 4. P. 359–370.
13. Baranov V.G. Experimental Diabetes Mellitus. Moscow: Nauka. 1983. 240 p.
14. Karkishchenko N.N. The Basics of Biomodelling. Moscow: VPK. 2004. 608 p.
15. Lukačínová A., Hubková B., Rácz O., Ništiar F. // Diabetes Mellitus – Insights and Perspectives / Ed. Oluwafemi O. Oguntibeju. L.: InTech, 2013. Ch. 13.
16. King A.J. // Br. J. Pharmacol. 2012. V. 166. № 3. P. 877–894.
17. Choi S.B., Park C.H., Choi M.K., Jun D.W., Park S. // J. Biotech. Biochem. 2004. V. 68. P. 2257–2264.
18. Masiello P. // Internat. J. Biochem. Ceil Biol. 2006. V. 38. № 5–6. P. 873–893.
19. Green E.A., Flavel R.A. // Immunol. Rev. 1999. V. 169. P. 11–22.
20. Yang Y., Santamaria P. // Clin. Sci. (London). 2006. V. 110. № 6. P. 627–639.
21. Lenzen S., Tiedge M., Elsner M., Lortz S., Weiss H., Jörns A., Klöppel G., Wedekind D., Prokop C.M., Hedrich H.J. // Diabetologia. 2001. № 44. P. 1189–1196.
22. Wallis R.H., Wang K., Marandi L., Hsieh E., Ning T., Chao G.Y., Sarmiento J., Paterson A.D., Poussier P. // Diabetes. 2009. № 58. P. 1007–1017.
23. Todd J.A., Wicker LS. // Immunity. 2001. V. 15. № 3. P. 387–395.
24. Driver J.P., Serreze D.V., Chen Y.G. // Semin. Immunopathol. 2011. № 33. P. 67–87.
25. Niens M., Grier A.E., Marron M., Kay T.W., Greiner D.L., Serreze D.V. // Diabetes. 2011. № 60. P. 1229–1236.
26. Herrath M.G., Nepom G.T. // J. Exp. Med. 2005. V. 202. № 9. P. 1159–1162.
27. Herrath M.G., Nepom G.T. // Nat. Immunol. 2009. V. 10. № 2. P. 129–132.
28. Chan O., Inouye K., Akirav E.M., Park E., Riddell M.C., Matthews S.G., Vranic M. // Am. J. Physiol. Regul. Integr. Comp. Physiol. 2005. V. 289. № 1. P. 235–246.
29. Mathews C.E. // Pediatr. Diabetes. 2005. V. 6. № 3. P. 165–177.
30. Yoon J.W., Jun H.S. // Ann. N. Y. Acad. Sci. 2001. № 928. P. 200–211.
31. Wicker L.S., Clark J., Fraser H.I., Garner V.E., Gonzalez-Munoz A., Healy B., Howlett S., Hunter K., Rainbow D., Rosa R.L., et al. //J. Autoimmun. 2005. № 25 (Suppl.). P. 29–33.
32. Toyoda H., Formby B. // Bioessays. 1998. V. 20. № 9. P. 750–757.
33. O'Reilly L.A., Gu D., Sarvetnick N. // Diabetes. 1997. V. 46. P. 4599–4606.
34. Brown G.R., Silva M.D.,Thompson P.A., Beutler B. // Diabetologia. 1998. V. 41. № 12. P. 1502–1510.
35. Gonzalez C., Ménissier De Murcia J., Janiak P., Bidouard J.P., Beauvais C., Karray S., Garchon H.J., Lévi-Strauss M. // Diabetes. 2002. V. 51. № 5. P. 1470–1476.
36. Babaya N., Ikegami H., Fujisawa T., Nojima K., Itoi-Babaya M., Inoue K., Ohno T., Shibata M., Ogihara T. // Biochem. Biophys. Res. Commun. 2005. V. 328. № 1. P. 158–164.
37. Masutani M., Suzuki H., Kamada N., Watanabe M., Ueda O., Nozaki T., Jishage K., Watanabe T., Sugimoto T., Nakagama H. // Proc. Natl. Acad. Sci. USA. 1999. V. 96. № 5. P. 2301–2304.
38. Baxter A.G., Duckworth R.C. // Drug Discovery Today. 2004. № 4. P. 451–455.
39. Turk J., Corbett J.A., Ramanadham S., Bohrer A. // Biochem. Biophis. Res. Commun. 1993. V. 197. № 3. P. 1458–1464.
40. Hosokawa M., Doici W., Thorens B. // Biochem. Biophys. Res. Commun. 2001. V. 289. № 5. P. 1114–1117.
41. Roep B.O., Atkinson M., Herrath M. // Nat. Rev. Immunol. 2004. V. 4. № 12. P. 989–997.
42. Mordes J.P., Bortell R., Blankenhorn E.P., Rossini A.A., Greiner D.L. // ILAR J. 2004. V. 45. № 3. P. 278–291.
43. Mathews C.E., Langley S.H., Leiter E.H. // Transplantation. 2002. V. 73. № 8. P. 1333–1336.
44. Zhou C., Pridgen B., King N., Xu J., Breslow J.L. // J. Lipid Res. 2011. V. 52. № 8. P. 1483–1493.
45. Drel V.R., Pacher P., Stavniichuk R., Xu W., Zhang J., Kuchmerovska T.M., Slusher B., Obrosova I.G. // Int. J. Mol. Med. 2011. № 28. P. 629–635.
46. Cailat-Zucman S., Bach J.F. // Clin. Rev. Allerg. Immunol. 2000. V. 19. № 3. P. 227–246.
47. Vandewalle C.L., Falorni A., Lernmark A., Goubert P., Dorchy H., Coucke W., Semakula C., Van der Auwera B., Kaufman L., Schuit F.C. // Diabetes Care. 1997. V. 20. № 10. P. 1547–1552.
48. Chen H., Zheng C., Zhang X., Li J., Li J., Zheng L., Huang K. // Peptides. 2011. V. 32. № 8. P. 1634–1639.
49. Dufrane D., van Steenberghe M., Guiot Y., Goebbels R.M., Saliez A., Gianello P. // Transplantation. 2006. № 81. P. 36–45.
50. Rackham C.L., Chagastelles P.C., Nardi N.B., Hauge-Evans A.C., Jones P.M., King A.J. // Diabetologia. 2011. № 54. P. 1127–1135.
51. Jederstrom G., Grasjo J., Nordin A., Sjoholm I., Andersson A. // Diabetes Technol. Ther. 2005. V. 7. № 6. P. 948–957.
52. Kargar C., Ktorza A. // Diabetes Obes. Metab. 2008. № 10 (Suppl. 4). P. 43–53.
53. Deeds M.C., Anderson J.M., Armstrong A.S., Gastineau D.A., Hiddinga H.J., Jahangir A., Eberhardt N.L., Kudva Y.C. // Lab. Anim. 2011. V. 45. № 3. P. 131–140.
54. Makhlouf L., Duvivier-Kali V.F., Bonner-Weir S., Dieperink H., Weir G.C., Sayegh M.H. // Transplantation. 2003. V. 76. № 4. P. 657–664.
55. Sheshala R., Peh K.K., Darwis Y. // Drug Dev. Ind. Pharm. 2009. V. 35. № 11. P. 1364–1374.
56. Baeyens L., De B.S., Lardon J., Mfopou J.K., Rooman I., Bouwens L. // Diabetologia. 2005. V. 48. № 1. P. 49–57.
57. Arai T., Kaneko H., Takagi H., Ogino T., Sasaki M., Matsumoto H., Sugawara M. // Vet. Res. Commun. 1996. V. 20. № 3. P. 215–224.

58. Yang H., Wrigth J.R. // Endocrinology. 2002. V. 143. № 7. P. 2491–2495.
59. Orlovskiy M.A. // Journal AMS of Ukraine. 2006. V.12. № 2. P. 255–268.
60. Hayashi K., Kojima R., Ito M. // Biol. Pharm. Bull. 2006. V. 29. № 6. P. 1110–1119.
61. Srinivasan K., Ramarao P. // Indian J. Med. Res. 2007. V. 125. № 3. P. 451–472.
62. Kromann H., Christy M., Lernmark A., Nedergaard M., Nerup J. // Diabetologia. 1982. V. 22. № 3. P. 194–198.
63. Orlovskiy M.A. // Pathology. 2004. V.1. № 1. P. 21–26.
64. Reddy S., Sandler S. // Autoimmunity. 1995. V. 22. № 2. P. 121–126.
65. Wright J.R., Abraham C., Dickson B.C. // Gen. Comp. Endocrinol. 1999. V. 114. № 3. P. 413–440.
66. El-Seweidy M.M., El-Swefy S.E., Ameen R.S., Hachem R.M. // Parmacol. Res. 2000. V. 45. № 5. P. 391–398.
67. Gai W., Schott-Ohly P., Schulte im Walde S., Gleichmann H. // Exp. Clin. Endocrinol. Diabetes. 2004. V. 112. № 1. P. 29–37.
68. Sharma B.R., Kim M.S., Rhyu D.Y. // J. Tradit. Chin. Med. 2016. V. 36. № 1. P. 71–77.
69. Gu D., Arnuch M., Sawyer S.P., Sarvetnick N. // Am. J. Physiol. 1995. V. 269. № 6. P. 1089–1094.
70. Fisher M.M., Perez Chumbiauca C.N., Mather K.J., Mirmira R.G., Tersey S.A. // Endocrinology. 2013. V. 154. № 9. P. 3476–3481.
71. Lee J.H., Yang S.H., Oh J.M., Lee M.G. // J. Pharm. Pharmacol. 2010. V. 62. № 1. P. 1–23.
72. Szkudelski T. // Physiol. Res. 2001. V. 50. № 6. P. 537–546.
73. Lenzen S. // Diabetologia. 2008. № 51. P. 216–226.
74. Mythili M.D., Vyas R., Akila G., Gunasekaran S. // Microsc. Res. Tech. 2004. V. 63. № 5. P. 274–281.
75. Imai Y., Patel H.R., Hawkins E.J., Doliba N.M., Matschinsky F.M., Ahima R.S. // Endocrinology. 2007. V. 148. № 12. P. 5716–5723.
76. Cardinal J.W., Allan D.J., Cameron D.P. // J. Mol. Endocrinol. 1999. V. 22. № 1. P. 65–70.
77. Cardinal J.W., Allan D.J., Cameron D.P. // Endocrinology. 1998. V. 139. № 6. P. 2885–2891.
78. Bellmann K., Wenz A., Radons J., Burkart V., Kleemann R., Kolb H. // J. Clin. Invest. 1995. V. 95. № 6. P. 2840–2845.
79. Burkart V., Blaeser K., Kolb H. // Horm. Metab. Res. 1999. V. 31. № 12. P. 641–644.
80. Charron M.J., Bonner-Weir S. // Nat. Med. 1999. V. 5. № 3. P. 268–270.
81. Elsner M., Guldbakke B., Tiedge M., Munday R., Lenzen S. // Diabetologia. 2000. V. 43. № 12. P. 1528–1533.
82. Dekel Y., Glucksam Y., Elron-Gross I., Margalit R. // Lab. Anim. (NY). 2009. V. 38. № 2. P. 55–60.
83. Lee J.Y., Kim M.J., Moon C.K., Chung J.H. // Biochem. Pharmac. 1993. V. 46. № 11. P. 2111–2113.
84. Wada R., Yagihashi S. // Virchows Archiv. 2004. V. 444. № 4. P. 375–382.
85. Heitmeier M.R., Scarim A.L., Corbett J.A. // J. Biol. Chem. 1997. V. 272. № 21. P. 13697–13704.
86. Chaudhry Z.Z., Morris D.L., Moss D.R., Sims E.K., Chiong Y., Kono T., Evans-Molina C. // Lab. Anim. 2013. V. 47. № 4. P. 257–265.
87. Husseiny M.I., Kaye A., Zebadua E., Kandeel .F, Ferreri K. // PLoS One. 2014. V. 9. № 4. P. 94591.
88. Akirav E.M., Lebastchi J., Galvan E.M., Henegariu O., Akirav M., Ablamunits V., Lizardi P.M., Herold K.C. // Proc. Natl. Acad. Sci. USA. 2011. V. 108. № 47. P. 19018–19023.
89. Yamamoto H., Uchigata Y., Okamoto H. // Nature. 1981. V. 294. № 5838. P. 284–286.
90. Simonsson E., Ahreacute B. // Eur. J. Pharm. 1998. V. 350. № 2–3. P. 243–250.
91. Stevens R.B., Sutherland D.E., Ansite J.D., Saxena M., Rossini T.J., Levay-Young B.K., Hering B.J., Mills C.D. // J. Immunol. 1987. V. 159. № 11. P. 5329–5335.
92. Fisher M.M., Watkins R.A., Blum J., Evans-Molina C., Chalasani N., DiMeglio LA., Mather K.J., Tersey S.A., Mirmira R.G. // Diabetes. 2015. V. 64. № 11. P. 3867–3872.
93. Szkudelski T. // Exp. Biol. Med. (Maywood). 2012. V. 237. № 5. P. 481–490.
94. Tsuji A., Sakurai H. // Bioch. Biophys. Res. Commun. 1998. V. 245. № 1. P. 11–16.
95. Howart F.C., Qureschi A., Shahin A., Lukic M.L. // Mol. Cell. Biochem. 2005. V. 269. № 1–2. P. 103–108.
96. Andreone T., Meares G.P., Hughes K.J., Hansen P.A., Corbett J.A. // Am. J. Physiol. Endocrinol. Metab. 2012. V. 303. № 2. P. 172–179.
97. Arnush M., Scarim A.L., Heitmeier M.R., Kelly C.B., Corbett J.A. // J. Immunol. 1998. V. 160. № 6. P. 2684–2691.
98. Rabinovitch A. // Diabet. Met. 1998. V. 14. № 2. P. 129–151.
99. Leiter E.H., von Herrath M. // Diabetologia. 2004. V. 47. № 10. P. 1657–1660.
100. Roep B.O., Atkinson M. // Diabetologia. 2004. V. 47. № 10. P. 1650–1656.
101. Mestas J., Hughes C.C. // J. Immunol. 2004. V. 172. № 5. P. 2731–2738.

The Effect of TNF and VEGF on the Properties of Ea.hy926 Endothelial Cells in a Model of Multi-Cellular Spheroids

S. Sh. Gapizov[1,2*], L. E. Petrovskaya[1], L. N. Shingarova[1], E. V. Svirschevskaya[1], D. A. Dolgikh[1,2] and M. P. Kirpichnikov[1,2]

[1]Shemyakin–Ovchinnikov Institute of Bioorganic Chemistry, Russian Academy of Sciences, Miklukho-Maklaya Str. 16/10, Moscow, 117997, Russia

[2]Lomonosov Moscow State University, Department of Biology, Leninskie Gory 1, bldg. 12, Moscow, 119234, Russia

*E-mail: gsultan3@gmail.com

Received: November 29, 2017; in final form February 27, 2018

ABSTRACT **Endothelial cells play a major role in the development of inflammation and neoangiogenesis in cancer and chronic inflammatory diseases. In 3D cultures, cells are under conditions that closely resemble those existing in healthy and disease-stricken human organs and tissues. Therefore, the development of a 3D model based on the Ea.hy926 endothelial cell line is an urgent need in molecular and cellular biology. Cell cultivation on an anti-adhesive substrate under static conditions was shown to lead to the formation of spheroids (3D cultures). Expression of ICAM-1 and VEGFR-2 and production of cytokines were screened in 2D and 3D cultures in the presence of TNF and VEGF. According to flow cytometry and confocal microscopy data, TNF significantly increased the expression of the cell adhesion molecule ICAM-1 in both 2D and 3D cultures but did not affect the expression level of VEGFR-2. Increased production of pro-inflammatory (IL-8, IL-6, IP-10) and anti-inflammatory (IL-10, TGF-β 1–3) factors was observed in spontaneous 3D cultures but not in 2D cultures, which was confirmed by flow cytometry and qPCR. TNF-induced secretion of IL-10, GM-CSF, and IL-6 was 11-, 4.7-, and 1.6-fold higher, respectively, in 3D cultures compared to 2D cultures. Thus, the use of a Ea.hy926 3D cell culture is a promising approach in studying the effects of anti- and pro-inflammatory agents on endothelial cells.**

KEWORDS **2D and 3D cultures, αvβ3-integrin, vascular endothelial growth factor receptor 2, intercellular adhesion molecule, tumor necrosis factor, inflammation.**

ABBREVIATIONS **2D – two-dimensional conditions; 3D – three-dimensional conditions; qPCR – quantitative polymerase chain reaction; ICAM-1 – intercellular adhesion molecule 1; IFN – interferon; IL – interleukin; TNF – tumor necrosis factor; VCAM-1 – vascular cell adhesion molecule 1; VEGF A – vascular endothelial growth factor A; VEGFR-2 – vascular endothelial growth factor receptor 2.**

INTRODUCTION

Cancer and chronic inflammatory diseases involving various human organs and tissues are a serious medical and societal problem. The tumor necrosis factor alpha (TNF-α) has been shown to play the key role in the development and maintenance of inflammation in diseases, such as rheumatoid arthritis, psoriasis, Crohn's disease, etc. [1, 2]. Both the inflammatory process and tumor growth are accompanied by tissue hypoxia, which leads to the formation of new blood vessels under the influence of the vascular endothelial growth factor (VEGF), which is secreted by epithelial cells in conditions of hypoxia [3, 4]. The expression level of αvβ3-integrin in endothelial cells is known to be significantly increased in tumor vessels [5]. In endothelial cells, TNF and VEGF have been shown to stimulate the expression of adhesion and inflammation molecules, in particular ICAM-1 and VCAM-1, the vascular endothelial growth factor receptor 2 (VEGFR-2), PECAM-1, and P- and E-selectins, induce the release of the von Willebrand factor from Weibel-Palade bodies, as well as enhance the secretion of the cytokines IL-6 and IL-8, monocyte chemotaxis protein 1 (MCP-1), and the granulocyte-macrophage colony-stimulating factor (GM-CSF) [6–11]. A change in the expression of endothelial surface proteins ensures the inhibition of leukocytes at the site of an inflammation, as well as their adhesion and transendothelial migration [12]. The *in vitro* response corresponds to the *in vivo* processes occurring under the influence of pro-inflammatory stimuli, which makes

it possible to use an endothelial cell culture to simulate inflammation processes in the body.

The use of therapeutic agents capable of suppressing angiogenesis partially slows down the pathological process. In particular, anti-VEGF antibodies (Bevacizumab), a low-molecular-weight inhibitor of VEGF (Aflibercept), anti-TNF antibodies (Adalimumab, Infliximab, and Etanercept), and a number of anti-integrin antibodies (Vedolizumab and anti-α4β7 integrin antibodies) have been developed and clinically used [13–15]. The αvβ3-integrin inhibitor known as Cilengitide, the antibodies Etaracizumab, and other drugs are undergoing clinical trials [16–18]. The disadvantage of low-molecular-weight drugs is that the patient quickly develops resistance to them [19]. Antibodies also have a number of disadvantages; in particular, the high cost of production of humanized recombinant antibodies limits the number of patients who can afford the therapy. On the other hand, antibodies have a large molecular weight, which prevents their deep penetration into tissues [19, 20].

The development of antibody analogues for creating immunoconjugates with antitumor drugs and/or vascular growth inhibitors will improve the treatment of tumor and chronic inflammatory diseases and expand the range of patients that can receive adequate therapy [19]. Primary screening of new drugs requires an *in vitro* cell model with properties that are as close as possible to *in vivo* conditions. Currently, interactions between anti-inflammatory drugs and endothelial cells are analyzed using primary cultures derived from the umbilical vein of healthy donors (human umbilical vein endothelial cells, HUVECs) or the Ea.hy926 hybrid line [21–23]. It is preferable to use a stable line, because the functional characteristics of HUVECs may depend on the quality of cell isolation and on the donor; in addition, donor cells are not always available and the number of passages of primary cells is limited [24]. The functional characteristics of HUVECs and Ea.hy926 largely coincide; in particular, both cell types change the expression of adhesion molecules and production of IL-6 and IL-8 in response to TNF [25–27].

In the body, small vessels and capillaries are predominantly composed of endotheliocytes; in larger vessels, the wall is formed by endothelial cells, connective tissue, and smooth muscles. A monoculture of endothelial cells largely simulates the capillary structure; in this case, the use of multicellular spheroids of endothelial cells enables one to study the effects of various drugs not only on endothelial cells, but also on their associates with the connective matrix formed in 3D cultures [28–31]. Earlier, there have been attempts to develop 3D cultures of endothelial cells by clinostatting [32–35]. This method is based on rotating a cell culture in a gravity field, which leads to the formation of spheroids on the monolayer culture surface. The purpose of the present work was to develop a static 3D culture model based on the Ea.hy926 endothelial cell line and compare the responses of 2D and 3D cultures to TNF and VEGF.

EXPERIMENTAL

Reagents from Bio-Rad (USA), Sigma (USA), Merck (USA), Panreac (Spain), and PanEco (Russia) were used in the study. Solutions were prepared in Milli-Q deionized water. The recombinant proteins TNF (produced in the Laboratory of Protein Engineering of the Institute of Bioorganic Chemistry) and VEGFA165 (Protein Synthesis, Russia) were used.

Cell cultures

A human Ea.hy926 endothelial cell line (ATCC, CRL-2922) provided by A.A. Sokolovskaya (Research Institute of General Pathology and Pathophysiology) with the permission of Dr. C.-J. Edgell (University of North Carolina) was used in the study. Cells were incubated in a DMEM/F12 medium (PanEco, Russia) supplemented with 10% inactivated bovine fetal serum (HyClon, USA), 50 μg/mL gentamicin sulfate, and 2 mM *L*-glutamine (PanEco). To form three-dimensional cultures, the well surface of a 24-well plate (Costar) was coated with poly-2-hydroxyethyl methacrylate (pHEMA) (Sigma). Each well was seeded with 5×10^5 cells per 1 mL of the growth medium. The cells were cultured under standard conditions in a CO_2 incubator for 48 h until the formation of a confluent monolayer (2D culture) or spheroids (3D culture).

Confocal microscopy

To analyze the expression of surface adhesion molecules in the 2D endothelial cell cultures, sterile glass coverslips were placed in six-well plates; 1×10^5 cells in 200 μL of medium were put on each coverslip and incubated in a CO_2 incubator under standard conditions for 16 h to produce a confluent monolayer. To analyze the 3D cultures of Ea.hy926 cells, spheroids were pipetted and transferred into the wells of a 96-well plate. Cell cultures were added with recombinant TNF or VEGFA proteins to a concentration of 25 ng/mL each and incubated for 5 h. The cells were stained with mouse monoclonal antibodies to human ICAM-1 (CD56) and VEGFR-2 (Flk-1), as well as anti-mouse IgG secondary antibodies labeled with CFL488 (Santa Cruz Biotechnology, USA) or Alexa Fluor 555 (Invitrogen, USA). Antibodies were added to a concentration of 0.2 μg/mL for 1 h. The cells were incubated in a CO_2 incubator at a rotation speed of 40 rpm. Cell nuclei were stained with Hoechst 33342 (Sigma). After completion of incubation,

the 2D and 3D cultures were fixed with 1% paraformaldehyde at room temperature for 10 min and then washed with phosphate buffered saline (PBS). After fixation, the cells were washed from primary antibodies and incubated with secondary antibodies in PBS (1 : 1000 dilution) at 37°C for 40 min. After washing, the cells were polymerized on glass slides using a Mowiol 4.88 (Calbiochem, Germany) medium and left overnight at room temperature. Images were acquired and analyzed using a Nikon Eclipse TE2000-E confocal microscope (Japan).

Flow cytometry

The expression of the surface molecules ICAM-1 and VEGFR-2 in all samples was assessed using a FACScan flow cytometer (BD, USA). To prepare a suspension, cells from 2D and 3D cultures were treated with a trypsin/EDTA solution (PanEco), washed in PBS containing 1% bovine serum albumin and 0.05% NaN_3 (PBSA), combined with the appropriate antibodies, and incubated in the dark at 4°C for 60 min. After washing, the cells were stained with secondary fluorescently labeled antibodies (4°C, in the dark, 60 min). Before the analysis, propidium iodide (0.5 μg/mL) was added to the samples for differential staining of dead cells. In each sample, 10,000 cells were analyzed. The data were analyzed using the WinMDI 2.9 software.

Production of humoral factors

Production of cytokines and chemokines by Ea.hy926 cells cultured under 2D and 3D conditions was analyzed by flow cytometry with microparticles on a FACS Calibur instrument (BD, USA) according to the manufacturer's protocol (BioRad, USA).

Quantitative PCR (qPCR)

Total mRNA was isolated using an RNeasy Mini Kit (Qiagen, USA) and purified from DNA contamination by treating it with DNase I (Fermentas, USA). cDNA was synthetized using a First Strand cDNA Synthesis kit (Thermo Scientific, USA). The concentration of mRNA and cDNA was determined using a NanoDrop 2000 device (Thermo Scientific). The resulting cDNA was used as a template for quantitative PCR (qPCR) with specific primers (*Table 1*) [36] and a qPCRmix-HS SYBR mixture (Eurogen, Russia) on a Lightcycler 480 instrument (Roche, USA). The reaction mixture consisted of 50 ng of cDNA, primers (0.120 μM per sample), the qPCRmix-HS SYBR (5x) mixture, and Milli-Q water. The annealing temperature was adjusted in accordance with the primer melting point. The data were sequentially processed using the Convert Light-Cycler 480 and LineRegPCR software. The expression of each gene was analyzed in triplicate.

Statistics

The obtained data were analyzed with parametric methods using the Excel software; The Cell Quest software was used for the analysis of flow cytometry data. Differences were considered to be statistically significant at $p < 0.05$.

RESULTS AND DISCUSSION

Expression of adhesion molecules by Ea.hy926 cells in 2D and 3D cultures

Normally, the endothelial cells lining the vessels are interconnected by ICAM-1, VCAM-1, and PECAM-1 adhesion molecules, as well as by a number of other actin-associated molecules, which enables the rapid cytoskeletal rearrangement necessary for leukocyte extravasation into tissues during an inflammation [6]. Unlike endothelial cells, epithelial cells are interconnected via tighter cadherin contacts that are linked to the keratin filaments of the cytoskeleton. Epithelial cells form 3D cultures of varying densities, depending

Table 1. Primers for qPCR [36]

Gene	Primer	Nucleotide sequence, 5' → 3'	Amplicon size, b.p.	T_m, °C
β-actin	BAf	TCATGTTTGAGACCTTCAACAC	512	55
	BAr	GTCTTTGCGGATGTCCACG		
GM-CSF	GMf	CTGCTGCTGAGATGAATGAAACAG	195	55
	GMr	GCACAGGAAGTTTCCGGGGT		
ICAM-1	ICAMf	ACCATGGAGCCAATTTCTC	590	51
	ICAMr	ACAATCCCTCTCGTCCAG		
IL-6	IL6d	GATGCAATAACCACCCCTGACCC	173	52
	IL6r	CAATCTGAGGTGCCCATGCTAC		
VEGFR-2	VEGFR2f	ATGCTCAGCAGGATGGCAA	320	53
	VEGFR2r	TTTGGTTCTGTCTTCCAAAGT		

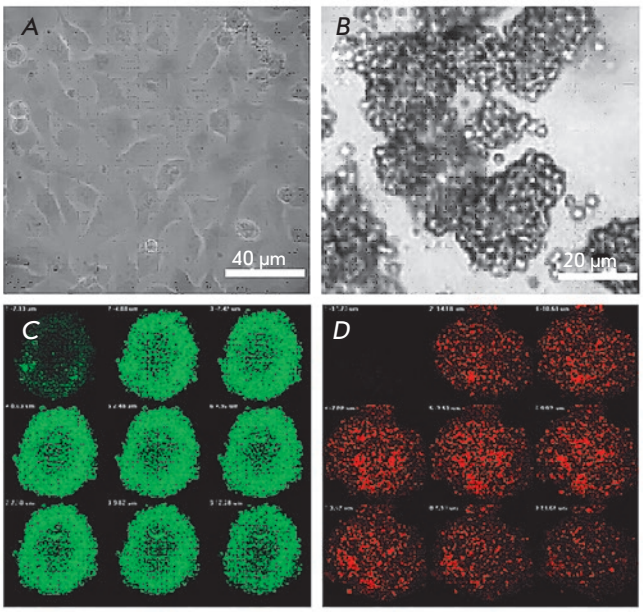

Fig. 1. Morphology of Ea.hy926 cells under 2D and 3D cultivation conditions. Ea.hy926 cells 48 h after transfer onto a culture plate (*A*) or a plate with an anti-adhesive coating pHEMA (*B*); light microscopy. Z-stacks of 3D cultures stained with antibodies to ICAM-1 (*C*, green) and VEGFR-2 (*D*, red); confocal microscopy

on the number of cadherin contacts [37]. Previously, there had been no attempts to produce 3D cultures of endothelial cells which would be similar to epithelial cell cultures. Clinostatted cultures, called 3D-cultures in some works, are monolayer cultures grown by rotation in a gravity field [32–35]. Cultivation for 5 to 6 days results in the development of spheroids on the monolayer surface, which are used for an analysis [33]. However, this prolonged cultivation disables the evaluation of the effects of fast-acting factors: e.g., TNF.

In this study, Ea.hy926 cells were cultured on an anti-adhesive pHEMA substrate, which resulted in the formation (within 18 h) of 200–400 μm cell clusters indestructible by pipetting (*Fig. 1B*), which confirmed the formation of intercellular contacts throughout the cell surface. In the 2D culture, cells formed a tight monolayer where they formed contacts only along the perimeter (*Fig. 1A*). A confocal analysis of 3D cultures revealed a different expression level of adhesion molecules, depending on the location of the cells in the culture. For example, in Ea.hy926 3D cultures, the level of ICAM-1 expression is higher in cells of the surface layer (*Fig. 1C*), while VEGFR-2 is uniformly expressed by all cells of the spheroid (*Fig. 1D*). Reduced expression of adhesion molecules inside the spheroid is associated with the formation of a hierarchy of cells. The presence of adhesion contacts throughout the cell surface reduces the expression of adhesion molecules – the cell is in the equilibrium state. On the spheroid surface, cells are in contact with the lower layer and have no contacts on the apical surface, which stimulates the expression of adhesion molecules and mimics damage repair in epithelial tissues. Unlike ICAM-1, VEGFR-2 is uniformly expressed throughout the bulk of the spheroid: therefore, endothelial cells, like epithelial cells, proved able of forming internally hierarchical spheroids in static cultures.

Earlier, studies of Ea.hy926 clinostatted cultures had revealed differences in the expression of adhesion molecules, as well as in spontaneous and TNF-induced cytokine production; in this case, both inhibition [38] and stimulation of the production of several proteins were detected [39]. Expression of adhesion molecules in static 2D and 3D Ea.hy926 cultures in response to TNF and VEGF activation was analyzed using pre-adjusted cell activation conditions. Expression of ICAM-1, VEGFR-2, αvβ3-integrin, and VCAM-1 in the 2D culture under the influence of TNF and VEGF was analyzed by flow cytometry in both early (24 hour incubation) and "old" (72–96 hour incubation) cultures. In addition, the dynamics of the changes in the expression of surface molecules under the influence of factors was studied. There were no changes in the expression of αvβ3-integrin and VCAM-1 (data not shown). VEGF also had no stimulating effect on any of the adhesion molecules. For this reason, the effect of TNF was studied further. TNF was found to act most effectively on early cultures (18–24 h). The effect develops rapidly, achieves a maximum 2–10 h after the addition of TNF, and decreases to control values in 24–36 h. Five hours after the addition of TNF, the expression of ICAM-1 in early cultures increased 13-fold, while the expression of VEGFR-2 remained almost unchanged (*Fig. 2*, *Table 2*). *Figure 2* presents confocal microphotographs of 2D cultures stained with antibodies to ICAM-1 and VEGFR-2 (*Fig. 2C, F*), which show the typical membrane location of these molecules.

The comparative data on TNF- and VEGF-induced expression of ICAM-1 and VEGFR-2 in 2D and 3D Ea.hy926 cultures are shown in *Fig. 3*. A more homogeneous pool of cells was shown to form in 3D-cultures. For example, 10–20% of cells in 2D cultures do not express adhesion molecules (a peak in the autofluorescence area), but this parameter is significantly lower (0–5%) in 3D cultures. Unlike ICAM-1, spontaneous expression of VEGFR-2 in 3D cultures is reduced by 50%, despite the absence of the first peak (*Table 2, Fig. 3D*). In all 3D cultures, expression of VEGFR-2 was statistically significantly lower than in 2D cultures, which demonstrates the role of contact interactions in the expression of VEGFR-2 by Ea.hy926 cells.

Table 2. Effect of TNF and VEGF on the expression of ICAM-1 and VEGFR-2 by Ea.hy926 cells in 2D and 3D cultures

Culture	Expression	Control	TNF	p	VEGF	p
2D	ICAM-1	49 ± 11	862 ± 148*	< 0.001	57 ± 14	> 0.05
3D	ICAM-1	70 ± 15	630 ± 93	< 0.001	63 ± 14	> 0.05
2D	VEGFR-2	59± 11	71 ± 18	> 0.05	67 ± 16	> 0.05
3D	VEGFR-2	32 ± 8**	35 ± 8**	>0.05	28 ± 7**	> 0.05

The data are presented as relative fluorescence units.
*TNF and VEGF were added to a concentration of 25 ng/mL in the last 5 hours of incubation. Expression was assessed by flow cytometry. The effect of a statistically significant increase in TNFα-induced expression compared to the control is shown in bold.
**Statistically significant reduction in VEGFR-2 expression in 3D compared to that in 2D.

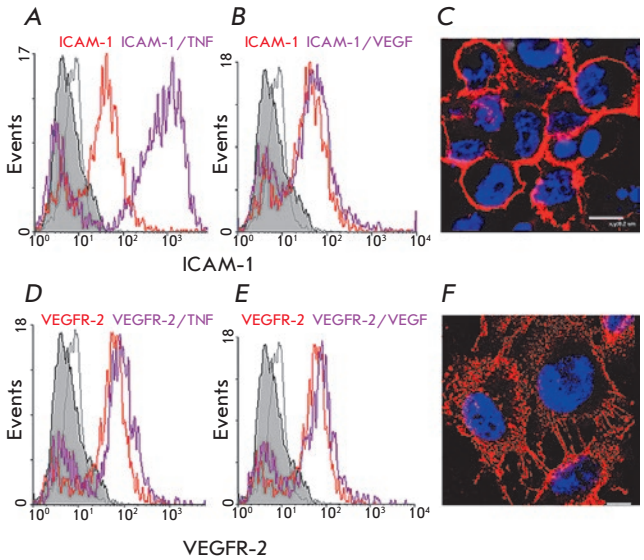

Fig. 2. Expression of ICAM-1 and VEGFR-2 in Ea.hy926 cells under the influence of TNF and VEGF A analyzed by confocal microscopy and flow cytometry. *A*, *B*, *D*, *E* – the Y axis is the mean fluorescence intensity; the X axis is the number of events. Ea.hy926 cells were grown under 2D conditions until a confluent monolayer. TNF (*A* and *D*) or VEGF (*B* and *E*) were added (25 ng/mL). The incubation time is 5 hours. Expression of certain proteins by the cells is displayed as fluorescence peaks of antibodies bound to the proteins. The solid gray peak is unstained cells; the gray line is cells with secondary antibodies (negative control); the red line is inactivated cells stained with specific antibodies; the purple line is cells stained with specific antibodies after stimulation by factors. *C* and *F* are representative confocal images of cells stained with antibodies to ICAM-1 (*C*, red) and VEGFR-2 (*F*, red). Cell nuclei are stained with Hoechst 33342 (blue). The scale bar equals C – 8 μm, F – 5 μm

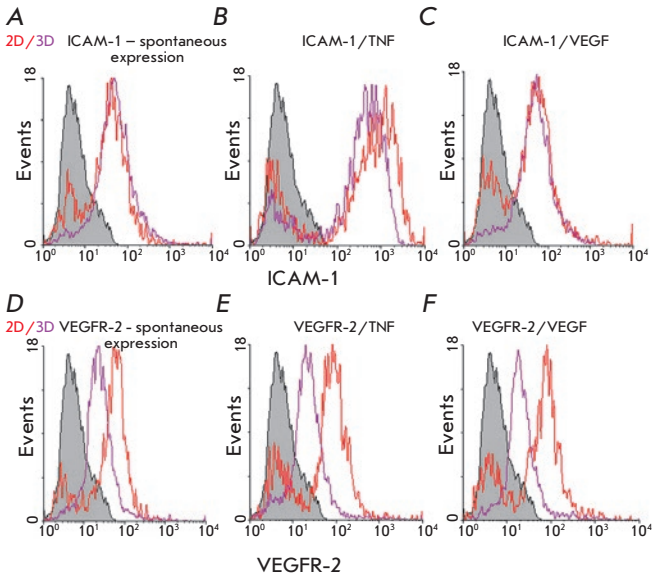

Fig. 3. ICAM-1 and VEGFR-2 expression in TNF- or VEGFA-treated Ea.hy926 cells under 2D and 3D conditions compared by flow cytometry. The Y axis is the mean fluorescence intensity; the X axis is the number of events. Ea.hy926 cells were grown under 2D or 3D conditions for 3 days and stained with antibodies to ICAM-1 (*A*–*C*) or VEGFR-2 (*D*–*F*). Cultures were added with TNF (*B*, *E*) or VEGF (*C*, *F*) to a concentration of 25 ng/mL within the last 5 hours. The solid gray peak is the autofluorescence of unstained cells; the red line is the autofluorescence peak of 2D culture cells stained with specific antibodies; the violet line is the autofluorescence peak of 3D culture cells stained in the same way

Expression of ICAM-1 in both 3D and 2D cultures was enhanced by TNF, but the increase was less pronounced in 2D cultures (7- and 11-fold, respectively). In this case, a negative population emerged, like in all 2D cultures (*Fig. 3B*). VEGF did not affect the expression of adhesion molecules in 3D cultures.

In general, the influence of various factors on the expression level of adhesion molecules in 3D cultures was insignificant compared to that in 2D cultures.

Production of cytokines by Ea.hy926 cells in 2D and 3D cultures

One of the indicators of endothelial cell activation is the production of humoral factors: cytokines, chemokines, and growth factors. Because there were no changes in the expression level of adhesion molecules under the influence of VEGF, the production of cytokines in 2D and 3D cultures was analyzed only in the presence of TNF. We analyzed the production of eleven factors, including IL-2, -4, -6, -8, -10, GM-CSF, IFN-γ, transforming growth factors beta (TGF-β) 1–3, and chemokine IP-10. In the absence of TNF, Ea.hy926 cells were found to produce a significant amount of only IL-8 (13.7g/mL) and TGF-β1 (7.5 ng/mL), with the production in 3D cultures being significantly higher (2- to 3-fold) (*Fig. 4A, B*). Under the influence of TNF, production of IL-8 in 2D cultures (19 ng/mL) increased to a spontaneous level in 3D cultures (22 ng/mL) and did not change in 3D cultures (*Fig. 4C, D*). Treatment with TNF resulted in a cytokine production comparable in 2D and 3D cultures, which decreased in the IL-6 > IL-10 > IL-2 > IFN-γ > IL-4 series (*Fig. 4C, D*). The ratio of spontaneous and TNF-induced production 3D/2D is shown in *Fig. 4E,F*. Spontaneous 3D cultures produced statistically significantly larger (2- to 5-fold) amounts of IL-8, IL-6, IL-10, TGF-β 1–3, and IP-10, while they almost lacked (below the detection limit in 2D cultures) IL-2, IL-4, IFN-γ, and GM-CSF (*Fig. 4E*). In TNF-stimulated cultures, the main difference occurred in the production of GM-CSF and IL-10 (*Fig. 4F*). Secretion of IL-10, GM-CSF, and IL-6 in 3D cultures compared to that in 2D cultures increased 11-, 4.7-, and 1.6-fold, respectively. At the same time, secretion of IL-4, IFN-γ, TGF-β2, and TGF-β3 in 3D cultures compared to that in 2D cultures decreased 2-, 1.4-, 1.6-, and 1.6-fold, respectively (*Fig. 4F*).

Comparison of mRNA and protein synthesis by Ea.hy926 cells in 2D and 3D cultures

Early events in Ea.hy926 cultures after TNF activation were analyzed based on the expression of the *ICAM-1*, *VEGFR-2*, *GM-CSF*, and *IL-6* genes evaluated by qPCR. The qPCR data are normalized to the expression of actin mRNA and presented as a relative gene expression (RGE) that is calculated by the formula $RGE = 2^{-ddCt}$ [40]. This method assesses the change in the number of gene copies in TNF-activated 2D and 3D cultures compared to that in the control (*Fig. 5A*). It is also possible to compare gene expression under 3D and 2D conditions in the presence and absence of TNF (*Fig. 5C*). *Figure 5* compares the expression of VEGFR-2 and ICAM-1 in Ea.hy926 cell cultures without stimulation and after stimulation with TNF for 5 h, assessed by qPCR (*Fig. 5A, C*) and flow cytometry (*Fig. 5B, D*). TNF significantly increased the synthesis of ICAM-1 mRNA both in 2D and 3D cultures (*Fig. 5A*), which correlated with the flow cytometry data (*Fig. 5B*). The effect of TNF was lower in 3D cultures. According to the qPCR data, expression of VEGFR-2 increased slightly, but reliably (*Fig. 5C*); in this case, the protein level evaluated by flow cytometry did not change. The difference in the data may be associated with non-optimal qPCR conditions (different length of the primers, *Table 1*). In any case, the effect of TNF on the expression of the ICAM-1 gene was significantly greater than on VEGFR-2.

Expression of the *GM-CSF* and *IL-6* genes was analyzed in a similar manner. RNA was isolated 5 h after the addition of TNF. Parallel cultures were used to analyze the synthesis of proteins; the supernatant was harvested 30 h after activation by TNF.

Figure 6 shows the level of spontaneous and TNF-induced synthesis of mRNA and the production of GM-CSF and IL-6 proteins. Under the influence of TNF, both the synthesis of mRNA and the production of both proteins were enhanced. Stimulation of GM-CSF was more pronounced in 3D cultures, whereas stimulation of IL-6 was more effective in 2D cultures (*Fig. 6A, B*). Comparison of the efficiency of mRNA and protein synthesis in 2D and 3D cultures did not reveal differences in the level of gene expression (*Fig. 6C*). Spontaneous production of GM-CSF was identical under 2D and 3D conditions, whereas IL-6 production in 3D cultures was significantly higher. Upon stimulation with TNF, the differences shrank and higher production of both GM-CSF and IL-6 was observed in 3D cultures (*Fig. 6D*).

CONCLUSION

For the first time, we have demonstrated that Ea.hy926 endothelial cells can be cultured on an anti-adhesive substrate under static conditions. In spontaneous Ea.hy926 cultures under 3D conditions, the production of both pro-inflammatory and anti-inflammatory factors is increased compared to that under 2D conditions, which enables a more detailed analysis when testing new therapeutic agents. TNF activation similarly affects Ea.hy926 cells cultured under 2D or 3D conditions,

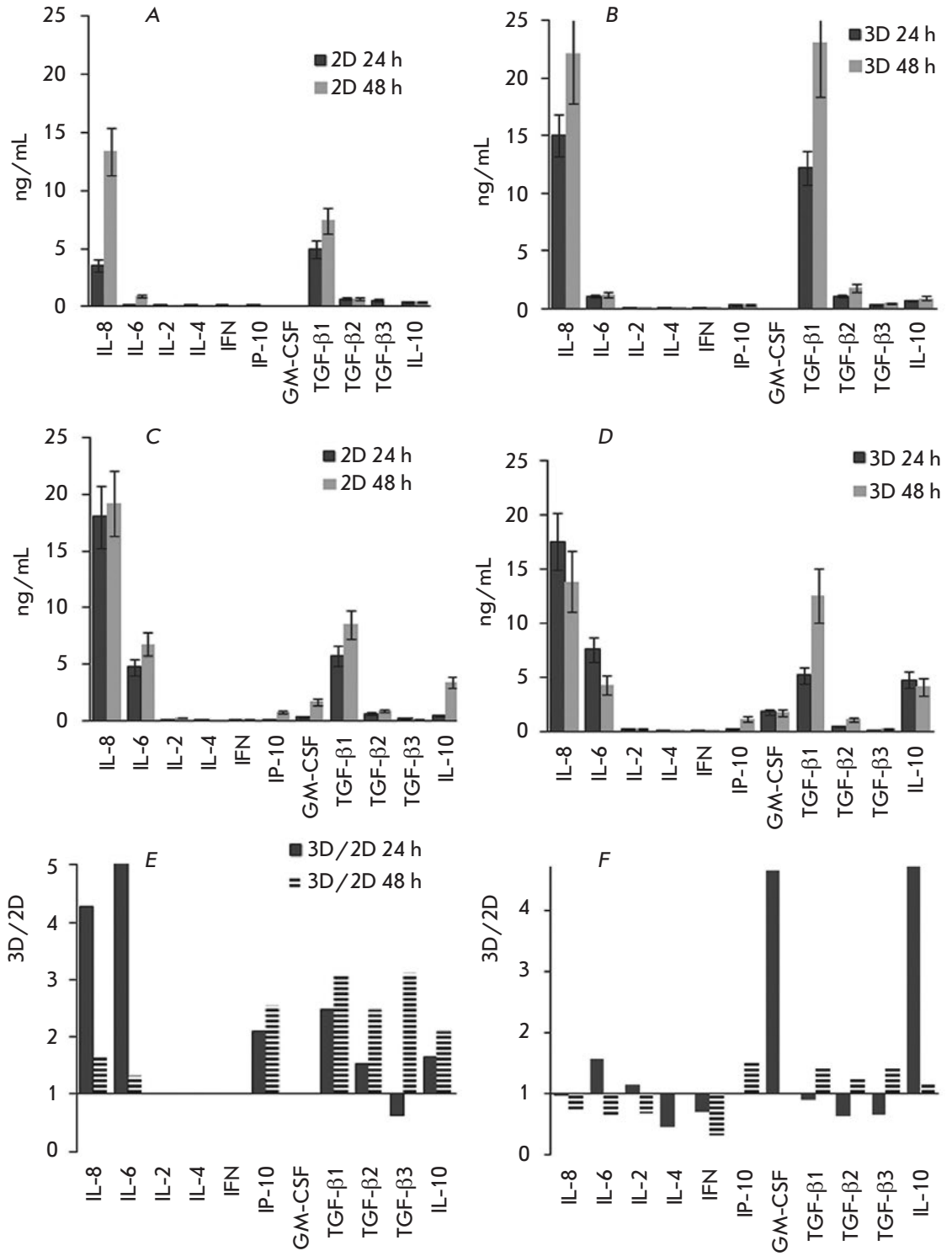

Fig. 4. Secretion of humoral factors by Ea.hy926 cells cultured under 2D and 3D conditions. Ea.hy926 cells were cultured in 24-well plates until adhesion or on an anti-adhesive substrate to form 3D cultures. Then, TNF was added to the medium to a concentration of 25 ng/mL. Supernatants were harvested 24 and 48 h after TNF addition. Production of soluble factors in 2D (*A* and *C*) or in 3D (*B* and *D*) cultures without TNF (*A* and *B*) and after TNF addition (*C* and *D*). The ratio of factor concentrations in 3D/2D cultures without stimulation (*E*) and after TNF addition (*F*). The concentration was determined by flow cytometry with microparticles according to the manufacturer's protocol (BioRad) using calibration curves

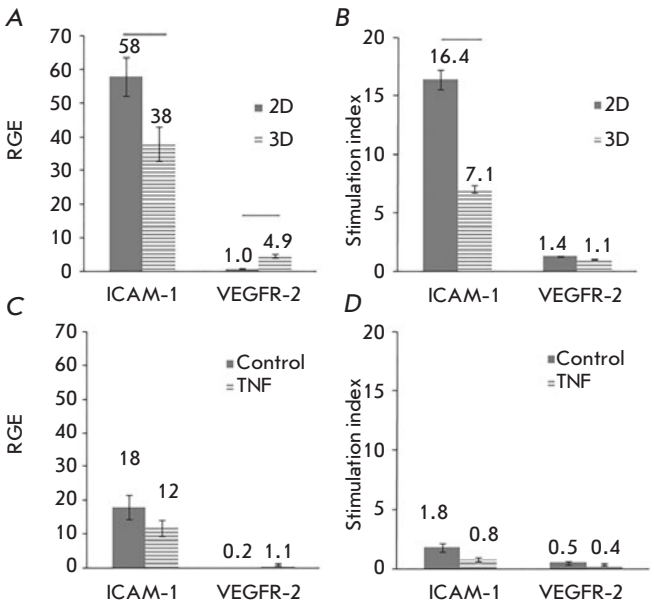

Fig. 5. Expression of VEGFR-2 and ICAM-1 in Ea.hy926 cell cultures with and without addition of TNF analyzed by qPCR and flow cytometry. Ea.hy926 cells were grown under 2D (*A* and *B*) and 3D (*C* and *D*) conditions for 18 h to form a monolayer or spheroids, and then TNF was added to a concentration of 25 ng/mL. After 5 h, a portion of the cultures was used for the generation of mRNA, cDNA synthesis, and qPCR (*A* and *C*). Parallel cultures were incubated for 36 h and analyzed by flow cytometry after staining with antibodies to VEGFR-2 and ICAM-1 (*B* and *D*). The statistically significant difference (<0.05) is indicated by bars. The data are presented as a relative gene expression (RGE) (*A* and *C*). RGE was calculated by the formula RGE = 2^{-ddCt} [40], where 2D cultures with TNF were compared to control without TNF, and 3D cultures with TNF were compared to control without TNF (*A*). Similarly, 3D was compared to 2D and without TNF (*C*). Cytometry data are presented as a ratio of MFI in a TNF-activated culture to that in the control without TNF (*B*) or MFI in a 3D culture to that in a 2D culture (*D*)

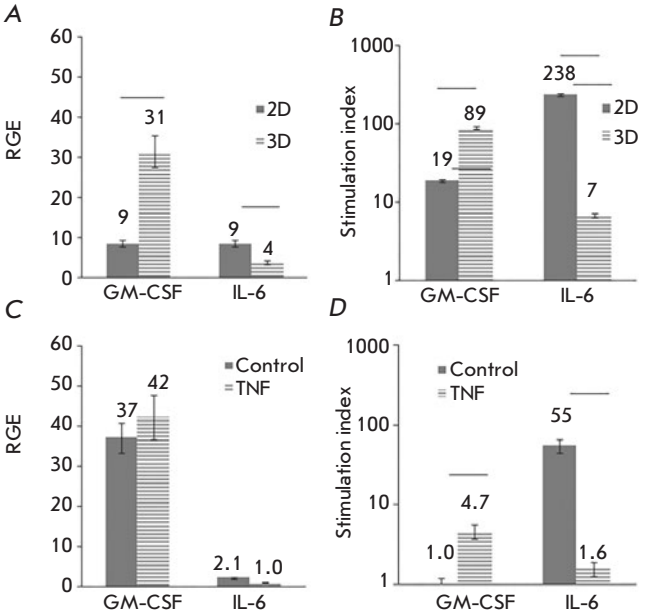

Fig. 6. Production of GM-CSF and IL-6 in Ea.hy926 cell cultures with and without the addition of TNF analyzed by qPCR (*A* and *C*) and flow cytometry (*B* and *D*). Culture conditions and data processing were identical to those in *Figure 5*

except for a 4- to 5-fold increase in the production of GM-CSF and IL-10 in 3D cultures. The most typical markers of Ea.hy926 cells are the adhesion molecule ICAM-1 and soluble factors IL-6, IL-8, TGF-β1, and IL-10. 3D cultures are easy to manipulate; they can be transferred onto new plates, e.g., 96-well plates, which enables one to study a panel of drugs in different dilutions. Confocal microscopy analysis does not require growing cells on glass slides. All these facts make the 3D culture of Ea.hy926 cells convenient for the screening of new anti-inflammatory and angiostatic drugs. ●

The authors are grateful to S.A. Kondrat'eva of the Laboratory of Human Genes Structure and Functions of the Institute of Bioorganic Chemistry of the Russian Academy of Sciences for assistance in processing qPCR data.

This work was supported by a grant from the Program of the Presidium of the Russian Academy of Sciences "Molecular and cellular biology," a grant from the President of the Russian Federation for state support to the leading scientific schools of the Russian Federation NSh-8384.2016.4, and a grant from the UMNIK program of the Foundation for the Promotion of Small Forms of Enterprises in the Science and Technology Sphere.

REFERENCES

1. Astrakhantseva I.V., Efimov G.A., Drutskaya M.S., Kruglov A.A., Nedospasov S.A. // Biochemistry. 2014. V. 79. № 12. P. 1308–1321.

2. Petrovskaya L.E., Shingarova L.N., Kryukova E.A., Boldyreva E.F., Yakimov S.A., Guryanova S.V., Novoseletsky V.N., Dolgikh D.A., Kirpichnikov M.P. // Biochemistry. 2012. V. 77. № 1. P. 79–89.

3. Arjamaa O., Aaltonen V., Piippo N., Csont T., Petrovski G., Kaarniranta K., Kauppinen A. // Graefe's Arch. Clin. Exp. Ophthalmol. 2017. Doi: 10.1007/s00417-017-3711-0
4. Song H., Kim Y., Cho H., Kim S., Kang M., Kim J., Min H., Kang J., Yoon J., Kim C. // Am. J. Respir. Cell Mol. Biol. 2017. Doi: 10.1165/rcmb.2016-0080OC
5. Bauer K., Mierke C., Behrens J. // Int. J. Cancer. 2007. V. 121. № 9. P. 1910–1918.
6. Pober J.S., Sessa W.C. // Nat. Rev. Immunol. 2007. V. 7. P. 803–815.
7. Bouis D., Hospers G.A., Meijer C., Molema G., Mulder N.H. // Angiogenesis. 2001. V. 4. № 2. P. 91–102.
8. Cervenak L., Morbidelli L., Donati D., Donnini S., Kambayashi T., Wilson J.L., Axelson H., Castaños-Velez E., Ljunggren H.G., Malefyt R.D. // Blood. 2000. V. 96. № 7. P. 2568–2573.
9. Meager A. // Cytokine Growth Factor Rev. 1999. V. 10. № 1. P. 27–39.
10. Galley H.F., Blaylock M.G., Dubbels A.M., Webster N.R. // Cell Biol. Internat. 2000. V. 24. № 2. P. 91–99.
11. Melder R.J., Koenig G.C., Witwer B.P., Safabakhsh N., Munn L.L., Jain R.K. // Nat. Med. 1996. V. 2. № 9. P. 992–997.
12. Madri J.A., Graesser D., Haas T. // Biochem. Cell Biol. 1996. V. 74. № 6. P. 749–757.
13. Moens S., Goveia J., Stapor P., Cantelmo A., Carmeliet P. // Cytokine Growth Factor Rev. 2014. V. 25. № 4. P. 473–482.
14. Komaki Y., Yamada A., Komaki F., Kudaravalli P., Micic D., Ido A., Sakuraba A. // J. Autoimmunity. 2017. V. 79. P. 4–16.
15. Bergqvist V., Hertervig E., Gedeon P., Kopljar M., Griph H., Kinhult S., Carneiro A., Marsal J. // Cancer Immunol. Immunotherapy. 2017. V. 66. № 5. P. 581–592.
16. Manegold C., Vansteenkiste J., Cardenal F., Schuette W., Woll P., Ulsperger E., Kerber A., Eckmayr J., von Pawel J. // Invest. New Drugs. 2013. V. 31. № 1. P. 175–182.
17. Hersey P., Sosman J., O'Day S., Richards J., Bedikian A., Gonzalez R., Sharfman W., Weber R., Logan T., Buzoianu M., et al. // Cancer. 2010. V. 116. № 6. P. 1526–1534.
18. Liu Y., Goswami R., Liu C., Sinha S. // Mol. Pharm. 2015. V. 12. № 7. P. 2544–2550.
19. Deyev S., Lebedenko E., Petrovskaya L., Dolgikh D., Gabibov A., Kirpichnikov M. // Russ. Chem. Rev. 2015. V. 84. № 1. P. 1–26.
20. Gebauer M., Skerra A. // Curr. Opin. Chem. Biol. 2009. V. 13. № 3. P. 245–255.
21. Oost B.A., Edgell C.-J.S., Hay C.W., MacGillivray R.T.-A. // Biochem. Cell. Biol. 1986. V. 64. № 7. P. 699–705.
22. Edgell C.-J., McDonald C.C., Graham J.B. // Cell Biology. 1983. V. 80. № 12. P. 3734–3737.
23. Bauer J., Marcolis M., Schreiner C., Edgell C.-J., Azizkhan J., Lazarowski E., Juliano R.L. // J. Cell. Physiol. 1992. V. 153. № 3. P. 437–449.
24. Heiss M., Hellstrom M., Kalen M., May T., Weber H., Hecker M., Augustin H., Korff T. // FASEB J. 2015. V. 29. № 7. P. 3076–3084.
25. Scheglovitova O.N., Sklyankina N.N., Boldyreva N.V., Babayants A.A., Frolova I.S., Kapkaeva M.R. // Vestnik of the RAMS. 2014. V. 3. № 4. P. 31–35.
26. Riesbeck K., Billström A., Tordsson J., Brodin T., Kristensson K., Dohlsten M. // Clin. Diagn. Lab. Immunol. 1998. V. 5. № 5. P. 675–682.
27. Chao C., Lii C., Tsai I., Li C., Liu K., Tsai C., Chen H. // J. Agric. Food Chem. 2011. V. 59. P. 5263–5271.
28. Hirschhaeuser F., Menne H., Dittfeld C., West J., Mueller-Klieser W., Kunz-Schughart L. // J. Biotechnol. 2010. V. 148. P. 3–15.
29. Fennema E., Rivron N., Rouwkema J., Blitterswijk C., Boer J. // Trends Biotechnol. 2013. V. 31. № 2. P. 108–115.
30. Page H., Flood P., Reynaud E.G. // Cell Tissue Res. 2013. V. 352. P. 123–131.
31. Breslin S., O'Driscoll L. // Drug Discovery Today. 2013. V. 18. № 5–6. P. 240–249.
32. Ma X., Sickmann A., Pietsch J., Wildgruber R., Weber G., Infanger M., Bauer J., Grimm D. // Proteomics. 2014. V. 14. № 6. P. 689–698.
33. Ma X., Wehland M., Schulz H., Saar K., Hübner N., Infanger M., Bauer J., Grimm D. // PLoS One. 2013. V. 8. № 5. P. 1–10.
34. Sokolovskaya A.A., Ignashkova T.I., Bochenkova A.V., Moskovtsev A.A., Baranov V.M., Kubatiev A.A. // Acta Astronautica. 2014. V. 99. P. 16–23.
35. Grimm D., Bauer J., Ulbrich C., Westphal K., Wehland M., Infanger M., Aleshcheva G., Pietsch J., Ghardi M., Beck M., et al. // Tissue Engineering: Part A. 2010. V. 16. № 5. P. 1559–1573.
36. Unger R.E., Krump-Konvalinkova V., Peters K., Kirkpatrick C.J. // Microvascular Res. 2002. V. 64. P. 384–397.
37. Kim J.B. // Semin. Cancer Biol. 2005. V. 15. № 5. P. 365–377.
38. Griffoni C., Di Molfetta S., Fantozzi L., Zanetti C., Pippia P., Tomasi V., Spisni E. // J. Cell Biochem. 2011. V. 112. № 1. P. 265–272.
39. Sanchez-Bustamante C., Kelm J-M., Mitta B., Fussenegger M. // Biotechnol. Bioeng. 2006. V. 93. № 1. P. 169–180.
40. Livak K.J., Schmittgen T.D. // Methods. 2001. V. 25. № 4. P. 402–408.

The *PTENP1* Pseudogene, Unlike the *PTEN* Gene, Is Methylated in Normal Endometrium, As Well As in Endometrial Hyperplasias and Carcinomas in Middle-Aged and Elderly Females

T. F. Kovalenko[1], K. V. Morozova[2], L. A. Ozolinya[2], I. A. Lapina[2], L. I. Patrushev[1*]

[1]Shemyakin-Ovchinnikov Institute of Bioorganic Chemistry Russian Academy of Sciences, Miklukho-Maklaya Str. 16/10, Moscow, 117997, Russia

[2]Pirogov Russian National Research Medical University, Ostrovitjanova Str. 1, Moscow, 117997, Russia

*E-mail: patrush@ibch.ru

Received: March 09, 2017; in final form October 03, 2017

ABSTRACT **The tumor suppressor PTEN controls multiple cellular functions, including cell cycle, apoptosis, senescence, transcription, and mRNA translation of numerous genes. In tumor cells, PTEN is frequently inactivated by genetic mutations and epimutations. The aim of this study was to investigate the methylation patterns of the *PTEN* gene and its pseudogene *PTENP1* as potential genetic markers of endometrial hyperplasia (EH) and endometrial carcinoma (EC). Methylation of the 5'-terminal regions of the *PTEN* and *PTENP1* sequences was studied using methyl-sensitive PCR of genomic DNA isolated from 57 cancer, 43 endometrial hyperplasia, and normal tissue samples of 24 females aged 17–34 years and 19 females aged 45–65 years, as well as 20 peripheral venous blood samples of EC patients. None of the analyzed DNA samples carried a methylated *PTEN* gene. On the contrary, the *PTENP1* pseudogene was methylated in all analyzed tissues, except for the peripheral blood. Comparison of *PTENP1* methylation rates revealed no differences between the EC and EH groups ($0.80 < p < 0.50$). In all these groups, the methylation level was high (71–77% in patients *vs.* 58% in controls). Differences in *PTENP1* methylation rates between normal endometrium in young (4%) and middle-aged and elderly (58%) females were significant ($p < 0.001$). These findings suggest that *PTENP1* pseudogene methylation may reflect age-related changes in the body and is not directly related to the endometrium pathology under study. It is assumed that, depending on the influence of a methylated *PTENP1* pseudogene on *PTEN* gene expression, the pseudogene methylation may protect against the development of EC and/or serve as a marker of a precancerous condition of endometrial cells.**

KEYWORDS **endometrial carcinoma, endometrial hyperplasia, DNA methylation, *PTEN*, *PTENP1*, long non-coding RNA.**

ABBREVIATIONS **asRNA – antisence RNA; ceRNA – competing endogenous RNA; EC – endometrial carcinoma; EH – endometrial hyperplasia; lncRNA – long non-coding RNA; MAE – middle-aged (45–55 years) and elderly (> 55 years) females; miRNA – micro RNA; MRE – microRNA recognition element; PICS – PTEN-loss-induced cellular senescence; PTEN – phosphatase and tensin homolog; sRNA – sense RNA.**

INTRODUCTION

Endometrial carcinoma (EC) is one of the most common cancers of the female reproductive tract, with the EC rate accounting for 4.8% of all cancers in females [1]. The risk of EC increases with age: by the age of 75, the cumulative risks of the disease reach 1%, and deaths – 0.2%. Although EC is considered as a postmenopausal disease that develops in females older than 50 years, up to 14% of clinical EC cases are diagnosed in premenopausal age; of these, only 5% occurr in females under 40 years [2–4]. Growing rates of obesity and metabolic syndrome in the populations of Europe and North America, which are accompanied by an increase in the level of endogenous estrogens, as well as the general aging of the population in these countries suggest a significant increase in the incidence rate of the disease

in these regions in the near future [5]. All these facts dictate the need to study etiology, as well as search for biomarkers, for an early diagnosis of EC to prevent and provide for timely adequate treatment of the disease.

Depending on the field of application in medicine, biomarkers are usually divided into prognostic, predictive, and pharmacodynamic [6]. Biomarkers of the first type are used to assess a disease's severity and the survival rate of patients regardless of the treatment. Predictive biomarkers predict the response of patients to the treatment, and pharmacodynamic biomarkers predict the patient's response to drugs, with allowance for the genetic characteristics of the molecular targets of the used drugs, as well as the enzymes of their metabolism.

On the basis of biomarkers, ECs are traditionally divided into two subtypes [1, 7–9]. The most common and usually sporadic type I Es are usually characterized by the presence of highly differentiated cells and are histologically endometrioid, with tumor cells having the normal diploid karyotype and microsatellite instability (MSI) and expressing estrogen receptors (ERs) and progesterone receptors (PRs). In the case of type I ECs, mutations in the *TP53* tumor suppressor gene are rare and patients have a good chance of recovering. In contrast, type II ECs do not belong to endometrioid tumors and contain low-differentiated cells, many of which are characterized by aneuploidy, an absence of genetic changes in the p53 protein, and lack of ER and PR expression. In this case, the disease course has an unfavorable prognosis. Based on the data of a histological and molecular genetic analysis, type II ECs may be divided into several additional subtypes, including serous and clear-cell ECs, as well as sarcinosarcoma [1]. A recent meta-analysis of mutations in endometrial tumors using deep sequencing of genomic DNA also revealed a significant heterogeneity of their mutational spectra and enabled researchers to divide ECs into four groups [7].

One of the risk factors for EC is the hyperplastic processes in the endometrium, which occur in a setting of an imbalance of endogenous steroid hormones: estrogens and progesterone [10–12]. EH is characterized by excessive proliferation of cells, which is accompanied by typical morphological changes in tissue. According to the 1994 WHO classification, endometrial hyperplasia includes EH without atypia and EH with atypia, which, in turn, are divided into simple and complex forms [10, 11]. Timely identified EHs usually respond well to therapy. However, complex EHs without atypia and with atypia are transformed into EC in approximately 25 and 50% of cases, respectively [13]. Both cancer and hyperplasia are associated, to varying degrees, with control over cell proliferation, which is accompanied by an increase in the number of cells per unit volume of tissue.

Mutations in the genes of the PI3K/AKT signaling pathway are more typical of EC cells than other types of tumor cells [7, 14]. Serine-threonine protein kinase AKT regulates many cellular functions [15]. The most important negative regulator of signal transduction through this pathway is dual specificity phosphatase PTEN. Mutations in the *PTEN* gene that is located on chromosome 10q23.3 are often detected in EH and in 93% of EC cases. The main PTEN substrate is a secondary messenger phosphatidylinositol-(3,4,5)-trisphosphate (PIP3); under the action of PTEN, PIP3 loses the 3'-phosphate group, transforming into PIP2. Dephosphorylated PIP2 is incapable of activating AKT, which blocks signal transduction through this pathway and suppresses many cellular activities and functions, including cell cycle, apoptosis, cell mobility and polarity, cellular senescence, stem cell renewal, and transcription and translation processes. The suppressor properties of PTEN are also associated with its alternative protein phosphatase activity that is involved in the dephosphorylation of pro-apoptotic proteins, protein kinases, and transcription factors [15–17]. Recently, extracellular and intranuclear suppressor PTEN functions independent of its phosphatase activity were discovered [18]. All these facts suggest that PTEN is an important prognostic and predictive biomarker of carcinogenesis [19] and shed light on the molecular mechanisms of PTEN involvement in the etiology of EC and emphasize the need to study the regulation of its activity in health and in EC.

In normal tissues, the *PTEN* gene is expressed constitutively and its functions are under strict control [17, 20]. The *PTEN* activity is regulated at all levels of its expression: via activation and suppression of transcription [21–23]; post-transcriptionally, at the mRNA level, with the involvement of numerous microRNAs [24, 25]; at the post-translational level, through covalent modifications to a protein product and interactions with numerous membrane, cytoplasmic, and nuclear proteins [20]. Both positive and negative control over the *PTEN* gene transcription involves several transcription factors, and suppression of *PTEN* transcription involves epigenetic mechanisms. The latter include methylation of the promoter DNA regions of the *PTEN* gene, as well as chromatin histone deacetylation at the promoter. Therefore, the available data demonstrate that inactivation of the *PTEN* tumor suppressor gene, which is associated with tumor progression in EH and EC, can occur under the influence of both genetic and epigenetic mutations.

The processed (intron-free) pseudogene *PTENP1* located on chromosome 9p13.3 has 98.6% homology

with the functional *PTEN* gene but does not express the PTEN protein, due to mutation-induced loss of the translation initiation codon [26]. *PTENP1* is usually transcribed to form three long non-coding RNAs (lncRNAs): one sense RNA (sRNA) and two antisense, α and β, RNAs (asRNAs) [27]. Transcription occurs from two opposite overlapping promoters, and the resulting transcripts perform important regulatory functions: sRNA exhibits competing endogenous RNA (ceRNA) properties in the cell [28–30]. According to this mechanism, the microRNA (miRNA) binding sites, MREs, located on pseudogene sRNAs compete with *PTEN* gene mRNA MREs for the specific miRNAs interacting with them, preventing their inhibitory effect on the translocation of PTEN mRNA. Polyadenylated asRNA-β acts similarly. It interacts with the 5'-end of non-polyadenylated PTENP1-sRNA and stabilizes it, enabling a higher competing action of the latter. In contrast, asNRNA-α enables delivery of at least two proteins involved in chromatin rearrangement (DNA methyltransferase 3A (DNMT3A) and the enhancer of Zeste homolog 2 (EZH2)) to the *PTEN* gene promoter [27]. These proteins enable histone H3 lysine 27 trimethylation (H3K27me3), a marker of inactive chromatin with suppressed transcription. A divergent effect of *PTENP1* pseudogene transcripts on the expression of the *PTEN* tumor suppressor gene suggests the need for fine regulation of their ratio in the cell. The mechanisms of this regulation, which may be impaired in tumors, have not been studied. Indeed, *PTENP1* pseudogene deletions have been found in sporadic rectal tumors [28], as well as in primary and metastatic melanoma [31]. Another potential mechanism of *PTENP1* pseudogene inactivation by methylation of its promoter region was identified in lung cancer [32] and, recently, in clear cell renal cancer [33].

Previously, we had discovered methylation of the 5'-terminal promoter region of the *PTENP1* pseudogene in EC and EH [34]. In the present work, *PTENP1* methylation in EC and EH was studied in detail and methylation of the studied pseudogene region was, for the first time, detected in normal endometrial cells of middle-aged and elderly (MAE) females. In addition, we analyzed the methylation status of *PTEN* gene promoter regions that had not been previously studied in EC and EH.

EXPERIMENTAL

Patients and tissue samples

In this study, we used tissue samples from 143 female patients from the Blokhin Russian Cancer Research Center and Moscow Clinical Hospitals No. 4 and 55. The study included tissue samples from 57 EC patients (mean age, 61.9 ± 7.8 years) and 43 patients with simple endometrial hyperplasia (mean age, 52.1 ± 6.5 years). In addition, we studied peripheral venous blood in 20 EC patients from the main group (mean age, 57.1 ± 7.6 years) who were detected with *PTENP1* methylation in the endometrium. The control group consisted of 43 females with a histologically intact endometrium who were examined because of suspicion of endometrial precancer. This group included two subgroups: 24 females aged 17 to 34 years (mean age, 24.2 ± 4.8 years) and 19 females aged 45 to 65 years (mean age, 52.5 ± 6.0 years). Comparison of the mean age in the control subgroup (45–65 years) and the group of EC patients (57 patients) using the Mann-Whitney test revealed statistically significant differences ($p < 0.05$). For this reason, when comparing *PTENP1* pseudogene methylation, we excluded females older than 59 years from the group of EC patients and allocated a subgroup of 24 patients (48–59 years; mean age, 54.3 ± 3.4 years) who did not differ from the controls in this parameter ($p = 0.095$). We used both fresh-frozen tissues obtained during surgery or biopsy and samples fixed with formalin and embedded in paraffin blocks. Peripheral venous blood was collected by puncturing the ulnar vein. A 3.8% sodium citrate solution was added at a 1 : 9 ratio as an anticoagulant. The EC stages were classified in accordance with the International Federation of Obstetrics and Gynecology (FIGO) recommendations. The histological EC type was identified in accordance with the World Health Organization recommendations. Consent to data processing was obtained from all patients included in the study.

Isolation and bisulfite conversion of DNA

Genomic DNA was isolated by a standard technique using phenol and guanidine chloride [35]. In the case of tissue samples embedded in paraffin blocks, each block was ground to 10 μm fragments using a microtome. Next, a sample was deparaffinized and DNA was extracted using a slightly modified procedure [36]. The DNA concentration was determined using a Qubit fluorometer (Invitrogen, USA). The bisulfite conversion was performed using an EpiTect Bisulfite Kit (Qiagen, Germany) according to the manufacturer's protocol.

Methyl-sensitive PCR

The reaction mixture (25 μL) contained 67 mM Tris-HCl (pH 8.8), 16.6 mM $(NH_4)_2SO_4$, 0.01% Tween 20, 2 mM $MgCl_2$, four deoxyribonucleoside triphosphates (0.2 mM each; Sibenzyme, Russia), forward and reverse primers (0.5 μM each), 25 ng of bisulfite converted DNA, and 0.5–1.0 units of Taq-DNA polymerase. Taq-DNA polymerase was produced using the recombinant *E. coli* PVG-A1 strain according to a slightly modified pro-

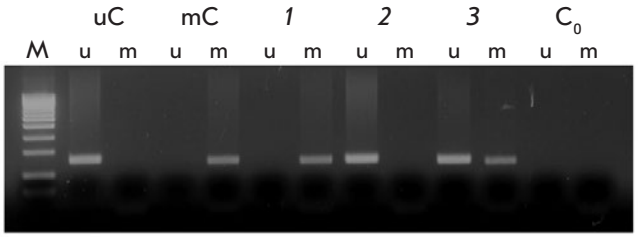

Fig. 1. Analysis of the methylation status of the *PTENP1* pseudogene 5′-terminal region by methyl-sensitive PCR. U and m are products of PCR amplification with primers to an unmethylated or methylated template, respectively. Bisulfite-treated DNA templates: uC – a peripheral blood sample (unmethylated control); mC – a peripheral blood sample methylated by SssI methylase (methylated control); 1–3 – tumor DNA samples with (1) methylated *PTENP1*, (2) unmethylated *PTENP1*, and (3) partially methylated *PTENP1* (some of the tumor cells had unmethylated *PTENP1*); C_0 – amplification without a DNA template; M – a molecular weight marker

cedure by Patrushev et al. [37]. As a fully methylated control, we used DNA isolated from human blood lymphocytes, methylated with SssI methylase (Sibenzyme, Russia) *in vitro*, and treated with sodium bisulfite. Sodium bisulfite-converted DNA from blood lymphocytes served as unmethylated control. After PCR on a Mastercycler pro thermal cycler (Eppendorf, Germany), amplification products were analyzed by electrophoresis on a 3% agarose gel stained with ethidium bromide. A 100 + 50 bp DNA marker (Sibenzyme, Russia) was used as a molecular weight marker. A typical result obtained using methyl-sensitive PCR is shown in *Fig. 1*. Primer sequences, as well as PCR amplification conditions for each pair of primers, are presented in *Table 1*. Annealing temperature for each pair was optimized in a temperature gradient to exclude nonspecific annealing of primers. In addition, the optimal number of cycles was determined to prevent the formation of nonspecific PCR products due to over-amplification. The primers reported in [32] were used for the analysis of the 5'-terminal region of the *PTENP1* pseudogene. The *PN2* region of the *PTEN* gene promoter (*Fig. 2*) was analyzed using primers developed by the authors. The methylation status of the *PN4* and *PN5* loci was analyzed using primers [38] and [32], respectively.

Statistical analysis

The statistical analysis was performed using the SPSS v.22 software package (SPSS Inc.). Differences in the methylation rates of the *PTENP1* pseudogene among groups were assessed using a two-sided Chi-square test and the Fisher exact test. The statistical differences in the mean age among groups were assessed using the Mann-Whitney test.

Table 1. PCR primers and conditions used to determine the methylation status of promoters of the *PTEN* gene and *PTENP1* pseudogene

Primer	Nucleotide sequence, 5'->3'	T_a, °C	Number of PCR cycles	PCR product size, b.p.
PNP1-U-F	TTGTAGTTGTGATGGAAGTTTGAAT	64	33	156
PNP1-U-R	CCACCCCCACAAATACTCACA			
PNP1-M-F	TGTAGTCGTGATGGAAGTTTGAAT	63	33	152
PNP1-M-R	CCCCCGCGAATACTCACG			
PN2-U-F	TTGTAGTTATGATGGAAGTTTGAG	61	33	165
PN2-U-R	CCACCACCACAAACCAACCA			
PN2-M-F	TTGTAGTTATGATGGAAGTTTGAG	61	33	162
PN2-M-R	CGCCGCAAACCGACCGA			
PN4-U-F	GTTGGGGTGTGTGGAGTTTGGTT	61	36	135
PN4-U-R	CCCTCAAACTCCAAATCAATTCACAA			
PN4-M-F	CGCGCGGAGTTTGGTTTCG	62	32	117
PN4-M-R	CAAATCGATTCGCGACGTCG			
PN5-U-F	TATTAGTTTGGGGATTTTTTTTTTGT	60	36	186
PN5-U-R	CCCAACCCTTCCTACACCACA			
PN5-M-F	GTTTGGGGATTTTTTTTTCGC	60	36	178
PN5-M-R	AACCCTTCCTACGCCGCG			

Note. M – methylated; U – unmethylated; F – a forward primer; R – a reverse primer; PNP – primers for amplification of pseudogene regions; PN – primers for amplification of *PTEN* gene regions.

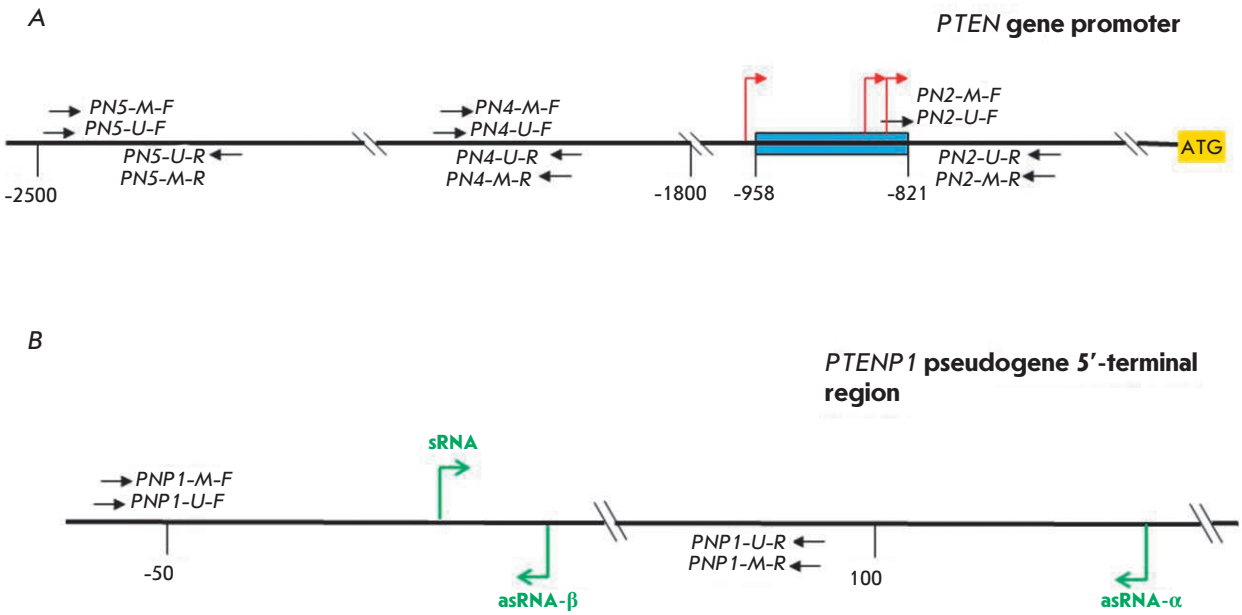

Fig. 2. Studied regions of the *PTEN* gene (A) and *PTENP1* pseudogene (B). A blue rectangle denotes the minimum promoter region of the *PTEN* gene; bent red and green arrows denote the main transcription initiation sites of the *PTEN* gene and of *PTENP1* pseudogene, respectively; black arrows indicate the location of primers for MS PCR; sRNA is sense *PTENP1* RNA; asRNA-α(-β) is antisense *PTENP1* RNA-α(-β); the numbers denote the distance from the ATG codon (A) or sRNA synthesis start site (B)

Table 2. Methylation of promoters of the *PTEN* gene and *PTENP1* pseudogene in normal, hyperplastic, and malignant endometrial tissues

Gene	Blood	Normal endometrium, mean age (extreme values)		Hyperplasia without atypia	Hyperplasia with atypia	Endometrial carcinoma
		24 (17–34)	52.5 (45–65)			
PTEN	0.00 (0/25)*	0.00 (0/24)	0.00 (0/19)	0.00 (0/30)	0.00 (0/13)	0.00 (0/57)
PTENP1	0.00 (0/25)	4.17 (1/24)	57.89 (11/19)	73.33 (22/30)	76.92 (10/13)	70.83 (17/24)**
P		<0.001***		0.351****	0.450****	0.521****

Note. Two-sided Fisher exact test.
*First digit – a percentage of methylated DNA samples; second digit – the number of methylated samples; third digit – the total number of samples.
**A subgroup of patients with age similar to that of the reference control group was selected from the main group of 57 patients with EC.
***Normal endometrium 24 (17–34) *vs.* 52.5 (45–65).
****Compared to normal endometrium 52.5 (45–65).

RESULTS

In this study, we examined three regions near the minimal promoter of the *PTEN* gene, including CpG sequences, which could have potentially been methylated and not analyzed previously in EC (*Fig. 2*). A sequence flanked by *PN2* primers is located 685 bp upstream of the ATG-codon and adjoins directly to the minimal promoter. The region situated between *PN4* primers is located 1,913 bp upstream of the ATG codon. Methylation of this region was studied in melanoma [38]. A sequence situated between *PN5* primers the methylation of which has already been studied in lung cancer is located 2,300 bp upstream of the ATG codon [32].

Starting the study, we first found that the *PTEN* gene was not methylated in the studied promoter regions in any of the DNA samples isolated from the analyzed tissues, including EC, EH, and normal endometrium (*Table 2*). Although this did not exclude genetic mutations in the gene, it indicated that the gene in our patients could not be inactivated by this epigenetic mechanism. Therefore, given the published data, we supposed that *PTEN* inactivation might occur via the

known mechanism of ceRNA through suppression of *PTENP1* pseudogene transcription by methylation of its 5'-terminal region.

Indeed, a high rate of *PTENP1* methylation was found in all endometrial tissue samples, except for the normal endometrium of young females (*Table 2*). At the same time, 73% (8 out of 11, *Table 2*) of normal endometrium samples from MAE females with methylated *PTENP1* were mosaic: i.e., they contained some amount of cells with an unmethylated or partially methylated pseudogene (data not shown). Mosaic methylation of the pseudogene was also detected in several endometrial tissue samples of patients with EH and EC (e.g., *Fig. 1*, lines *3u* and *3m*), which might be due to contamination of tumor biopsy samples by normal cells. Methylation was tissue-specific and was absent in the blood of patients. Comparison of the *PTENP1* methylation rates in the EC and EH groups and in the control group of MAE females did not reveal statistically significant differences between them ($0.45 < p < 0.35$). In all groups, the methylation level was high (71–77% in patients *vs.* 58% in control subgroup 2). At the same time, the mean age of the EC and EH patients included in the study was similar to the mean age of the females in control subgroup 2 (54.3, 52.1, and 52.5 years, respectively). There were also no significant differences in *PTENP1* methylation in subgroups of the main EC group, where patients were divided based on clinical and pathological characteristics: age, disease stage, depth of tumor invasion into the myometrium, differentiation degree of cancer cells, and tumor subtypes (*Table 3*). However, statistically significant differences in the rates of *PTENP1* methylation were found in the normal endometrium of young females (4%) and MAE females (58%) ($p < 0.001$). These results were unexpected. They suggest that *PTENP1* pseudogene methylation reflects primarily age-related changes in the human body and is not directly related to the studied endometrial pathology.

DISCUSSION

In 2001, Salvesen and co-workers tried to analyze the methylation status of the *PTEN* gene promoter in EC. Methylation was detected in 19% of patients. However, these data proved to be erroneous because they did not take into account the high homology between the gene and its pseudogene *PTENP1* [39]. Later, Zysman and co-workers also studied the methylation of the *PTEN* promoter region in EC [40]. In this case, *PTEN*-specific primers were used for methyl-sensitive PCR. Two sites were analyzed: the first one – in the minimal promoter of the *PTEN* gene; the second – near the ATG codon. Both sites were found to be unmethylated. These data suggest that studies of the *PTEN* gene promoter using primers not differentiating between *PTEN* and its pseudogene have detected methylation of *PTENP1*, but not *PTEN*. The methylation status of other *PTEN* gene regions in EC and EH has no longer been analyzed using *PTEN*-specific primers. However, methylation of other promoter regions of this gene was also found in other oncological diseases [32, 38, 41]. Therefore, we supposed that EC tissues might contain methylated sequences of the *PTEN* gene promoter region, with some of them having been previously analyzed and some being new, not studied yet in this disease. Thus, we decided to study a new locus located in the immediate vicinity of the minimum promoter, as well as two distally located sequences that had been analyzed previously (*Fig. 2*, see the Results section for more details). One of them, located between *PN4* primers, was methylated in 60% of melanoma cases [38].

We demonstrated that the analyzed sequences of the *PTEN* gene promoter region were not methylated in any of the studied tissue samples. Given these and published data, we concluded that methylation of the *PTEN* gene promoter was not involved in its inactivation in EC and EH, at least in our patients. Therefore, we supposed that suppression of *PTEN* gene expression in this case might occur via a competing endogenous RNA mechanism or via the involvement of asRNAs through inhibition of *PTENP1* pseudogene transcription by methylation of its promoter region.

In fact, we found a high rate of methylation of the 5'-terminal *PTENP1* region in patients with EC (70.83%), as well as EH with and without atypia (76.92% and 73.33%, respectively, *Table 2*). These results are consistent with the published data. In particular, methylation of the 5'-terminal region of the *PTENP1* pseudogene was detected in 66% of small cell lung cancer cases [32]. However, pseudogene methylation in the endometrial samples of healthy females aged 45–65 years was unexpected. Methylation in this control subgroup occurred in 57.89% of cases. At the same time, *PTENP1* methylation occurred in only 4% of healthy young females aged 17 to 34 years (*Table 2*). The differences in the DNA methylation rates in these subgroups were statistically significant ($p < 0.001$). A further analysis revealed no significant differences in the rates of *PTENP1* methylation between healthy MAE females and patients with EC and EH. Also, there was no correlation between pseudogene methylation and EC stages, cell differentiation degree, depth of invasion into the myometrium, or cancer subtypes (*Table 3*). It should also be emphasized that there is an absence of methylation in the blood of EC patients with pseudogene methylation in the endometrium. These facts indicate the tissue-specific nature of this phenomenon that accompanies changes in a healthy endometrium during aging of the human body.

Table 3. Association of *PTENP1* pseudogene methylation with the clinical and pathological characteristics of endometrial cancer patients

Clinical and pathological characteristics	n	M(U)	M, %	p
Mean age (extreme values)				0.784
55 (48–60)	27	19(8)	70.37	
68 (61–76)	30	20(10)	66.66	
FIGO stage				1.00
I	46	31(15)	67.39	
II + III	11	8(3)	72.73	
Invasion into endometrium				0.359
Yes	17	10(7)	58.82	
No	40	29(11)	72.50	
Tumor differentiation				0.774
high (G1)	31	21(10)	67.74	
moderate and low (G2 + G3)	26	19(7)	73.08	
Bokhman subtype				
I	19	14(5)	73.68	1.00
II	11	8(3)	72.73	

Note. Two-sided Fisher exact test; M – methylated; U – unmethylated.

At present, we do not know how the discovered methylation of the studied *PTENP1* pseudogene region affects its expression and the expression of the *PTEN* gene. There are three potential consequences of the methylation: no effect on *PTEN* expression; suppression of *PTEN* activity; and stimulation of *PTEN* activity. The three *PTENP1*-lncRNAs (*Fig. 2*) synthesized from the studied promoter, which were mentioned in the Introduction section, have an opposite effect [27]. *PTENP1*-asRNA-α inhibits *PTEN* transcription through heterochromatinization of its promoter by trimethylation of histone H3 in this chromatin region. *PTENP1*-sRNA that competes with *PTEN*-mRNA for miRNA acts as ceRNA, and *PTENP1*-asRNA-β stabilizes *PTENP1*-sRNA. The physiological outcome of pseudogene methylation will depend on changes in the ratio among these three *PTENP1*-RNAs in endometrial cells. Stabilization or stimulation of *PTEN* tumor suppressor gene activity during preferential simultaneous synthesis of *PTENP1*-sRNA and *PTENP1*-asRNA-β can protect against carcinogenesis. The consequence of suppressing its activity may be dual. Partial *PTEN* inactivation via this epigenetic mechanism may be a marker of the precancerous state of endometrial cells. At the same time, its complete rapid inactivation might also perform protective functions in aging endometrial cells.

Recently, the P. Pandolfi group discovered a new PTEN-dependent mechanism of cell aging, which was called *PTEN*-loss-induced cellular senescence (PICS) [42]. Unlike classical aging mechanisms, e.g., due to hyperactivation of oncogenes, PICS (at least in mice [42] and the primary cells of human epithelium [43]) can rapidly develop in nonproliferating cells in the absence of a cellular response to DNA damage. In this case, the development of PICS depends on the activity level of intracellular PTEN. Cell aging and cell cycle blockage via this mechanism in nonmalignant cells occur upon complete inactivation of *PTEN*, whereas its partial inactivation may be accompanied by the initiation of carcinogenesis and proliferation of malignized cells [42]. Therefore, we may suppose that *PTEN* that is partially inactivated by somatic mutations in endometrial cells bears the risk of cell malignant transformation. Therefore, complete suppression of the cell cycle and prevention of tumor growth via this mechanism require rapid complete inactivation of *PTEN*. This could apparently occur via the suppression of *PTENP1* pseudogene transcription through methylation of its promoter and/or depletion of ceRNA, whose function is performed by *PTENP1*-sRNA. If this assumption is correct, *PTENP1* methylation may be considered as one of the elements of protection from aging cells with a high risk of malignant transformation. In this case, the *PTENP1* methylation found in EH and EC cells may be a consequence of a preceding or still ongoing fight with their malignant transformation. To confirm or disprove this model, further studies of the effect of *PTENP1* methylation on the expression of the *PTEN* gene are required.

CONCLUSION

This study of normal tissues, malignant tumors, and endometrial hyperplasias in females of different ages revealed that the promoter region of the *PTEN* tumor suppressor gene was not methylated in any of the cases. In contrast to this, the bi-directional promoter of the *PTENP1* pseudogene was methylated at a high frequency in all studied tissues, except for the endometrium of young healthy females, as well as the blood of endometrial cancer patients. We think that *PTENP1* pseudogene methylation reflects the age-related changes in the human body and may not be directly related to the studied endometrial pathology. We suggest that, depending on the effect of methylated *PTENP1* on the expression of the *PTEN* gene, pseudogene methylation may protect the body from the development of EC or serve as a marker of a precancerous state of cells. To select between these alternatives, it is necessary to further investigate the effect of *PTENP1* methylation on *PTEN* gene expression in cultured human cells. ●

This study was supported by the Russian Foundation for Basic Research (grant No. 14-08-00801).

REFERENCES

1. Morice P., Leary A., Creutzberg C., Abu-Rustum N., Darai E. // Lancet. 2016. V. 387. № 10023. P. 1094–1108.
2. Evans-Metcalf E.R., Brooks S.E., Reale F.R., Baker S.P. // Obstet. Gynecol. 1998. V. 91. P. 349–354.
3. Duska L.R., Garrett A., Rueda B.R., Haas J., Chang Y., Fuller A.F. // Gynecol. Oncol. 2001. V. 83. P. 388–393.
4. Garg K., Soslow R.A. // Arch. Pathol. Lab. Med. 2014. V. 138. P. 335–342.
5. Sheikh M.A., Althouse A.D., Freese K.E., Soisson S., Edwards R.P., Welburn S., Sukumvanich P., Comerci J., Kelley J., LaPorte R.E., et al. // Future Oncol. 2014. V. 10. P. 2561–2568.
6. Werner H.M.J., Salvesen H.B. // Curr. Oncol. Rep. 2014. V. 16. P. 403.
7. Cancer Genome Atlas Research Network, Kandoth C., Schultz N., Cherniack A.D., Akbani R., Liu Y., Shen H., et al. // Nature. 2013. V. 497. № 7447. P. 67–73.
8. Bokhman J.V. // Gynecol. Oncol. 1983. V. 15. P. 10–17.
9. Tsikouras P., Bouchlariotou S., Vrachnis N., Dafopoulos A., Galazios G., Csorba R., von Tempelhoff F.G. // Eur. J. Obstetr. Gynecol. Reprod. Biol. 2013. V. 169. P. 1–9.
10. Mazur M.T. // Annals Diagn. Pathol. 2005. V. 9. P. 174–181.
11. Sivridis E., Giatromanolaki A. // Virchows Arch. 2008. V. 453. P. 223–231.
12. Mills A.M., Longacre T.A. // Semin. Diagn. Pathol. 2010. V. 27. P. 199–214.
13. Wise M.R., Jordan V., Lagas A., Showell M., Wong N. Lensen S., Farquhar C.M. // Am. J. Obst. Gynecol. 2016. V. 214. № 6. P. 689.e1-689.e17.
14. Kandoth C., McLellan M.D., Vandin F., Ye K., Niu B., Lu C., Xie M., Zhang Q., McMichael J.F., Wyczalkowski M.A., et al. // Nature. 2013. V. 502. P. 333–339.
15. Blanco-Aparicio C., Renner OLeal J.F.M., Carnero A. // Carcinogenesis. 2007. V. 28. № 7. P. 1379–1386.
16. Matias-Guiu X., Prat J. // Histopathology. 2013. V. 62. P. 111–112.
17. Song M.S., Salmena L., Pandolfi P.P. // Nat. Rev. Mol. Cell Biol. 2012. V. 13. P. 283–296.
18. Milella M., Falcone I., Conciatori F., Cesta Incani U., Del Curatolo A., Inzerilli N., Nuzzo C.M., Vaccaro V., Vari S., Cognetti F., Ciuffreda L. // Front. Oncol. 2015. V. 5. P. 24.
19. McCabe N., Kennedy R.D., Prise K.M. // Oncoscience. 2016. V. 3. № 2. P. 54–55.
20. Brito M.B., Goulielmaki E., Papakonstanti E.A. // Front. Oncol. 2015. V. 5. P. 166.
21. Stambolic V., MacPherson D., Sas D., Lin Y., Snow B., Jang Y., Benchimol S., Mak T.W. // Mol. Cell. 2001. V. 8. № 2. P. 317–325.
22. Song L.B., Li J., Liao W.T., Feng Y., Yu C.P., Hu L.J., Kong Q.L., Xu L.H., Zhang X., Liu W.L. et al. // J. Clin. Invest. 2009. V. 119. № 12. P. 3626–3636.
23. Whelan J.T., Forbes S.L., Bertrand F.E. // Cell Cycle. 2007. V. 6. № 1. P. 80–84.
24. He L. // Sci. Signal. 2010. V. 3. P. 146, pe39.
25. Poliseno L., Salmena L., Riccardi L., Fornari A., Song M.S., Hobbs R.M., Sportoletti P., Varmeh S., Egia A., Fedele G., et al. // Sci. Signal. 2010. V. 3. P. 117, ra29.
26. Dahia P.L.M., FitzGerald M.G., Zhang X., Marsh D.J., Zheng Z., Pietsch T., von Deimling A., Haluska F.G., Haber D.A., Eng C. // Oncogene. 1998. V. 16. P. 2403–2406.
27. Johnsson P., Ackley A., Vidarsdottir L., Lui W., Corcoran M., Grander D., Morris K.V. // Nat. Struct. Mol. Biol. 2013. V. 20. № 4. P. 440–446.
28. Poliseno L., Salmena L., Zhang J., Carver B., Haveman W.J., Pandolfi P.P. // Nature. 2010. V. 465. P. 1033–1038.
29. Tay Y., Kats L., Salmena L., Weiss D., Tan S.M., Ala U., Karreth F., Poliseno L., Provero P., Di Cunto F., et al. // Cell. 2011. V. 147. P. 344–357.
30. Poliseno L., Pandolfi P.P. // Methods. 2015. V. 77–78. P. 41–50.
31. Poliseno L., Haimovic A., Christos P.J., Vega Y. Saenz de Miera E.C., Shapiro R., Pavlick A., Berman R.S., Darvishian F., Osman I. // J. Invest. Dermatol. 2011. V. 131. № 12. P. 2497–2500.
32. Marsit C.J., Zheng S., Aldape K., Hinds P.W., Nelson H.H., Wiencke J.K., Kelsey K.T. // Hum. Pathol. 2005. V. 6. № 7. P. 768–776.
33. Yu G., Yao W., Gumireddy K., Li A., Wang J., Xiao W., Chen K., Xiao H., Li H., Tang K. // Mol. Cancer Ther. 2014. V. 13. № 12. P. 3086–3097.
34. Kovalenko T.F., Sorokina A.V., Ozolinya L.A., Patrushev L.I. // Bioorg. Khim. 2013. V. 39. № 4. P. 445–453.
35. Lindblom B., Holmlund G. // Gene Anal. Techn. 1998. № 5. P. 97–101.
36. Pikor L.A., Enfield K.S., Cameron H., Lam W.L. // J. Visual. Exp. 2011. e2763. P. 1–3.
37. Patrushev L.I., Valiaev A.G., Golovchenko P.A., Vinogradov S.V., Chikindas M.L., Kiselev V.I. // Mol. Biol. (Mosk.). 1993. V. 27. № 5. P. 1100–1112.
38. Lahtz Ch., Stranzenbach R., Fielder E., Hembola P., Dammann R.H. // J. Invest. Dermatol. 2010. V. 130. P. 620–622.
39. Salvesen H.B., Mac Donald N., Ryan A., Jacobs I.J., Lynch E.D., Akslen L.A., Das S. // Int. J. Cancer. 2001. V. 91. P. 22–26.
40. Zysman M.A., Chapman W.B., Bapat B. // Am. J. Pathol. 2002. V. 160. № 3. P. 795–800.
41. Garcia J.M., Silva J., Peña C., Garcia V., Rodriquez R., Cruz M.A., Cantos B., Provencio M., España P., Bonilla F. // Genes. Chromosomes Cancer. 2004. V. 41. P. 117–124.
42. Alimonti A., Nardella C., Chen Z., Clohessy J.G., Carracedo A., Trotman L.C., Cheng K., Varmeh S., Kozma S.C., Thomas G., et al. // J. Clin. Invest. 2010. V. 120. P. 681–693.
43. Childs B.G., Durik M., Baker D.J., van Deursen J.M. // Nat. Med. 2015. V. 21. P. 1424–1435.

A Highly Productive CHO Cell Line Secreting Human Blood Clotting Factor IX

S. V. Kovnir[1], N. A. Orlova[1], M. I. Shakhparonov[2], K. G. Skryabin[1], A. G. Gabibov[2], I. I. Vorobiev[1,2*]

[1]Institute of Bioengineering of the Federal Research Centre "Fundamentals of Biotechnology" of the Russian Academy of Sciences, 60-let Oktjabrja Ave. 7, bldg. 1, Moscow, 117312, Russia

[2]M. M. Shemyakin–Yu. A. Ovchinnikov Institute of Bioorganic Chemistry of the Russian Academy of Sciences, Miklukho-Maklaya Str. 16/10, Moscow, 117997, Russia

*E-mail: ptichman@gmail.com

Received: March 03, 2017; in final form February 05, 2018

ABSTRACT **Hemophilia B patients suffer from an inherited blood-clotting defect and require regular administration of blood-clotting factor IX replacement therapy. Recombinant human factor IX produced in cultured CHO cells is nearly identical to natural, plasma-derived factor IX and is widely used in clinical practice. Development of a biosimilar recombinant human factor IX for medical applications requires the generation of a clonal cell line with the highest specific productivity possible and a high level of specific procoagulant activity of the secreted factor IX. We previously developed plasmid vectors, p1.1 and p1.2, based on the untranslated regions of the translation elongation factor 1 alpha gene from Chinese hamster. These vectors allow one to perform the methotrexate-driven amplification of the genome-integrated target genes and co-transfect auxiliary genes linked to various resistance markers. The natural open reading frame region of the factor IX gene was cloned in the p1.1 vector plasmid and transfected to CHO DG44 cells. Three consecutive amplification rounds and subsequent cell cloning yielded a producer cell line with a specific productivity of 10.7 ± 0.4 pg/cell/day. The procoagulant activity of the secreted factor IX was restored nearly completely by co-transfection of the producer cells by p1.2 plasmids bearing genes of the soluble truncated variant of human PACE/furin signal protease and vitamin K oxidoreductase from Chinese hamster. The resulting clonal cell line 3B12-86 was able to secrete factor IX in a protein-free medium up to a 6 IU/ml titer under plain batch culturing conditions. The copy number of the genome-integrated factor IX gene for the 3B12-86 cell line was only 20 copies/genome; the copy numbers of the genome-integrated genes of PACE/furin and vitamin K oxidoreductase were 3 and 2 copies/genome, respectively. Factor IX protein secreted by the 3B12-86 cell line was purified by three consecutive chromatography rounds to a specific activity of up to 230 IU/mg, with the overall yield > 30%. The developed clonal producer cell line and the purification process employed in this work allow for economically sound industrial-scale production of biosimilar factor IX for hemophilia B therapy.**

KEYWORDS **blood clotting factor IX, hemophilia B, heterologous protein expression system.**

ABBREVIATIONS **CHO – Chinese hamster ovary cells (*Cricetulus griseus*); DHFR – dihydrofolate reductase [EC 1.5.1.3]; EBV – Epstein–Barr virus; EMCV – encephalomyocarditis virus; FIX – clotting factor IX; HAT – a mixture of hypoxanthine, aminopterin, and thymidine; HT – a mixture of hypoxanthine and thymidine; IRES – internal ribosome entry site; MTX – methotrexate; PBS – phosphate buffered saline; VKORC1 – vitamin K epoxide reductase complex subunit 1 (EC 1.17.4.4); APTT – activated partial thromboplastin time; BSA – bovine serum albumin; IU – international unit of factor IX activity (corresponds to the amount of factor IX in 1 ml of pooled plasma from healthy donors); ORF – open reading frame; RT-PCR – real-time polymerase chain reaction.**

INTRODUCTION

Factor IX (FIX) is the proenzyme of serine protease from the blood coagulation cascade which hydrolyzes the arginine–isoleucine bond in a factor X molecule in the presence of Ca^{2+} and membrane phospholipids to yield activated factor X (FXa). The noncovalent complex of the factors IXa, VIIIa, and X bound to the phospholipid membrane (tenase) is the key element of the positive feedback loop of the coagulation cascade.

The *FIX* gene resides on the X chromosome. A congenital absence of this gene or a low level of functionally active factor IX cause hemophilia B, the X-linked recessive genetic disorder that occurs in approximately one out of 30,000 males. In particular, the hemophilia

among European royal families (Royal family disease) was believed to have been caused by point mutation in the *FIX* gene, leading to incorrect splicing of its mRNA and the emergence of an inactive, truncated FIX protein [1].

Therapy for hemophilia B was initially limited to periodic transfusions of blood plasma, then later replaced with prothrombin complex concentrates (a mixture of vitamin K-dependent blood clotting factors IX, II, VII, and X). The risk of thrombosis was the key limitation to this therapy. Blood plasma fractionation using the Cohn's method gave rise to FIX drugs characterized by a higher purity but containing admixtures of activated FIX (FIXa) and other clotting factors: so, the risk of thrombotic episodes persisted. Additional immunoaffinity purification of FIX has made it possible to completely remove these admixtures; however, it did not eliminate the risk of viral or prion infection that exists when other products of blood plasma processing are used. Natural FIX products prepared by purification using immobilized monoclonal mouse antibodies can also cause an allergic response to mouse immunoglobulin and potentially contribute to the emergence of FIX-neutralizing antibodies; i.e., the inhibitor form of hemophilia B [2].

Cloning FIX cDNA [3] and the first successful attempts at producing recombinant FIX in heterologous systems [4, 5] were performed in 1980–1985. In 1986, a FIX producer with an appreciably high specific productivity was obtained on the basis of a CHO cell line [6]. The recombinant FIX product, nonacog alfa (BeneFIX™), was approved for use in the USA and European Union member states in 1997. Production of this drug involves no animal-derived ingredients or donor plasma components. Nonacog alfa is secreted in CHO cells cultured in a medium free of serum or any other animal-derived products. Isolation and purification of FIX involves four chromatographic rounds, without the use of immunoaffinity chromatography. Potentially present viruses are removed by nanofiltration on a filter with a cut-off threshold of 70 kDa.Ready-to-use nonacog alfa is formulated without human albumin [7].

Circulating mature FIX has a molecular weight of ~57 kDa and an average plasma concentration of ~90 nM. FIX consists of four structural domains: the Gla domain, two EGF-like domains (EGF is the epidermal growth factor), and the C-terminal serine protease domain. The N-terminal signal peptide of FIX is cleaved upon translocation of polypeptide into the endoplasmic reticulum; the propeptide directly upstream from the Gla domain is cleaved upon secretion of a mature protein. The activation peptide residing between the second EGF-like domain and the serine protease domain is cleaved at FIX activation. FIX activation in the coagulation cascade is performed by activated factor XI (the intrinsic pathway) or activated factor VII (the extrinsic pathway).

The Gla domain carrying 12 γ-carboxylated Glu residues is located at the N-terminus of a mature FIX molecule. This domain ensures binding of FIX and FIXa to the surface of endothelial cells [8]. The first EGF-like FIX domain contains a high-affinity binding site for a calcium ion and ensures interplay of FIX with factor VIIIa and the tissue factor (factor III). The second EGF-like FIX domain is involved in the formation of the FIXa–FVIIIa–FX complex. It is linked to the serine protease domain via the activation peptide and the single disulfide bond.

The activation peptide FIX contains many post-translational modification sites that affect the properties of FIX, including N-linked oligosaccharides [9]. As a result, the only significant difference between the recombinant FIXa secreted in CHO cells and natural FIXa consists in the level of β-hydroxylation of the Asp64 residue: 0.24 mol/mol in natural FIX versus 0.4 mol/mol in recombinant FIX [8]. Blocking this post-translational modification by inhibitors of 2-ketoglutarate dioxygenase does not substantially alter the procoagulant activity of FIX. The C-terminal domain of serine protease accounts for ~50% of the total weight of FIX; the active site in it is hidden by the activation peptide and becomes exposed once the peptide is cleaved.

Among all post-translational modifications, only γ-carboxylation in the Gla domain is directly responsible for the procoagulant activity of FIX. Nevertheless, the recombinant FIX produced in CHO cells has only one significant difference from the natural FIX used as a drug: recovery of the FIX procoagulant activity *in vivo* in patients receiving an infusion of recombinant FIX was on average 1.29-fold lower than that for a natural concentrate of human FIX [10]. The reasons for the lower level of procoagulant activity recovery of recombinant FIX are yet to be elucidated, since comparative clinical trials evaluating the pharmacokinetics of nFIX products have shown that recombinant FIX has a longer half-life: 36 h for recombinant FIX versus 32.7 h for natural FIX [11]. The possible reason for the reduced activity recovery of recombinant FIX *in vivo* can be the fact that there is no Tyr158 sulfation and/or Ser155 phosphorylation within the activation peptide; however, evidence that supports this hypothesis has been obtained only for animal models of hemophilia B [12].

In many cases, the productivity of the systems of heterologous expression of the human *FIX* gene depends on the ability of the host cell to properly perform its post-translational modification rather than by the level of FIX biosynthesis. In particular, a signifi-

cant percentage of FIX secreted in CHO cells is inactive at almost any level of specific productivity, since it contains an unprocessed propeptide that completely inhibits the functioning of the Gla domain. Normal processing of FIX propeptide can be restored upon coexpression of subtilisin/kexin-like convertase PACE/furin or convertase PC5 homologous to it. An optimal level of propeptide cleavage in secreted FIX can be achieved upon coexpression of the truncated variant of human PACE/furin also secreted in the culture medium. Hence, propeptide cleavage can occur not only in the Golgi apparatus, but also in the extracellular space [7].

FIX activity also depends on the degree of γ-carboxylation of the Glu residues in the Gla domain. In fully active FIX, the first 10 Glu residues out of the 12 need to be converted into Gla residues. In a natural FIX molecule, all 12 Glu residues in the Gla domain are fully γ-carboxylated while the degree of modification of the last two residues is reduced in recombinant FIX products, which does not affect the properties of FIX. The conventional method for purifying recombinant FIX by anion-exchange chromatography involving elution with a $CaCl_2$ solution at a low ionic strength efficiently removes FIX molecules with a nonfunctional Gla domain. Therefore, an insufficiently high degree of γ-carboxylation of FIX is more likely to affect the yield of the target product rather than the specific procoagulant activity of purified FIX. The total number of Gla residues in purified recombinant FIX secreted in CHO cells can be as high as 11.5 per protein molecule, while specific procoagulant activity is no lewer than 200 IU/mg, identical to that of the natural protein.

The reaction of γ-carboxylation of Glu residues in vitamin K-dependent protein molecules is driven by vitamin K-dependent γ-glutamyl carboxylase (GGCX [EC 4.1.1.90]) [13]. The reaction takes place in the lumen of the endoplasmic reticulum and precedes proprotein translocation to the Golgi compartment. Dissolved carbon dioxide is a source of the carboxyl group being attached, while the reduced dihydroquinone form of vitamin K (KH_2) acts as an electron donor and a co-factor of GGCX. The reduced dihydroquinone form of vitamin K (KH_2) is converted to quinone 2,3-epoxide (K>O). For the γ-carboxylation reaction, the KH_2 concentration in the lumen of endoplasmic reticulum needs to be permanently maintained rather high. Reduction of K>O to KH_2 in vertebrate cells is catalyzed by the VKOR enzyme complex or VKORC (vitamin K oxidoreductase complex), the integral protein (vitamin K 2,3-epoxide-reductase complex subunit 1 (VKORC1 [EC 1.17.4.4]) being its main component) [14].

The attempts at achieving overexpression of the gene encoding human coagulation factor VII (the vitamin K-dependent protein whose Gla domain is functionally active only if all 12 Glu residues are fully γ-carboxylated) in CHO cells showed that the proportion of functionally active FVII molecules is very low and that GGCX overexpression does not increase the specific activity of FVII. Meanwhile, overexpression of the *FVII* gene in a HepG2 cell line (human hepatocellular carcinoma cells) and BHK (baby hamster kidney) cells derived from the Syrian hamster allows one to produce a predominantly functionally active protein. The varying activity levels of the VKOR complex are the reason why different cells have different abilities to ensure the γ-carboxylation reaction. Overexpression of the human *VKORC1* gene in a CHO cell line allows one to obtain a functionally active product and significantly enhance the rate of factor VII secretion [15].

Similar data were obtained for FIX secreted by BHK cells [16]. In the factor IX expression systems in CHO cells limited by the processing level of the propeptide of the target protein, the degree of γ-carboxylation ensured by the endogenous VKORC1 enzyme was sufficiently high to produce a fully functionally active factor IX [7]. Nevertheless, when expression of the *FIX* gene is significantly upregulated, the degree of γ-carboxylation of Glu residues in the Gla domain can drop, as evidenced by the strong difference in the level of FIX secretion by HepG2 cells (transformed hepatocytes) and cell lines derived from other tissues [17]. HepG2 cells exhibit high VKORC1 activity, thus being more efficient in FIX secretion.

Transfection with a plasmid encoding the known human *VKORC1* gene was considered to be the conventional method to enhance vitamin K oxidoreductase activity in cultured cells. However, the relative catalytic efficiency of this method in other mammalian cells is not so evident. VKORC1 orthologs in different mammalian species are not fully homologous; their *in vitro* catalytic efficiencies differ by approximately fourfold [18]. The protein composition of the VKOR complex is yet to be identified. Thioredoxin-like proteins from the lumen of the endoplasmic reticulum, including TMX, are considered to be the most likely source of electrons for the functioning of VKORC1 [19]. The membrane topology of VKORC1 was determined only by analogy to the bacterial protein from *Synechococcus* sp. The spatial electron transport chain to cysteine residues in the VKORC1 active site has not been described yet, as opposed to its homolog, VKORC1L1 [20].

We have put forward the hypothesis that the low activity of the VKOR complex in CHO cells can be due to insufficient expression of the gene coding for VKORC1 from Chinese hamster rather than because of its insufficient catalytic efficiency. Therefore, the required maximum level of human FIX secretion in CHO cells

can be ensured by coexpressing the target gene, the soluble variant of human PACE/furin, and VKORC1 from Chinese hamster. The target level of expression of the auxiliary genes can be determined by choosing clonal producer cell lines according to the percentage of coagulationally active FIX molecules with a cleaved propeptide. The objective of this study was to produce and characterize these cell lines that secrete FIX.

EXPERIMENTAL

Generation of genetic constructs for gene expression

Generation of the expression vectors p1.1, p1.2-Zeo, and p1.2-Hyg was described earlier in [21]. The DNA fragments encoding the target open reading frames (ORFs) of the human *FIX* gene, the human or Chinese hamster *VKORC1* gene, or human furin and fused with the Kozak consensus sequence (GCCGCCATGG) [22] were produced by PCR using proper adapter oligonucleotide primers. The PCR products were isolated from 1% agarose gel using Wizard SV Gel and PCR Clean-Up System reagent kits (Promega, USA) and ligated with a pAL-TA vector (Evrogen, Russia) using DNA ligase from bacteriophage T4 (Fermentas, Lithuania). PCR was performed using oligonucleotide primers and mixtures for the PCR Encyclo PCR kit, Tersus polymerase mix, and ScreenMix-HS (Evrogen, Russia) on a PTC-100 Thermal Cycler (MJ Research, USA). Molecular cloning was performed on a TOP10 *Escherichia coli* strain (Invitrogen, USA). Plasmid DNA was isolated using a GeneJET Plasmid Miniprep Kit (Fermentas, Lithuania).

The commercially available clone of human FIX cDNA, pCMV6-XL4/NM_000133.2 (sc126517, Origene, USA), and adapter primers AD-9-AbsF and AD-9-NheR (*Table 1*) were used as a source of FIX ORF. The ORF sequence of human VKORC1 was amplified from the pCMV6-XL4/ NM_024006.4 plasmid (sc112318, Origene, USA) with AD-hVKO-AbsIF and AD-hVKO-NheIR primers.

Total RNA was isolated from $2 \cdot 10^6$ CHO DG44 cells using TRI Reagent (MRC) in order to obtain the *VKORC1* ORF from Chinese hamster. cDNA was synthesized using a Mint kit (Evrogen, Russia) and 2 μl of the RNA template. cDNA was amplified using an Encyclo PCR Kit; the vkof1, vkof2, and vkor1 primers were used to perform PCR of the ORF region. The PCR product was cloned into the pAL-TA vector to yield plasmid pAL-CHOVKORC1. The nucleotide sequence of the inserted fragment was deposited into the GenBank database (accession number, JQ400047.1) on April 3, 2012. The amino acid sequence of the VKORC1 ORF from CHO DG44 cells was deposited into the GenBank database (accession number, AFG26681.1) on April 3, 2012.

Table 1. The primers used to clone and sequence the expression plasmids

Primer	Nucleotide sequence 5'→3'
FIX	
AD-9-AbsF	ttcctcgaggccgccaccatgcagcgcgtgaa-catg
AD-9-NheR	atgctagctttcattaagtgagctttg
9SQf	cggtatgtcaactggattaag
9-AS	ctgctggttcacaggactt
VKORC1	
vkof1	gtcgacatgggcaccacctgag
vkof2	gacatgggca ccacctggag gagccc
vkor1	ctcagggccttttggccttgtgttc
AD-CVKO-AbsIF	ttcctcgaggccgccaccatgggcaccacctgg
AD-CVKO-NheIR	atgctagctcagggcctttt ggcct
AD-hVKO-AbsIF	ttcctcgaggccgccaccatgggcagcacctgg-ggga
AD-hVKO-NheIR	atgctagctcagtgcctcttagccttg
Furin	
AD-FUR-AbsF	ttcctcgaggccgccaccatggagctgaggccctg
AD-FUR-NheR	aatctagactatcactcaggcaggtgtgagggc
IP-fVQ-F	gctgcagagggagcctcaagtacagtggctg-gaacagcaggtg
IP-fVQ-R	cacctgctgttccagccactgtactt-gaggctccctctgcagc
SQ-FUR639-F	caacggtgtctgtggtgtagg
SQ-FUR1228-F	gcccacctcaatgccaacg
SQ-FUR1563-R	cagggtggagcgggtg
SQ-fVQ-R	gttccagccactgtacttg
Primers targeting the vectors	
T7prom	taatacgactcactataggg
SP6	gatttaggtgacactatag
3CH1-Rev	acaaacagttctgagaccg
SQ-5CH6-F	gccgctgcttcctgtgac
IRESArev	aggtttccgggccctcacattg

The PCR product containing the VKORC1 ORF from Chinese hamster with restriction sites for subcloning insertion into an expression vector was obtained using the AD-CVKO-AbsIF and AD-CVKO-NheIR adapter primers and plasmid pAL-CHOVKORC1 as a template.

Human PACE/furin ORF was obtained by PCR using the AD-FUR-AbsF and AD-FUR-XbaR adapter primers and plasmid SC118550 (Origene, USA) as a template. The PCR product containing the ORF of the soluble deletion variant of human PACE/furin pro-

tease, with two amino acids deleted (VQ), was cloned into the pAL-TA vector to yield plasmid pAL-Fur. The ORF was then brought in line with the reference sequence NM_002569 by adding six missing nucleotides by inverse PCR using the IP-fVQ-F and IP-fVQ-R primers. Mutagenesis was carried out according to the procedure described in [23], with the following modifications: the primers were phosphorylated with bacteriophage T4 polynucleotide kinase (SibEnzyme, Russia) in bacteriophage T4 DNA ligase buffer (Fermentas, Lithuania) for 30 min at 37°C. PCR was performed using an Encyclo PCR kit according to the following scheme: one cycle for 4 min at 94°C, 2 min at 50°C, and 2 min at 72°C; 11 cycles for 1 min at 94°C, 1 min at 55°C, and 2 min at 72°C. The mixture was diluted twice with normal-strength *Dpn*I endonuclease buffer; 10 AU of this endonuclease was added, and the mixture was incubated at 37°C for 30 min and subsequently at 72°C in the presence of Pfu DNA polymerase (2.5 AU) for another 30 min. The PCR product was purified and ligated. A specific SQ-fVQ-R oligonucleotide was used to search for the regions of altered DNA by colony PCR.

The resulting plasmids pAL-F9, pAL-hVKORC1-AN, pAL-CHOVKORC1-AN, and pAL-FurVQ were sequenced within the insert; the correct ORF areas were cloned into the expression vectors p1.1, p1.2-Zeo or p1.2-Hyg at the *Abs*I–*Nhe*I sites. DNA for transfection was isolated using an EndoFree Plasmid MaxiKit (Qiagen, USA) or a GeneJet™ Midi kit (Fermentas, Lithuania). Prior to transfection, we sequenced the main functional elements of the vectors and repeatedly sequenced the regions of the target ORFs. The plasmids were linearized with *Pvu*I (p1.1 and p1.2-Zeo) or *BspH*I endonucleases (p1.2-Hygro), precipitated with ethanol, dissolved in phosphate-buffered saline (PBS), and sterilized by filtration through filters with a 0.22 μm pore size (Millipore, USA).

Culturing of CHO DG44 cells (Invitrogen, USA) and transfection with plasmid p1.1-F9 were carried out according to the procedure described in [21]. Forty-eight hours post-transfection, the cells were transferred into a CD CHO medium (Invitrogen, USA) supplemented with 200 nM methotrexate (MTX) and 8 mM glutamine and cultured by passing the cells every 3–4 days until a cell viability above 85% was restored (for a total of ~20 days). The resulting cell population was cloned by limited dilution (1 cell per well) in the MTX-free EX-CELL® CHO Cloning Medium (Sigma-Aldrich) supplemented with 8 mM glutamine. The productive clones were identified by ELISA; the selected clones were transferred sequentially into 24-well plates and then, into 6-well plates with the ProCHO 5 culture mixture (Lonza, Switzerland) supplemented with 8 mM glutamine, and cultured in the suspension mode. The most productive cultures were selected by ELISA among the clonal cultures that retained viability upon suspension cultivation. The p1.1-F9-T2/S clone was used for further amplification.

Amplification was carried out in Erlenmeyer flasks containing 30 ml of a ProCHO medium supplemented with 8 mM glutamine and 1, 2, and 4 μM MTX until the cell viability was restored (15–20 days). The cell culture generated in the presence of 4 μM MTX and exhibiting the highest specific productivity was used for the second round of limiting dilution cloning. Clone 3B12 was selected, readapted for suspension cultivation in the ProCHO 5 medium, and used for sequential co-transfection of the linearized plasmids p1.2-Hyg-Fur and p1.2-Zeo-VKORC. The stably transfected populations were selected using hygromycin B and zeocin antibiotics, respectively. The polyclonal population 3B12-Fur-VC was used to perform final cloning by limiting dilutions according to the procedure described above. The resulting clones were sequentially subdivided into groups according to the expression level of soluble PACE/furin and the level of procoagulationally active FIX. The selected clones were readapted to a ProCHO 5 medium supplemented with 8 mM glutamine and 1 μM vitamin K3 (menadione sulfate, Sigma-Aldrich) and suspension cultivation in Erlenmeyer flasks.

Real-time PCR

RT-PCR was conducted using an iCycler iQ real-time PCR system (Bio-Rad, USA) and qPCRmix-HS SYBR master mix (Evrogen, Russia) supplemented with a SYBR Green I intercalating dye. Each reaction was repeated 3 times in a volume of 25 μl in 3–5 replicas. Genomic DNA was isolated using a Wizard SV Genomic DNA Purification System kit (Promega, USA). Total RNA was isolated using an RNeasy Mini Kit (Qiagen, USA). In order to obtain the required amounts of cDNA, we used 1 μg of total RNA and the Mint kit (Evrogen, Russia).

The primers for RT-PCR were selected using the Beacon Designer v7.51 software; primer specificity was tested using the NCBI BLAST tool (http://www.ncbi.nlm.nih.gov/blast/Blast.cgi). Primers not homologous to the nucleotide sequences of Chinese hamster (specific to the FIX region and IRES-DHFR) were applied. The RT-PCR data were processed using the iCycler Iq4 software, including calculation of the reaction efficiency. The copy number of expression cassette integrated into the genome was calculated using a calibration curve plotted for serial dilutions of plasmid p1.1-F9. The PCR results were compared to those of a control amplicon of the *PPIB* gene, which is present only once in the genome of CHO cells, by

Table 2. Specific real-time PCR primers

Primer	Nucleotide sequence 5' → 3'
RT-F9-F	ttagatgtaacatgtaacattaagaatggcag
RT-F9-R	cattaaatgattgggtgctttgag
RT-ID-F	gccacaagatctgccaccatg
RT-ID-R	gtaggtctccgttcttgccaatc
RT-HYG-F	ttcggctccaacaatgtc
RT-HYG-R	gtctgctgctccatacaag
RT-Zeo-F	agttgaccagtgccgttcc
RT-Zeo-R	ggcgaagtcgtcctccac
RT-FURC-F	agcgggacctgaatgtgaag
RT-FURC-R	ggtggttcttctcgatgcca
RT-PPIB-F	gcaggcaaagacaccaatg
RT-PPIB-R	ctccaccttcctcactacatc
RT-bACT-F	gctcttttccagccttcctt
RT-bACT-R	gagccagagcagtgatctcc
RT-cVKOspN-F	aacgggtttgccgtcagaac
RT-cVKOspN-R	cggtaatcctcgtctcgg
RT-cVKOspC-F	gggcttgatgttgcttaatttc
RT-cVKOspC-R	gcaggtgttaggggtaatatg

searching against the NCBI Nucleotide Collection database using the BLAST algorithm.

The mRNA expression level was calculated using the relative ΔΔCq method for primers with a known PCR efficiency. The relative increase in the expression level (times) of the gene normalized with respect to the control gene was determined using the formula taken from [24].

Table 2 lists the primers used to assess the copy number of the expression cassette integrated into the genome and the mRNA level.

Southern blot hybridization

DNA was biotinylated using a Biotin DecaLabel DNA Labeling Kit (Fermentas, Lithuania). Either plasmid pAL-ID carrying replication initiation domains of the β-lactamase gene identical to those in the expression plasmids p1.1, EMCV IRES, ORF DHFR [21], or the amplification product of plasmid p1.1-F9 from the AD-9-AbsF and AD-9-NheR primers corresponding to FIX ORF was used as a template to generate probes. The genomic DNA to be used for Southern blotting was cleaved with *Apa*I endonuclease for 16 h, and the DNA fragments were separated in 0.8% agarose gel. The gel was prepared and transferred to a Amersham Hybond-N+ membrane (GE Healthcare, USA) in a buffer with a high ionic strength of 20 × SSC (3 M NaCl, 0.3 M sodium citrate) for 16 h in accordance with the membrane manufacturer's protocol. DNA was fixed by heating the membrane to 80°C for 2 h. Prehybridization and hybridization were carried out according to the procedure described in [25] in a solution containing 7% sodium dodecyl sulfate, 0.5 M sodium phosphate, and 1% bovine serum albumin (BSA), pH 7.2, for 16 h at 65°C. The membrane was washed according to the manufacturer's protocol; detection was performed using a Biotin Chromogenic Detection Kit (Fermentas, Lithuania).

ELISA measurement of FIX concentration

The FIX concentration was measured using rabbit anti-FIX polyclonal antibodies (LifeSpan BioSciences, USA) (50 ng/well) as an immobilized antibody according to the procedure described in [26]. HIX-1 mouse monoclonal antibodies (F2645, Sigma Aldrich) were used as a specific antibody. The samples, either undiluted or diluted with PBS supplemented with 1% BSA, were placed into the wells. The percentage of FIX molecules with an uncleaved propeptide was measured by ELISA using affinity purified rabbit antibodies targeting the synthetic peptide corresponding to human FIX propeptide as immobilized antibodies according to the procedure reported in [27]. The key ELISA steps were performed as described above.

The procoagulant activity of FIX was determined by activated partial thromboplastin time (APTT) assay using a Factor IX assay (Renam, Russia). Recombinant FIX within the BeneFIX drug (Wyeth, USA) was used as an activity reference standard. The measurements were conducted using a ThromboScreen 400c optical coagulometer (Pacific Hemostasis, USA).

Measuring furin activity

Furin activity was determined using a peptide substrate with a detachable 7-amino-4-methylcoumarin moiety Pyr-Arg-Thr-Lys-Arg-AMC (344935, Merck Millipore, USA) according to the procedure described in [27].

Measuring VKORC1 activity

VKORC1 activity was measured using DTT as an electron donor according to the procedure described in [28]. The substrate of the enzyme reaction, vitamin K1 2-3 epoxide (K>O), was synthesized from the quinone form of vitamin K1 (Sigma Aldrich, USA) and purified [29].

Isolation and purification of FIX

FIX was isolated and purified as follows: the culture medium was loaded into a column packed with the

Capto MMC sorbent and equilibrated with a 20 mM sodium citrate solution, pH 7.0, 100 mM NaCl, 0.02% Tween 80; and washed with a 20 mM sodium citrate solution, pH 7.0, 0.1 M NaCl. FIX was eluted with a 20 mM sodium citrate solution, pH 6.5, 200 mM NaCl, 0.5 M arginine, and 0.02% Tween 80. The eluate was diluted fourfold with water, loaded into a column packed with the Capto Q sorbent and equilibrated with a 50 mM Tris-HCl solution, pH 8.0; 100 mM NaCl; washed with a 50 mM Tris-HCl solution, pH 8.0; 200 mM NaCl; and eluted stepwise with the following solutions: 50 mM Tris-HCl pH 8.0; 10 mM $CaCl_2$, and 100–500 mM NaCl. The eluate fractions containing FIX exhibiting full procoagulant activity were diluted twofold with water and loaded into a column packed with the Capto Heparin sorbent and equilibrated with a 50 mM Tris-HCl solution, pH 7.5; 100 mM NaCl. The column was washed with a 50 mM Tris-HCl solution, pH 7.5; 200 mM NaCl. FIX was eluted with a 50 mM Tris-HCl solution, pH 7.5; 500 mM NaCl. The purified FIX solution was concentrated by ultrafiltration using a VivaFlow200 cassette with a 10 kDa PES membrane (Sartorius Stedim, Germany) and transferred into a storage solution containing 8 mM *L*-histidine, 0.8% sucrose, 208 mM glycine, pH 7.2, and 0.004% Tween 80. The purified FIX solution was divided into aliquot parts, frozen, and stored at temperatures below −70°C.

RESULTS AND DISCUSSION

Generation of CHO cells expressing the gene coding for human factor IX

The FIX ORF sequence with the inserted synthetic Kozak consensus sequence and a block of stop codons was cloned into the previously designed expression vector p1.1, which was based on noncoding regions of the translation elongation factor 1-alpha of Chinese hamster to yield the expression plasmid p1.1-F9 (*Fig. 1*).

Long genomic regions flanking the gene encoding translation elongation factor 1-alpha of Chinese hamster ensured the high expression level of the target genes and maintained this level constant during several months of sequential passaging [21]. The ORF sequence of the *FIX* gene in plasmid p1.1-F9 was linked to the selection marker, murine dihydrofolate reductase (DHFR), by the attenuated internal ribosome binding site of the encephalomyocarditis virus (EMCV IRES), thus ensuring expression of single bicistronic mRNA. This structure provides the strongest possible linkage between the target gene and the selection marker, which is required for amplification of the gene cassettes integrated into the genome of producer cells.

Plasmid p1.1-F9 was linearized, with the β-lactamase gene being destroyed, and used to transfect CHO DG44 cells with both *dhfr* alleles being defective. Forty-eight hours post-transfection, the cells were subjected to primary selection in the presence of three different methotrexate concentrations (50, 100, and 200 nM). Stably transfected cell populations were obtained in all three cases; the FIX secretion levels determined by ELISA were 0.69 ± 0.04, 1.05 ± 0.05, and 1.83 ± 0.24 μg/ml, respectively; the population doubling time for the cell cultures was 27–29 h. The maximum FIX titer was detected in the culture obtained in the presence of 200 nm MTX; therefore, immunoblotting of the intracellular FIX and FIX secreted by this cell culture was performed (*Fig. 2A*). No immunoreactive bands of FIX with an incorrect molecular weight were revealed, thus indirectly indicating that the gene cassettes integrated into the cell genome were not damaged. The resulting polyclonal culture was used to clone cells by limiting dilution. The clonal cell lines secreting FIX with maximum product titer were readapted to the suspension cultivation conditions in a medium with neither nucleotides nor DHFR inhibitors added. The levels of FIX secretion by the three most productive clonal lines after 3 days of cultivation were 11.9 ± 0.4, 12.3 ± 0.4, and 9.9 ± 0.3 μg/ml. The clonal line p1.1-F9-T2/S with specific productivity (Qp) of 2.99 ± 0.06 pg/cell/day and a population doubling time of 22.5 h was chosen for further experiments.

The productivity of the clonal cell line was enhanced by amplifying the target genes in the presence of methotrexate at increasing concentrations. Raising the MTX concentration to 4 μM yielded an oligoclonal cell line with Qp = 5.97 ± 0.18 pg/cell/day, which was used for the second round of limiting dilution cloning. Among the 12 most productive cell clones readapted to suspension cultivation, we selected the clone p1.1-F9-T2/4k-3B12 (referred to as 3B12 in the text and figures below) with Qp = 10.7 ± 0.4 pg/cell/day and a population doubling time of 20.2 h (*Fig. 2B*).

Production of the cell lines secreting biologically active FIX

FIX secreted by the 3B12 clonal cell line was almost completely inactive. The procoagulant activity of FIX in the culture medium was 0.22 IU/ml at a total concentration of 59 μg/ml (determined by ELISA), which corresponded to specific activity comprising 1.8% of that of natural human factor IX. Two reasons are known for the absence of biological activity in FIX: insufficient γ-carboxylation of its Gla domain [7] and retention of propeptide in the secreted FIX molecule so that efficient processing of FIX propeptide by host-cell endogenous proteases belonging to the PACE/furin family becomes impossible [7].

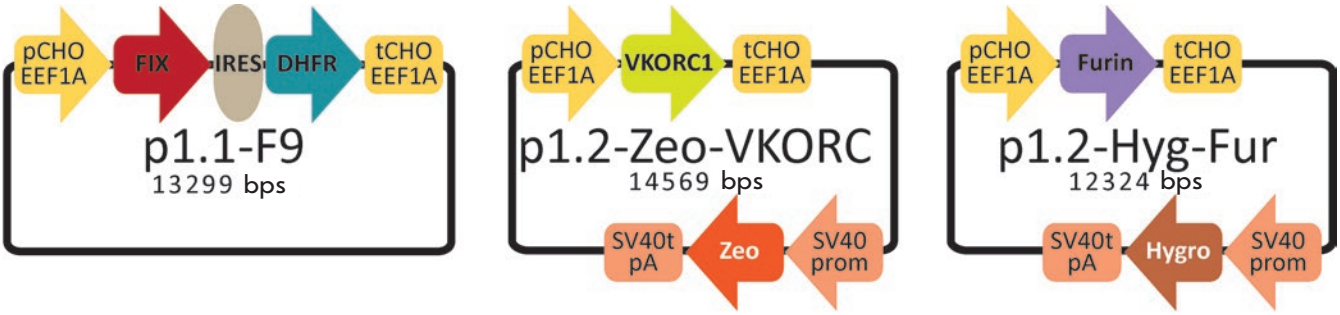

Fig. 1. Maps of the expression plasmids p1.1-F9, p1.2-Zeo-VKORC, and p1.2-Hyg-Fur. pCHO EEF1A – functional promoter of the gene of Chinese hamster translation elongation factor 1 alpha, the 5′ untranslated region of this gene and nontranscribing DNA regions flanking this gene; IRES – internal ribosome binding site of the EMCV; DHFR – the open reading frame of the mouse DHFR gene used for selection and genome amplification in eukaryotic cells; tCHO EEF1A – polyadenylation signal, the transcription terminator of the Chinese hamster translation elongation factor 1 alpha gene and the corresponding 3′ nontranscribing DNA region flanking the aforesaid gene; FIX – open reading frame of the human blood clotting factor IX; VKORC – open reading frame of the Chinese hamster VKORC1 gene; SV40 prom – immediate early promoter of the SV40 virus; SV40t pA – transcription terminator and polyadenylation sequence of the SV40 virus; Zeo – open reading frame of the Sh ble gene (*Streptoalloteichus hindustanus* bleomycin) conferring zeocin resistance; Furin – open reading frame of the human PACE/furin protease gene; Hygro – open reading frame of the hygromycin phosphotransferase gene (*E.coli* hpt). Promoter directions are depicted by arrows

Proper processing of human factor IX propeptide can be ensured by coexpressing the gene encoding signal protease of human PACE/furin. To coexpress the soluble truncated variant of human PACE/furin, we used vector p1.2-HYG that is similar to vector p1.1 but carries the gene coding for hygromycin phosphate transferase under the control of the SV40 promoter (that ensures resistance to hygromycin B) that lies outside the *EEF1A* gene (*Fig. 1*).

In order to achieve overexpression of endogenous VKORC1, we cloned the open reading frame sequence of the *vkorc1* gene from cDNA of CHO DG44 cells using primers homologous to the start and end of the ORF of the murine *vkorc1* gene. Sequencing of the cloned PCR product revealed approximately the same level of homology between the *vkorc1* gene from Chinese hamster and the murine and human *vkorc1* genes (*Fig. 2C*). Unlike its orthologs in other mammals, VKORC1 from Chinese hamster carries a RRR motif [30] flanking the first transmembrane domain and shows much lower homology with the human *vkorc1* gene (*Fig. 2D*).

The characterized ORF sequence of the *vkorc1* gene from Chinese hamster was deposited into the GenBank database (accession number, AFG26681.1) and cloned into vector p1.2-Zeo to yield plasmid p1.2-Zeo-VKORC1 (*Fig. 1*). The same expression vector was also used to generate the control construct p1.2-Zeo-hVKORC1 carrying the ORF sequence of the human *vkorc1* gene.

Stably transfected polyclonal populations expressing both orthologs of the *vkorc1* gene were produced using CHO DG44 cells. The vitamin K oxidoreductase activity in cell lysate was measured, and the copy number of the integrated expression cassettes was determined. Overexpression of both *vkorc1* orthologs significantly increased the oxidoreductase activity in cell lysate (*Table 3*), while the specific enzyme activity ensured by VKORC1 from Chinese hamster was threefold higher than that ensured by human VKORC1, with the copy numbers of the integrated cassettes being almost equal (5.8 ± 0.3 and 5.5 ± 0.5 copies/genome for the *vkorc1* gene of Chinese hamster and human *vkorc1*, respectively). The transcription levels did not differ significantly for both orthologs: in VKORC1 mRNA from Chinese hamster, it was 0.12 ± 0.03% of the level

Table 3. The VKORC1 activity level in stably transfected cells

Plasmid	Specific VKORC1 activity, % of substrate conversion per 1 mg/ml of total protein in the lysate for 1 h	The relative level of increase in VKORC1 activity, times
Intact CHO DG44 cells	0.38	–
p1.2-Zeo-VKORC1	9.21	24.2
p1.2-Zeo-hVKORC1	3.03	8.0

Note: specific activities were calculated for the linear regions of the curve showing substrate conversion versus total protein concentration in lysates.

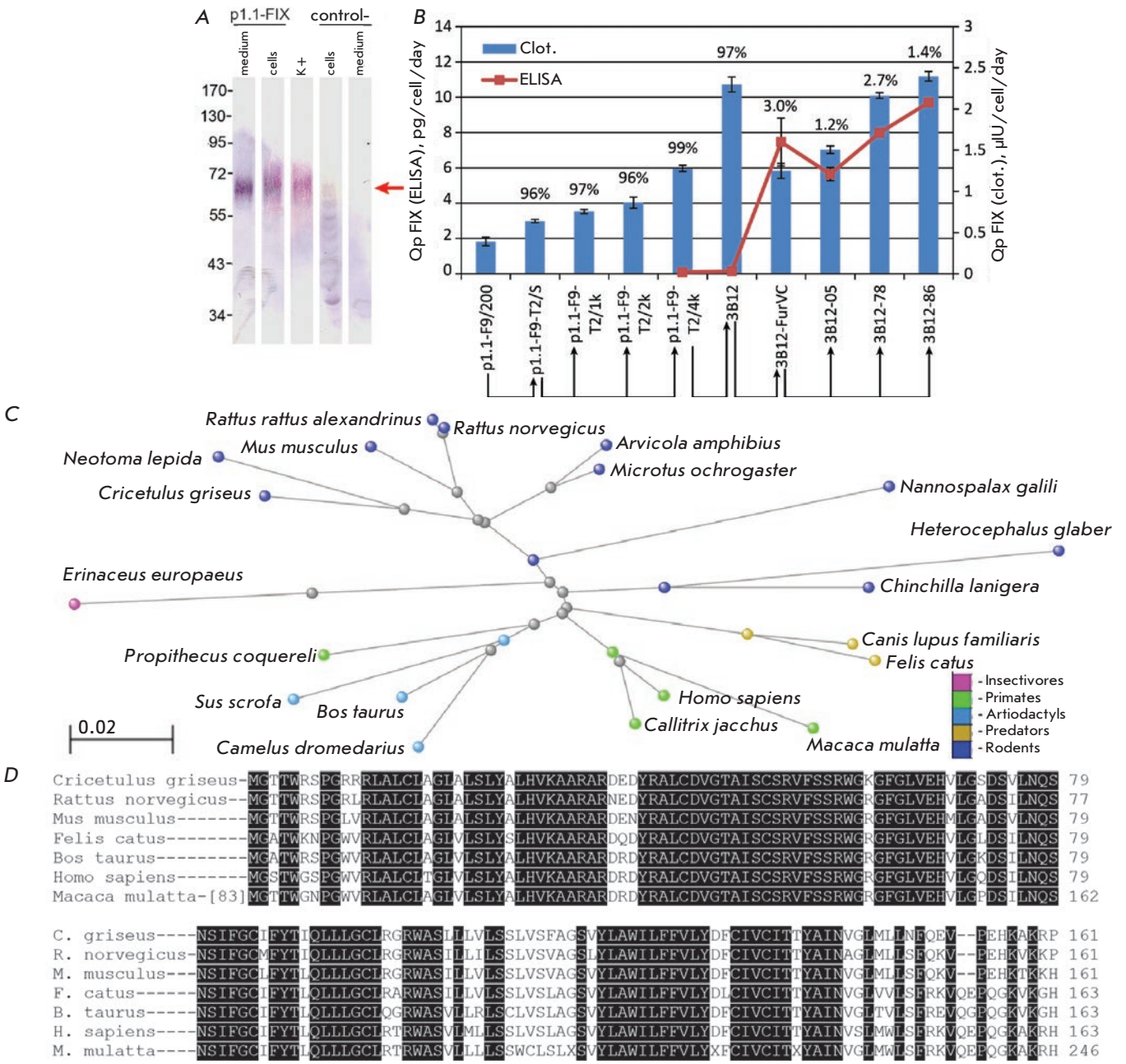

Fig. 2. The integrity of the intracellular and extracellular FIX polypeptide chain for the p1.1-F9-T2/S cell line, FIX secretion level and the change in clotting activity for various producer cell lines; the phylogenetic tree for the Chinese hamster VKORC1 protein. Panel *A* – Western blotting of the secreted and intracellular FIX. SDS-PAGE under reducing conditions, detection by polyclonal anti-FIX antibodies, the molecular weight of the marker bands is shown in kDa. Denotation: "K+" – recombinant FIX standard; "control-" – untransfected CHO DG44 cells. The mature FIX position is depicted by an arrow. Panel *B* – FIX secretion level and the degree of propeptide processing for cell populations and clonal lines. ELISA-determined specific productivity is shown as bars (left axis). Specific productivity as the clotting activity is shown as a broken line (right axis). The percentage of FIX molecules without the propeptide was determined by ELISA and is shown as numbers above the bars. Specific productivity for both methods is shown as the mean value; error bars represent the standard deviation, n=2. The scheme of production of cell populations and clonal lines is shown with arrows. Panel C – The taxonomic tree for a mammalian VKORC1 protein visualized using the Tree Viewer software (NCBI, USA). The scale bar represents the evolutionary distance measured as the number of substitutions per amino acid residue. Panel D – multiple alignment of the amino acid sequences of VKORC1 variants for the selected mammalian species. Conservative amino acid residues are shown against a black background

of β-actin mRNA; in human VKORC1 mRNA, it was 0.09 ± 0.01; $P = 0.16$. Simultaneously, it was discovered that the highest rate of substrate conversion VK > O by the microsomal fraction of cells transfected with the human *VKORC1* gene is approximately 5% per hour, while being at least 9% per hour for the *VKORC1* gene from Chinese hamster (data not shown). Since overexpression of the autologous *vkorc1* gene in CHO cells makes it possible to achieve maximum vitamin K oxidoreductase activity, this variant of *vkorc1* was used for the transfection of cell lines secreting FIX.

The clonal 3B12 cells were sequentially transfected with the linearized plasmids p1.2-Zeo-VKORC and p1.2-Hygro-Fur. In the resulting population of stably transfected cells containing three gene cassettes for the expression of factor IX and two auxiliary enzymes, the specific procoagulant activity of FIX in the culture medium was 27% of the reference value; the percentage of secreted FIX molecules with the uncleaved propeptide determined by ELISA was only 3.1% (*Fig. 2B*). Hence, the activity of soluble human PACE/furin in the generated cell population was sufficiently high to ensure an almost complete propeptide cleavage; however, the degree of γ-carboxylation in most cells was insufficient for a proper formation of the Gla domain of FIX. It can be assumed that expression of auxiliary enzymes was not equally efficient in all stably transfected cells. However, unlike VKORC1, soluble PACE/furin secreted by some cells into the culture medium ensured propeptide cleavage in all the secreted FIX molecules.

In order to isolate cells where both auxiliary enzymes exhibit maximum efficiency (i.e., biologically active FIX is produced), we cloned the generated populations by limiting dilutions using the procoagulant activity of the secreted FIX and the peptidase activity level of PACE/furin in the culture medium as a criterion for selecting promising clones. Out of 199 primary cell clones, we chose 80 having maximum FIX concentration. Of those, 24 clones exhibiting the highest PACE/furin activity were selected, eventually yielding 12 clones with maximum procoagulant activity of FIX (data not shown). Five out of the 12 clonal lines were successfully adapted to suspension cultivation in the presence of water-soluble vitamin K3; specific procoagulant activity of FIX in all the clones was > 185 IU/mg. Among these five clones, we identified the main 3B12-86 line with Qp = 11.2 ± 0.3 pg/cell/day and two backup lines, 3B12-78 and 3B12-05.

The copy numbers of the *FIX* gene, the sequences of its selection marker and auxiliary genes in the genome of producer lines and parental cell populations were determined by quantitative PCR (*Fig. 3A,B*). The copy numbers of the FIX and DHFR ORF sequences did not differ significantly in the studied objects; i.e., no signs of fission of the target gene and the gene encoding the selection marker were revealed. In other words, the copy number of the gene encoding the selection marker separately from that of the target gene does not occur despite the amplification of the gene cassettes in the genome of producer cells. When generating the 3B12-86 cell line, changes in the copy number of the human *FIX* gene were revealed: the copy number of the *FIX* gene increased approximately fivefold after amplification, remained constant upon cloning of the amplified population, and subsequently dropped fourfold after plasmids had been cotransfected with the auxiliary genes and repeated cloning had been performed. Meanwhile, the specific productivity of the corresponding cell lines did not decrease. It is possible that once the selection pressure had been eliminated, the low-activity copies of the genetic cassette that had appeared during genomic amplification were rejected.

The copy numbers of the auxiliary genes in all the generated clonal cell lines were significantly lower than that of the *FIX* gene, because cell clones were not selected in accordance with the maximum activity of the *vkorc1* gene. Only one selection round was performed for PACE/furin, and one-third of all produced clones were selected.

In the main producer cell line, 3B12-86, we assessed the changes in the expression levels of several of the housekeeping genes involved in the biosynthesis and post-translational processing of proteins by RT-PCR (*Fig. 3C*). None of the tested genes showed any significant changes in its expression level, thus indicating that there are no substantial alterations in biosynthesis and protein processing in host cells secreting FIX with the achieved productivity.

Evaluation of the integrity of the open reading frame sequence in the target gene

We demonstrated by PCR using genomic DNA and primers specific to the promoter and terminator regions of the employed expression vectors that the predominant PCR products have the correct size (*Fig. 4A*). Namely, a product consisting of 2942 bps corresponding to p1.1-F9 was revealed; amplicons 2511 and 852 bps long corresponding to the ORF sequences of VKORC1 and PACE/furin were also detected for genomic DNA from 3B12-86 cells. Similar amplification of cDNA from the 3B12-86 cell line using primers homologous to the beginning and end regions of the FIX ORF also revealed only a product of the target size (*Fig. 4B*), thus indicating that there are neither long deletions/insertions in the FIX ORF sequence nor mutations that alter splicing of FIX mRNA.

Southern blot analysis of genomic DNA from the 3B12-86 cell line using a probe targeting the FIX ORF

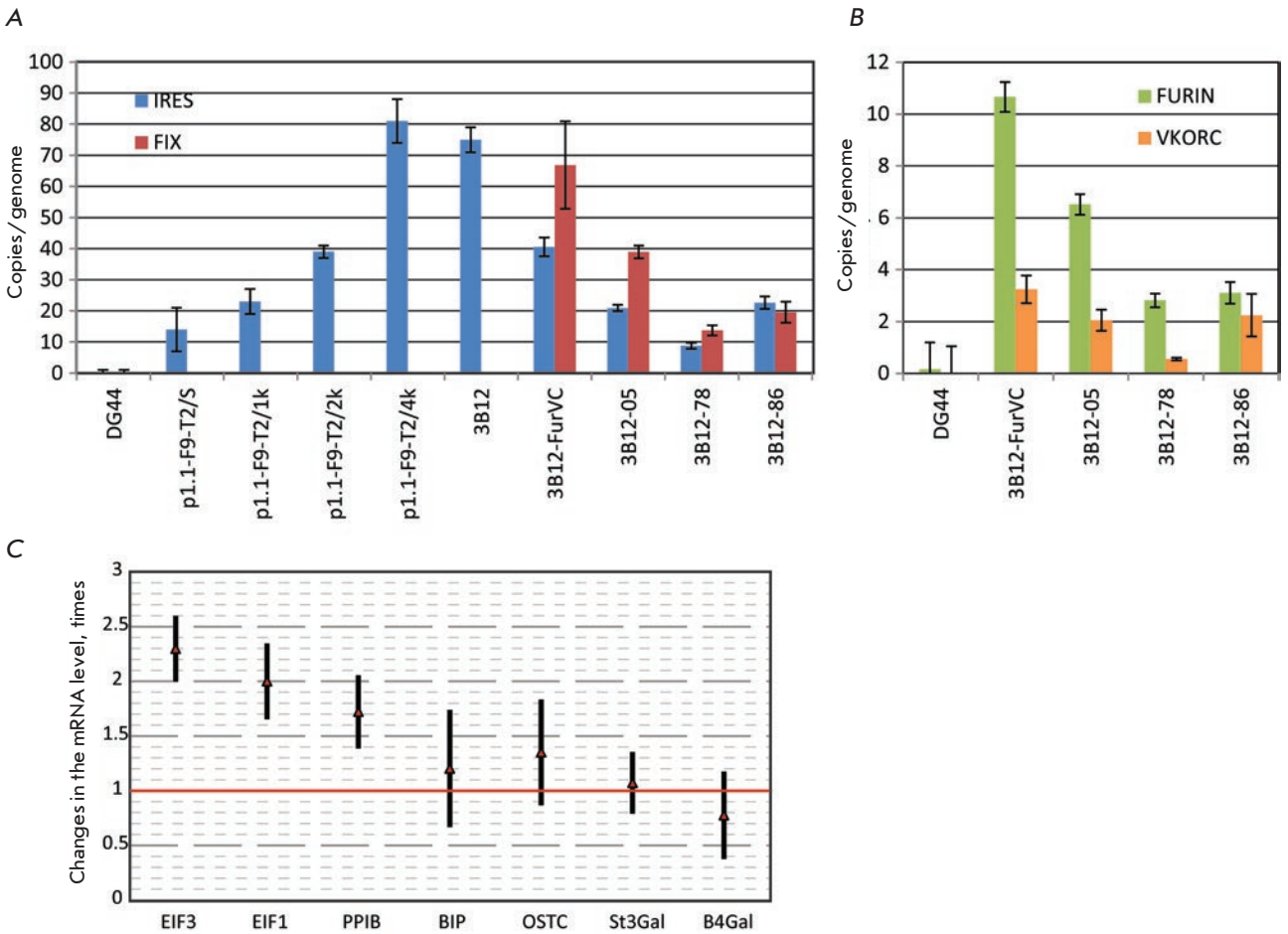

Fig. 3. Copy numbers of the target gene and auxiliary genes of furin and VKORC1 in the genome of producer cells; the expression levels of the housekeeping genes for the 3B12-86 cell line determined by quantitative PCR. Panel A – gene copy numbers for the FIX ORF region and the selection marker region (IRES). Denotation: IRES – the amplicon consisting of the IRES fragment and the adjacent DHFR ORF fragment; FIX – the amplicon from the ORF of the FIX gene. Panel B – gene copy numbers for the auxiliary genes of furin and VKORC1. Denotation: FURIN – the amplicon from the ORF of the furin gene; VKORC – the amplicon from the ORF of the VKORC1 gene. Panel C – alterations of the expression levels of the CHO genes involved in translation and post-translational protein modifications in the FIX-secreting cell line as compared to the untransfected control CHO DG44 cells. The results were normalized with respect to the beta-actin mRNA levels. Denotation: EIF1 – eukaryotic translation initiation factor 1a; EIF3 – eukaryotic translation initiation factor 3; PPIB – peptidylprolyl isomerase B; BiP – immune globulin binding protein (Grp78); OSTC – oligosaccharyl transferase complex; St3gal – alpha-2,3-sialyltransferase 3; B4gal – beta-1,4-galactosyltransferase 1. For all panels, the error bars represent a standard deviation (n=3–4), one representative experiment out of three runs is shown

sequence revealed one restriction fragment 1921 bps long (*Fig. 4C*), thus indicating that the producer genome does not carry gene cassettes integrated to rupture DNA in the FIX ORF sequence. Southern blot analysis using a probe targeting the regions of plasmid DNA corresponding to the domain of plasmid replication initiation and the sequence of the *bla* gene found two restriction fragments: a heavy fragment (~3700 bps) approximately corresponding to the calculated cassette integration at the site of its linearization by PvuI restrictase and a short fragment (~800 bps) putatively corresponding to cassette integration involving DNA deletion near the PvuI site. Pseudo-Northern blotting of cDNA produced from the 3B12-86 and 3B12-78 cell lines also revealed only FIX mRNA of the expected length (*Fig. 4D*).

The absence of mutations in the FIX ORF sequence was also confirmed by PCR amplification of the entire FIX ORF sequence from the genomic DNA produced by the 3B12-86 cell line, cloning PCR amplicon, and se-

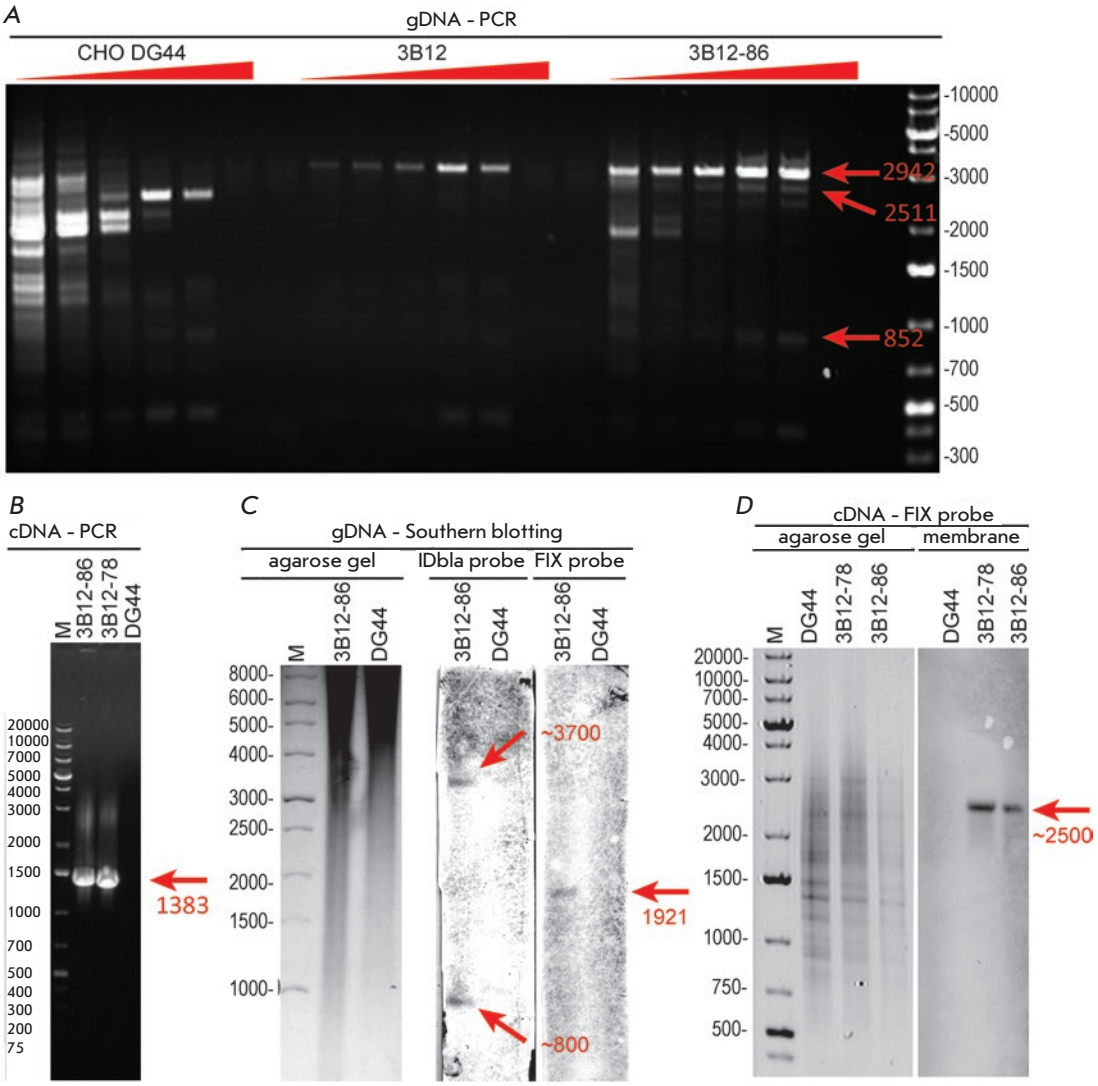

Fig. 4. Analysis of target gene integrity in the genomic DNA and cDNA from producer cell lines by PCR, RT-PCR, Southern blotting and pseudo-Northern blotting. DNA ladder bands are shown as bps. Panel A – amplification of whole ORF regions of the target genes in genomic DNA (gDNA) by PCR. The annealing temperature gradient is shown with red triangles; the linear shift in annealing temperature was from 53 to 68 °C. The expected amplification products of the *FIX*, furin, and *VKORC1* genes are shown with red arrows. Panel B – RT-PCR products for total mRNA with primers towards the 5′- and 3′- ends of the FIX ORF; the amplification product of expected size is shown with a red arrow. Panel C – Southern blotting of gDNA with biotin-labeled probes. The IDbla probe is the probe targeting the IRES and DHFR regions, the ampicillin resistance gene (the *bla* gene) and the region of plasmid origin of replication (ori). The FIX probe is the probe targeting the FIX ORF region. Sizes of the detected target restriction fragments are shown with arrows. Negative agarose gel images; the membrane images were contrast-enhanced to add visibility. Panel D – Analysis of cDNA by pseudo-Northern blotting. Denotation is the same as that in panel C. The actual position and size of FIX cDNA are shown with an arrow

quencing of the insert in three plasmid clones. Changes in the FIX ORF sequence were revealed in none of these cases (data not shown).

FIX isolation and purification

FIX was isolated from the conditioned 3B12-86 cell medium and purified using three sequential stages: (1) multimodal chromatography using the Capto MMC sorbent that allows one to isolate FIX from the conditioned medium without any additional preparative stages; (2) pseudo-affinity chromatography utilizing a Capto Q anion-exchange resin and elution of correct IX molecules by a calcium chloride solution with a low ionic strength; and (3) affinity chromatography on a

Table 4. FIX purification

Fraction name	FIX:Ag, IU/ml	Fraction volume, ml	FIX:C, IU/ml	FIX:Ag, IU	Total protein quantified by UV spectrophotometric assay, mg	FIX:C, IU	FIX:C/ protein, IU/mg	FIX:Ag/ /protein, IU/mg	Yield of the stage with respect to FIX:Ag	Overall yield with respect to FIX:Ag	Percentage of FIX with propeptide, %
Culture medium	6.04	115	3.6	695	–	414	–	–	–	–	2.6
Capto MMC flow-through and eluate fractions	0.166	273	–	45	–	–	–	–	7%	–	–
Capto MMC eluate	64.79	9	–	583	4.28	–	–	136	84%	84%	–
Capto Q flow-through fraction	0.07	37	–	3	0.69	–	–	4	0.4%	–	–
Capto Q eluate 200 mM NaCl	0.05	12.5	–	1	0.48	–	–		–	–	–
Capto Q eluate 10 mM $CaCl_2$	31.75	9.2	25.2	292	1.51	232	154	194	50%	62%	2
Capto Q, 150 mM NaCl + 10 mM $CaCl_2$	12.95	10.5	–	136	0.88	–	–	154	23%		
Capto Q 200 mM NaCl + 10 mM $CaCl_2$	4.67	10.7	<1	50	0.83	<10.7	<12	60	9%	–	5.8
Capto Q 500 mM NaCl + 10 mM $CaCl_2$	13.87	4	–	55	0.57	–	–	98	10%	–	–
Capto Heparin flow-through fraction	0.72	18	–	13	–	–	–	–	3%	–	–
Capto Heparin eluate	36.10	9	38.6	325	1.46	347	237	222	76%	32%	<2

specialized Capto Heparin sorbent, which separates heparin-binding proteins from the remaining molecules. The overall yield of the product was 32%; and the specific procoagulant activity of the purified FIX was > 230 IU/mg, corresponding to that of the known recombinant FIX drug (*Table 4*). SDS-PAGE analysis (*Fig. 5*) showed that most FIX molecules were eluted from the Capto Q sorbent after Ca^{2+} had been added to the low-salt eluent, indicating that these FIX molecules have a properly formed Gla domain whose structural rearrangement upon chelation of Ca^{2+} ions causes elution of Gla proteins from the anion exchanger.

CONCLUSIONS

The previously developed set of vectors based on untranslated regions of the *EEF1A1* gene from Chinese hamster can be used to generate cell lines secreting large amounts of functionally active human FIX. The target gene can be amplified in the genome of producer cells by culturing cells in the presence of increasing MTX concentrations, thus enhancing FIX secretion manifold. A sufficient expression level of the auxiliary *vkorc1* and *PACE/furin* genes can be ensured by cotransfecting the "compatible plasmids" with antibiotic resistance genes. The generated clonal cell lines secreting FIX contain a relatively low copy number of the target gene and only several copies of the auxiliary genes in chromosomal DNA, which may contribute to maintaining the secretion level constant upon long-term cultivation.

A comparative analysis of the overexpressed orthologs of the gene encoding the VKORC1 enzyme has

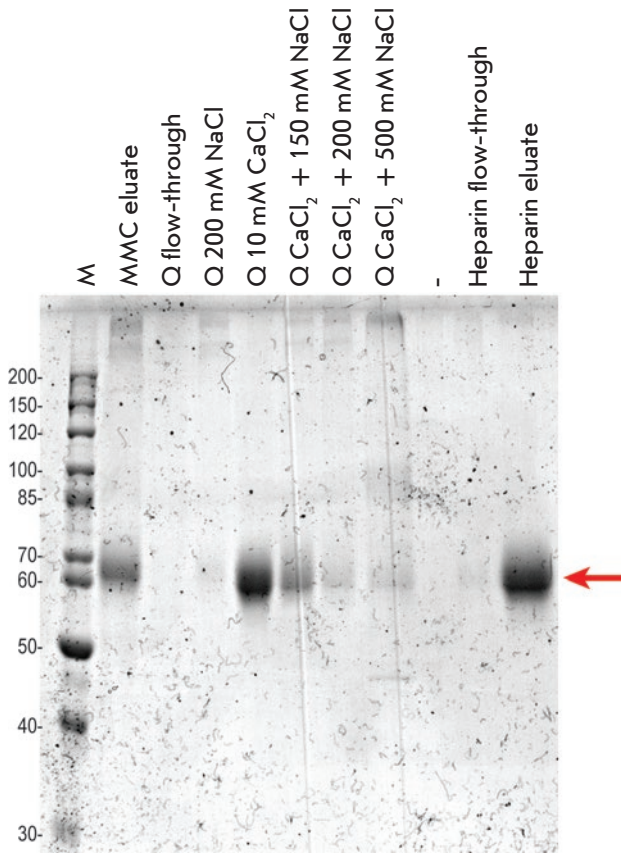

Fig. 5. SDS-PAGE analysis of the chromatography fractions obtained during the purification of FIX. Electrophoresis was performed under nonreducing conditions; molecular weights are given in kDa; colloidal Coomassie staining. Denotation: M – marker, eluate – the elution fraction from the corresponding column; flow-through – the flow-through fractions. The corresponding NaCl concentration in the elution solutions are given for the elution fractions from the Capto Q column; $CaCl_2$ concentration was 10 mM for all lanes

demonstrated that the enzyme activity ensured by the autologous VKORC1 from Chinese hamster is twice as high as that ensured by the artificial *vkorc1* gene, their copy numbers in the genome being identical. This method of overexpression of the *vkorc1* gene can be used to generate not only FIX producers, but also other vitamin K-dependent proteins in CHO cells. It seems especially promising to use the *vkorc1* gene from Chinese hamster to secrete human blood clotting factor VII in CHO cells. The BHK cell line that is currently employed for industrial-scale production of FVII combines a relatively high activity of the VKOR complex and a low total level of FVII secretion. Meanwhile, there are certain limitations to the cultivation mode: unlike CHO, this cell line requires fetal bovine serum to be present in the medium and can grow in a normal manner only under adhesion conditions.

The high specific productivity of the generated cell line secreting blood clotting factor FIX will make it possible to use 4- to 5-day-long plain batch cultivation to produce FIX on an industrial scale; the FIX titer will be ~6 IU/ml. This method of FIX production requires neither using specialized perfusion bioreactors nor elaborating methods to maintain cell culture viability for a long time, making industrial production of recombinant human factor IX much simpler and cheaper. ●

The authors are grateful to A.L. Berkovskiy for the valuable recommendations and reagents for coagulometry.

This study was supported by the Ministry of Industry of the Russian Federation (grant no. 121/13-FMP-0.507OK) and the Russian Foundation for Basic Research (grants nos. 16-34-01026 and 16-34-60242).

REFERENCES

1. Rogaev E.I., Grigorenko A.P., Faskhutdinova G., Kittler E.L., Moliaka Y.K. // Science. 2009. V. 326. № 5954. P. 817.
2. Puetz J., Soucie J.M., Kempton C.L., Monahan P.E. // Haemophilia. 2014. V. 20. № 1. P. 25–31.
3. Kurachi K., Davie E.W. // Proc. Natl. Acad. Sci. USA. 1982. V. 79. № 21. P. 6461–6464.
4. Anson D.S., Austen D.E., Brownlee G.G. // Nature. 1985. V. 315. № 6021. P. 683–685.
5. De la Salle H., Altenburger W., Elkaim R., Dott K., Dieterle A., Drillien R., Cazenave J.P., Tolstoshev P., Lecocq J.P. // Nature. 1985. V. 316. № 6025. P. 268–270.
6. Kaufman R.J., Wasley L.C., Furie B.C., Furie B., Shoemaker C.B. // J. Biol. Chem. 1986. V. 261. № 21. P. 9622–9628.
7. McGrath B.M., Walsh G. Directory of Therapeutic Enzymes. Boca Raton: CRC Press, 2005.
8. Derian C.K., VanDusen W., Przysiecki C.T., Walsh P.N., Berkner K.L., Kaufman R.J., Friedman P.A. // J. Biol. Chem. 1989. V. 264. № 12. P. 6615–6618.
9. Makino Y., Omichi K., Kuraya N., Ogawa H., Nishimura H., Iwanaga S., Hase S. // J. Biochem. 2000. V. 128. № 2. P. 175–180.
10. Poon M.C., Lillicrap D., Hensman C., Card R., Scully M.F. // Thromb. Haemost. 2002. V. 87. № 3. P. 431–435.
11. Lissitchkov T., Matysiak M., Zavilska K., Laguna P., Gercheva L., Antonov A., Moret A., Caunedo P., Aznar J.A., Woodward M.K., Paez A. // Haemophilia. 2013. V. 19. № 5. P. 674–678.
12. Bond M., Jankowski M., Patel H., Karnik S., Strang A., Xu B., Rouse J., Koza S., Letwin B., Steckert J., Amphleand G., Scoble H. // Semin. Hematol. 1998. V. 35. № 2 Suppl 2. P. 11–17.
13. Berkner K.L. // Annu. Rev. Nutr. 2005. V. 25. P. 127–149.
14. Garcia A.A., Reitsma P.H. // Vitam. Horm. 2008. V. 78. P. 23–33.

15. Bolt G., Steenstrup T.D., Kristensen C. // Thromb. Haemost. 2007. V. 98. № 5. P. 988–997.
16. Wajih N., Hutson S.M., Owen J., Wallin R. // J. Biol. Chem. 2005. V. 280. № 36. P. 31603–31607.
17. De Castilho Fernandes A., Fontes A., Gonsales N., Swiech K., Picanco-Castro V., Faca S., Covas D. // Biotechnol. Appl. Biochem. 2011. V. 58. № 4. P. 243–249.
18. Wilson C.R., Sauer J.M., Carlson G.P., Wallin R., Ward M.P., Hooser S.B. // Toxicology. 2003. V. 189. № 3. P. 191–198.
19. Schulman S., Wang B., Li W., Rapoport T.A. // Proc. Natl. Acad. Sci. USA. 2010. V. 107. № 34. P. 15027–15032.
20. Tie J.K., Jin D.Y., Stafford D.W. // J. Biol. Chem. 2014. V. 289. № 13. P. 9396–9407.
21. Orlova N.A., Kovnir S.V., Hodak J.A., Vorobiev I.I., Gabibov A.G., Skryabin K.G. // BMC Biotechnol. 2014. V. 14. P. 56.
22. Kozak M. // Nucl. Acids Res. 1987. V. 15. № 20. P. 8125–8148.
23. Griffin A.M., Griffin H.G. Molecular Biology: Current Innovations and Future Trends. Horizon Scientific Press, 1995.
24. Dussault A.A., Pouliot M. // Biol. Procd. Online. 2006. V. 8. P. 1–10.
25. Church G.M., Gilbert W. // Proc. Natl. Acad. Sci. USA. 1984. V. 81. № 7. P. 1991–1995.
26. Harlow E., Lane D. Antibodies: A Laboratory Manual. Cold Spring Harbor: Cold Spring Harbor Laboratory, 1988.
27. Bristol J.A., Furie B.C., Furie B. // J. Biol. Chem. 1993. V. 268. № 10. P. 7577–7584.
28. Rost S., Fregin A., Ivaskevicius V., Conzelmann E., Hortnagel K., Pelz H.J., Lappegard K., Seifried E., Scharrer I., Tuddenham E.G., Muller C.R., Strom T.M., Oldenburg J. // Nature. 2004. V. 427. № 6974. P. 537–541.
29. Tishler M., Fieser L.F., Wendler N.L. // J. Am. Chem. Soc. 1940. V. 62. № 10. P. 2866–2871.
30. Alves D.S., Castello-Banyuls J., Faura C.C., Ballesta J.J. // FEBS Lett. 2011. V. 585. № 8. P. 1169–1174.

Gene Expression in the Three-Spined Stickleback (*Gasterosteus aculeatus*) of Marine and Freshwater Ecotypes

S. M. Rastorguev[1*], A. V. Nedoluzhko[1], N. M. Gruzdeva[1], E. S. Boulygina[1], S. V. Tsygankova[1], D. Y. Oshchepkov[4], A. M. Mazur[2], E. B. Prokhortchouk[2,3], K. G. Skryabin[1,2,3]

[1]National Research Center "Kurchatov Institute", Kurchatov Sq. 1, Moscow, 123182, Russia

[2]Institute of Bioengineering, Research Center of Biotechnology of the Russian Academy of Sciences, Leninsky Ave. 33, bldg. 2, Moscow, 119071, Russia

[3]Faculty of Biology, Lomonosov Moscow State University, Leninskie Gory 1–12, Moscow, 119991, Russia

[4]Institute of Cytology and Genetics of the Siberian Division of Russian Academy of Sciences, Lavrentieva Ave. 10, Novosibirsk, 630090, Russia

*E-mail: rastorgueff@gmail.com

Received: December 09, 2016; in final form November 07, 2017

ABSTRACT **Three-spine stickleback *(Gasterosteus aculeatus)* is a well-known model organism that is routinely used to explore microevolution processes and speciation, and the number of studies related to this fish has been growing recently. The main reason for the increased interest is the processes of freshwater adaptation taking place in natural populations of this species. Freshwater three-spined stickleback populations form when marine water three-spined sticklebacks fish start spending their entire lifecycle in freshwater lakes and streams. To boot, these freshwater populations acquire novel biological traits during their adaptation to a freshwater environment. The processes taking place in these populations are of great interest to evolutionary biologists. Here, we present differential gene expression profiling in *G. aculeatus* gills, which was performed in marine and freshwater populations of sticklebacks. In total, 2,982 differentially expressed genes between marine and freshwater populations were discovered. We assumed that differentially expressed genes were distributed not randomly along stickleback chromosomes and that they are regularly observed in the "divergence islands" that are responsible for stickleback freshwater adaptation.**

KEYWORDS **three-spined stickleback, *Gasterosteus aculeatus*, gene expression, differential expression, RNA-seq, osmoregulation, GO-analysis, speciation.**

INTRODUCTION

Three-spined stickleback *(Gasterosteus aculeatus)* (*Fig. 1*) is a well-known model organism that is commonly used to explore the adaptive speciation process [1], since its marine form colonizes freshwater areas across the entire coastline of the Northern Hemisphere. A marine population of three-spined stickleback usually uses freshwater streams and lakes for spawning. However, isolation in a new habitat leads to the formation of a freshwater resident population, whose morphology changes over time as other features that make survival possible in new conditions develop. This feature makes it possible to use this small fish as a model for studying adaptive evolution in similar habitat conditions.

To date, a number of investigations have been published on the genome-wide changes that occur in three-spined stickleback during the process of adaptive speciation [2–4], which describe genomic "divergence islands" where the nucleotide substitutions characteristic of the freshwater form are concentrated. There are studies that describe the differential expression of stickleback genes in the kidneys of marine and freshwater specimen and the changes that occur after the introduction a freshwater specimen to a marine environment [5], as well as changes in the muscles, epithelial and bone tissues of marine and freshwater stickleback populations in studies of the plasticity of gene expression during colonization of freshwater habitats [6]. In addition, the differential expression of *G. aculeatus* genes in the tissues of the kidney and spleen in lake and river fish was evaluated in a study of the immune response to parasitic fauna [7].

The differences in the expression of genes in marine and freshwater forms have been widely studied in other models. Diadromous fish are especially suitable for this type of research, since they can live in both marine and fresh water and have physiological mechanisms for adaptation to water of differing salinity. In addition, global changes in gene expression in the marine

and freshwater forms of such species as *Plecoglossus altivelis* ayu [8], Japanese river acne *Anguilla japonica* [9], European acne *A. anguilla* [10], tilapia *Oreochromis mossambicus* [11, 12], *Fundulus heteroclotus* [13], common laurel *Dicentrarchus labrax* [14], sockeye *Oncorhynchus nerka* [15], arctic char *Salvelinus alpinus* [16] are studied by the RNA-seq method. In most cases, the RNA-seq method is used to evaluate subsequent changes in gene expression after changes in the external environment with gills as the target tissue. The categories of gene ontology (GO, Gene Ontology), which are enriched in experimental groups, have been identified, and metabolic and biochemical pathways, which play an important role in adaptation to changes in osmotic conditions, have been proposed. In particular, it has been shown that changes in osmotic conditions lead to changes in the expression of the genes that encode transport proteins and ion channels [12], the genes responsible for cell growth and proliferation, apoptosis and molecular transport, protein synthesis, and energy metabolism [9, 11, 13]. The active involvement of transcription factors in this process [15], which indicates an extensive effect of changing osmotic conditions on gene expression, deserves special mention.

Examination of gene expression can shed light on such fundamental problems of genetics as the connection between structure and functions in the eukaryotic genome. It is generally believed that genes in the eukaryotic genome are distributed randomly without forming any functional clusters similar to bacterial operons. However, there is evidence that this statement is false: statistical analysis of genome-wide data and transcription analysis data have demonstrated that genes in the eukaryotes genome are not distributed randomly but are organized into co-expressed clusters [17, 18]. Moreover, it has been shown that the genes of Arctic char [16], orthologous to the genes of three-spined stickleback, which are differentially expressed in the gills of fish from fresh and marine water, are much closer to each other than they would have been in a random arrangement, which confirms the hypothesis of a cluster organization of the eukaryotic genome. However, it would be of interest to compare these data with gene expression in three-spined stickleback.

In this paper, we present the results of a RNA-seq analysis of the genes expressed in the gills of marine and freshwater forms of three-spined stickleback; we have identified genes whose expression levels differ significantly in these two forms. We used gills as the target tissue, because they play an important role in the osmotic balance, and they are easy to isolate, which reduces the errors associated with the collection of material for the study. We elucidated the genomic localization of differentially expressed genes. For each chromosome, we calculated the ratio of the intergenic distances of such genes to the mean in the chromosome. We additionally performed functional and Gene Ontology analyses, identified the biochemical pathways enriched with the identified genes, and compared the data obtained with previously published data for other species. The ratio of differentially expressed genes to the genomic "divergence islands" involved in the adaptation of three-spined stickleback to a freshwater habitat was determined [4].

Fig. 1. Three-spined stickleback. Freshwater form. Stickleback female (top), stickleback male in breeding dress (bottom)

EXPERIMENTAL

Samples of marine three-spined stickleback (hereinafter referred to as "M") were collected from the White Sea, near the N.A. Pertsov White Sea Biological Station of Moscow State University (WSBS, MSU, Primorskiy settlements, Murmansk Region). Freshwater samples (hereinafter referred to as "F") were collected from the Machinnoye Lake, not far from the village of Tchkalovsky, Loukhskiy district, Republic of Karelia. Based on its location above sea level, the approximate age of the lake after desalination is 700 years [4, 19]. The lake contains only resident freshwater forms, since the stream leading from the lake into the sea is swampy and impassable for anadromous stickleback. In addition, the risk of collection error was reduced due to the significant morphological differences between the marine and freshwater forms [20]. To synchronize the physiological status of the samples, only males in breeding dress were selected.

The collected samples were kept for 4 days, each in their own water in the aquariums at the WSBS to synchronize the stress factor, which may differ depending on the collection conditions. Afterwards, the gills were isolated and fixed in a IntactRNA® reagent ("Eurogen", Russia).

RNA from the gill tissue of *G. aculeatus* (five samples from each experimental group) was isolated according to a standard protocol using a TRIzol® reagent (Invitrogen, USA). The RNA concentration for each sample was determined using a BioAnalyzer 2100 (RNA 6000 Nano Kit) (Agilent, USA).

To obtain cDNA libraries, cDNA was first synthesized on the RNA template using a set of Mint® reagents ("Eurogen", Russia) according to the manufacturer's instructions. Then, 10 indexed pair-end libraries for sequencing on Illumina analyzers (Illumina, USA) were prepared using the NEBNext Library Prep Kit for Illumina (NEB, UK). The concentration and purity of the libraries were determined using an Agilent Bioanalyzer 2100 instrument (Agilent Technologies, USA), followed by sequencing on Illumina HiSeq 1500 with a length of 2 × 75 nucleotides.

To identify the genes which are differentially expressed in the marine and freshwater samples of three-spined stickleback, the Illumina nucleotide reads were mapped on the *G. aculeatus* reference genome from the Ensembl database (BROAD S1, Feb 2006, assembly 81; http://www.ensembl.org) [21] using the *bowtie2* software package [22] with the set of parameters "-very-sensitive-local." As a result, SAM (Sequence Alignment/Map) files [23] were produced, which were further processed (compression, sorting, indexing) using the *SAMtools* package [23, 24]. The relative activity of each gene was determined according to the coverage of this gene by nucleotide reads on the reference genome after the mapping of each library. The coverage was determined using the *coverageBed* tool from the *bedtools* software package [25], using the bed-file with gene coordinates from Ensembl, and an indexed bam file obtained as a result of mapping of the nucleotide reads. The mapping data for each library was collated in a single table using a perl script. Statistical analysis of differential expression was performed using the edgeR package [26] of the R software for statistical computations (http://www.r-progect.org).

The analysis of gene ontologies (GO-Gene Ontology) and the analysis of biochemical pathways were carried out using the PANTHER (Protein Annotation through Evolutionary Rela- tionships) software (http://pantherdb.org) [27], after translating the Ensembl ID of stickleback genes into human orthologic genes with the help of BioMart Ensembl service, because this software does not use the genome of three-spined stickleback as a reference for searching for enriched GO categories. This utility uses the GO PANTHER library, based on models that use the hidden Markov chain algorithm to identify enrichment categories. Both "full" and reduced GO slim categories are used.

The intergenic distances for the complete set of genes of three-spined stickleback were compared with the distances between the genes responsible for osmoregulation using a perl script. Using the coordinates of the genes on each chromosome (indicated in bed-files from Ensembl's ftp server), the distance from each gene to all other genes of a given chromosome was measured and the same was done for all genes of the genome, resulting in an array of intergenic distances in nucleotides. A similar procedure was carried out for those genes that were differentially expressed in the gills of the marine and freshwater forms. We transferred the two acquired arrays to the t.test function of the R software for statistical computation, producing the difference indices for the two arrays.

The work was carried out using the equipment of the Center for Collective Use "Complex for Modeling and Data Processing of Mega-Class Research Facilities" of the Kurchatov Institute, http://ckp.nrcki.ru.

Table 1. Number of Illumina reads

Library	Number of clusters	Number of reads	Reads mapped on genes	Total for marine and freshwater forms	
				produced	mapped
M2	10566712	21133424	17993109	85438630	74093974
M3	10577457	21154914	18161521		
M4	10262893	20525786	18489001		
M5	11312253	22624506	19450343		
F1	13523593	27047186	24692145	110690898	103570453
F2	15715663	31431326	28960967		
F4	13359490	26718980	26307475		
F5	12746703	25493406	23609866		

*Sequencing statistics. The number of Illumina reads were obtained for each RNA-library and for the marine and freshwater stickleback populations altogether.

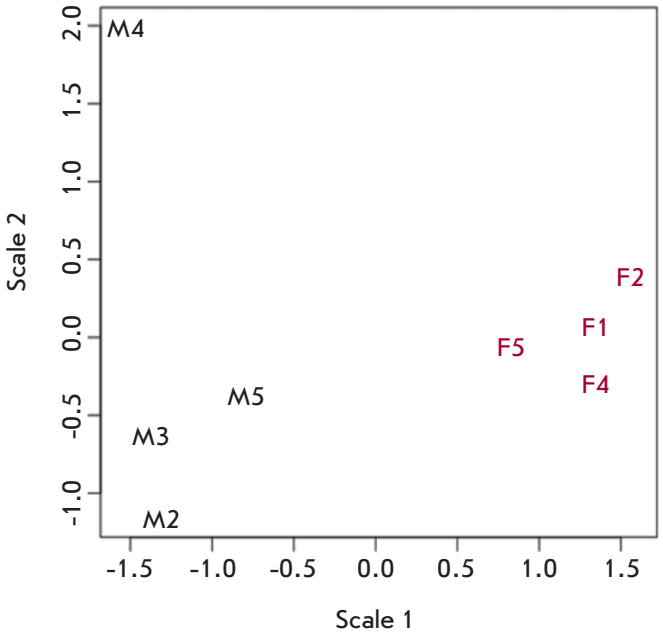

Fig. 2. Multi-dimensional scaling (MDS) plot of marine and freshwater stickleback based on normalized gene expression profiles in RNA-seq libraries. Marine samples are marked with red dots (M), freshwater samples are marked with blue ones. The indexes correspond to the RNA-libraries index numbers

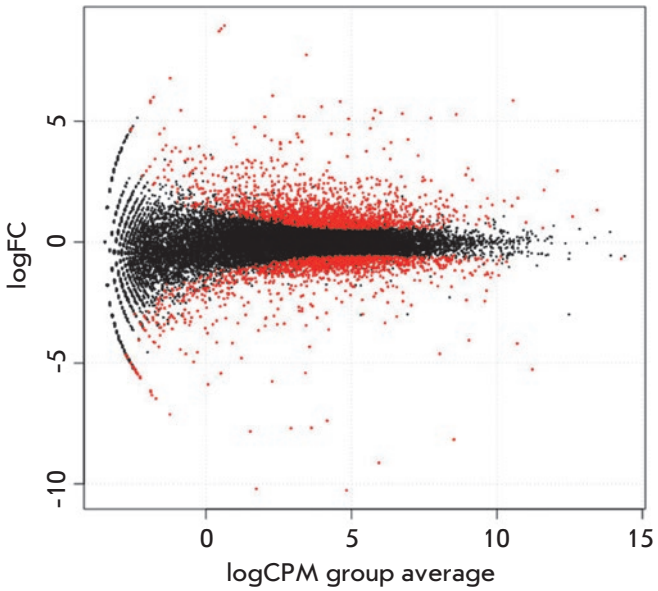

Fig. 3. Genes differentially expressed in three-spined stickleback gills. The dependency of logCPM (logarithm of count per million) on logFC (logarithm of fold change). These are binary logarithms. Marine vs freshwater differential genes, with more than 95% statistical support, marked with red dots

Table 2. Genes with the widest difference in expression level between marine and freshwater stickleback samples

Ensembl gene ID	logFC	logCPM	*P*-value	FDR
ENSGACG00000013714	-4.193912	10.693346	2.116876e-51	4.753656e-47
ENSGACG00000011986	-5.259545	11.215562	6.575861e-51	7.383376e-47
ENSGACG00000001275	3.860307	6.117474	2.371864e-46	1.775419e-42
ENSGACG00000014967	4.253744	6.943885	6.017277e-41	3.378099e-37
ENSGACG00000018764	-4.056880	9.038716	2.477170e-40	1.112547e-36
ENSGACG00000014959	4.706814	5.650018	7.523387e-40	2.815753e-36
ENSGACG00000003404	-4.617256	8.036567	5.344099e-37	1.714387e-33
ENSGACG00000001373	3.762800	5.512202	4.071101e-35	1.061745e-31
ENSGACG00000019813	5.816259	4.613614	4.255301e-35	1.061745e-31
ENSGACG00000014691	4.449242	4.901331	9.436192e-35	2.118991e-31

Note. logFC – binary logarithm of expression fold change, logCPM count per million – expression level characteristic, *P*-value – difference in expression, FDR – (false discovery rate) – *P*-value, normalized for multiple comparisons.

RESULTS AND DISCUSSION

Initially, five samples of stickleback from marine and freshwater populations were selected for the study of differential expression. However, the preparation of cDNA libraries revealed that two samples (one from each population) were of poor quality and they were excluded from the subsequent analysis. Therefore, four cDNA libraries, suitable for sequencing on the Illumina platform, were obtained for each group.

The total number of reads of 75 nucleotides in length was 85438630 and 110690898 in the libraries from the marine and freshwater samples, respectively. Nucleotide reads (177664427 in total) were mapped on the genes annotated in the *G. aculeatus* genome from the

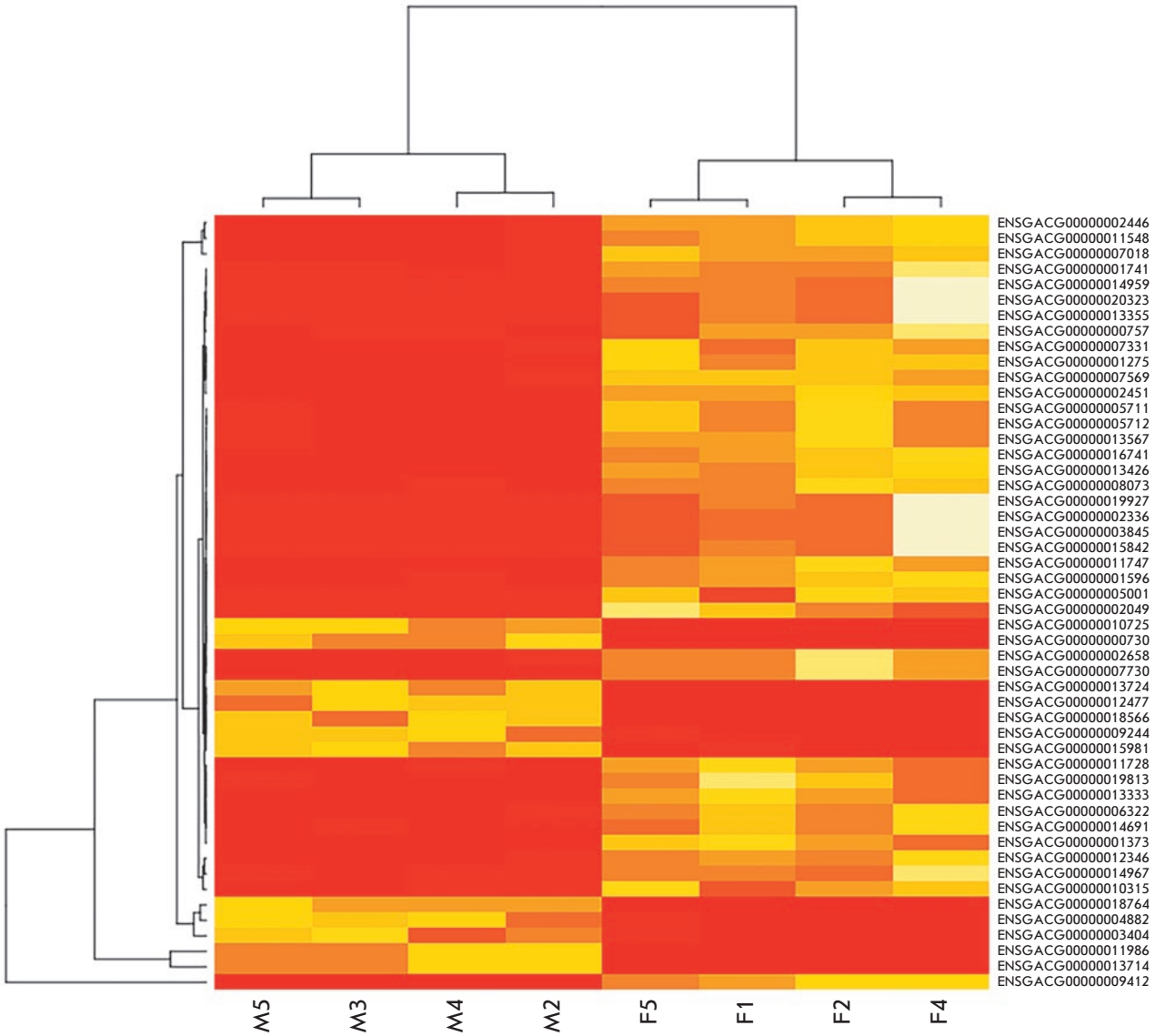

Fig. 4. Heat map diagram of the 50 most differentially expressed genes in the gill samples of marine and freshwater three-spined sticklebacks. The expression values are normalized using CPM (count per million) measure. The heat map indicates up-regulation (red) and down-regulation (yellow). The columns represent individual tissue samples (M – marine, F – freshwater), and rows represent gene names. The marine and freshwater stickleback samples are grouped separately Differences in the grouping of marine and freshwater specimen are visible

Ensembl database. The information on the number of nucleotide reads obtained as a result of the experiment and the mapping statistics are presented in *Table 1*.

After mapping of the data on the *G. aculeatus* genome, the nucleotide reads mapped on each of the annotated three-spined stickleback genes were counted and the activity of each gene was normalized using the edgeR package.

A MDS (Multi Dimensional Scaling) graph was constructed using the data on the coverage of annotated genes; in this graph, the arrangement of the samples corresponds to the differences in the expression of their genes. There were significant differences in the expression of genes in marine and freshwater stickleback samples. At the same time, samples of each group formed a fairly tight cluster (with the exception of the M4 marine sample), which indicates good synchronization of the physiological processes between the samples studied (*Fig. 2*).

Differential expression was established using the edgeR package [26], which calculates the variance of the expression index for each gene. Genes were consid-

Table 3. The intergenic distances for a whole gene set and differentially expressed genes in three-spined stickleback.

Chromosome	Length, b.p. according to Ensembl	Number of genes	Number of differentially expressed genes	Mean intergene distance, b.p.	Mean between differentially expressed genes, b.p.	*P*-value**
groupI	28185914	1647	150	9760533	10405738	< 2.2e-16
groupII	23295652	1158	113	7517040	7507226	0.8372
groupIII	16798506	1226	104	5325760	5764740	< 2.2e-16
groupIV	32632948	1719	171	11075843	10983967	0.04622
groupV	12251397	980	128	4198998	4022731	1.14e-13
groupVI	17083675	965	93	5605389	5223090	< 2.2e-16
groupVII	27937443	1726	183	9642342	10137264	< 2.2e-16
groupVIII	19368704	1177	128	6508569	6477095	0.387
groupIX	20249479	1374	149	6868532	6267635	< 2.2e-16
groupX	15657440	1050	107	5286434	5883914	< 2.2e-16
groupXI	16706052	1344	185	5543259	5455211	4.402e-05
groupXII	18401067	1301	116	6049383	6006811	0.2558
groupXIII	20083130	1303	137	6640756	6646041	0.8806
groupXIV	15246461	984	94	5118033	5192484	0.06052
groupXV	16198764	1026	114	5102727	5321175	2.422e-10
groupXVI	18115788	1063	97	5635724	5357195	6.306e-12
groupXVII	14603141	929	93	4897567	4834424	0.08998
groupXVIII	16282716	1020	101	5251120	4896094	< 2.2e-16
groupXIX	20240660	1373	132	6414729	6790731	< 2.2e-16
groupXX	19732071	1259	113	5868160	5362585	< 2.2e-16
groupXXI	11717487	599	71	3488145	2936194	< 2.2e-16

*The analysis was performed for each chromosome separately.
**The last column contains an indicator of the statistical significance of differences in the intergenic distance.

ered differently expressed if the difference between their activity and the mean was significantly higher than the variance. When calculating differential expression, the degree of gene activity is also important: for poorly expressed genes, the deviation from the mean should be higher for the difference in expression to be recognized as reliable. *Figure 3* illustrates the information presented above: differentially expressed genes (red dots) are genes whose expression not only deviated significantly from the mean, but also was on a fairly high level.

When comparing marine and freshwater specimens, statistically significant differences were found in the expression of 2,982 out of 22,456 annotated genes of *G. aculeatus* (significance level 95%). The expression of 1,304 genes was higher in marine stickleback, and the expression of 1,678 genes was higher in the freshwater form. *Table 2* shows 10 genes with the highest difference in expression in individuals of different ecotypes.

Figure 4 graphically represents the results of the differential analysis of 50 genes whose level of expression is most significantly different in the three-spined stickleback experimental groups. It was shown (similarly to MDS-graph) that marine and freshwater specimens differ considerably in their level of expression of some genes (judging by the clustering of the samples at the top of the figure). Moreover, 50 of the analyzed genes are predominantly genes whose expression is enhanced in marine samples.

The results of the functional analysis are shown in *Fig. 5*. The genes which are UP-expressed ("over-expressed") in the gills of the marine stickleback deviate to the right of the point of origin, while DOWN-expressed genes deviate to the left. UP- and DOWN-expressed genes can be interpreted as marine and freshwater ones, respectively. In addition, among the genes differentially expressed in the marine form, the content of genes associated with transmembrane functions and the cytoskeleton, e.g. those associated with the activity of ionic and anionic channels, transmembrane transporters, substrate-specific transmembrane transport activity, as well as other categories associated with membranes, proved significantly higher. This is quite logical and can be attributed to the fact that the maintenance of intracellular homeostasis in different osmotic conditions requires significant activi-

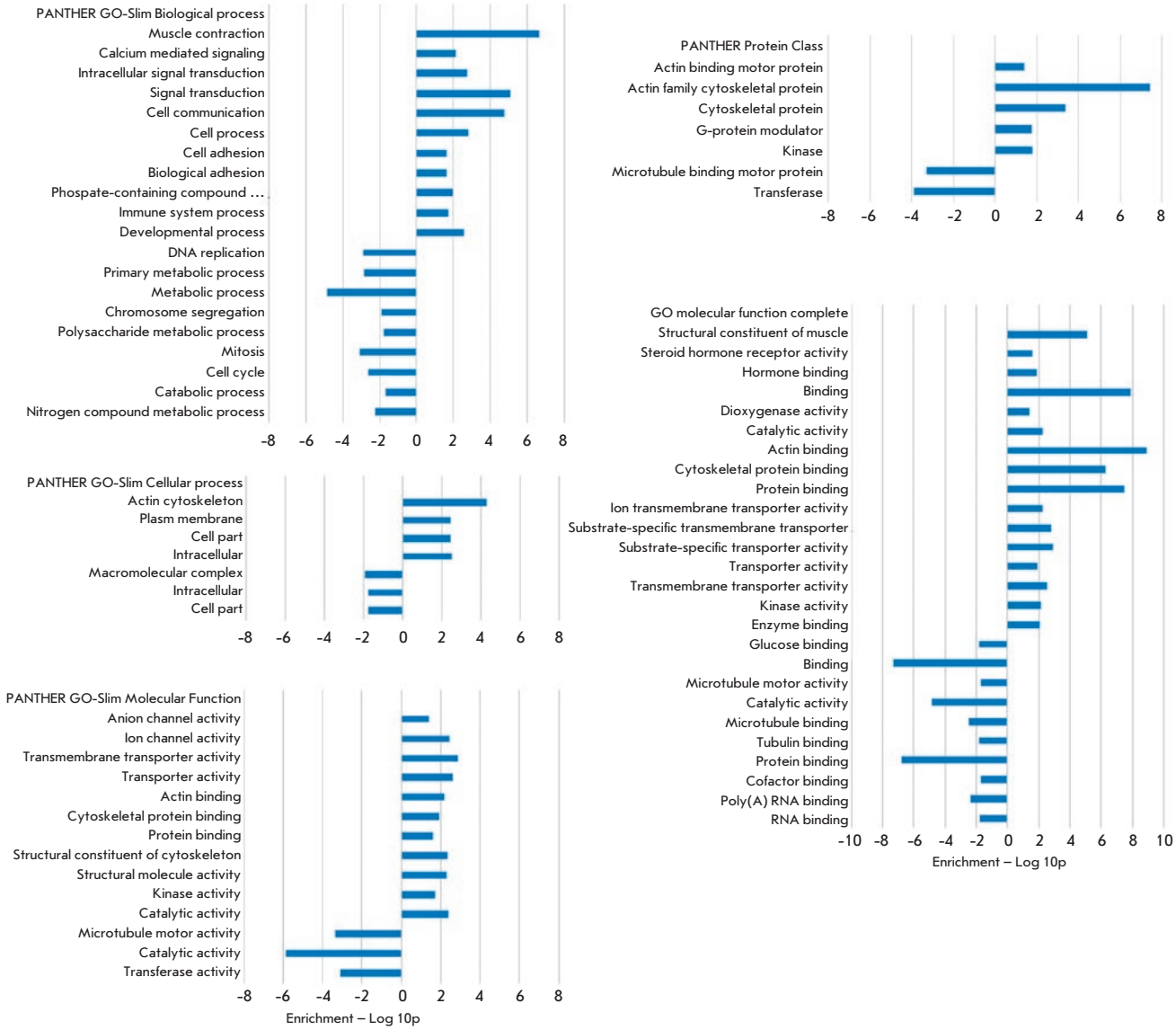

Fig. 5. Statistically significant gene ontology terms for differently expressed genes in marine and freshwater stickleback gill samples. Increased expression level of specific functional categories in marine sticklebacks, in relation to freshwater sticklebacks, equals to the deviation of Enrichment -Log10p in positive value. The names of the database for GO categories are indicated in the upper left corner of each barplot

ty by transmembrane systems. Among the genes whose expression is increased in the freshwater form, there are many genes associated with the cell cycle: DNA replication, mitosis, chromosome segregation, as well as those associated with intracellular transport and microtubules. Differences in the processes of cell division can be associated with different rates of development of stickleback in the sea and in fresh water, which, in turn, can be defined by the temperature regime. However, this phenomenon requires further study and explanation.

The content of genes associated with muscle activity is increased among the differentially expressed genes of the marine form, which can be explained, for example, by the need for males of marine sticklebacks to migrate to the coast where the spawning takes place before the mating season, whereas in freshwater forms such movement is unnecessary, as spawning occurs directly in the habitat. The differences in the immune processes in the two forms of stickleback, apparently, may be due to differences in the freshwater and marine parasitic fauna that affects stickleback [28].

Our results only weakly correlate with the data for other fish species [9, 11–13, 15]. Is this related to the methodological features of the functional analysis of the gene lists or do different species adapt differently to saline conditions? This issue remains open and requires more in-depth studies. However, there is evidence in favor of the idea that the response to changes in osmotic conditions can be individual. For example, a study of changes in gene expression in the gills of two related arctic char larvae (*S. alpinus*) revealed 1,045 and 1,544 genes differentially expressed in each of these lines, respectively [16]. At the same time, only 257 genes were common; i.e. in less than a quarter of the genes responding to changes in osmotic conditions expression changed in a similar way. And this in representatives of just one species!

Based on the intergenic distances for a complete set of genes of three-spined stickleback and the distances between the genes participating in osmoregulation, the distribution of differentially expressed genes on the chromosome is indeed not accidental. For example, the distance between genes whose regulation varies with change in osmotic conditions does not statistically differ from the intergenic distances of other genes only in seven out of 21 chromosomes of three-spined stickleback (*Table 3*). This confirms the hypothesis that the genes in the eukaryotic genome are not distributed randomly but are combined into co-expressed clusters [17, 18]. This result suggests that we still do not know much about the structure of the eukaryotic genome.

The previously published results of the search for single nucleotide polymorphisms associated with marine and freshwater forms in the genome of three-spined stickleback [3, 4] showed that such polymorphisms are predominantly localized in small parts of the genome called "divergence islands." We compared the localization of the differentially expressed genes we had identified with the position of the "divergence islands" involved in the adaptation of stickleback to fresh water. Out of 2,982 differentially expressed genes, 28 were found in the islands of adaptive divergence, which is significantly higher than the number of random coincidences. All in all, there are 212 of the 29,245 annotated three-spined stickleback genes in the divergence islets (according to the Poisson test, at *P*-value is 0.0001). This fact seems quite natural, since if there are single nucleotide polymorphisms in certain loci that differ in the marine and freshwater specimens of three-spined stickleback, then it is logical to assume that the expression of genes in these loci will differ as well with rather high probability, because some polymorphisms can be in the regulatory elements of these genes.

CONCLUSION

Summarizing the results presented in this work, let us emphasize that the use of modern methods of parallel sequencing to determine the activity of gene expression allowed us to identify an array of genes and the range of mechanisms involved in the process under study. Using the example of the adaptation of three-spined stickleback to changes in osmotic conditions, it has been shown that genes whose expression varies with the osmotic response are actively involved in such processes as regulation of the cell cycle, membrane transport, immunity, muscle contractions, etc. At the same time, a comparison of the enriched categories of differentially expressed genes with the results obtained earlier in other research centers reveals a low universality of the molecular mechanisms of adaptation to change in habitat conditions. This phenomenon requires further study. ●

The authors express their gratitude to the staff of the All-Russian Scientific Research Institute of Fisheries and Oceanography (VNIRO) N.S. Myuge and A.E. Barmintseva for their assistance in collecting samples, discussing the results, and providing a photograph of the investigated model (Figure 1). Special thanks to the staff of the I.D Papanin Institute of Biology of Inland Water of the Russian Academy of Sciences B.A. Levin and A.A. Bolotovsky for their help in collecting material from Mashinnoye lake.

This work is supported by grants from RFBR (No. 14-04-01237) for collection of samples and data analysis and RNF (№ 14-24-00175) for preparation and sequencing of cDNA libraries. Functional analysis of genes was supported by budget project (No. 0324-2018-0017).

REFERENCES

1. Hagen D., Gilbertson L. // Evolution. 1972. V. 26. P. 32–51.
2. Hohenlohe P.A., Bassham S., Currey M.C., Cresko W.A. // Philos. Transact. Royal Soc. B. 2012. V. 367. P. 395–408.
3. Jones F.C., Grabherr M.G., Chan Y.F., Russell P., Mauceli E., Johnson J., Swofford R., Pirun M., Zody M.C., White S., et al. // Nature. 2012. V. 484. P. 55–61.
4. Terekhanova N., Logacheva M., Penin A., Neretina T., Barmintseva A., Bazykin G., Kondrashov A., Mugue N. // PLoS Genet. 2014. V. 10. № 10. e1004696.
5. Wang G., Yang E., Smith K.J., Zeng Y., Ji G., Connon R., Fangue N.A., Cai J.J. // Front. Genet. 2014. V. 5. P. 312.
6. Morris M.R.J., Richard R., Leder E.H., Barrett R.D.H., Aubin-Horth N., Rogers S.M. // Mol. Ecol. 2014. V. 23. P. 3226–3240.
7. Huang Y., Chain F.J.J., Panchal M., Eizaguirre C., Kalbe M., Lenz T.L., Samonte I.E., Stoll M., Bornberg-Bauer E., Reusch T.B.H., et al. // Mol. Ecol. 2016. V. 25. P. 943–958.

8. Lu X.-J., Zhang H., Yang G.-J., Li M.-Y., Chen J. // Dongwuxue Yanjiu. 2016. V. 37. № 3. P. 126–135.
9. Lai K.P., Li J.-W., Gu J., Chan T.-F., Tse W.K.F., Wong C.K.C. // BMC Genomics. 2015. V. 16. P. 1072.
10. Kalujnaia S., McWilliam I.S., Zaguinaiko V.A., Feilen A.L., Nicholson J., Hazon N., Cutler C.P., Cramb G. // Physiol. Genomics. 2007. V. 31. P. 385–401.
11. Lam S.H., Lui E.Y., Li Z., Cai S., Sung W.-K., Mathavan S., Lam T.J., Ip Y.K. // BMC Genomics. 2014. V. 15. P. 921.
12. Ronkin D., Seroussi E., Nitzan T., Doron-Faigenboim A., Cnaani A. // Comp. Biochem. Physiol. Part D: Genomics and Proteomics. 2015. V. 13. P. 35–43.
13. Whitehead A., Roach J.L., Zhang S., Galvez F. // J. Exp. Biol. 2012. V. 215. P. 1293–1305.
14. Boutet I., Long Ky C.L., Bonhomme F. // Gene. 2006. V. 379. P. 40–50.
15. Evans T.G., Hammill E., Kaukinen K., Schulze A.D., Patterson D.A., English K.K., Curtis J.M.R., Miller K.M. // Mol. Ecol. 2011. V. 20. P. 4472–4489.
16. Norman J.D., Ferguson M.M., Danzmann R.G. // J. Exp. Biol. 2014. V. 217. P. 4029–4042.
17. Hurst L.D., Pál C., Lercher M.J. // Nat. Rev. Genet. 2004. V. 5. P. 299–310.
18. Ng Y.K., Wu W., Zhang L. // BMC Genomics. 2009. V. 10. P. 42.
19. Kolka V.V., Korsakova O.P. // Proc. MSTU. 2005. V. 15. P. 349–356.
20. McKinnon J.S., Rundle H.D. // Trends Ecol. Evol. 2002. V. 17. P. 480–488.
21. Cunningham F., Amode M.R., Barrell D., Beal K., Billis K., Brent S., Carvalho-Silva D., Clapham P., Coates G., Fitzgerald S., et al. // Nucl. Acids Res. 2015. V. 43. D662–669.
22. Langmead B., Salzberg S.L. // Nat. Meth. 2012. V. 9. P. 357–359.
23. Li H., Handsaker B., Wysoker A., Fennell T., Ruan J., Homer N., Marth G., Abecasis G., Durbin R. // Bioinformatics. 2009. V. 25. P. 2078–2079.
24. Li H. // Bioinformatics. 2011. V. 27. P. 2987–2993.
25. Quinlan A.R., Hall I.M. // Bioinformatics. 2010. V. 26. P. 841–842.
26. Robinson M.D., McCarthy D.J., Smyth G.K. // Bioinformatics. 2010. V. 26. P. 139–140.
27. Nesvizhskii A.I., Keller A., Kolker E., Aebersold R. // Anal. Chem. 2003. V. 75. P. 4646–4658.
28. Scharsack J.P., Franke F., Erin N.I., Kuske A., Büscher J., Stolz H., Samonte I.E., Kurtz J., Kalbe M. // Zoology (Jena). 2016. V. 119. № 4. P. 375–383.

New Experimental Models of Retinal Degeneration for Screening Molecular Photochromic Ion Channel Blockers

A. Yu. Rotov[1,2], L. A. Astakhova[2], V. S. Sitnikova[1,2], A. A. Evdokimov[3], V. M. Boitsov[4], M. V. Dubina[4], M. N. Ryazantsev[5,6*], M. L. Firsov[2]

[1]Peter the Great St. Petersburg Polytechnic University, Polytekhnicheskaya Str. 29, St. Petersburg, 195251, Russia

[2]Sechenov Institute of Evolutionary Physiology and Biochemistry, Russian Academy of Sciences, Toreza Ave. 44, St. Petersburg, 194223, Russia

[3]St. Petersburg State Chemical–Pharmaceutical Academy, Professor Popov Str. 14, St. Petersburg, 197376, Russia

[4]St. Petersburg National Research Academic University, Russian Academy of Sciences, Khlopina Str. 8/3A, St. Petersburg, 194021, Russia

[5]St. Petersburg State University, Institute of Chemistry, Universitetskiy Ave. 26, St. Petersburg, Petergof, 198504, Russia

[6]St. Petersburg National Research University of Information Technologies, Mechanics and Optics, Kronverkskiy Ave. 49, St. Petersburg, 197101, Russia

*E-mail: mikhail.n.ryazantsev@gmail.com

Received May 20, 2017; in final form January 24, 2018

ABSTRACT **Application of molecular photochromic ion channel blockers to recover the visual function of a degenerated retina is one of the promising trends in photopharmacology. To this day, several photochromic azobenzene-based compounds have been proposed and their functionality has been demonstrated on cell lines and knockout mouse models. Further advance necessitates testing of the physiological activity of a great number of new compounds. The goal of this study is to propose animal models of photoreceptor degeneration that are easier to obtain than knockout mouse models but include the main features required for testing the physiological activity of molecular photoswitches. Two amphibian-based models were proposed. The first model was obtained by mechanical deletion of the photoreceptor outer segments. The second model was obtained by intraocular injection of tunicamycin to induce the degeneration of rods and cones. To test our models, we used 2-[(4-{(E)-[4-(acryloylaminophenyl]diazenyl}phenyl)amino]-N,N,N-triethyl-2-oxoethanammonium chloride (AAQ), one of the compounds that have been studied in other physiological models. The electroretinograms recorded from our models before and after AAQ treatment are in agreement with the results obtained on knockout mouse models and reported in other studies. Hence, the proposed models can be used for primary screening of molecular photochromic ion channel blockers.**

KEYWORDS **photoreceptor degeneration, retinal degeneration, photochromic ion-channel blockers, photopharmacology, vision.**

ABBREVIATIONS **AAQ – 2-[(4-{(E)-[4-acryloylaminophenyl]diazenyl}phenyl)amino]-N,N,N-triethyl-2-oxoethaneammonium chloride acrylamide-azobenzene-quaternary ammonium; ERG – electroretinogram.**

INTRODUCTION

Retinitis pigmentosa and age-related macular degeneration, which result in progressive degeneration of the retina, are widespread visual disorders [1, 2]. Progression of these disorders leads to the death of rods and cones, while other types of neurons in the retina – ganglion, amacrine, bipolar and horizontal cells – survive (*Fig. 1 A,B*). Transmission of information to the brain ceases due to the loss of photoreceptor cells; i.e., the visual function is lost.

To this day, no curative treatment for these diseases has been achieved. Therefore, new strategies aimed at visual restoration after complete photoreceptor degeneration are under active development. Several approaches in dealing with the problem have been proposed. For example, implanted electronic retinal

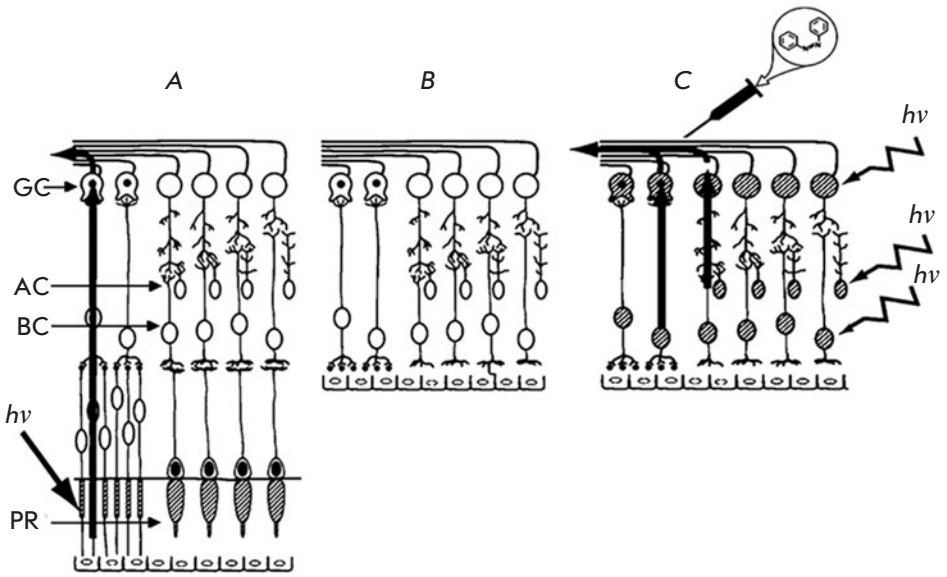

Fig. 1. A schematic image of the retina. *A* – intact retina; *B* – retina with degenerated photoreceptors; *C* – retina with degenerated photoreceptors after the injection of photochromic compounds. *GC* – ganglion cells, *AC* – amacrine cells, *BC* – bipolar cells, *PR* – photoreceptors, *hv* – incident light. The light-sensitive cells are marked with hatching. Because the horizontal cells do not have direct access to the ganglion cells, they are not shown in the figure. The figure is adapted from ref. [3] (with changes)

prostheses have been shown to partially restore visual function in patients with total vision loss [4]. Transplantation of stem cells into the retina has restored reaction to light in blind mice [5]; transplantation of the retinal pigment epithelium has allowed to enhance vision in patients with age-related macular degeneration [6]. Another approach, the optogenetic one, implies incorporation of light-sensitive proteins into the retinal neurons using genetic engineering methods. These can be bacterial opsins (light-activated ion channels) or hybrid proteins containing light-sensitive domains of visual pigments and the C-terminal domains of metabotropic receptors that induce intracellular signaling. Both optogenetic methods lead to partial restoration of light-induced processes [7, 8].

However, all these approaches are characterized either by high invasiveness or by the irreversibility of adverse side effects. An alternative method for the restoration of the visual function of the retina with degenerated photoreceptors has been recently proposed. It involves the injection of photosensitive molecules into the retina, which can bind to the voltage-dependent potassium channels in the membrane of survived cells (ganglion, amacrine, bipolar and horizontal ones). However, the latter three types of cells have no direct access to ganglion cells; for this reason, they will not be further considered in this work. The bound molecule exists in the trans-form and blocks the ion current through the channel, until a photon with a specific wavelength is absorbed. The photochromic compound then isomerizes into its cis-form that does not block an ion channel, thus inducing an ionic current, changing the membrane potential, and generating a photoresponse (*Fig. 2*). The molecule isomerizes back into its stable trans-form either in darkness or under illumination with light of a longer wavelength [10]. Thus, the cells activated by the photochromic blocker start to respond to light stimulation in a specific range of wavelengths in order to restore afferent signaling from the eye to the brain (*Fig. 1C*).

The promise of such an approach has been demonstrated in electrophysiological experiments on HEK293 cells expressing potential-dependent potassium channels and on cultured hippocampal neurons [11]. In both cases, the cells acquired photosensitivity. Experiments with blind rd1 mice with a knockout Pde6b gene demonstrated a response to light stimulation in an isolated retina and a retina incubated with a photochromic compound and a change in the behavioral response to light in animals that had received an intraocular injection of the drug [12, 13].

Further research in this direction requires physiological screening of a large number of compounds to select the most effective ones. For this reason, an animal model of photoreceptor-specific retinal degeneration that is simpler than the model with knockout mice is required. We have created two new amphibian-based models. The first model was obtained by mechanical removal of its photoreceptor outer segments. In the second model, the degeneration of rods and cones was achieved by intraocular injection of antibiotic tunicamycin. Tunicamycin is known to disturb opsin glycosylation and the formation of membrane discs in outer photoreceptor segments, which leads to their degradation within 15–25 days [14, 15]. The advantage of this model over the mouse models mentioned above consists

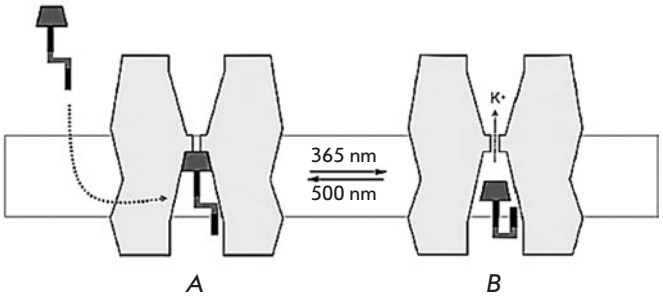

Fig. 2. The mechanism of action of molecular photochromic compounds on K^+ channels. *A* – the trans-form of the photochromic compound blocks the flow of ions through the channel, *B* – the cis-form does not prevent the flow of ions. The transition from one conformation to another takes place after light of a specific wavelength has been absorbed. The figure is adapted from ref. [9] (with changes)

in the simplicity of manipulations with the retina of cold-blooded animals compared to warm-blooded ones.

Several models of photoreceptor degeneration in cold-blooded animals have been developed thus far, but all of them use fish [16], including the models that use tunicamycin injections. Yet, performing intravital control over retinal degeneration is more complicated for a fish-based model than it is for amphibian-based ones.

EXPERIMENTAL

Synthesis of acrylamide-azobenzene-quaternary ammonium (AAQ, scheme)

4-[(E)-(4-Nitrophenyl)diazenyl]aniline (1a). 4-Nitroaniline (16.9 g, 0.12 mol) was partially dissolved in a mixture of water (50 mL) and concentrated aqueous HCl (50 mL) under heating in a water bath. The mixture was then cooled by pouring it into iced water, and a solution of sodium nitrite (8.4 g, 0.12 mol) in water (31 mL) was added under cooling on an ice bath. The resulting homogeneous mixture was stirred for 1 h; an ice-cold solution of aniline (11.4 g, 0.12 mmol) in a mixture of water (122 mL) and concentrated aqueous HCl (25 mL) was then added drop-wise for 30 min at 0–5 °C. After stirring in the ice-water bath for 2 h, the mixture was neutralized with aq. NH_3. The resulting mixture was filtered and washed with water and ethanol. The red–brown powder was dried in vacuo to give (**1a)** with a 66% yield. R_f = 0.74 (hexane–ethyl acetate 1:1 v/v). ^{1}H NMR (400 MHz, $CDCl_3$): δ 4.41 (Br. s, 2H), 6.63 (d, J = 8.1 Hz, 2H), 7.88 (d, J = 8.1 Hz, 2H), 8.08 (d, J = 8.7 Hz, 2H), 8.35 (d, J = 8.7 Hz, 2H).

4,4'-(E)-Diazene-1,2-diyldianiline (1b). A solution of amine (**1a)** (5.0 g, 18.5 mmol) and sodium sulfide nonahydrate (9.80 g, 37 mmol, 2 equiv) in ethanol (300 ml) was refluxed for 3 h. The solvent was evaporated under vacuum. The obtained brown oil was re-dissolved in a mixture of water (250 ml) and brine (15 ml). The product was extracted with ethyl acetate (3 x 100 ml), dried over magnesium sulfate, concentrated (to about 50 ml), and passed through a short pad of silica gel (25 g). Compound **(1b)** (3.2 g, 80%) was obtained as a reddish solid (mp. 234-237°C). R_f = 0.55 (hexane–ethyl acetate 1:1 v/v). ^{1}H NMR (400 MHz, DMSO-d_6) δ 5.73 (s, 4H), 6.61 (d, J = 8.7 Hz, 4H), 7.52 (d, J = 8.7 Hz, 4H). ^{13}C NMR (100 MHz, DMSO-d_6) δ 113.3, 124.2, 142.8, 151.4.

N-{4-[(E)-(4-Aminophenyl)diazenyl]phenyl}acrylamide (2a) and N,N'-[(E)-diazene-1,2-diylbis(4,1-phenylene)] bisacrylamide (2b). A solution of acryloyl chloride in dichloromethane (0.38 ml, 4.7 mmol) was added drop-wise to a solution of amine **(1b)** (1.0 g) in dichloromethane (200 ml) at 0°C. The obtained reaction mixture was stirred at room temperature for 12 h. After that, the solvent was evaporated. The products were analyzed by thin-layer chromatography (TLC) and then separated by column chromatography using silica with hexane: ethyl acetate as an eluent.

Compound **(2a)**: orange-red solid (19%); ^{1}H NMR (400 MHz, DMSO-d_6): 4.72 (s, 2H), 5.78 (dd, *J* = 10 and 2 Hz, 1H), 6.31 (dd, *J* = 17 and 2 Hz, 1H), 6.47 (dd, *J* = 17 and 10 Hz, 1H), 7.65 (d, *J* = 8.7, 2H), 7.79-7.94 (m, 6H), 10.34 (s, 1H). ^{13}C NMR (100 MHz, DMSO-d_6): 114.6 (2C), 121.3 (2C), 124.2 (2C), 125.7, 127.9 (2C), 132.4, 141.3, 145.3, 149.9, 152.5, 164.5. HRMS (ESI): *m/z* $[M + H]^+$ calcd for $C_{15}H_{16}N_4O$: 268.1319, found: 268.1324.

Compound **(2b)**: brown-red solid (42%); ^{1}H NMR (400 MHz, DMSO-d_6): 5.82 (dd, *J* = 10 and 2 Hz, 2H), 6.33 (dd, *J* = 17 and 2 Hz, 2H), 6.50 (dd, *J* = 17 and 10 Hz, 2H), 7.85–7.93 (m, 8H), 10.51 (s, 1H). HRMS (ESI): *m/z* $[M + H]^+$ calcd for $C_{18}H_{18}N_4O_2$: 322.1424, found: 322.1431.

N-[4-((E)-{4-[(2-Chloroacetyl)amino]phenyl}diazenyl) phenyl]acrylamide (3). A solution of chloroacetyl chloride (0.17 ml, 1.2 equiv.) in dichloromethane (5 ml) was added to a vigorously stirred solution of amine **(2a)** (1.8 mmol, 0.5 g) and DIPEA (0.9 ml, 3 equiv.) in dichloromethane (15 ml) at 0°C. The reaction mixture was stirred at room temperature for 12 h, quenched with water, and mixed with dichloromethane (2 × 20 ml). The combined organic layers were washed with a 5% aqueous HCl solution (15 ml) and water (15 ml), dried over sodium sulfate, and evaporated. The crude product was purified by flash chromatography using silica with hexane-ethyl acetate as an eluent to give rise to

(3) as a red solid with a 53% yield. ^{1}H NMR (400 MHz, DMSO-d_6): δ 4.32 (s, 2H), 5.83 (dd, J = 10 and 2 Hz, 1H), 6.32 (dd, J = 17 and 2 Hz, 1H), 6.50 (dd, J = 17 and 10 Hz, 1H), 7.81–7.90 (m, 8H), 10.48 (s, 1H), 10.64 (s, 1H). HRMS (ESI): m/z $[M + H]^+$ calcd for $C_{17}H_{17}ClN_4O_2$: 344.1035, found: 344.1031.

2-[(4-{(E)-[4-(acryloylaminophenyl]diazenyl}phenyl) amino]-N,N,N-triethyl-2-oxoethanammonium chloride (4, AAQ). Triethylamine (0.2 mL) was added to the solution of compound **(3)** (0.3 g, 0.9 mmol) in dimethylformamide (5.0 mL). The mixture was then heated for 12 h at 50°C in a nitrogen atmosphere. The reaction mixture was cooled to room temperature, and the solvent was removed in vacuo. The resulting red solid was dissolved in distilled water, and the insoluble precipitate was filtered off. Water was removed under vacuum to obtain pure compound **(4)** as a red solid with a 45% yield. ^{1}H NMR (400 MHz, D_2O): δ 1.12 (t, J = 7 Hz, 9H), 3.37 (m, 6H), 4.35 (s, 2H), 5.77 (dd, J = 10 and 2 Hz, 1H), 6.29 (dd, J = 17 and 2 Hz, 1H), 6.47 (dd, J = 17 and 10 Hz, 1H), 7.69–7.75 (m, 4H), 7.82-7.89 (m, 4H), 11.71 (s, 1H), 12.11 (s, 1H). ^{13}C NMR (100 MHz, D_2O): 7.8 (3C), 53.3, 56.5 (3C), 120.5 (2C), 121.1 (2C), 123.2, 125.2 (2C), 128.8 (2C), 132.8, 141.8, 142.6, 148.5, 149.7, 160.4, 163.9. HRMS (ESI): m/z $[M - Cl]^+$ calcd for $C_{23}H_{31}N_5O_2$: 409.2472, found: 409.2469.

The models of photoreceptor degeneration in cold-blooded animals

Marsh frogs (*Rana ridibunda*) caught in the Astrakhan Region of Russia were used in our experiments. The animals were kept in the vivarium of the Institute at 20°C and 12/12 light cycle; they were fed flour worms.

The model with mechanical removal of photoreceptors

First, the method of mechanical removal of the photoreceptor layer from the retina was tested. The retina extracted from the eyecup was placed on a filter paper sheet with the photoreceptors on the paper surface. The outer segments of the photoreceptors are connected to the inner segment layers by a thin cilium that can be easily broken. Thus, we just needed to remove the paper with the photoreceptor layer on it to obtain a retina model devoid of light-sensitive outer photoreceptor segments.

The obtained model was tested in electrophysiological experiments. The preparation was placed in a chamber filled with an amphibian Ringer solution. Two identical silver/silver chloride electrodes (World Precision Instruments, Inc., USA) in contact with the medium from different sides of the retina were used for transretinal ERG recording. The composition of the Ringer solution for preparations of the isolated retina was as follows: 90 mM NaCl, 2.5 mM KCl, 1.4 mM $MgCl_2$, 10 mM glucose, 1.05 mM $CaCl_2$, 5 mM $NaHCO_3$, 5 mM HEPES, 0.05 mM EDTA, and 50 mg/l bovine serum albumin. White (415–745 nm) and ultraviolet (UV, 365 nm) LEDs were used for stimulation. Signal intensity was controlled by changing the electric current flowing through the LEDs and by using neutral-density filters. ERG was recorded with 5 ms sampling for each point with analogous filtration in the 0–100 Hz band using an 8-pole Bessel filter. The experimental setup controlling program was custom written in the laboratory using Microsoft Visual Basic 96.

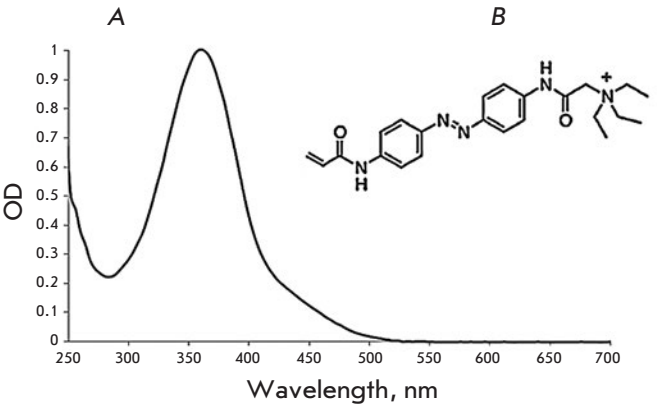

Fig. 3. *A* – spectrum of the trans-form of AAQ in the amphibian Ringer solution; *B* – the structural formula of AAQ

The model of the retina without photoreceptors was tested using a AAQ photochromic compound whose efficiency was known from the study performed on knockout mice [12]. The retina was placed in a chamber filled a witha 1 mM AAQ solution (the Ringer solution was used as a solvent) and incubated for 30 min. The chamber containing the retina sample was then filled with a pure Ringer solution, and ERG was recorded. AAQ is known to change conformation under illumination with a 365-nm wavelength (*Fig. 3*). For this reason, the sample was tested using brief flashes and long exposures to UV LED. Green light was used as the control signal (520 nm, white LED with an appropriate color filter).

The model of tunicamycin-induced photoreceptor degeneration

A tunicamycin solution (Sigma, 1 μg of the antibiotic per 10 g of frog weight) in DMSO at a concentration of 0.5 mg/ml was injected into one eye of the frogs. The second eye was used as the control; the same volume of pure DMSO was injected into it. *In vivo* ERG was recorded 2 h after the injection and then subsequently

with a 7-day interval. Before the injections and ERG recordings, the frogs were anesthetized with a MS-222 drug (Sigma, 1 mg/ml aqueous solution). Recording from the surface of the eye cornea was performed using the same experimental setup as the one used for ERG recordings from the isolated retina. To achieve such recordings, a silver wire electrode that was in contact with the cornea through a conductive ophthalmic gel was used; a white diffuser ensuring a uniform distribution of light over the pupil area was employed. A silver wire electrode inserted into the oral cavity of the animal was used as the control electrode. Light stimulation was performed with short (10 ms), white LED flashes. Thus, the entire process of photoreceptor degeneration was monitored. After the photoresponse in animals had disappeared, they were decapitated and a preparation of the retina devoid of photoreceptors was obtained. The parameters (sampling and the filtering band) were the same as those used during ERG recording from the isolated retina with mechanically removed photoreceptors.

The retina preparation extracted from the eye that had been exposed to tunicamycin and lost photosensitivity was additionally tested for lack of ERG in Ringer solution and then in a the presence of a photochromic compound, AAQ, in the same manner as the model with mechanically removed photoreceptors.

Morphological control over photoreceptor degeneration

After the photoresponse in the tunicamycin-exposed eye had disappeared, the eyecups of three decapitated frogs were taken for the subsequent histological investigation. The fixation protocol was the same as described by Sillman et al. [18]. The eyecups were placed into a 1% glutaraldehyde solution in 0.1 M phosphate buffer for 1.5 h. The preparations were then rinsed with a 4% paraformaldehyde solution in 0.1 M phosphate buffer for 4 h and kept in a 1% paraformaldehyde solution for several weeks. The preparations were then washed with 0.1 M phosphate buffer, dehydrated with ethanol, and fixed in a LR White epoxy resin (Fluka). Slices (1–3 μm thick) were prepared using an LKB ultramicrotome, stained with toluidine blue, and assessed by light microscopy to identify the layer of photoreceptor cells.

RESULTS AND DISCUSSION

Synthesis of acrylamide-azobenzene-quaternary ammonium (AAQ)

Water-soluble acrylamide-azobenzene-quaternary ammonium was synthesized in several simple stages from simple and easily accessible compounds. The azo group was inserted via the reaction of the corresponding diazonium salt with aniline (*scheme*). The obtained 4-nitroazobenzene **(1a)** was reduced to 4,4'-diaminoazobenzene **(1b)** with sodium sulfide in boiling ethanol (*scheme*). Monosubstituted 4,4'-diamonoazobenzene **(2a)** was obtained via the reaction between azobenzene **(1b)** and acrylic acid chloride. The corresponding diadduct was formed as a by-product of this reaction **(2b)** (*scheme*). A quaternary ammonium cation was inserted into the target product in two stages (*scheme*). The amide **(3)** was produced in the reaction between aminoazobenzene **(2a)** and chloroacetic acid. The reaction between the resulting chloroacetyl chloride and triethylamine gave rise to target compound **(4), (AAQ)** with moderate yields.

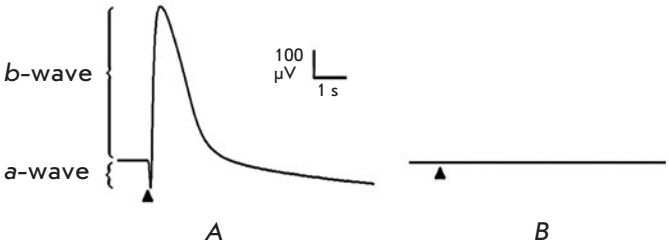

Fig. 4. *A* – ERG of the intact retina preparation in response to light stimulation. *B* – ERG of the retina preparation after mechanical removal of photoreceptors. Stimulation was performed with green light (520 nm; duration of the flash, 10 ms; flash intensity, 2.9×10^6 photons/μm^2/s). The moment of flash is shown with a triangle

Photoreceptor degeneration models in cold-blooded animals

The model with mechanical removal of photoreceptors. An ERG of the intact retina sample contains both expected components: a-wave characterizing the hyperpolarization of photoreceptors and b-wave arising from the function of Müller cells and bipolar cells (*Fig. 4A*). Either a lack of response to UV and visible light stimulation or weak residual responses with an amplitude of several μV is observed after the photoreceptor layer has been mechanically removed (*Fig. 4*). The residual response retains only the b-wave, while the a-wave completely disappears (*Fig. 5A, C*). These results demonstrate that the employed approach allows one to obtain a working model of retinal degeneration which can be used in further studies.

Results of incubation in AAQ solution. As expected, stimulation of a retina sample after its incubation in the AAQ solution with green light led to naught response (*Fig. 5B*). No response to brief flashes of UV light oc-

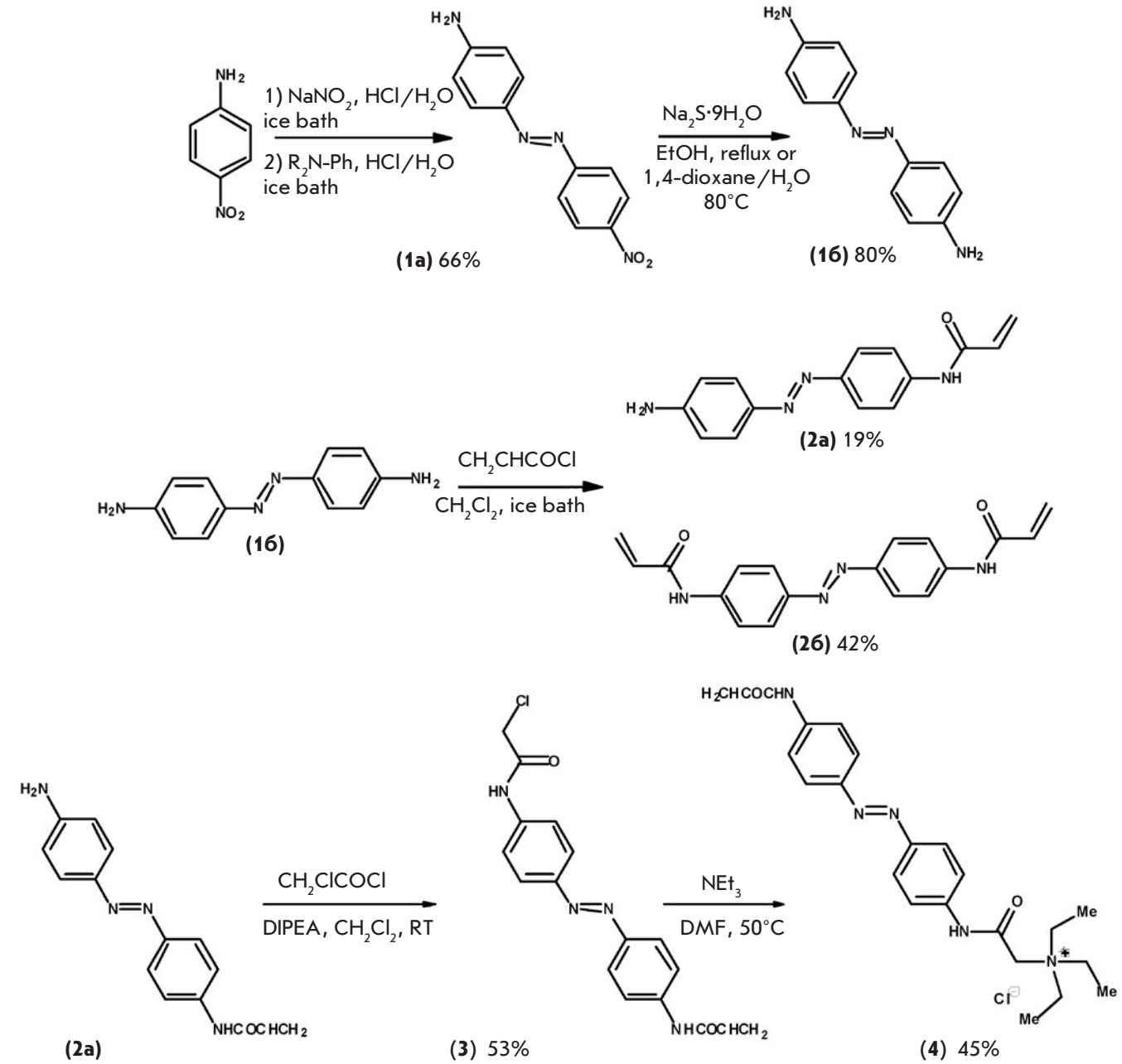

Scheme. Synthesis of acrylamide-azobenzene-quaternary ammonium

curred, while long-term UV light stimulation led to a response pointed in the same direction as a normal ERG a-wave with an amplitude ranging from 10 to 100 μV (*Fig. 5D*). This response ceased right after the illumination had been turned off. The potential had either never returned to its initial value or the process was very slow. The amplitude of the occurring response depended on the intensity of the light stimuli: the higher the intensity of the UV stimuli, the larger the change in the potential was (*Fig. 6*).

The model of tunicamycin-induced photoreceptor degeneration

Injections of tunicamycin led to a progressing decrease in the response amplitude to brief flashes of light (*Fig. 7*). As one can see in *Fig. 7, panel a*, the ERG amplitude for the eye with tunicamycin injection gradually decreased and completely disappeared on days 14–21. On the contrary, the ERG of the control eye into which a pure solvent (DMSO) was injected (*Fig. 7, panel b*) did not change.

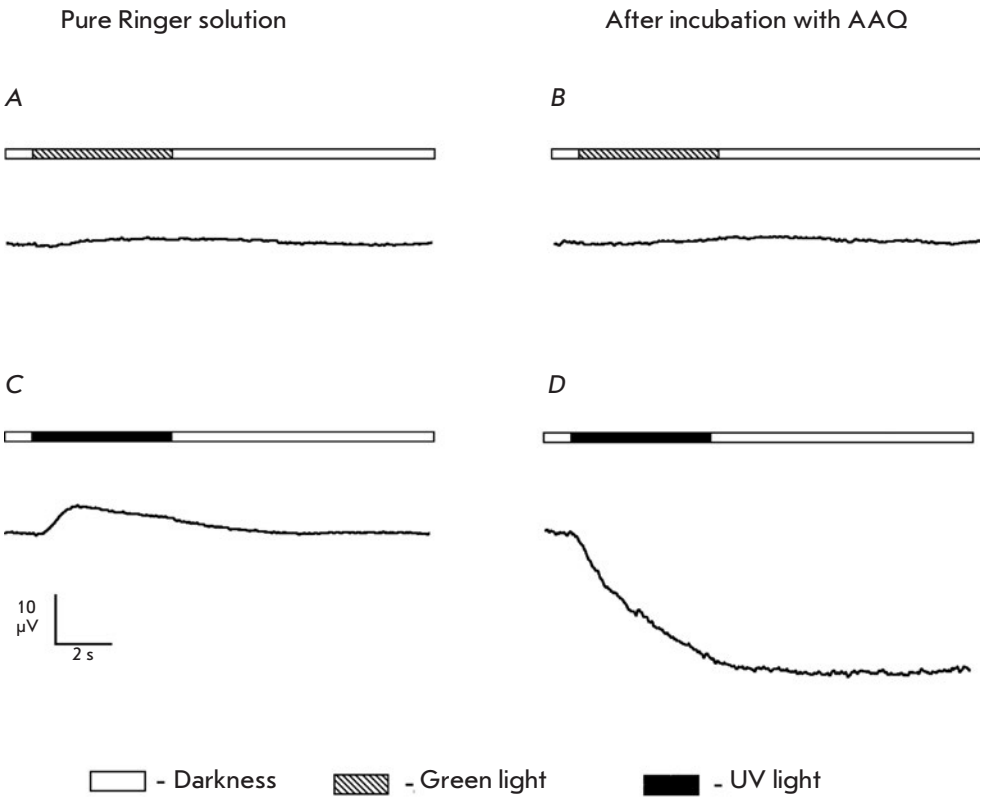

Fig. 5. Comparison of the trans-retinal ERG of retina with mechanically removed photoreceptors that occurs in response to green and UV light stimuli in a pure Ringer solution (*A*,*C*) and after 30 min of incubation in 1 mM AAQ (*B*,*D*). The scheme of stimulation is given for each plot. The stimulation duration is 5 s. The intensity of green light (520 nm) is 2.9×10^8 photons/μm^2/s; the intensity of UV light (365 nm), 6.5×10^8 photons/μm^2/s

Microscopy of the eyecup slices confirmed that exposure to tunicamycin caused selective degeneration of photoreceptor cells. In *Fig. 8A* showing a transverse section of the eyecup from the control eye (DMSO injection), all retinal layers are well-distinguishable. In the retina of the eye exposed to tunicamycin, the layer of photoreceptor cells is absent (*Fig. 8B*) but bipolar, amacrine, and ganglion cells remain. Therefore, such a degeneration model can be used to test molecular photochromic compounds. The isolated retina of the eye exposed to tunicamycin responded to stimulation with neither green nor UV light (*Fig. 9 A*,*C*), which is consistent with the results of *in vivo* ERG recordings and shows that the performed manipulations yielded the desired result: a model of photoreceptor degeneration was obtained.

Results of incubation in AAQ solution

Incubation in the AAQ solution induced a response to long-term UV illumination unidirectional to that of a normal ERG a-wave, with an amplitude of 10–30 μV (*Fig. 9 B*,*D*), similar to the model of retina with mechanically removed photoreceptors. The signal recorded after the illumination was turned off remained stable, thus indicating that the nature of the response is identical to that of the model with mechanically removed photoreceptors. Stimulation with green light did not lead to any response.

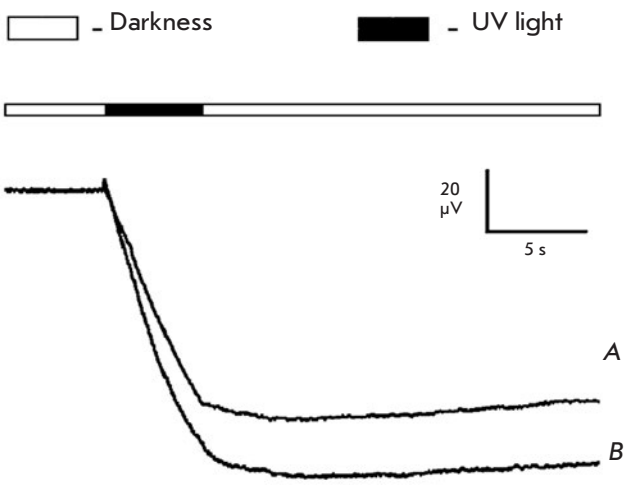

Fig. 6. The response of the retina with mechanically removed photoreceptors to long-term (5 s) UV illumination (365 nm) of differing intensity after incubation with AAQ. *A* – intensity, 2.7×10^8 photons/μm^2/s, *B* – intensity, 6.5×10^8 photons/μm^2/s

The results show that AAQ restores photosensitivity to a model preparation in the near-UV region, possibly

via light-dependent regulation of ion channels by the photochromic compound. Both models of degenerated retina yield similar results.

CONCLUSIONS

In this study, we have introduced two experimental models of photoreceptor degeneration that can be used for the primary screening of new molecular photochromic potassium channel blockers.

The findings on the effect of AAQ on ERG obtained in this study show good agreement with the results reported by other authors who demonstrated that this compound is able to impart photosensitivity in the UV region to the degenerated retina [12]. The effect of molecular photochromic compounds demonstrated by the authors was as follows: the frequency of spike generation by ganglion cells increased significantly under long-term UV stimulation (a multi-electrode array was used for recording), while returning to the initial level after the light had been turned off or replaced with green light. We have demonstrated in this study that a different pattern is observed upon alternation of UV stimulus and a dark cycle or a UV stimulus and green light: the potential changes only during exposure to UV, while signal intensity remains stable under dark conditions or under illumination with green light but does not return to its initial level (*Fig. 10*).

Our data also indicate that AAQ cannot be regarded as a substance for vision restoration to be used in clinical practice not only because it is unable to function under light visible to the human eye, but also due to its ultra-slow response to a light stimulus. However, the amphibian-based models of photoreceptor degeneration proposed in this work can be used to test new compounds and identify the most promising ones. The approach with mechanical photoreceptor removal allows one to quickly obtain a model preparation; therefore, its application accelerates the screening of photochromic compounds. On the contrary, tunicamycin-induced photoreceptor degeneration is a gradual process and the changes inherent to common retina-degeneration diseases, such as retinitis pigmentosa or age-related macular degeneration, have time to occur [19]. There-

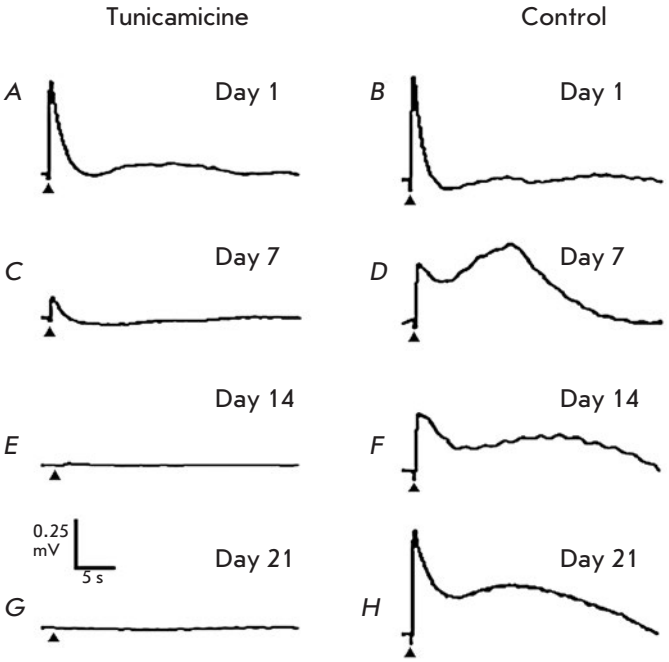

Fig. 7. ERG registered from the cornea of an anesthetized frog at different periods of time post-injection. *A, C, E, G* – from the eye into which tunicamycin was injected; *B, D, F, H* – from the eye into which only DMSO was injected. Stimulation with white light (range, 415–745 nm); flash duration, 10 ms; intensity, ~9 W/μm^2 of the pupil area. The moment of flash is shown with a triangle

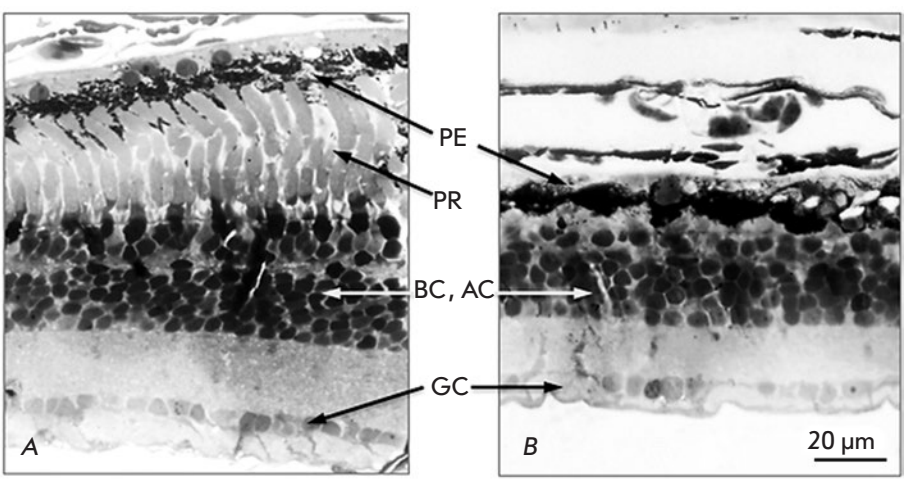

Fig. 8. Light microscopy images of retina preparations. *A* – the retina of the control eye into which DMSO was injected. *B* – the retina of the eye into which tunicamycin was injected. *PE* – pigment epithelium, *GC* – ganglionic cells, *AC* – amacrine cells, *BC* – bipolar cells, *PR* – photoreceptors. The photoreceptor layer is absent, but other cell types remained in the retina exposed to tunicamycin

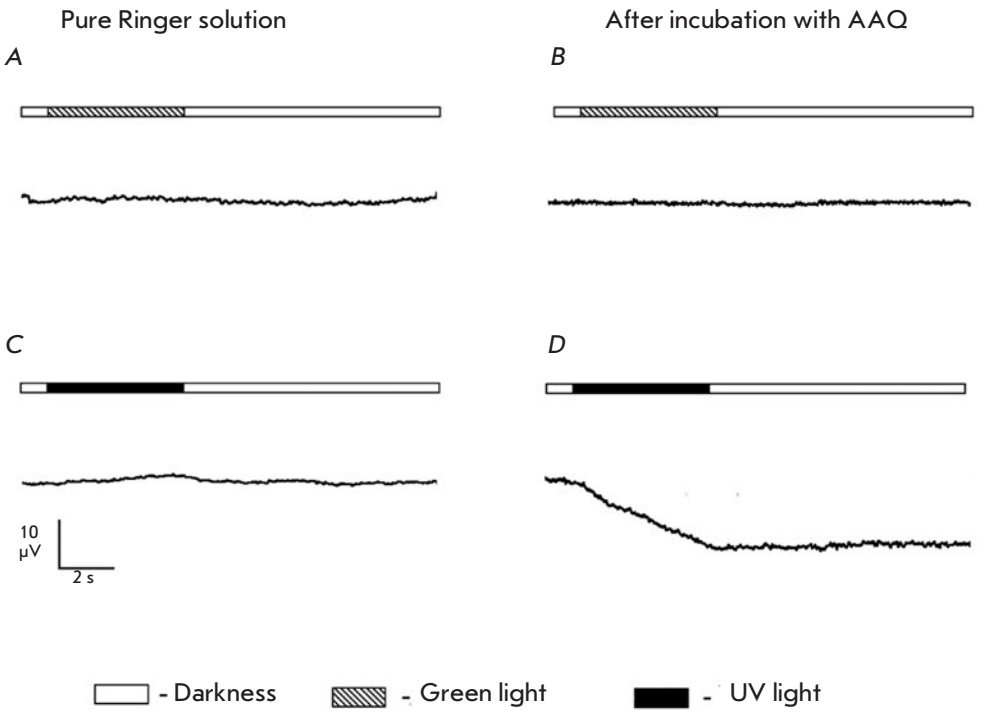

Fig. 9. Comparison of the transretinal ERG of the retina degenerated after being exposed to tunicamycin, which occurs in response to illumination with green and UV light in a pure Ringer solution (*A*, *C*) and after 30 min of incubation in 1 mM AAQ (*B*, *D*). The scheme of light stimulation is given for each diagram. Duration of each light stimulation is 5 s. The intensity of green light (520 nm) is 2.9×10^8 photons/μm²/s; the intensity of UV light (365 nm) is 6.5×10^8 photons/μm²/s

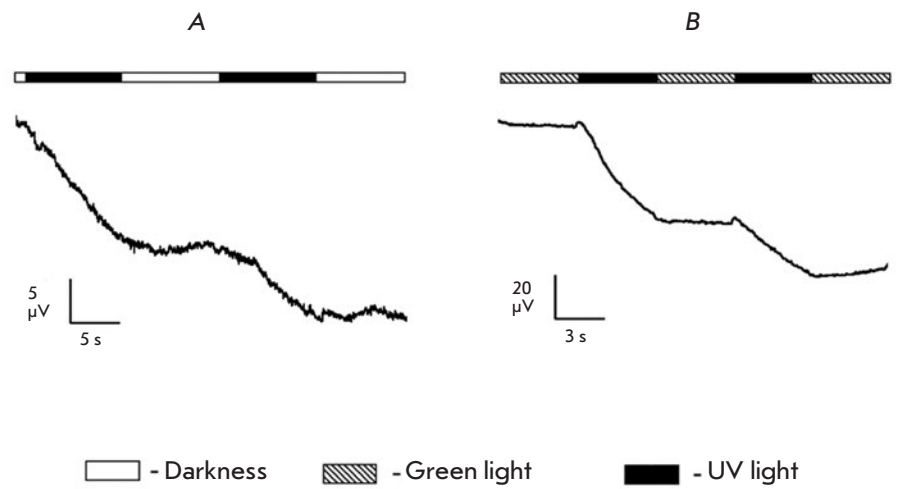

Fig. 10. *A* –ERG of the retina degenerated after being exposed to tunicamycin under alteration of UV illumination (365 nm) and dark cycles after 30 min of incubation in 1 mM AAQ. B – ERG of the retina with mechanically removed photoreceptors under alteration of illumination with UV (365 nm) and green light (520 nm) after 30 min of incubation in 1 mM AAQ. The scheme of light stimulation is given for each diagram. The intensity of green light is 2.9×10^8 photons/μm²/s; the intensity of UV light is 6.5×10^8 photons/μm²/s

fore, the tunicamycin model allows one to study the action of molecular photochromic compounds on a model that is closer to a degenerated retina.

The model of tunicamycin degeneration can be further tested using laboratory rats in order to obtain a model that would be more valid for humans and to investigate the effect of these compounds on the retina of warm-blooded animals. Attempts to create a model of tunicamycin photoreceptor degeneration on rats have already been reported [20], but the action of molecular photochromic compounds under this model has not been studied yet. ●

The authors are grateful to V.I. Govardovskii (Sechenov Institute of Evolutionary Physiology and Biochemistry, Russian Academy of Sciences).

This work was supported by the Russian Foundation for Basic Research (grant no. 15-29-03872 ofi_m), the Skolkovo Foundation (grant agreement for Russian Educational and Research Organization no. 7 dated December 19, 2017), and Skolkovo Institute of Science and Technology (General agreement no. 3663-MRA dated December 25, 2017).

REFERENCES

1. Hamel C. // Orphanet J. Rare Dis. 2006. V. 1 (1). P. 1–40.
2. Guadagni V., Novelli E., Piano I., Gargini C., Strettoi E. // Prog. Retinal Eye Res. 2015. V. 48. P. 62–81.
3. Weiland J.D., Cho A.K., Humayun M.S. // Ophthalmology. 2011. V. 118 (11). P. 2227–2237.
4. Lamba D.A., Gust J., Reh T.A. // Cell Stem Cell. 2009. V. 4 (1). P. 73–79.
5. Schwartz S.D., Hubschman J.P., Heilwell G., Franco-Cardenas V., Pan C.K., Ostrick R.M., Mickunas E., Gay R., Klimanskaya I., Lanza R. // Lancet. 2012. V. 379 (9817). P. 713–720.
6. Sahel J. A., Roska B. // Annu. Rev. Neurosci. 2013. V. 36. P. 467–488.
7. van Wyk M., Pielecka-Fortuna J., Löwel S., Kleinlogel S. // PLoS Biol. 2015. V. 13 (5). P. e1002143.
8. Banghart M.R., Mourot A., Fortin D.L., Yao J.Z., Kramer R.H., Trauner D. // Angewandte Chem. Internat. Ed. 2009. V. 48 (48). P. 9097–9101.
9. Fortin D.L., Banghart M.R., Dunn T.W., Borges K., Wagenaar D.A., Gaudry Q., Karakossian M.H., Otis T.S., Kristan W.B., Trauner D., Kramer R.H. // Nat. Meth. 2008. V. 5 (4). P. 331–338.
10. Polosukhina A., Litt J., Tochitsky I., Nemargut J., Sychev Y., De Kouchkovsky I., Huang T., Borges K., Trauner D., van Gelder R.N., Kramer R.H. // Neuron. 2012. V. 75 (2). P. 271–282.
11. Tochitsky I., Polosukhina A., Degtyar V.E., Gallerani N., Smith C.M., Friedman A., van Gelder R.N., Trauner D., Kaufer D., Kramer R.H. // Neuron. 2014. V. 81 (4). P. 800–813.
12. Fliesler S.J., Basinger S.F. // Proc. Natl. Acad. Sci. USA. 1985. V. 82 (4). P. 1116–1120.
13. Fliesler S.J., Rapp L.M., Hollyfield J.G. // Nature. 1984. V. 311 (5986). P. 575–577.
14. Blanco-Sánchez B., Clément A., Phillips J.B., Westerfield M. // Meth. Cell Biol. 2017. V. 138. P. 415–467.
15. Negishi K., Sugawara K., Shinagawa S., Teranishi T., Kuo C.H., Takasaki Y. // Developmental Bain Res. 1991. V. 63 (1–2). P. 71–83.
16. Sillman A.J., Govardovskii V.I., Röhlich P., Southard J.A., Loew E.R. // J. Comparative Physiol. A: Neuroethology, Sensory, Neural, and Behavioral Physiol. 1997. V. 181 (2). P. 89–101.
17. Marc R., Pfeiffer R., Jones B. // ACS Chem. Neurosci. 2014. V. 5 (10). P. 895–901.
18. Shirai Y., Mori A., Nakahara T., Sakamoto K., Ishii K. // Biol. Pharmaceut. Bull. 2015. V. 38 (7). P. 1076–1080.
19. Drivas T.G., Bennett J. // Neuron. 2012. V. 75 (2). P. 185–187.
20. Mourot A., Kienzler M.A., Banghart M.R., Fehrentz T., Huber F.M., Stein M., Kramer R.H., Trauner D. // ACS Chem. Neurosci. 2011. V. 2 (9). P. 536–543.

Influence of the Linking Order of Fragments of HA2 and M2e of the influenza A Virus to Flagellin on the Properties of Recombinant Proteins

L. A. Stepanova[1*], R. Y. Kotlyarov[2], M. A. Shuklina[1], E. A. Blochina[2], M. V. Sergeeva[1], M. V. Potapchuk[1], A. A. Kovaleva[1], N. V. Ravin[2], L. M. Tsybalova[1]

[1]Research Institute of Influenza, Russian Federation Ministry of Health, Prof. Popova Str.15/17, St. Petersburg, 197376, Russia

[2]Institute of Bioengineering, Research Center of Biotechnology of the Russian Academy of Sciences, Leninsky Ave. 33, bldg. 2, Moscow, 119071, Russia

*E-mail: stepanoval60@mail.ru

Received: December 28, 2017; in final form January 23, 2018

ABSTRACT **The ectodomain of the M2 protein (M2e) and the conserved fragment of the second subunit of hemagglutinin (HA2) are promising candidates for broadly protective vaccines. In this paper, we report on the design of chimeric constructs with differing orders of linkage of four tandem copies of M2e and the conserved fragment of HA2 (76–130) from phylogenetic group II influenza A viruses to the C-terminus of flagellin. The 3D-structure of two chimeric proteins showed that interior location of the M2e tandem copies (Flg-4M2e-HA2) provides partial α-helix formation nontypical of native M2e on the virion surface. The C-terminal position of the M2e tandem copies (Flg-HA2-4M2e) largely retained its native M2e conformation. These conformational differences in the structure of the two chimeric proteins were shown to affect their immunogenic properties. Different antibody levels induced by the chimeric proteins were detected. The protein Flg-HA2-4M2e was more immunogenic as compared to Flg-4M2e-HA2, with the former offering full protection to mice against a lethal challenge. We obtained evidence suggesting that the order of linkage of target antigens in a fusion protein may influence the 3D conformation of the chimeric construct, which leads to changes in immunogenicity and protective potency.**

KEYWORDS **influenza, vaccine, HA2, M2e, recombinant protein, flagellin.**

ABBREVIATIONS **M2e – ectodomain of M2 protein of influenza A viruses, HA – hemagglutinin, HA2 – second subunit of hemagglutinin, Flg – flagellin, BALF – bronchoalveolar lavage fluid, ELISA – enzyme-linked immunosorbent assay, OD – optical density, GMT – geometric mean titer, TCID50 – 50% tissues cytopathogenic infectious virus dose.**

INTRODUCTION

The development a new generation of vaccines capable of providing protection against various influenza A viruses, as well as severe forms of influenza A, for at least 5 years is a global challenge. Influenza A conserved proteins (M2, HA2, M1, NP) have emerged as promising targets for vaccine design. A number of studies that have assessed the highly conserved ectodomain of the M2 protein (M2e) of the influenza A virus as a vaccine antigen have shown potent immunogenicity and efficacy in animals, as well as safety and immunogenicity in humans [1–7]. M2e-based vaccines are not for prophylactic use and do not prevent infection, but they reduce clinical signs by limiting virus replication and offering cross-protection [8–11]. The protection offered by M2e-based vaccines is attributed to antibody production [8, 10, 12, 13]. The mechanism of M2e-induced immunity is mediated by antibody-dependent cellular cytotoxicity and antibody-dependent cell mediated phagocytosis. In contrast to anti-HA antibodies, anti-M2e-antibodies do not prevent virus infection and are not neutralizing, but they can eliminate infected cells by an antibody-dependent cellular cytoxicity mechanism and thus reduce viral replication [9, 11, 14].

Recently, an enormous research effort has been focused on the HA2 subunit conserved within the phylogenetic group that mediates the fusion of cellular and viral membranes in endosomes, resulting in entry of the ribonucleic complex into the cytoplasm [15]. Monoclonal antibodies that react with the epitopes localized in the stem region of HA are cross-reactive and can neutralize influenza viruses within one phylogenetic

group [16–22]. There are studies that have been devoted to the search for the most promising epitopes HA2 of influenza A viruses I and II phylogenetic groups (amino acid residues (aa) 38–59, 23–185, 1–172, 76–103, 35–107). The identification of these sites allowed researchers to design recombinant proteins [23–27]. Animal studies have shown that such proteins elicit both humoral and cytotoxic T-cell mediated responses. Moreover, they protect animals against a lethal challenge from homologous and heterologous influenza A viruses from one phylogenetic group.

However, a vaccine carrying several conserved protein epitopes which induce humoral and T-cell-mediated responses and neutralize a broad range of influenza virus strains would offer a more effective protection.

Flagellin represents an appropriate platform for the development of recombinant vaccines against various pathogens of viral and bacterial origin [2, 28]. The adjuvant effect of flagellin is mediated via the TLR5 signaling pathway in CD11c+ antigen-presenting cells, which explains the increase in the immunogenic potential of antigens fused to flagellin and the ability to enhance the CD4+ T-mediated humoral response [28–31]. The role of flagellin as a vaccine platform and an adjuvant at the same time has been demonstrated in multiple infection models, including influenza [2, 6, 27, 32–34].

In this study, we report on the eventuality of producing a recombinant protein containing conserved epitopes of the M2 and HA proteins fused to the C-terminus of full-length flagellin. We designed two chimeric proteins with differing orders of linkage of four tandem copies of M2e and a conserved fragment of HA2 (76–130) from phylogenetic group II influenza A viruses to the C-terminus of flagellin. We compared the effect of different insertion points of the target antigens into flagellin on the structure, stability, and immunogenicity of the recombinant proteins.

EXPERIMENTAL SECTION

Selection of a conserved HA2 region from influenza A virus phylogenetic group II

A search for amino acid sequences for our analysis was carried out using the GenBank and GISAID databases. In order to construct consensuses, sequences were aligned using the MAFFT server (http://mafft.cbrc.jp/alignment/server/index.html) and using either the FFT-NS-I or FFT-NS-2 algorithm (depending on the number of sequences) [35] and analyzed using the Unipro UGENE v.1.14.0 software [36]. Alignment and sequence analysis were performed using the Vector NTI (v10.0) software (Invitrogen, USA). A search for experimental B-cell and CD4+ T-cell epitopes homologous to HA2 fragments was performed in the Immune Epitope Database [37]. A search for possible CD8+ T-cell epitopes was conducted using the NetCTLpan 1.1 server [38] with default search parameters. Three-dimensional HA structure (4JTV models - 4O5I A/Victoria/06/2011 H3N2 - from the RCSB Protein Data Bank) was visualized using the Chimera (1.9) [39]. Visualization of the three-dimensional structures of recombinant proteins was carried out using Chimera 1.5.3 [39]. For homology modeling of the 3D structure of recombinant proteins on primary sequence we used the open web resource Phyre2 [40].

Construction of expression vectors

The pQE30 plasmid (Qiagen) was used to construct vectors for the expression of chimeric proteins with different insertion points of target antigens. The chimeric protein Flg-4M2e-HA2 contains flagellin (Flg) from *Salmonella typhimurium*, carrying at the C-terminus four copies of the M2e peptide (two copies M2e consensus among human influenza viruses A – M2eh and two copies of M2e from A/H5N1 – M2ek) and the HA2 subunit conserved region of influenza A viruses from the second phylogenetic group. In the second chimeric protein Flg-HA2-4M2e, the HA2-fragment was linked first to the C-terminus of flagellin, followed by four M2e copies. The chimeric genes were designed using common genetic engineering techniques. The flagellin gene was amplified from the *S. typhimurium* genome by PCR and cloned. Nucleotide sequences encoding the consensus HA2 sequence (aa 76–130) of influenza A viruses of phylogenic group II and tandem copies of M2e were synthesized *in vitro*. The HA2 expression in *Escherichia coli* cells was codon-optimized. As a result, vectors expressing pQE30_Flg_HA2_4M2e and pQE30_Flg_4M2e_HA2 were prepared.

Expression and purification of chimeric proteins

The *E. coli* strain DLT1270 was transformed with the pQE30/Flg-HA2-4M2e and pQE30/Flg-4M2e-HA2 plasmids for chimeric proteins expression. The strains DLT1270 are derived from DH10B [41] containing the lactose repressor gene *lacI* intergrated into the bacterial genome. *E. coli* strains were grown in a LB medium supplemented with ampicillin until the mid-log phase (OD_{600} = 0.4–0.7) at 37°C, followed by induction with IPTG at a concentration of 0.1 mM and culturing for another 4 h at 37°C. The cells were treated with lysozyme. The produced chimeric proteins were purified from lysed cells by metal-affinity chromatography on a Ni-column.

Electrophoresis and western-blot

Polyacrylamide gel electrophoresis (PAGE) was run under denaturing conditions according to the Laemmli

protocol [42]. Protein samples were mixed with a sample buffer containing beta-mercaptoethanol, boiled for 7 min, and separated on a 8-16% acrylamide gradient gel. The electrophoresis was run at 10-12 mA for 1.5 h. The gel was fixed in 10% acetic acid. Protein bands were visualized by staining with Coomassie G-250 for 18 h. The proteins were electro-transferred onto a nitrocellulose membrane (BioRad, USA) in a transfer buffer (TB) (0.03 M glycine, 0.04 M Tris, 0.037% sodium dodecyl sulfate, 20% ethanol). The transfer was performed in a Bio-Rad Mini Trans-Blot system (BioRad, USA) at a constant current of 200 mA in the cold (+4°C) for 1.5 h. After the transfer, the nitrocellulose membranes were blocked in 3% BSA (bovine serum albumin, Amresco, EU) in phosphate buffered saline (PBS) overnight at room temperature. Protein bands were visualized by incubation with mouse monoclonal anti-M2e antibodies 14C2 (ab5416, Abcam, UK). The membrane was incubated with primary antibodies diluted in PBS with 0.1% Tween 20 (PBS-T) and 3% BSA, followed by a wash in PBS-T. The bound mouse antibodies were then evaluated with peroxidase-labeled secondary antibodies (goat anti-mouse IgG, Abcam, UK) at room temperature for 1 h and incubated in a TMB (tetramethylbenzidine) Immunoblot solution (Invitrogen, USA) for 5 min.

Mouse immunization

Female Balb/c mice (16–18 g) were purchased from the Stolbovaya mouse farm at the State Scientific Center of Biomedical Technologies, Russian Academy of Medical Sciences. The mice were housed at the vivarium of the Research Institute of Influenza of the Ministry of Healthcare of the Russian Federation according to their in-house animal care guidelines. The animals were immunized with Flg-4M2e-HA2 or Flg-HA2-4M2e chimeric proteins intranasally (following inhalation anesthesia with 2–3% isoflurane, 30% O_2, 70% N_2O) three times at 2 week intervals at a dose of 6 μg/0.1 ml. The control mice were intranasally injected with 0.1 ml PBS.

Sampling of sera and bronchoalveolar lavage fluids

Serum samples and bronchoalveolar lavage fluids (BALF) were obtained from five mice of each group 14 days post third immunization following euthanasia in a CO_2-chamber (Vet Tech Solutions, UK). Serum was harvested after clot formation at 37°C for 30 min. Blood clots were placed on ice for cooling for 1 h and centrifuged at 400 g for 15 min. The obtained serum was aliquoted (30 μl) and frozen at −20°C.

To collect BALF, the sacrificed animals were secured in supine position on the operating table. The ventral skin was incised from the lover jaw along the midline to expose the trachea. The lower part of the exposed trachea was cannulated 3–5 mm deep to assess the lung lumen. The lungs were lavaged twice via the cannula with 1 ml PBS. The collected BALF samples were centrifuged at 400 g for 15 min and the supernatant aliquoted and stored at −20°C.

Synthetic peptides

The immunogenicity of the chimeric proteins was evaluated with the following synthetic peptides supplied by the Scientific Production Association "Verta":

M2ek SLLTEVETP**T**RNEW**E**CRC**S**DSSD (M2e of influenza virus A/Kurgan/05/05 (H5N1)),

M2eh SLLTEVETP**I**RNEW**G**CRC**N**DSSD (consensus M2e sequence in human influenza A viruses). The different amino acid residues are indicated in bold font and underlined.

ELISA

Antigen-specific IgG and IgA levels in immunized mice were evaluated with ELISA in high adhesion 96-well plates (Greiner, Germany). The plates were coated with M2e-peptides (5 μg/ml) or purified virus A/Aichi/2/68 (H3N2) (2 μg/ml) in PBS (pH 7.2) overnight at 4°C.

The plates were blocked with PBS in 5% FBS (300 μl/well) at room temperature for 1 h, followed by three washes with PBS-T. The plate wells were loaded with 100 μl 2-fold serum dilutions or BALF in blocking buffer and incubated at room temperature for 1 h. Goat polyclonal anti-mouse IgG and IgA peroxidase labeled (Abcam, UK) in a dilution of 1 : 20,000. TMB was used as a substrate (BD Bioscience, USA). The incubation time was 15 min. The optical density (OD) was measured at 450 nm using an iMark microplate reader (Bio-Rad, USA). The maximum serum dilution that had an optical density at least 2 times higher than the twice mean value of the blank was taken as the titer

Viruses and challenge of mice

In this study, we used influenza virus A/Aichi/2/68 (H3N2) received from the Collection of Influenza and Acute Respiratory Viruses of the laboratory of evolution of the influenza virus at the Research Institute of Influenza of the Ministry of Healthcare of the Russian Federation. Influenza virus A/Aichi/2/68 (H3N2) is a mouse-adapted virus obtained by the Research Institute of influenza by serial mouse/egg passages. The mouse-adapted virus A/Aichi/2/68 (H3N2) retains the antigenic properties of the wild-type strain but acquires a lethal phenotype for mice. The amino acid sequence of the surface proteins (M2, NA и HA) of the mouse-adapted strain was identical to that of the parental strain [6]. On day 14 post third immunization, Balb/c mice (eight mice in the experimental and con-

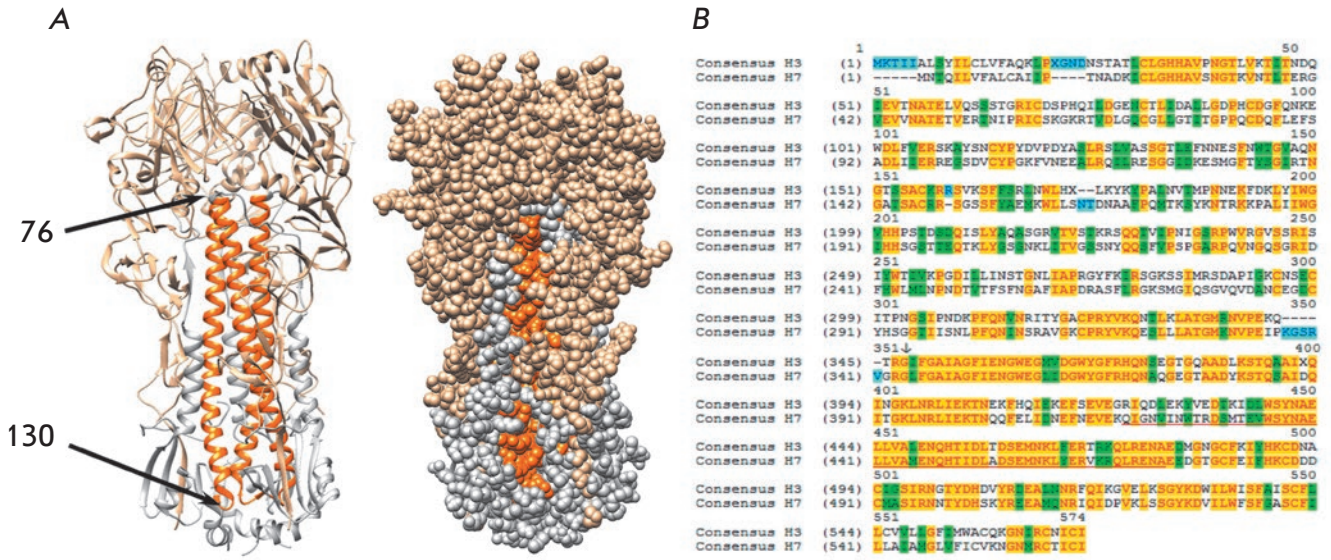

Fig. 1. A – Three-dimensional structure (trimer, 4JTV RCSB Protein Data Bank model) of HA of influenza A/H3N2 virus (phylogenetic group II). HA1 subunit is in beige; HA2, in grey; and HA2 fragment 76–130 is in orange. B – Alignment of consensus HA sequences of human influenza A/H3N2 and A/H7N9 influenza viruses (including human isolates), both from phylogenetic group II. The start of the HA2 subunit is marked with an arrow. The 76–130 region is underlined in red, the identical regions are in yellow, substitutions for chemically similar residues are in green, amino acid substitutions are colorless, and insertions are blue.

trol groups) were challenged with the mouse-adapted A/Aichi/2/68 (H3N2) strain at a dose of 5LD50. The virus was administered intranasally in a volume of 50 µl/mouse following inhalation anesthesia (2–3% isoflurane, 30% O_2, 70% N_2O). The protective effect of chimeric proteins was measured daily by weight loss and survival rates over a post-challenge period. Control mice were used as negative control in challenge studies.

Influenza virus replication in lungs

Mice (three from each group) intranasally received the influenza viruses A/Aichi/2/68 (H3N2), A/PR/8/34 (H1N1), and A/Kurgan/5/05 (H5N1) with 5 times the LD50 doses (5LD50) on day 14 post third immunization. On day 6 post challenge, the mice were euthanatized (in a CO_2- euthanasia chamber, Vet Tech Solutions) and their lungs aseptically extracted. The lungs were homogenized in 2.7 ml PBS (Tissue Lyser II homogenizer, Qiagen, USA) to obtain a 10% (w/v) suspension, centrifuged at 400 g at 4°C for 15 min to remove cellular debris and stored at −20°C. The MDCK cell culture in the MEM medium grown in 96-well plates was used for virus titration. Culture cells were infected with 10-fold dilutions (10^{-1} to 10^{-8}) of the lung homogenate in quadruplicates and incubated in a thermostat (36.0 ± 0.5°C) for 72 h. Following incubation, culture suspensions were transferred into the 96-well plates for immunological assays, followed by the addition of an equal volume of 1% chicken erythrocytes in PBS. The viral titers were determined by hemagglutination test with 0.5% chicken erythrocytes. The viral titers were calculated by the Reed and Muench method. A value opposite to the decimal logarithm of the highest virus dilution showing a positive HA reaction was taken as the titer. Virus titers were expressed as a lg 50% tissue culture infectious dose ($TCID_{50}$).

Statistics

The statistical analysis was done by using GraphPad Prizm v6.0. Statistically significant differences in the antibody levels between groups were tested using the nonparametric Mann-Whitney test. Survival rates were compared with the Montel-Cox test. Differences were considered significant at $p < 0.05$.

RESULTS AND DISCUSSION

HA2 fragment analysis (76–130) of influenza viruses from the second phylogenetic group

The HA2 fragment (76–130) is a large α-helix in the second subunit of HA partially exposed to the HA surface (*Fig. 1A*). Consensus HA sequences of influenza A viruses from the phylogenetic group II (H3 and H7 subtypes) share 63.6 % identity within the HA2 (76–130) region

Fig. 2. *A* – Experimental *B*- and CD4+ T-cell epitopes that are > 90 % homologous to the consensus HA2 region spanning aa 76–130. The data obtained from the IEDB database. Mismatched amino acids are in red, the B-cell epitope is in green. *B* – Predicted CD8+ T-cell epitopes within the 76–130 region of HA2 for a given set of HLA alleles. Epitopes are predicted by the NetCTLpan1.1 Server [38]

(*Fig. 1B*). When substitutions of amino acid residues for chemically similar ones are taken into account, the HA sequences exhibit 80% homology. For the influenza viruses of phylogenetic group II, predicted B- and CD4+ T- cell epitopes are located in the first portion of the 76–130 region (*Fig. 2A*). In addition, the HA2(76–130) of influenza viruses of phylogenetic group II contains the predicted CD8+ T- cell epitopes of different HLA alleles (*Fig. 2B*).

Design of chimeric proteins

The M2eh consensus sequence across human influenza A virus strains, the M2ek sequence of the influenza A/Kurgan/05/200 (H5N1) virus, the HA2 (76–130) fragment of hemagglutinin of phylogenetic group II were selected as conserved peptides to be used in the vaccine design (*Fig. 3*).

We constructed genes expressing chimeric proteins that contain M2e-peptides of different influenza virus subtypes and a conserved fragment of the second HA subunit of influenza A viruses of phylogenetic group II linked at the C-terminus of flagellin in a different sequence order (*Fig. 3*). The chimeric protein Flg-HA2-4M2e consists of the 76–130 region of the second HA subunit of influenza viruses from phylogenetic group II and four tandem copies of M2e (M2h-M2k-M2h-M2k) sequentially fused to the C-terminus of the flagellin molecule. In fusion protein Flg-4M2e-HA2, four tandem copies of M2e (M2h-M2k-M2h-M2k) were linked to the C-terminus of flagellin, followed by the HA2(76-130) fragment. The M2e copies are separated from each other and from HA2 by glycine-rich linkers. The assembly of the chimeric genes was carried out in the expression vector pQE30. The flagellin gene, without its own start codon, was cloned into the BamHI site of the vector. The

M2h – is a M2e consensus sequence of human influenza A viruses:
SLLTEVETPIRNEWGCRCNDSSD
M2k – M2e from A/Kurgan/05/2005 H5N1:
SLLTEVETPTRNEWECRCSDSSD
HA2 – HA2 (76–130) fragment of influenza viruses A from the phylogenetic group II:
RIQDLEKYVEDTKIDLWSYNAELLVALENQHTIDLTDSEMNKLFEKTRRQLRENA

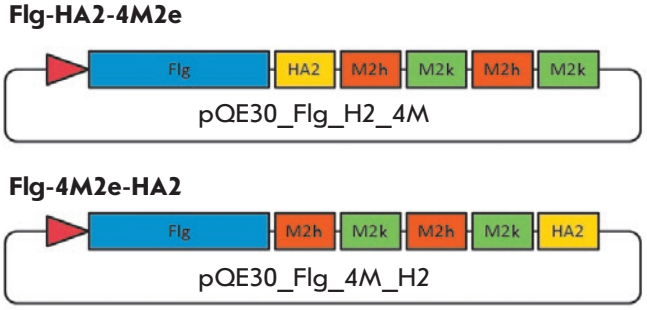

Fig. 3. Structure of the chimeric proteins Flg-HA2-4M2e and Flg-4M2e-HA2. The blue block depicts flagellin of *S. typhimurium*; the orange block depicts the consensus M2e sequence of human influenza A viruses; the green block depicts the M2e peptide of influenza A/Kurgan/5/05 RG (H5N1) virus; the yellow block depicts the aa 76–130 of HA2 of influenza viruses from phylogenetic group II

expression allowed us to produce recombinant flagellin with the N-terminal 6-His tag needed for purification by metal-affinity chromatography.

The chimeric genes were constructed using common genetic engineering techniques. The flagellin gene was

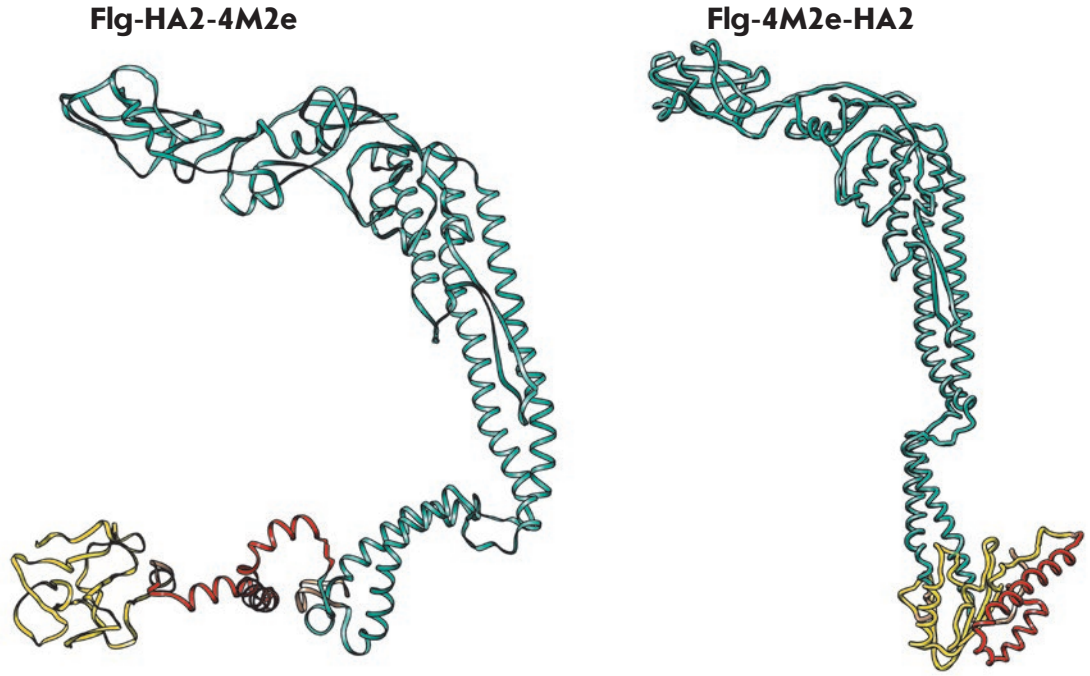

Fig. 4. Modeling of 3D- structures of monomeric chimeric proteins Flg-HA2-4M2e and Flg-4M2e-HA2. M2e-peptides are in yellow, HA2 are in red, and Flg is in blue. Protein models are predicted using the Phyre2 server. Structures are visualized with the UCSF Chimera tool

produced by amplification of *S. typhimurium* genomic DNA and cloned. The HA2 nucleotide sequences and M2e tandem copies were generated *in vitro*. Overall, we created pQE30_Flg_HA2-4M2e and pQE30_ Flg_4M2e-HA2 vectors expressing the corresponding proteins.

Homology modeling of 3D structures of the Flg-HA2-4M2e and Flg-4M2e-HA2 proteins showed retention of the alpha-helical structure within the 76–130 region of HA2 regardless of the sequence order (*Fig. 4*). It is tempting to say that the native structure of the HA2 fragment seems to remain intact and that the obtained chimeric proteins are immunogenic, including eliciting an antibody response to the structural epitopes occurring in the native HA structure. However, the two chimeric proteins do differ in structure. The chimeric protein carrying the HA2 peptide at the C-terminus displays a more compact structure. The 3D-structure of four M2e tandem copies differed between the two chimeric proteins. When positioned between Flg and HA2 (Flg-4M2e-HA2), the M2e repeats adopted a partial alpha-helical configuration, which does not occur in the native M2e structure on the surface of the virion or infected cells (*Fig. 4*). The terminal position of the M2e tandem copies (Flg-HA2-4M2e) did not significantly alter the intrinsically unstructured M2e conformation existing in the M2 protein. These conformational differences in the structure of the two chimeric proteins may affect their immunogenic properties.

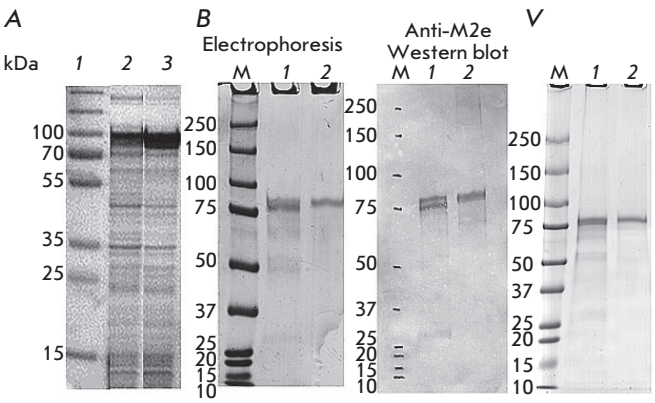

Fig. 5. *A* – Expression of the chimeric proteins in *E. coli* cells. *Lane 1*, molecular weight markers, kDa (Fermentas, EU); lane *2*, lysed cells transformed with the pQE30 Flg_HA2_4M2e vector following induction; lane *3*, lysed cells transformed with the pQE30 Flg_4M2e_HA2 vector following induction; *B* – Chimeric proteins Flg-HA2-4M2e and Flg-4M2e-HA2 purified by Ni-affinity chromatography. Electrophoretic profiles and results of western blot analysis using anti-M2e monoclonal antibodies (14C2) are shown; *C* — Recombinant proteins Flg-HA2-4M2e and Flg-4M2e-HA2 following a 2-month storage period at 4°C. Electrophoretic profiles are shown: M is a molecular weight marker, *1* – Flg-HA2-4M2e, *2* – Flg-4M2e-HA2

Production and purification of chimeric proteins

The genes encoding the chimeric proteins Flg-4M2e-HA2 and Flg-HA2-4M2e were cloned into the pQE30 vector and expressed in *E. coli* DLT1270 cells (*Fig. 5A*). The expected molecular weight of the two proteins, 73.9 kDa, was in agreement with the molecular weight resolved by electrophoretic migration on

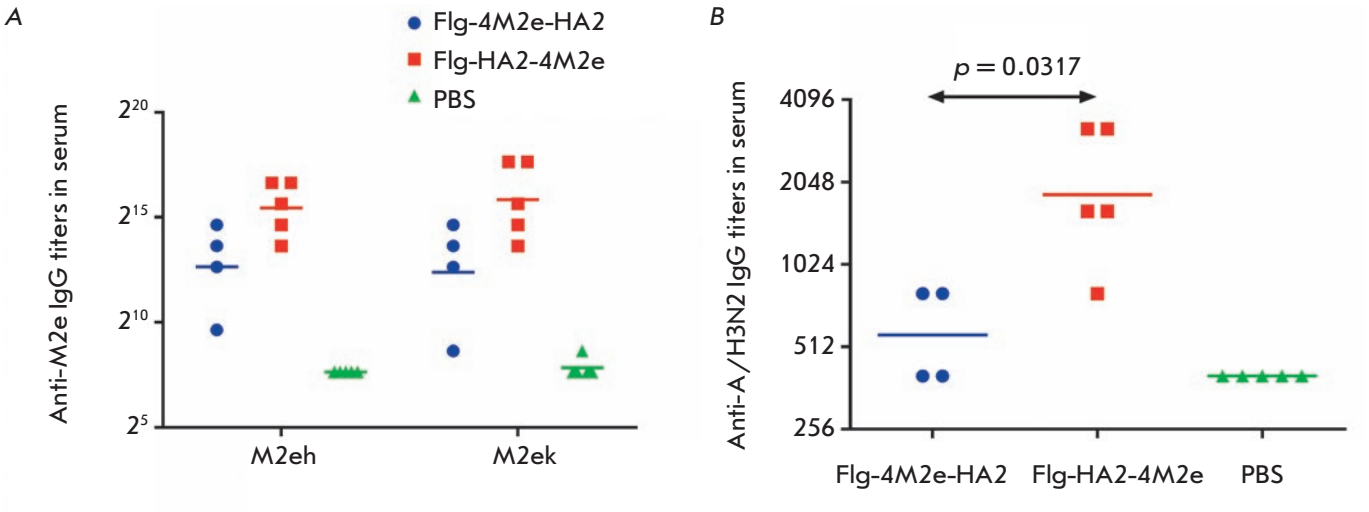

Fig. 6. Serum antibody titers in mice of experimental and control groups on day 14 post third immunization with Flg-HA2-4M2e and Flg-4M2e-HA2. Serum IgG levels to the target antigens: A — M2e peptides; B — influenza virus A/Aichi/2/68 (H3N2)

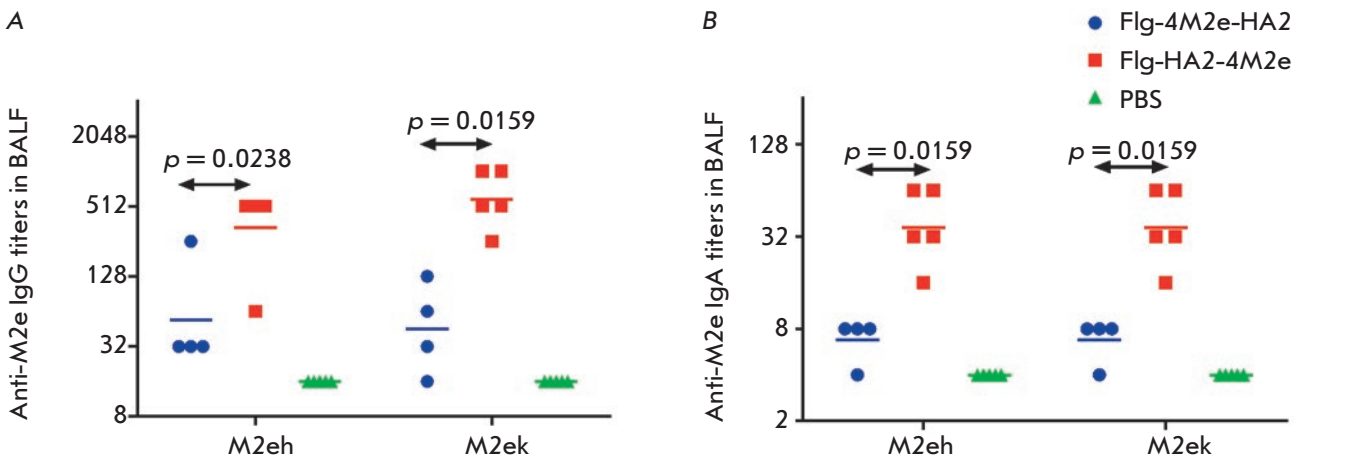

Fig. 7. BALF antibody titers to M2e peptides in mice of experimental and control groups on day 14 post third immunization with Flg-HA2-4M2e and Flg-4M2e-HA2: A – IgG; B – IgA

PAGE (*Fig. 5B*). The purified proteins Flg-4M2e-HA2 and Flg-HA2-4M2e were recognized by the monoclonal anti-M2e antibodies 14C2 in western blot (*Fig. 5B*). Since 14C2 antibodies recognize only the protective epitope M2e [14, 43], these findings confirm that the M2e peptide is present in both proteins. Both chimeric proteins showed robust stability. When stored at 4°C for 2 months, no sign of degradation was detected (*Fig. 5C*).

Comparison of the immunogenic properties of the Flg-HA2-4M2e and Flg-4M2e-HA2 proteins

The immunogenicity of the proteins Flg-HA2-4M2e and Flg-4M2e-HA2 were evaluated in Balb/c mice immunized intranasally three times. On day 14 post third immunization, sera and BALF samples of five mice were tested by ELISA for anti-M2e- and anti-A(H3N2)-antibodies. The mice immunized with Flg-HA2-4M2e or Flg-4M2e-HA2 showed no difference in anti-M2eh and anti-M2ek IgG levels in serum ($p > 0.05$) (*Fig. 6A*). However, the geometric mean titer (GMT) of the anti-M2e IgG levels in mice that had intranasally received Flg-HA2-4M2e was 4- to 6-fold higher than in mice immunized with Flg-4M2e-HA2. The level of anti-HA2 IgG against influenza virus A/Aichi/2/68 (H3N2) was significantly higher in mice immunized with Flg-HA2-4M2e (*Fig. 6B*) ($p = 0.0317$).

The mucosal IgA and IgG responses to M2eh and M2ek antigens were evaluated in BALF of five mice from each group on day 14 post third immunization. As shown in *Fig. 7*, intranasal immunization with the

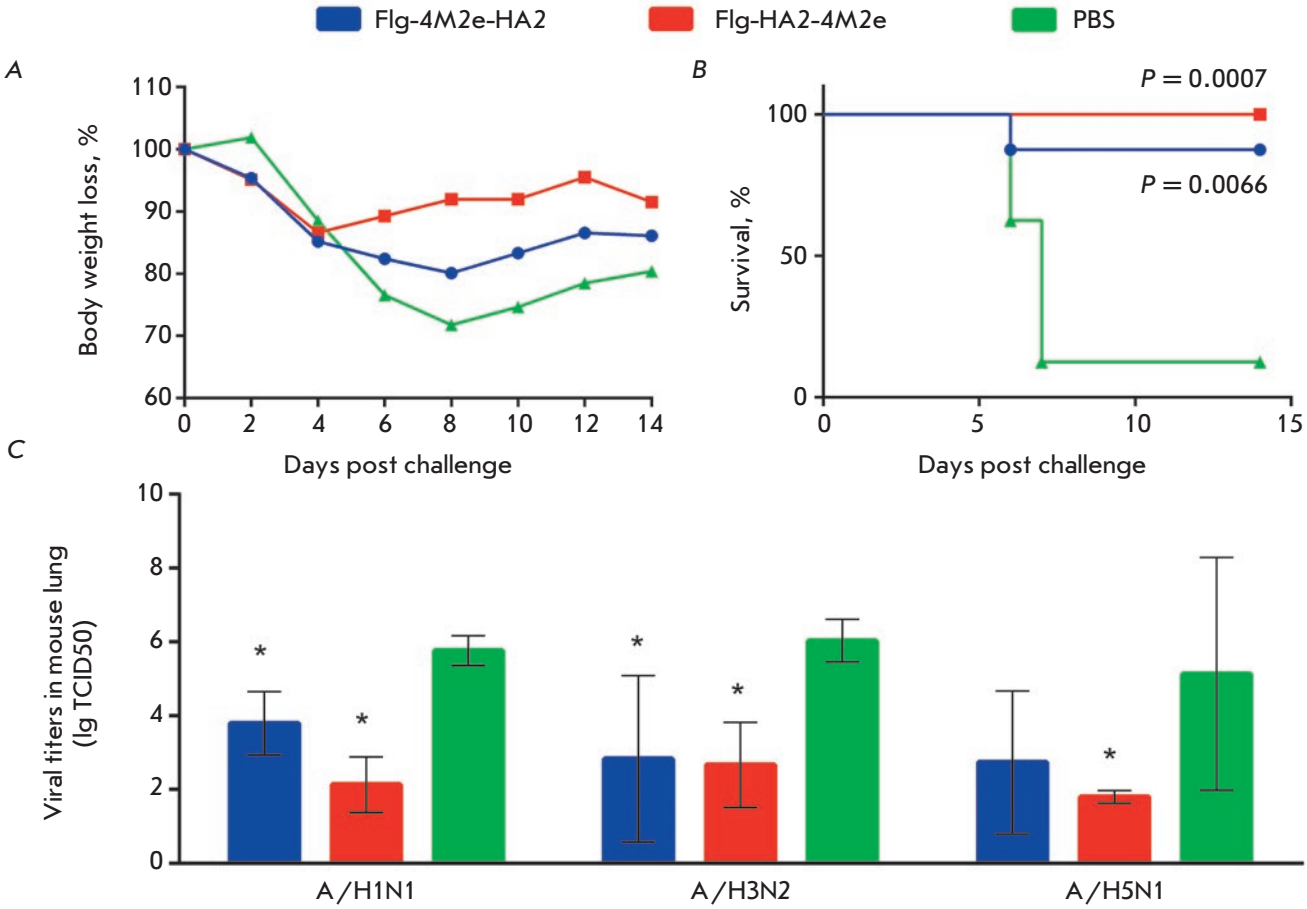

Fig. 8. Protective effects of Flg-HA2-4M2e and Flg-4M2e-HA2. On day 14 post third immunization, mice were intranasally challenged with influenza virus A/Aichi/2/68 (H3N2) at a dose of $5LD_{50}$. Body weight loss (*A*) and survival (*B*) were monitored daily for 14 days. The *p* value was calculated using the Mantel-Cox test. C – viral replication in mouse lung. On day 14 post third immunization, mice were intranasally challenged with influenza viruses A/Aichi/2/68 (H3N2), A/PR/8/34(H1N1), and A/Kurgan/5/05 (H5N1) at $5LD_{50}$. Viral titers were evaluated on day 6 post challenge. Results are given as lg TCID50. The limit of detection was 0.5 lg TCID50. The statistical significance between experimental and control groups was assessed using the nonparametric Mann-Whitney test. *The differences were considered significant when $p < 0.05$

chimeric protein Flg-HA2-4M2e promoted much higher anti-M2e IgG and IgA levels than Flg-4M2e-HA2 ($p < 0.05$). This result demonstrates that the C-terminal position of M2e in Flg-HA2-4M2e shows more immunogenicity as compared to the inside position of M2e (Flg-4M2e-HA2).

Comparison of the protective potency of Flg-HA2-4M2e and Flg-4M2e-HA2

To evaluate the protective properties of the chimeric proteins, mice (8 mice/group) were immunized with Flg-HA2-4M2e or Flg-4M2e-HA2 and challenged with influenza virus A/Aichi/2/68 (H3N2) with 5LD50 on day 14 post third immunization. PBS-inoculated mice that received lethal influenza A/Aichi/2/68 (H3N2) were used as a negative control. The infected mice were monitored daily for body weight changes (as a measure of influenza infection severity) and survival for 14 days. *Figure 8A* demonstrates that mice immunized with the Flg-HA2-4M2e protein showed no more than a 13% body weight loss by day 4 post challenge, whereas mice immunized with the Flg-4M2e-HA2 protein exhibited a 20% decrease in body weight by day 8 post challenge. The maximum body weight loss in the control mice was 28% by day 8 post challenge. These findings show that immunization with Flg-HA2-4M2e offers a milder course of infection compared with the Flg-4M2e-HA2 protein (*Fig. 8A*). Immunization of mice with the fusion

protein Flg-HA2-4M2e provided complete protection (*Fig 8 B.*) from a lethal challenge (100% survival), whereas the survival rate of mice treated with Flg-4M2e-HA2 was 87.5%.($p = 0.0007$ and $p = 0.0066$, respectively, Montel-Cox test). The lethal challenge of PBS-inoculated mice resulted in a 12.5% survival rate.

After 14 days post third immunization, all groups (3 mice/group) were intranasally challenged with the influenza viruses A/PR/8/34 (H1N1), A/Aichi/2/68 (H3N2), and A/Kurgan/05/05 (H5N1) with a 5LD50 dose. On day 6 post challenge, mice were sacrificed to measure virus titers in their lungs. Mice from both immunized groups had lower viral titers as compared to control mice (*Fig. 8C*). The immunization with Flg-HA2-4M2e led to a 3.7, 3.3, and 3.3 lg reduction in viral titers after challenge with the influenza viruses A/PR/8/34 (H1N1), A/Aichi/2/68 (H3N2), and A/Kurgan/05/05 (H5N1), respectively. These values significantly differed from mock-inoculated mice ($p < 0.05$, Mann-Whitney Test). The chimeric protein Flg-4M2eh-HA2 induced a milder decrease in virus replication levels in the lungs (2.0, 3.2 and 2.4 lg, respectively), although the differences from the control group were significant ($p < 0.05$).

CONCLUSION

The highly conserved ectodomain of the matrix protein M2 and the conserved regions of the second HA subunit are promising antigens for the development of influenza vaccines with a broad spectrum of protection. The design of a candidate vaccine protein with two or more conserved target antigens that could induce different arms of immune responses (antibodies with different modes of action, CD4+, CD8+ T-lymphocytes) would boost the efficacy of such protein-based vaccines. The recombinant protein based on flagellin and the conserved antigens of two influenza proteins (M2e and aa 76–130 of of HA2) combines the adjuvant activity of flagellin due to TLR5 recognition, a highly conserved structure of M2e between human and avian influenza A virus strains, and a conserved fragment of the second subunit of HA with B-cell, as well as CD4+ and CD8+ T-cell epitopes.

We designed two chimeric proteins based on flagellin varying the insertion points of M2e peptides of different influenza A subtypes and the conserved fragment of the second subunit of HA. The possibility of producing a stable recombinant protein with two targeted antigens (heterologous M2e and HA2 (76–130) fused with flagellin was demonstrated. Such a protein is immunogenic, and it stimulates the formation of antibodies to both M2e and the influenza virus. The recombinant protein protected mice from a lethal challenge and significantly reduced the viral load in their lungs. We found that differing orders of linkage of target antigens to flagellin in the chimeric protein affect the 3D structure of the constructs, its immunogenicity, and protective potency. The two chimeric proteins induced different levels of antibody production, and the Flg-HA2-4M2e protein with a terminus position of M2e peptides was superior to an interior M2e position in the Flg-4M2eh-HA2 protein. Differences in protective effect between the two variants of protein design were also observed. Full protection and rapid recovery of animal weight after a small decline following a lethal challenge was observed in mice immunized with the Flg-HA2-4M2e protein. Moreover, this protein effected a greater reduction of viral titers in the lungs of the animals as compared to Flg-4M2eh-HA2.

Further research would be aimed at clarifying the role of each of the targeted antigens in the fusion protein in the formation of protective immunity, immune response duration, and the duration of its conservation and cross-protective effect. ●

This work was supported by the Russian Scientific Foundation (grant № 15-14-00043).

REFERENCES

1. Fan J., Liang X., Horton M.S., Perry H.C., Citron M.P., Heidecker G.J., Fu T.M., Joyce J., Przysiecki C.T., Keller P.M., et al. // Vaccine. 2004. V. 22. № 23–24. P. 2993–3003.
2. Huleatt J.W., Nakaar V., Desai P., Huang Y., Hewitt D., Jecobs A., Tang J., McDonald W., Song L., Evans R.K., et al. // Vaccine. 2008. V. 26. № 2. P. 201–214.
3. Fiers W., De Filette M., El Bakkouri K., Schepens B., Roose K., Schotsaert M., Birkett A., Saelens X. // Vaccine. 2009. V. 27. № 45. P. 6280–6283.
4. Schotsaert M., De Filette M., Fiers W., Saelens X. // Expert Rev. Vaccines. 2009. V. 8. № 4. P. 499–508.
5. Turley C.B., Rupp R.E., Johnson C., Taylor D.N., Wolfson J., Tussey L., Kavita U., Stanberry L., Shaw A. // Vaccine. 2011. V. 29. № 32. P. 5145–5152.
6. Stepanova L.A., Kotlyarov R.Y., Kovaleva A.A., Potapchuk M.V., Korotkov A.V., Sergeeva M.V., Kasianenko M.A., Kuprianov V.V., Ravin N.V., Tsybalova L.M., et al. // PLoS One. 2015. V. 10. № 3. P. e0119520.
7. Tsybalova L.M., Stepanova L.A., Kuprianov V.V., Blokhina E.A., Potapchuk M.V., Korotkov A.V., Gorshkov A.N., Kasyanenko M.A., Ravin N.V., Kiselev O.I. // Vaccine. 2015. V. 33. № 29. P. 3398–3406.
8. Neirynck S., Deroo T., Saelens X., Vanlandschoot P., Jou W.M., Fiers W. // Nat. Med. 1999. V. 5. № 10. P. 1157–1163.
9. Mozdanovska K., Maiese K., Furchner M., Gerhard W. // Virology. 1999. V. 254. № 1. P. 138–146.
10. Tompkins S.M., Zhao Z.C., Lo C.Y., Misplon J.A., Liu T., Ye Z., Hogan R.J. Wu Z., Benton K.A., Tumpey T.M., Epstein S.L. // Emerg. Infect. Dis. 2007. V. 13. № 3. P. 426–435.

11. Beerli R.R., Bauer M., Schmitz N., Buser R.B., Gwerder M., Muntwiler S., Renner W.A., Saudan P., Bachmann M.F. // Virol. J. 2009. V. 6. P. 224–235.
12. Jegerlehner A., Schmitz N., Storni T., Bachmann M.F. // J. Immunol. 2004. V. 172. . P. 5598–5605.
13. El Bakkouri K., Descamps F., De Filette M., Smet A., Festjens E., Birkett A., van Rooijen N., Verbeek S., Fiers W., Saelens X. // J. Immunol. 2011. V. 186. P. 1022–1031.
14. Treanor J.J., Tierney E.L., Zebedee SL., Lamb R.A., Murphy B.R. // J. Virol. 1990. V. 64. P. 1375–1377.
15. Gerhard W., Mozdzanowska K., Zharikova D. // Emerg. Infect. Dis. 2006. V. 12. № 14. P. 569–574.
16. Trosby M., van den Brink E., Jongeneelen M., Poon L.L., Alard P., Cornelissen L., Bakker A., Cox F., van Deventer E., Guan Y., et al. // PLoS One. 2008. V. 3. № 12. P. e3942.
17. Prabhu N., Prabakaran M., Ho H.T., Velumani S., Qiang J., Goutama M., Kwang J. // J. Virol. 2009. V. 83. № 6. P. 2553–2562.
18. Wang T.T., Tan G. S., Hai R., Pica N., Petersen E., Moran T.M., Peter Palese P. // PLoS Pathogens. 2010a. V. 6. № 2. P. e1000796.
19. Wei C.J., Boyington J.C., McTamney P.M., Kong W.P., Pearce M.B., Xu L., Andersen H., Rao S., Tumpey T.M., Yang Z.Y., et al. // Science. 2010. V. 329. № 5995. P. 1060–1064.
20. Corti D., Voss J., Gamblin S.J., Codoni G., Macagno A., Jarrossay D., Vachieri S.G., Pinna D., Minola A., Vanzetta F., et al. // Science. 2011. V. 333. № 6044. P. 850–856.
21. Wrammert J., Koutsonanos D., Li G.M., Edupuganti S., Sui J., Morrissey M., McCausland M., Skountzou I., Hornig M., LipkinW.I., et al. // J. Exp. Med. 2011. V. 208. № 1. P. 181–193.
22. Ekiert D.C., Friesen R.H., Bhabha G., Kwaks T., Jongeneelen M., Yu W., Ophorst C., Cox F., Korse H.J., Brandenburg B., et al. // Science. 2011. V. 333. № 6044. P. 843–850.
23. Wang T.T., Tan G.S., Hai R., Pica N., Ngai L., Ekiert D.C., Wilson I.A., García-Sastre A., Moran T.M., Palese P. // Proc. Natl. Acad. Sci. USA. 2010b. V. 107. № 44. P. 18979–18984.
24. Bommakanti G., Citron M.P., Hepler R.W., Callahan C., Heidecker G.J., Najar T.A., Lu X., Joyce J.G., Shiver J.W., Casimiro D.R., et al. // Proc. Natl. Acad. Sci. USA. 2010. V. 107. № 31. P. 13701–13706.
25. Schneemann A., Speir J.A., Tan G.S., Khayat R., Ekiert D.C., Matsuoka Y., Wilson I.A. // J. Virol. 2012. V. 86. № 21. P. 11686–11697.
26. Stanekova Z., Adkins I., Kosova M., Janulíkova J., Sebo P., Vareckova E. // Antiviral Res. 2013. V. 97. № 1. P. 24–35.
27. Stepanova L.A., Sergeeva M.V., Shuklina M.A., Shaldzhyan A.A., Potapchuk M.V., Korotkov A.V., Tsybalova L.M. // Acta Naturae. 2016. V. 8. № 2. P. 116–126.
28. Delaney K.N., Phipps J.P., Johnson J.B., Mizel S.B. // Viral Immunol. 2010. V. 23. P. 201–210.
29. Cuadros C., Lopez-Hernandez F.G., Dominguez A.L., McClelland M., Lustgarten J. // Infect. Immun. 2004. V. 72. P. 2810–2816.
30. Honko A.N., Sriranganathan N., Lees C.J., Mizel S.B. // Infect. Immun. 2006. V. 74. P. 1113–1120.
31. Bates J.T., Honko A.N., Graff A.H., Kock N., Mizel S.B. // Mech. Ageing Dev. 2008. V. 129. P. 271–281.
32. Song L., Zhang Y., Yun N.E., Poussard A.L., Smith J.N., Smith J.K., Borisevich V., Linde J.J., Zacks M.A., Li H., et al. // Vaccine. 2009. V. 27. № 42. P. 5875–5884.
33. Wang B.-Z., Xu R., Quan F.-S., Kang S.M., Wang L., Compans R.W. // PLoS One. 2010. V. 5. P. e13972.
34. Liu G., Tarbet B., Song L., Reiserova L., Weaver B., Chen Y., Li H., Hou F., Liu X., Parent J., et al. // PLos One. 2011. V. 6. № 6. P. e20928.
35. Katoh K., Misawa K., Kuma K., Miyata T. // Nucl. Acids Res. 2002. V. 30. № 14. P. 3059–3066.
36. Okonechnikov K., Golosova O., Fursov M. // Bioinformatics. 2012. V. 28. № 8. P. 1166–1167.
37. Vita R., Zarebski L., Greenbaum J.A., Emami H., Hoof I., Salimi N., Damle R., Sette A., Peters B. // Nucl. Acids Res. 2010. V. 38. Database issue. P. D854–D862.
38. Stranzl T., Larsen M.V., Lundegaard C., Nielsen M. // Immunogenetics. 2010. V. 62. № 6. P. 357–368.
39. Pettersen E.F., Goddard T.D., Huang C.C., Couch G.S., Greenblatt D.M., Meng E.C., Ferrin T.E. // J. Comput. Chem. 2004. V. 25. № 13. P. 1605–1612.
40 Kelley L.A., Sternberg M.J. // Nat. Protoc. 2009. V. 4. № 3. P. 363–371.
41. Grant S., Jessee J., Bloom F., Hanahan D. // Proc. Natl. Acad. Sci. USA. 1990. V. 87. № 12. P. 4645–4649.
42. Laemmli U.K. // Nature. 1970. V. 227. № 5259. P. 680–685.
43. Zharikova D., Mozdzanowska K., Feng J., Zhang M., Gerhard W. // J. Virol. 2005. V. 79. P. 6644–6654.

GENERAL RULES

Acta Naturae publishes experimental articles and reviews, as well as articles on topical issues, short reviews, and reports on the subjects of basic and applied life sciences and biotechnology.

The journal is published by the Park Media publishing house in both Russian and English.

The journal *Acta Naturae* is on the list of the leading periodicals of the Higher Attestation Commission of the Russian Ministry of Education and Science. The journal Acta Naturae is indexed in PubMed, Web of Science, Scopus and RCSI databases.

The editors of *Acta Naturae* ask of the authors that they follow certain guidelines listed below. Articles which fail to conform to these guidelines will be rejected without review. The editors will not consider articles whose results have already been published or are being considered by other publications.

The maximum length of a review, together with tables and references, cannot exceed 60,000 characters with spaces (approximately 30 pages, A4 format, 1.5 spacing, Times New Roman font, size 12) and cannot contain more than 16 figures.

Experimental articles should not exceed 30,000 symbols (approximately 15 pages in A4 format, including tables and references). They should contain no more than ten figures.

A short report must include the study's rationale, experimental material, and conclusions. A short report should not exceed 12,000 symbols (8 pages in A4 format including no more than 12 references). It should contain no more than four figures.

The manuscript and the accompanying documents should be sent to the Editorial Board in electronic form:
1) text in Word 2003 for Windows format;
2) the figures in TIFF format;
3) the text of the article and figures in one pdf file;
4) the article's title, the names and initials of the authors, the full name of the organizations, the abstract, keywords, abbreviations, figure captions, and Russian references should be translated to English;
5) the cover letter stating that the submitted manuscript has not been published elsewhere and is not under consideration for publication;
6) the license agreement (the agreement form can be downloaded from the website www.actanaturae.ru).

MANUSCRIPT FORMATTING

The manuscript should be formatted in the following manner:

- Article title. Bold font. The title should not be too long or too short and must be informative. The title should not exceed 100 characters. It should reflect the major result, the essence, and uniqueness of the work, names and initials of the authors.
- The corresponding author, who will also be working with the proofs, should be marked with a footnote *.
- Full name of the scientific organization and its departmental affiliation. If there are two or more scientific organizations involved, they should be linked by digital superscripts with the authors' names. Abstract. The structure of the abstract should be very clear and must reflect the following: it should introduce the reader to the main issue and describe the experimental approach, the possibility of practical use, and the possibility of further research in the field. The average length of an abstract is 20 lines (1,500 characters).
- Keywords (3 – 6). These should include the field of research, methods, experimental subject, and the specifics of the work. List of abbreviations.
- INTRODUCTION
- EXPERIMENTAL PROCEDURES
- RESULTS AND DISCUSSION
- CONCLUSION

  The organizations that funded the work should be listed at the end of this section with grant numbers in parenthesis.
- REFERENCES

  The in-text references should be in brackets, such as [1].

RECOMMENDATIONS ON THE TYPING AND FORMATTING OF THE TEXT

- We recommend the use of Microsoft Word 2003 for Windows text editing software.
- The Times New Roman font should be used. Standard font size is 12.
- The space between the lines is 1.5.
- Using more than one whole space between words is not recommended.
- We do not accept articles with automatic referencing; automatic word hyphenation; or automatic prohibition of hyphenation, listing, automatic indentation, etc.
- We recommend that tables be created using Word software options (Table → Insert Table) or MS Excel. Tables that were created manually (using lots of spaces without boxes) cannot be accepted.
- Initials and last names should always be separated by a whole space; for example, A. A. Ivanov.
- Throughout the text, all dates should appear in the "day.month.year" format, for example 02.05.1991, 26.12.1874, etc.
- There should be no periods after the title of the article, the authors' names, headings and subheadings, figure captions, units (s – second, g – gram, min – minute, h – hour, d – day, deg – degree).
- Periods should be used after footnotes (including those in tables), table comments, abstracts, and abbreviations (mon. – months, y. – years, m. temp. – melting temperature); however, they should not be used in subscripted indexes (T_m – melting temperature; $T_{p.t}$ – temperature of phase transition). One exception is mln – million, which should be used without a period.
- Decimal numbers should always contain a period and not a comma (0.25 and not 0,25).
- The hyphen ("-") is surrounded by two whole spaces, while the "minus," "interval," or "chemical bond" symbols do not require a space.
- The only symbol used for multiplication is "×"; the "×" symbol can only be used if it has a number to its

right. The "·" symbol is used for denoting complex compounds in chemical formulas and also noncovalent complexes (such as DNA·RNA, etc.).
- Formulas must use the letter of the Latin and Greek alphabets.
- Latin genera and species' names should be in italics, while the taxa of higher orders should be in regular font.
- Gene names (except for yeast genes) should be italicized, while names of proteins should be in regular font.
- Names of nucleotides (A, T, G, C, U), amino acids (Arg, Ile, Val, etc.), and phosphonucleotides (ATP, AMP, etc.) should be written with Latin letters in regular font.
- Numeration of bases in nucleic acids and amino acid residues should not be hyphenated (T34, Ala89).
- When choosing units of measurement, SI units are to be used.
- Molecular mass should be in Daltons (Da, KDa, MDa).
- The number of nucleotide pairs should be abbreviated (bp, kbp).
- The number of amino acids should be abbreviated to aa.
- Biochemical terms, such as the names of enzymes, should conform to IUPAC standards.
- The number of term and name abbreviations in the text should be kept to a minimum.
- Repeating the same data in the text, tables, and graphs is not allowed.

GUIDENESS FOR ILLUSTRATIONS

- Figures should be supplied in separate files. Only TIFF is accepted.
- Figures should have a resolution of no less than 300 dpi for color and half-tone images and no less than 500 dpi.
- Files should not have any additional layers.

REVIEW AND PREPARATION OF THE MANUSCRIPT FOR PRINT AND PUBLICATION

Articles are published on a first-come, first-served basis. The members of the editorial board have the right to recommend the expedited publishing of articles which are deemed to be a priority and have received good reviews.

Articles which have been received by the editorial board are assessed by the board members and then sent for external review, if needed. The choice of reviewers is up to the editorial board. The manuscript is sent on to reviewers who are experts in this field of research, and the editorial board makes its decisions based on the reviews of these experts. The article may be accepted as is, sent back for improvements, or rejected.

The editorial board can decide to reject an article if it does not conform to the guidelines set above.

The return of an article to the authors for improvement does not mean that the article has been accepted for publication. After the revised text has been received, a decision is made by the editorial board. The author must return the improved text, together with the responses to all comments. The date of acceptance is the day on which the final version of the article was received by the publisher.

A revised manuscript must be sent back to the publisher a week after the authors have received the comments; if not, the article is considered a resubmission.

E-mail is used at all the stages of communication between the author, editors, publishers, and reviewers, so it is of vital importance that the authors monitor the address that they list in the article and inform the publisher of any changes in due time.

After the layout for the relevant issue of the journal is ready, the publisher sends out PDF files to the authors for a final review.

Changes other than simple corrections in the text, figures, or tables are not allowed at the final review stage. If this is necessary, the issue is resolved by the editorial board.

FORMAT OF REFERENCES

The journal uses a numeric reference system, which means that references are denoted as numbers in the text (in brackets) which refer to the number in the reference list.

For books: the last name and initials of the author, full title of the book, location of publisher, publisher, year in which the work was published, and the volume or issue and the number of pages in the book.

For periodicals: the last name and initials of the author, title of the journal, year in which the work was published, volume, issue, first and last page of the article. Must specify the name of the first 10 authors. Ross M.T., Grafham D.V., Coffey A.J., Scherer S., McLay K., Muzny D., Platzer M., Howell G.R., Burrows C., Bird C.P., et al. // Nature. 2005. V. 434. № 7031. P. 325–337.

References to books which have Russian translations should be accompanied with references to the original material listing the required data.

References to doctoral thesis abstracts must include the last name and initials of the author, the title of the thesis, the location in which the work was performed, and the year of completion.

References to patents must include the last names and initials of the authors, the type of the patent document (the author's rights or patent), the patent number, the name of the country that issued the document, the international invention classification index, and the year of patent issue.

The list of references should be on a separate page. The tables should be on a separate page, and figure captions should also be on a separate page.

The following e-mail addresses can be used to contact the editorial staff: vera.knorre@gmail.com, actanaturae@gmail.com, tel.: (495) 727-38-60, (495) 930-87-07